

Investigation of Positron Emission Tomography for pharmacological assessment of Epidermal Growth Factor Receptor-directed therapies

A dissertation submitted to Imperial College London
Department of Surgery and Cancer
for the fulfilment of the requirements
for the degree of Doctor of Philosophy

by

Rozanna Slade

Declaration of Work

I hereby declare that this thesis and the work reported herein was composed and originated entirely by myself, with the exception of the chemical and radiochemical synthesis of the cyanoquinoline compounds, which were carried out by Dr Pisaneschi and the tumour sectioning for immunohistochemistry which was carried out by John Latigo.

Copyright Declaration

'The copyright of this thesis rests with the author and is made available under a Creative Commons Attribution Non-Commercial No Derivatives licence. Researchers are free to copy, distribute or transmit the thesis on the condition that they attribute it, that they do not use it for commercial purposes and that they do not alter, transform or build upon it. For any reuse or redistribution, researchers must make clear to others the licence terms of this work'

Acknowledgements

I would like to thank Cancer Research UK (CR-UK) for their financial support that allowed this project to be carried out.

I would like to express my appreciation to my supervisor Professor Aboagye for his valuable guidance throughout this project. I am grateful for everybody in Professor Aboagye's group for their help and support throughout my project. A special thanks to Dr. Pisaneschi who designed and synthesised the cyanoquinoline compounds used in this project. Thank you to Dr. Kaliszczak for his help with the proof reading of this thesis and Dr Nguyen for his supervision.

Finally, I would also like to thank my friends and family for their support during the last three years and especially for the help they gave me in the later stages of the preparation of this thesis.

Abstract

The epidermal growth factor receptor (EGFR) is overexpressed in many cancers including lung, breast, head and neck and brain. Furthermore, mutations of this receptor have been shown to play crucial roles in response to EGFR-targeted therapies in non small cell lung carcinoma (NSCLC) patients. Imaging EGFR or its function using positron emission tomography (PET) could aid in selection and monitoring patient's therapeutic response to small molecule tyrosine kinase inhibitors (TKIs) including gefitinib.

The aims of this project are first to further investigate the use of a series of cyanoquinoline tracers for imaging the EGFR and second to assess the role of PET imaging to predict early response to EGFR directed therapy such as gefitinib.

First, the uptake of a representative cyanoquinoline radiotracer, [¹⁸F](2E)-N-{4-[(3-chloro-4-fluorophenyl)amino]-3-cyano-7-ethoxyquinolin-6-yl)}4-([1-(2-fluoroethyl)-1H-1,2,3-triazol-4-yl]methyl*amino)but-2-enamide ([¹⁸F]FED6), was examined in cell lines harbouring mutant forms of EGFR. *In vitro* assays, evaluating the affinity of cyanoquinoline compounds for different mutant EGFR and *in vivo* PET imaging in NSCLC xenograft models expressing mutant or wild type (WT) EGFR were carried out. The lack of specificity for mutant vs WT EGFR and overall low tumour uptake led us to investigate the potential interaction of the radiotracer with members of the ABC transporters. *In vitro* experiments of radiolabelled [¹⁸F] showed substrate specificity of the cyanoquinoline tracer for at least two ABC transporters, ABCG2 and ABCB1. This was confirmed by inhibiting the activity of the transporters through drug and siRNA treatment. To overcome the transporter substrate specificity of FED6, investigations into a novel radiotracer, (2E)-N-{4-[(3-chloro-4-fluorophenyl)amino]-3-cyano-7-ethoxyquinolin-6-yl}-4-([1-[(2R,5S)-3-fluoro-4,5-dihydroxy-6-(hydroxymethyl)oxan-2-yl]-1H-1,2,3-triazol-4-yl]methyl)amino]but-2-enamide (FED20), designed so as to limit the affinity for the ABC transporters were carried out. These studies showed that FED20 lacked the substrate specificity for both ABCB1 and ABCG2, and maintained a strong affinity for EGFR.

Second, the role of choline kinase as a biomarker of response to gefitinib treatment in sensitive vs resistant NSCLC cell lines was investigated. *In vitro* western blots, Q-PCR, cell viability and cell cycle analysis assays were undertaken. *In vitro* cell uptake experiments using tritiated choline were compared with uptake of [¹⁸F]3' deoxy-3' Fluorothymidine (FLT) and [¹⁸F]Fluoro-D glucose (FDG). Higher levels of choline uptake were found in the sensitive compared to the resistant cell line whereas both [¹⁸F]FLT and [¹⁸F]FDG showed higher accumulation in the resistant versus sensitive cell line. These experiments confirmed that differential responses of the sensitive and the resistant cell lines to gefitinib treatment were detectable by tracer pulse-chase. *In vivo* PET imaging of NSCLC

xenografts using [^{18}F]FLT, [^{18}F]FDG and [^{18}F]D4Choline showed that gefitinib treatment was associated with a decrease in the fractional retention of all three tracers in the sensitive but not resistant NSCLC xenografts.

Table of Contents

CHAPTER 1: INTRODUCTION	17
1.1 EPIDERMAL GROWTH FACTOR RECEPTOR	18
1.1.1. MEMBER OF THE HUMAN EPIDERMAL GROWTH FACTOR RECEPTOR (HER) FAMILY	18
1.1.2. EGFR ACTIVATION AND SIGNAL TRANSDUCTION	19
1.2 EGFR AND CANCER	21
1.2.1 EGFR'S INVOLVEMENT IN MANY TYPES OF CANCER	22
1.2.2 EGFR GENE AMPLIFICATION	22
1.2.3 EGFR MUTATIONS	23
1.3 EGFR TARGETED CANCER THERAPIES	25
1.3.1 ANTIBODY BASED COMPOUNDS	25
1.3.2 SMALL MOLECULAR TKIS: FIRST GENERATION, ERLOTINIB AND GEFITINIB	25
1.3.3 RESISTANCE TO TKI TREATMENT	29
1.3.3.1 <i>Intrinsic resistance</i>	29
1.3.3.2 <i>Acquired resistance</i>	29
1.3.4 OVERCOMING RESISTANCE	31
1.3.4.1 <i>Second generation of TKI</i>	31
1.3.4.2 <i>Third generation of TKIs</i>	33
1.3.4.3 <i>Multitarget TKI and combination studies</i>	34
1.4 PET IMAGING OF EGFR	35
1.4.1 PRINCIPLES OF POSITRON EMISSION TOMOGRAPHY IMAGING	37
1.4.2 TRACERS USED IN THE CLINIC	39
1.4.3 PET IMAGING AND ITS APPLICATION IN THE STUDY OF EGFR	41
1.4.3.1 <i>Tracers developed from antibody therapeutic agents</i>	41
1.4.3.2 <i>Tracers developed from the first generation TKIs</i>	42
1.4.3.3 <i>Tracers developed from second generation of TKI's</i>	43
1.4.3.4 <i>FED Compounds</i>	45
1.5 BIOMARKERS OF RESPONSE, FAILURE OF RESPONSE TO TKI TREATMENT IN NSCLC	48
1.5.1 BIOMARKERS OBTAINED FROM TISSUE SAMPLES	48
1.5.2 PREDICTING RESPONSE TO TKI TREATMENT: PET IMAGING WITH [¹⁸ F]FDG AND [¹⁸ F]FLT	49
1.5.2.1 <i>Pre-clinical findings</i>	50
1.5.2.2 <i>Clinical findings</i>	50
1.6 CHOLINE METABOLISM IN CANCER	51
1.6.1 CHOLINE KINASE	52
1.6.2 <i>IN VIVO</i> IMAGING OF CHOLINE METABOLISM	54
1.6.2.1 <i>MRS</i>	55
1.6.2.2 <i>PET imaging of choline metabolism</i>	55
1.7 ATP BINDING CASSETTE (ABC) TRANSPORTERS AND TKI INTERACTION	56
1.7.1 ABC TRANSPORTERS	56
1.7.2 TKI AND ABC TRANSPORTER PROTEIN INTERACTION	58
1.7.3 TRACERS AND ABC TRANSPORTER INTERACTION	59
AIMS	61
CHAPTER 2: METHODS	62

2.1 CHEMICAL STRUCTURE ANALYSIS	63
2.2 CELL CULTURE.....	63
2.3 SIRNA TRANSFECTION	64
2.3.1. SIRNA TRANSFECTION IN 6-WELL PLATES	64
2.3.2. SIRNA IN 96-WELL PLATES	64
2.4 RNA QUANTIFICATION	65
2.4.1 RNA EXTRACTION	65
2.4.2 cDNA SYNTHESIS	65
2.4.3 RT-PCR	65
2.5 INHIBITION OF EGFR ACTIVATION	66
2.6 WESTERN BLOTTING	66
2.6.1 CELL LYSATE PREPARATION	67
2.6.2 SAMPLE PROCESSING.....	67
2.7 CELL VIABILITY ASSAY	68
2.7.1 GENERAL PROTOCOL	68
2.7.2 CELL VIABILITY ASSAY WITH DRUG PRE-TREATMENT	69
2.7.3 DATA ANALYSIS.....	69
2.8 EGFR TYROSINE KINASE ENZYME INHIBITION ASSAY	69
2.9 CALCEIN-AM ASSAY	70
2.10 HOECHST 33324 UPTAKE ASSAY.	70
2.11 CACO2 TRANSWELL ASSAY.	71
2.11.1 TRANSWELL PREPARATION.....	71
2.11.2 HPLC ANALYSIS.....	72
2.11.3 DATA ANALYSIS	72
2.11.4 MEMBRANE INTEGRITY.....	73
2.12 CASPASE GLOW ASSAY	73
2.13 CELL CYCLE ANALYSIS VIA FLOW CYTOMETRY USING PROPIDIUM IODIDE.....	74
2.14 RADIOPHARMACEUTICALS	74
2.15 CELL UPTAKE ASSAY.....	75
2.15.1 [³ H]CHOLINE	75
2.15.2 [¹⁸ F] UPTAKE EXPERIMENTS	76
2.16 IN VIVO.....	77
2.16.1 TUMOUR INOCULATION.....	77
2.16.2 POSITRON EMISSION TOMOGRAPHY IMAGING	77
2.16.3 BIODISTRIBUTION.....	79
2.16.4 TUMOUR LYSATE PREPARATION	80
2.17 STATISTICS	80
CHAPTER 3: IMAGING MUTANT EGFR WITH [¹⁸F]FED6.....	81
3.1 BINDING OF [¹⁸F]FED6 TO EGFR OVEREXPRESSING CELLS	82

3.2 SENSITIVITY OF WILD TYPE AND ACTIVE MUTANT EGFR EXPRESSING NSCLC TO FED6	83
3.3 [¹⁸F]FED6 <i>IN VITRO</i> AND <i>IN VIVO</i> UPTAKE IN A549 VS H1650	86
3.4 TESTING FED6 IN ACTIVE AND RESISTANT MUTANT NSCLC CELL LINES	89
3.4.1 WESTERN BLOT ANALYSIS OF GEFITINIB AND FED6 INHIBITION OF P-EGFR.	89
3.4.2 [¹⁸ F]FED6 <i>IN VITRO</i> UPTAKE IN ACTIVE AND RESISTANT MUTANT NSCLC CELLS.	91
CHAPTER 4: INTERACTION OF FED6 WITH ABC TRANSPORTERS	94
4.1 PHYSICO-CHEMICAL PROPERTIES OF COMPOUNDS CAN HELP PREDICT ABC TRANSPORTER SUBSTRATE SPECIFICITY.	95
4.2 TESTING FOR ABCB1, ABCG2, ABCC1 SUBSTRATE SPECIFICITY.	96
4.2.1 SUBSTRATE SPECIFICITY FOR ABCB1	96
4.2.2 SUBSTRATE SPECIFICITY FOR ABCG2.....	101
4.2.3 SUBSTRATE SPECIFICITY FOR ABCC1	104
4.2.4 ABC TRANSPORTERS AND UPTAKE OF [¹⁸ F]FED6 <i>IN VITRO</i>	106
4.2.5 CACO2 CELL PERMEABILITY ASSAY.	107
4.3 IMPACT OF ABC TRANSPORTER SUBSTRATE SPECIFICITY OF FED6 FOR IMAGING EGFR.	109
4.3.1 LEVELS OF ABC TRANSPORTERS ACROSS A PANEL OF CELL LINES.....	109
4.3.2 OVERCOMING ABCG2 EFFLUX.	110
4.3.2.1 <i>Inhibition of ABCG2 in MCF7MX cells.</i>	110
4.3.2.2 <i>Inhibition of ABCG2 in A431 cells in vitro and in vivo</i>	115
4.4 INVESTIGATION OF AN ALTERNATIVE CYANOQUINOLINE MOLECULE	121
4.4.1 AFFINITY OF FED20 FOR EGFR.....	121
4.4.2 SPECIFICITY OF FED20 FOR EGFR	123
4.4.3 SUBSTRATE SPECIFICITY OF FED20 FOR THE ABC TRANSPORTERS.	124
4.4.4 FED20 IN THE CONTEXT OF MUTANT EGFR IN NSCLC	126
CHAPTER 5: MONITORING RESPONSE TO GEFITINIB TREATMENT IN NSCLC	131
5.1 CHOLINE KINASE ALPHA AS A BIOMARKER OF RESPONSE TO GEFITINIB	132
5.1.1 <i>IN VITRO</i> ASSESSMENT OF CHOLINE KINASE ALPHA AS A BIOMARKER OF RESPONSE TO GEFITINIB TREATMENT IN PC9 AND PC9ER CELLS.....	132
5.1.1.1 <i>Cell cycle profile following 6, 24 and 48 h gefitinib treatment.</i>	133
5.1.1.2 <i>Apoptosis levels following 6, 24 and 48 h gefitinib treatment.</i>	136
5.1.1.3 <i>Changes to ChKα protein expression following 6, 24 and 48 h gefitinib treatment.</i>	137
5.1.1.4 <i>Levels of ChKα mRNA following 6, 24 and 48 h gefitinib treatment.</i>	140
5.1.1.5 [³ H]choline uptake following 6, 24 and 48 h gefitinib treatment.	141
5.1.2 <i>IN VIVO</i> [¹⁸ F]D4CHOLINE UPTAKE IN PC9 AND PC9ER XENOGRAFTS.	145
5.1.3 INVESTIGATING THE EGFR-CHKA-SRC COMPLEX.	150
5.1.3.1 <i>Changes in protein expression, [³H]choline uptake and apoptosis following 1, 6 and 24 h gefitinib treatment.</i>	151
5.1.3.2 <i>Changes in protein expression, [³H]choline uptake and apoptosis following 1, 6 and 24 h dasatinib treatment.</i>	156
5.1.3.3 <i>siRNA knock down of EGFR or SRC.</i>	160
5.2. OTHER CLINICALLY AVAILABLE TRACERS AND THEIR ROLE FOR IMAGING EARLY RESPONSE TO GEFITINIB TREATMENT.	162
5.2.1 [¹⁸ F]FDG.....	162

5.2.1.1 <i>In vitro</i> assessment of the role of [¹⁸ F]FDG as a biomarker of response to gefitinib treatment.	162
5.2.1.2 <i>In vivo</i> uptake of [¹⁸ F]FDG in PC9 and PC9ER xenograft.....	163
5.2.2 [¹⁸ F]FLT.....	167
5.2.2.1 <i>In vitro</i> assessment of the role of [¹⁸ F]FLT as a biomarker of response to gefitinib treatment.....	167
5.2.2.2 <i>In vivo</i> uptake of [¹⁸ F]FLT in PC9 and PC9ER xenograft.....	168
CHAPTER 6: DISCUSSION	175
6.1 IMAGING MUTANT EGFR	176
6.2 FED6 SUBSTRATE SPECIFICITY FOR THE ABC TRANSPORTERS.	178
6.2.1 FED6 IS A SUBSTRATE FOR ABCB1 AND ABCG2.....	179
6.2.2 OVERCOMING ABCG2 EFFLUX OF FED6.....	180
6.2.3 INVESTIGATION OF AN ALTERNATIVE CYANOQUINOLINE MOLECULE: FED20.....	182
6.3 CHKA AS A BIOMARKER OF RESPONSE TO GEFITINIB TREATMENT.	184
6.3.1 <i>IN VITRO</i> ASSESSMENT OF CHKA AS A BIOMARKER OF RESPONSE TO GEFITINIB TREATMENT IN PC9 AND PC9ER CELLS.....	185
6.3.2 ROLE OF SRC AND EGFR ACTIVITY ON CHKA ACTIVITY.....	186
6.3.3 <i>IN VIVO</i> [¹⁸ F]D4 CHOLINE UPTAKE IN PC9 AND PC9ER XENOGRAPHS.....	187
6.4 [¹⁸F]FDG AND [¹⁸F]FLT PET IMAGING OF RESPONSE TO GEFITINIB TREATMENT IN COMPARISON TO [¹⁸F]D4CHOLINE.	188
REFERENCES.....	190
APPENDIX.....	208

List of tables

Table 1: Summary of the outcome of first line TKI vs chemotherapy phase III clinical trials in patients expressing active mutant EGFR advanced NSCLC	28
Table 2: Summary of imaging modalities used pre-clinically and clinically.	36
Table 3: Methods for assessing EGFR.	37
Table 4: Radioisotopes used in PET imaging.	38
Table 5: Summary of cell lines used.	63
Table 6: List of Dharmacon ON TARGET plus- SMARTpool siRNA used.....	64
Table 7: Primers used for Q-PCR.....	66
Table 8: Source and working dilutions of antibodies used.....	68
Table 9: Physico-chemical properties of the FED series in relation to prediction of ABC transporter substrate specificity	96
Table 10: Growth inhibitory effect associated with the series of cyanoquinoline molecules in 3T3 and 3T3-MDR1 cells.	100
Table 11: Growth inhibitory effect associated with the series of cyanoquinoline molecules in MCF7 and MCF7MX cells.	102
Table 12: Growth inhibitory effect associated with the series of cyanoquinoline molecules in A549 and A549 cells treated with MK-571.....	105
Table 13: Physico-chemical properties of FED20.	122
Table 14: GI ₅₀ of gefitinib in PC9 and PC9ER cells.....	133
Table 15: GI ₅₀ values of PC9 and PC9ER cells treated with gefitinib for 72 h.	151
Table 16: GI ₅₀ values of PC9 and PC9ER cells treated with dasatinib for 72 h.....	156

List of figures

Figure 1: EGFR schematic structure.	19
Figure 2: EGFR phosphorylation and signal transduction.....	21
Figure 3: Summary of mutations of EGFR in NSCLC.	24
Figure 4: Covalent bond formation via Michael acceptor	31
Figure 5: Epidermal growth factor receptor tyrosine kinase inhibitor structures.	33
Figure 6: Principles of PET imaging.	39
Figure 7: Principles of [¹⁸ F]FDG and [¹⁸ F]FLT metabolism.	41
Figure 8: PET image of [¹⁸ F]-PEG6-IPQA in mouse xenografts.....	45
Figure 9: Radiolabelled irreversible inhibitors of EGFR.	47
Figure 10: Kennedy pathway.	52
Figure 11: Schematic of ChKα and metabolic control.	54
Figure 12: Topological and hypothetical schematic of typical ABC transporter in cellular membrane.	56
Figure 13: Diagram illustrating the overlapping substrate specificity for ABCB1, ABCG2 and ABCC1 transporters of a variety of drugs.	58
Figure 14: Schematic of transwell and transporter localisation on a Caco2 cell.	71
Figure 15: Schematic of phosphocholine extraction.	76
Figure 16: Schematic of drug treatments before PET scan	78
Figure 17: <i>In vitro</i> uptake of [¹⁸ F]FED6 following EGFR siRNA treatment.....	83
Figure 18: Inhibition of EGFR activation in WT and del 746-750 mutant EGFR expressing cells following gefitinib and FED6 treatment.	85
Figure 19: <i>In vitro</i> uptake of [¹⁸ F]FED6 in H1650, H358 and A549 cells.....	86
Figure 20: <i>In vivo</i> PET imaging of A549 and H1650 xenografts with [¹⁸ F]FED6.	88
Figure 21: p-EGFR and EGFR levels of A549 and H1650 tumours.....	89
Figure 22: Inhibition of EGFR activation in NSCLC following gefitinib and FED6 treatment.	90
Figure 23: <i>In vitro</i> uptake of [¹⁸ F]FED6 in NSCLC.	91
Figure 24: Correlation between [¹⁸ F]FED6 uptake, EGFR protein expression and FED6 IC ₅₀	92
Figure 25: ABCB1 protein expression in 3T3 and 3T3-MDR1.	97
Figure 26: Calcein fluorescence in 3T3 and 3T3-MDR1 cells following zosuquidar treatment.....	98
Figure 27: Cell viability curves showing reversal of resistance to vinblastine in 3T3-MDR1 following zosuquidar treatment.	99
Figure 28: Impact of zosuquidar on the cytotoxicity of cyanoquinoline derivatives.	100
Figure 29: Protein expression of ABCG2 in MCF7 and MCF7MX.	101
Figure 30: Cell viability assays showing reversal of resistance to mitoxantrone in MCF7MX following FTC treatment.	102
Figure 31. Impact of FTC on the cytotoxicity of cyanoquinoline derivatives.	103
Figure 32: Calcein fluorescence in A549 cells following MK-571 treatment.	104
Figure 33: Cell viability assays in A549 cells with and without pre-treatment with ABCC1 inhibitor MK-571.	105
Figure 34: Impact of MK-571 on the cytotoxicity of cyanoquinolines derivatives in A549 cells.....	106
Figure 35: [¹⁸ F]FED6 uptake in ABC transporter expressing cells.	107
Figure 36: Active efflux of cyanoquinoline derivatives across Caco2 cells.	108

Figure 37: Efflux ratio of cyanoquinoline compounds in the presence of ABC transporter inhibitors.	109
Figure 38: mRNA and protein expression of ABCB1 and ABCG2 in cell lines studied.	110
Figure 39: Hoechst 33324 uptake in MCF7 and MCF7MX cells following FTC or gefitinib pre-treatment.	112
Figure 40: Hoechst 33324 uptake in MCF7MX and MCF7 following siRNA and drug inhibition of ABCG2.	113
Figure 41: ABCG2 knock down in MCF7MX cells.	114
Figure 42: [¹⁸ F] FED6 uptake in MCF7MX cells following ABCG2 knock down or drug inhibition.	115
Figure 43: Hoechst 33324 uptake in A431 cells following ABCG2 siRNA transfection and drug treatment.	116
Figure 44: ABCG2 knock down in A431 cells.	117
Figure 45: [¹⁸ F]FED6 uptake in A431 cells following inhibition of ABCG2.	118
Figure 46: <i>In vivo</i> uptake of [¹⁸ F]FED6 in A431 xenograft after gefitinib pre-treatment.	120
Figure 47: p-EGFR and EGFR protein expression of A431 tumours following gefitinib treatment.	121
Figure 48: Inhibition of p-EGFR <i>via</i> FED20.	122
Figure 49: [¹⁸ F]FED20 uptake in high vs low EGFR expressing cells.	124
Figure 50: Efflux ratio of FED20 in Caco2 cells with and without pre-treatment with verapamil.	125
Figure 51: [¹⁸ F]FED20 uptake in ABC transporter expressing cells.	125
Figure 52: Differential FED20 inhibition of p-EGFR in NSCLC cell lines expressing mutant or wild type EGFR.	127
Figure 53: Differential uptake of [¹⁸ F]FED20 in active and resistant mutant EGFR.	128
Figure 54: Correlation between [¹⁸ F]FED20 uptake, EGFR protein expression and FED20 IC ₅₀ status.	129
Figure 55: Cell cycle profile of PC9 or PC9ER cells following 6, 24 and 48 h gefitinib treatment.	135
Figure 56: Apoptosis levels in PC9 and PC9ER cells following 6, 24 and 48 h gefitinib treatment.	137
Figure 57: Changes in choline kinase alpha protein expression following 6, 24 and 48 h gefitinib treatment in PC9 and PC9ER cells.	139
Figure 58: Changes to ChKα mRNA levels following 6, 24 and 48 h gefitinib treatment.	140
Figure 59: Whole cell [³ H]choline uptake in PC9 and PC9ER cells following 6, 24 and 48 h gefitinib treatment.	142
Figure 60: [³ H]phosphocholine levels in PC9 and PC9ER cells following 6, 24 and 48 h gefitinib treatment.	144
Figure 61: [¹⁸ F]D4choline PET imaging of PC9 and PC9ER xenografts following 48 h gefitinib treatment.	146
Figure 62: Tumour uptake parameters from [¹⁸ F]D4choline PET imaging of PC9 and PC9ER xenografts following 48 h gefitinib or vehicle treatment.	148
Figure 63: Representative immunohistochemistry analysis of PC9 and PC9ER tumour samples from [¹⁸ F]D4choline PET imaging.	149
Figure 64: Protein expression analysis from PC9 and PC9ER tumour lysates following [¹⁸ F]D4choline PET imaging.	150
Figure 65: Effect of 1, 6 and 24 h gefitinib treatment on protein expression in PC9 and PC9ER cells.	152
Figure 66: Changes in ChKα activity following 1, 6 and 24 h treatment with gefitinib.	154
Figure 67: Effect of 1, 6 and 24 h gefitinib treatment on apoptosis in PC9 and PC9ER cells.	155

Figure 68: Effect of 1, 6 and 24 h dasatinib treatment on protein expression in PC9 and PC9ER cells.	157
Figure 69: Changes in ChK α activity in PC9 and PC9ER cells following 1, 6 and 24 h dasatinib treatment.....	158
Figure 70: Apoptosis levels in PC9 and PC9ER cells following 1, 6 and 24 h dasatinib treatment.	159
Figure 71: [^3H]choline uptake following SRC and EGFR siRNA transfection of PC9 and PC9ER cells.	161
Figure 72: [^{18}F]FDG uptake in PC9 and PC9ER cells following gefitinib treatment for 1, 6 and 24 h.	162
Figure 73: [^{18}F]FDG PET imaging of PC9 and PC9ER xenografts following 48 h gefitinib treatment..	164
Figure 74: Tumour uptake parameters from [^{18}F]FDG PET imaging of PC9 and PC9ER xenografts following 48 h gefitinib treatment.	165
Figure 75: PC9 and PC9ER tumour lysate protein expression analysis from [^{18}F]FDG PET imaging...	166
Figure 76: [^{18}F]FLT uptake in PC9 and PC9ER cells following 48 h gefitinib treatment.....	167
Figure 77: [^{18}F]FLT PET imaging of PC9 and PC9ER xenografts following 48h gefitinib treatment. ...	170
Figure 78: Tumour uptake parameters from [^{18}F]FLT PET imaging of PC9 and PC9ER xenografts following 48 h gefitinib treatment.	171
Figure 79: PC9 and PC9ER tumour lysate protein expression analysis from [^{18}F]FLT PET imaging....	173

Abbreviations

ABC: ATP binding cassette
AKT: Protein kinase B
ALK: Anaplastic lymphoma kinase
BSA: Bovine serum albumin
ChK α : Choline kinase alpha
DAG: Diacylglycerol
EGFR: Epidermal growth factor receptor
EML4: Echinoderm microtubule associated protein 4
ERK: Extracellular signal-regulated kinase
FDA: Food and Drug Administration
FDG: Fluorodeoxyglucose
FED6: (2E)-N-{4-[(3-chloro-4-fluorophenyl)amino]-3-cyano-7-ethoxyquinolin-6-yl}-4-[[{1-(2-fluoroethyl)-1H-1,2,3-triazol-4-yl)methyl}amino]but-2-enamide
FED20: (2E)-N-{4-[(3-chloro-4-fluorophenyl)amino]-3-cyano-7-ethoxyquinolin-6-yl}-4-[[{1-[(2R,5S)-3-fluoro-4,5-dihydroxy-6-(hydroxymethyl)oxan-2-yl]-1H-1,2,3-triazol-4-yl)methyl}amino]but-2-enamide
FISH: Fluorescence in situ hybridization
FLT: 3' deoxy-3' Fluorothymidine
FRT: Fractional retention of the tracer
FTC: Fumitremorgin C
GLUT: Glucose transporter
H&E: Haematoxylin and eosin
HBSS: Hank's balanced salt solution
HER: Human Epidermal growth factor receptor
HPLC: High protein linked chromatography
ID: Injected dose
IHC: Immunohistochemistry
JAK: Janus kinase
KRAS: Kirsten rat sarcoma viral oncogene
mAb: Monoclonal antibody
MAPK: Mitogen activated protein kinase
MDR: Multi drug resistance
MEK: MAP/extracellular signalling
MET: Hepatocyte growth factor receptor
MRS: Magnetic resonance spectroscopy
m-TOR: mammalian target of rapamycin
NSCLC: Non small cell lung carcinoma
ORR: Objective response rate
OS: Overall survival
PBS: Phosphate buffer saline
PET: Positron Emission Tomography
PFS: Progression free survival
Pgp: Permeability glycoprotein
PI: Propidium iodide
PIP2: Phosphatidylinositol 4,5-bisphosphate
PIP3: Phosphatidylinositol (3,4,5)-triphosphate
PI3K: Phosphatidylinositol-3-kinase
PSA: Polar surface area
PTEN: Phosphatase and tensin homolog

PTK: Protein tyrosine kinase
RD: Refractory disease
RECIST: Response evaluation criteria in solid tumours
SRB: Sulforhodamine B
SRC: Sarcoma
STAT: Signal transducer and activator of transcription
TAC: Time activity curve
TBST: Tris-buffered saline and tween 20
TGF α : Transforming growth factor alpha
TK1: Thymidine kinase
TKI: Tyrosine kinase inhibitor
WT: Wild type

Chapter 1: Introduction

1.1 Epidermal growth factor receptor

1.1.1. Member of the human epidermal growth factor receptor (HER) family.

The epidermal growth factor receptor (EGFR) is a 170 kDA transmembrane tyrosine kinase receptor. It is a member of the HER family; also referred to as ERbB family of receptors, which includes HER2 (ERbB2), HER3 (ERbB3) and HER4 (ERbB4) (Yarden and Sliwkowski, 2001). EGFR is formed of several domains, which are depicted in Figure 1. The ligand binding occurs between domains I and III. Domains II and IV are cysteine rich and domain II plays an important role in the dimerisation of the EGFR. Indeed, a loop from domain II interacts with domain II of the dimerising receptor (Ogiso et al., 2002).

The kinase domain, which contains the ATP binding pocket, shares a strong sequence similarity with other members of the tyrosine kinase receptor family. Finally, the C-terminal domain is rich in tyrosine residues which become phosphorylated upon activation of the receptor and direct the signal transduction of the EGFR (Jorissen et al., 2003).

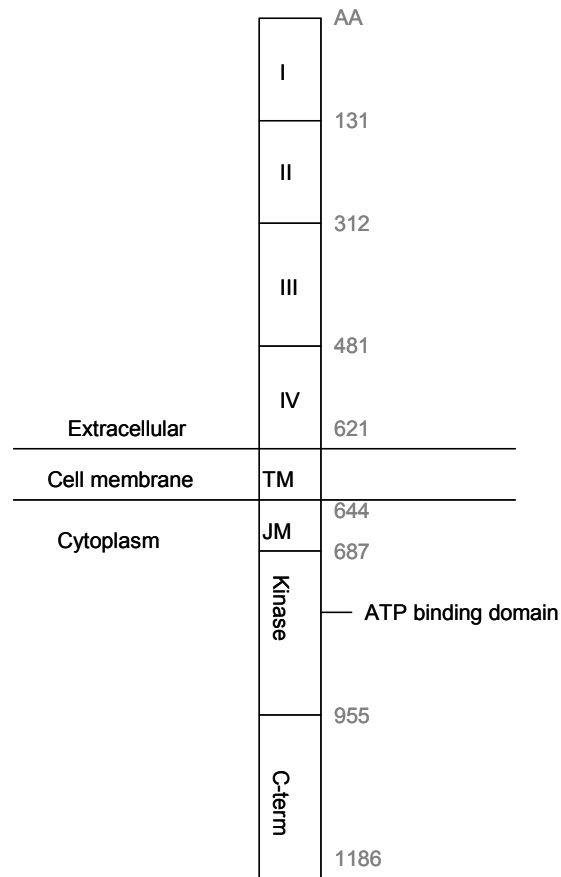


Figure 1: EGFR schematic structure.

Adapted from (Jorissen et al., 2003) AA: Amino acid I: Ligand binding domain 1, II: Cysteine rich domain 1, III: Ligand binding domain 2, IV: Cysteine rich domain 2, TM: Transmembrane domain, JM Juxtamembrane domain, c-term: Carboxy terminal domain.

1.1.2. EGFR activation and signal transduction

Ligands for the epidermal growth factor receptor contain an EGF-like domain along with three intramolecular disulphide bonds. These ligands are found as precursor proteins within the cell membrane and are converted to their active forms through proteolysis. Ligands include EGF, epiregulin, neuregulin, transforming growth factor α (TGF α) and betacellulin (Prenzel et al., 2001). Following ligand binding the receptor undergoes a conformational change and homo- or heterodimerises with another receptor from the ERB family of receptors. HER1-HER2 heterodimers are favourable and lead to the strongest biological signals. The receptor dimerisation leads to autophosphorylation at specific tyrosine residues within the intracellular region of EGFR (Yarden and Sliwkowski, 2001). A given adapter protein will bind to a specific phosphorylated tyrosine residue within the c-terminal domain of EGFR, as depicted in Figure 2. For example the tyrosine 1068

(Y1068) is the docking site for the adaptor protein Grb2 (Sebastian et al., 2006). The docking of Grb2 forms the beginning of the mitogen-activated protein kinase (MAPK) intracellular signal transduction pathway. A series of phosphorylation's leads to the activation of extracellular signal-regulated kinase (ERK) protein, which in turn activates transcription factor ELK and c-fos. These transcription factors regulate the expression of genes involved in cell proliferation, including cyclin D cell cycle protein. Thus, the activation of the MAPK pathway through EGFR leads to an increase in mitosis (Yarden and Sliwkowski, 2001).

Activated EGFR initiates many signal transduction pathways, (including: Janus kinase (JAK)/ Signal transducer and activator of transcription (STAT), Phosphatidylinositide 3-kinases (PI3K)/ protein kinase B (AKT)), which are involved in several aspects of cellular function including: proliferation, angiogenesis, cell adhesion and migration (Burgess, 2008). More recently it has been shown that EGFR dimerisation with HER3 also plays an important role in the regulation of cell proliferation by activating MAPK and PI3K/AKT pathways (Choi et al., 2012).

The complexity of the EGFR signalling network is accentuated further by the tight link and modulation of this network by other signalling pathways within the cell, for example, *via* active G-protein coupled receptors (Yarden and Sliwkowski, 2001).

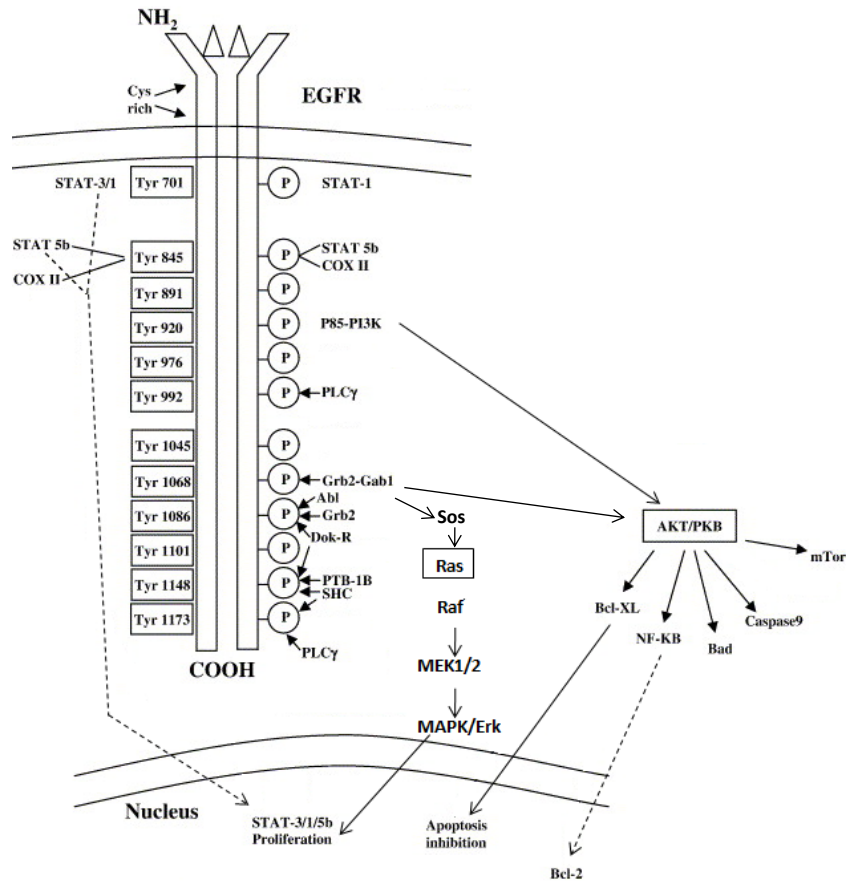


Figure 2: EGFR phosphorylation and signal transduction.

Following EGFR activation, several tyrosine residues can become phosphorylated. Secondary messengers including Grb2, Src binds to these phosphorylated residues and will initiate the intracellular signal transduction resulting in changes to proliferation, apoptosis and cell cycle progression (Sebastian et al., 2006, Felip and Rosell, 2006).

1.2 EGFR and cancer

The complex network of signal transduction pathways, which are affected by EGFR, explain the involvement of this tyrosine kinase receptor in different mechanisms of cancer. Indeed, modification to this receptor leads to not only an increase in proliferation but also a decrease in apoptosis and an increase in angiogenesis (Hynes and Lane, 2005, Sharma et al., 2007).

The involvement of EGFR in the development of cancer was first made from the study of viral oncogenes. It was found that EGFR is a homolog of the avian erythroblastosis virus (v-erb) oncogene (Downward et al., 1984b) and it was later demonstrated that cells in culture in which EGFR was overexpressed underwent malignant transformation (Di Fiore et al., 1987).

1.2.1 EGFR's involvement in many types of cancer

Since the first link between EGFR and cancer development was made, this receptor has been shown to be involved in a multitude of cancers. The involvement of EGFR in cancer development and progression can be the result of different factors including; gene amplification leading to overexpression of EGFR and increased activation of EGFR caused by activating mutations (Sebastian et al., 2006). However, it is the overexpression of EGFR, which has been the most reported. In a pathological setting, the number of EGFR molecules expressed per cell can increase to over a million from twenty to two hundred thousand in a physiological setting (Rowinsky, 2004). Abnormal expression of EGFR has been observed in head and neck, breast, uterus, oesophageal, pancreatic, non small cell lung carcinoma (NSCLC), prostate, colon, ovarian, bladder, brain and gastric cancer (Salomon et al., 1995). The percentage of tumours that overexpress EGFR differs greatly from cancer to cancer. For example, between 90 and 95 % of head and neck tumours overexpress EGFR, whereas changes in EGFR expression are only seen in 4 to 33 % of gastric tumours (Sebastian et al., 2006). EGFR overexpression has been shown to be linked to tumour initiation in glioma (Mazzoleni et al., 2010). Nicholson *et al* carried out a meta-analysis study in which they looked into over 200 studies and investigated the correlation between EGFR and cancer prognosis. They found that EGFR overexpression leads to increased aggressiveness of disease in head and neck, ovarian, cervical, bladder and oesophageal cancer (Nicholson et al., 2001). In contrast to this, they found a modest correlation between EGFR overexpression and disease outcome prediction in gastric, breast and colorectal cancer. Finally, in NSCLC only 3 out of the 10 studies they reviewed showed a relationship between EGFR overexpression and patient outcome prediction (Nicholson et al., 2001). Despite these differences of prevalence of EGFR overexpression in different cancers, overall, there was a strong correlation between high levels of EGFR expression and metastasis potential and later stage disease diagnosis (Sebastian et al., 2006).

1.2.2 EGFR gene amplification

Amplification of the gene coding for *EGFR* is one of the main events that leads to overexpression of EGFR. *EGFR* gene amplification is found in NSCLC, glioma, colorectal and bladder cancer (Rowinsky, 2004). It is also interesting to note that a correlation between EGFR gene copy number and tumour grade has been observed in cancers such as colorectal and bladder, while in other cancers including NSCLC no link between *EGFR* copy number and severity of disease have been found (Rowinsky, 2004).

1.2.3 EGFR Mutations

In addition to looking at changes in the expression of EGFR, investigation into EGFR mutations in human cancers has been carried out. EGFR mutations are highly prevalent in glioblastoma where *EGFR* gene rearrangement, which leads to mutant EGFR, is present in 63 to 75 % of patients. These gene rearrangements result in deletions of large sections of the *EGFR* gene. The most prevalent deletion mutation in glioblastoma involves the loss of exons 2 to 7 of the *EGFR* gene, which encode for the extracellular ligand binding domain of the receptor. The EGFRvIII mutant, which results from this in frame deletion, is constitutively active and no longer requires ligand binding for its activation (Gan et al., 2009).

Another mutation seen in glioblastoma, involves the deletion of the exons that encode the carboxyl terminal domain of EGFR, resulting in the EGFRIV mutant. A recent study has brought clarity to the mechanism of tumourgenicity of this mutant including the importance of the intrinsic tyrosine kinase activity and a role for the HSP90 chaperone (Pines et al., 2010).

The other cancer in which EGFR mutations have been extensively investigated is lung cancer, and will be reviewed below.

- Mutations involved in NSCLC

There are two forms of lung cancer, small cell lung carcinoma (SCLC) and NSCLC. NSCLC represents over 85 % of cases of lung cancer. NSCLC is characterised by modifications to a number of genes including, p53 mutation, kirsten rat sarcoma viral oncogene (KRAS) mutation, HER2 mutation, hepatocyte growth factor receptor (MET) mutation and amplification, anaplastic lymphoma kinase-echinoderm microtubule- associated protein 4 (ALK-EML4) fusion, as well as EGFR mutation, the latter will be discussed in the following paragraph (Herbst et al., 2008).

The mutational status of EGFR has been extensively studied in NSCLC and this mainly came from a surge in translational research in this field from 2004, in a bid to increase the efficacy of TKI therapy by selecting a responding group of patients. A number of different mutations in the *EGFR* gene have been recorded from studies involving NSCLC patients. The majority of these mutations affect regions of the gene, which encode for the tyrosine kinase domain (exons 18 to 21) (Gazdar, 2009). These mutations can be divided into different classes: single nucleotide substitutions, in frame deletions and insertions, as depicted in Figure 3.

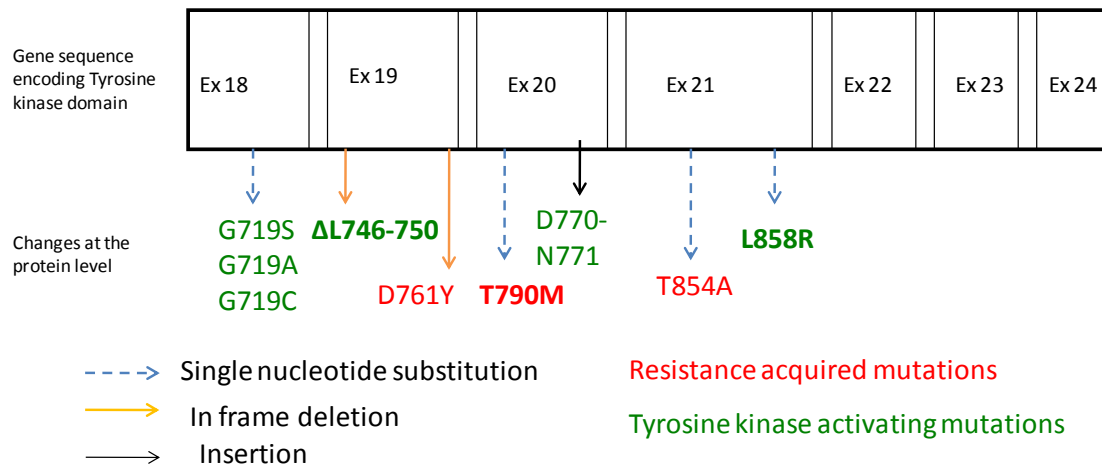


Figure 3: Summary of mutations of EGFR in NSCLC.

Mutations to the tyrosine kinase coding domain of EGFR can be classed as activating (indicated in green) or resistant (indicated in red) mutations. Adapted from (Mishani et al., 2008)

The frequency of mutations in the *EGFR* recorded in NSCLC patients has been found to range between 10 to 33 % (Pao and Miller, 2005, Dahabreh et al., 2010, Riely et al., 2006). In certain subtypes of NSCLC this value can be much higher with *EGFR* mutations identified in up to 44 % of adenocarcinoma patients, and the highest frequency of these somatic mutations are recorded in female patients that have no previous history of smoking and patients of Asian origin (Kosaka et al., 2004, Pao and Miller, 2005, Tanaka et al., 2010). The most frequent mutation, recorded in over 44 % of cases of EGFR mutations, involves an in frame deletion in exon 19, these deletions can vary in location and length but in the majority of cases result in the deletion of the tripeptide leucine 747, arginine 748 and glutamic acid 749 (Gazdar, 2009). The second most frequent mutation, occurring in over 40 % of cases, is the single nucleotide substitution which results in the leucine at position 858 being replaced by an arginine amino acid (L858R) (Sharma et al., 2007).

The mutations mentioned above, which occur within the tyrosine kinase domain of EGFR are classed as activating mutations. They have been shown to lead to an increased kinase activity of the receptor. EGFR molecules that contain an activating mutation, notably the leucine 858 to arginine mutation, showed a reduced affinity for ATP as measured by a higher K_m value for ATP (Carey et al., 2006, Yun et al., 2007).

The characteristics of mutant EGFR molecules have further been investigated using X ray crystallography data of both WT and mutant EGFR. The increase in activity of mutant EGFR is thought to originate from changes to the homeostasis between the inactive and active form of the receptor. The leucine residue 858 of EGFR lies within the P activation loop, and forms part of a

hydrophobic cluster of amino acids, which are involved in stabilising the molecule in an inactive conformation, by blocking the interaction with the activating part of the C helix (Yun et al., 2007). The X ray crystallography structure of the L858R mutant shows that the arginine residue causes a destabilisation of this “auto-inhibited” inactive conformation, leading to a constitutively active EGFR (Kumar et al., 2008).

Alongside the two most frequent mutations mentioned above, there are other rare mutations, which occur in under 1 % of NSCLC cases. These include point mutations in exon 20 of the *EGFR* gene. (Gazdar, 2009). The identification of mutant EGFR is very important as the different properties of these molecules often translate into differences in targeted drug response.

1.3 EGFR targeted cancer therapies

The involvement of EGFR in a broad range of cancers along with the central role it plays in many pathways of cell activity (Figure 2), including promoting proliferation, and inhibiting apoptosis, makes it an important target for cancer therapy. Two different approaches have been taken. The first involves inhibiting the binding of ligands to EGFR at the extracellular level, while the second approach consists of targeting the intracellular tyrosine kinase domain of EGFR.

1.3.1 Antibody based compounds

The first method for targeting EGFR involves the inhibition of ligand binding to EGFR by targeting the receptor with monoclonal antibodies (mAb). Cetuximab (Merck), a chimeric mouse-human monoclonal antibody was approved in 2004 by the food and drug administration (FDA) for use in treatment of colorectal cancer and in 2006 received approval for head and neck cancer (Mendelsohn and Baselga, 2006). Another mAb targeting EGFR is panitumumab. It was approved by the FDA in 2006, for metastatic colorectal cancer, following a successful clinical trial that showed progression free survival (PFS) of 96 days in patients receiving panitumumab compared to 60 days in patients receiving best standard of care. (Van Cutsem et al., 2007). A host of antibody fragments have also been developed and tested in animal models but have yet to make it to the clinic (Lammerts van Bueren et al., 2008, Friedman et al., 2008).

1.3.2 Small molecular TKIs: first generation, erlotinib and gefitinib

The second approach for targeting EGFR involves the use of small molecular TKIs. The first generation of these drugs include two molecules that are currently in clinical use in NSCLC, these are gefitinib and erlotinib. Both these compounds are defined as reversible TKIs due to the non-covalent

nature of their binding to EGFR. They showed good *in vitro* profiles with high selectivity and affinity for EGFR (Barker et al., 2001, Moyer et al., 1997). Phase I clinical trials demonstrated good tolerability of both drugs and phase II trials showed activity of the inhibitors as measured by objective response or disease control compared to chemotherapy which was given as standard of care (Swaisland et al., 2001, Fukuoka et al., 2003). This led to further investigation in phase III trials. However, several Phase III trials did not meet their outcomes with any improvement in overall survival compared to standard of care (Giaccone et al., 2004, Thatcher et al., 2005). This low level of response, to TKI treatment, in the majority of patients was contrasted by a strong and rapid response of a subgroup of patients (Lynch et al., 2004). Through translational work and retrospective studies, profiling the EGFR status of responders *versus* non-responders, it was established that patients who had active mutant forms of EGFR showed significantly higher response rates to gefitinib or erlotinib (Paez et al., 2004). In later clinical trials, in which patient selection was undertaken, response rates were greatly increased (Kris et al., 2003). The breakthrough trial in regards to EGFR mutational status and response to gefitinib was the iressa pan-Asia-study (IPASS), which compared gefitinib to carboplatin + paclitaxel in a first line treatment setting in NSCLC Asian patients (Mok et al., 2009). The primary end point of this trial was progression free survival. The authors showed that patients with EGFR activation mutations had a significantly higher PFS in the gefitinib arm compared to carboplatin + paclitaxel, while patients who were EGFR mutant negative showed lower PFS compared to carboplatin + paclitaxel. Furthermore, patients harbouring EGFR activation mutations had an objective response of 71.2 % in the gefitinib arm compared to 47.3 % in the carboplatin-paclitaxel arm. This was one of the first indications for the superiority of gefitinib treatment vs classical chemotherapeutics in adenocarcinoma patients, who possess mutant EGFR (Mok et al., 2009).

Since then, several randomised phase III trials have been carried out, comparing EGFR-TKI and chemotherapy in NSCLC patients that express active mutant EGFR. The results of these trials are summarised in Table 1. A common feature of all these trials was a higher objective response rate and higher PFS in the gefitinib treated arms compared to the chemotherapy arms. In addition, the overall survival was not improved in the TKI treated groups (Mok et al., 2009, Mitsudomi et al., 2010, A. Inoue, 2012, Rosell et al., 2012, Han et al., 2012). One explanation for this is the confounding effect of subsequent therapies once the studies had finished. Indeed, a large proportion of patients in the chemotherapy arm subsequently went on to receive TKI treatment. This proportion ranged from 59.3 % in the WJTOG3405 trial (Tetsuya Mitsudomi, 2012), to 96 % in the NEJ002 trial (A. Inoue, 2012).

Both gefitinib and erlotinib are currently approved for treatment of advanced NSCLC. In the UK, the national institute for health and care excellence (NICE) approved gefitinib for first line treatment in advanced or metastatic NSCLC in patients harbouring activation mutation in EGFR since July 2010. In addition to this, the FDA approved erlotinib in May 2013 for first line treatment of NSCLC harbouring activation mutant EGFR. Activation mutations have been shown to have both strong sensitivity and specificity as predictive biomarkers of response to TKI treatment. It has also been shown that EGFR mutations are a better predictor of TKI response compared to EGFR expression levels as assessed by methods such as immunohistochemistry and fluorescence *in situ* hybridization (Sholl et al., 2010).

Table 1: Summary of the outcome of first line TKI vs chemotherapy phase III clinical trials in patients expressing active mutant EGFR advanced NSCLC

clinical trial	Author	TKI and chemotherapy	Patient population	ORR(%)	PFS(months)	OS(months)
IPASS	(Mok et al., 2009)	Gefitinib	Asian patients with adenocarcinoma (Pan Asia)	71.2	9.6	21.6
		Carboplatin+ paclitaxel		47.3	6.3	21.9
WJTOG3405	(Mitsudomi et al., 2010, Tetsuya Mitsudomi, 2012)	Gefitinib	EGFR mutation positive Japanese	62.1	9.6	35.5
		Cisplatin+docetaxel		32.1	6.6	38.8
NEJ002	(Maemondo et al., 2010, A. Inoue, 2012)	Gefitinib	EGFR mutation positive japanese	73.7	10.8	27.7
		Carboplatin+Paclitaxel		30.7	5.4	26.6
OPTIMAL	(Zhou et al., 2011a)	Erlotinib	Chinese patients with EGFR activating mutations in Advanced NSCLC	83	13.7	22.69
		Carboplatin+gemcitabine		36	4.6	19.3
EURTAC	(Rosell et al., 2012)	Erlotinib	European NSCLC patients with active mutant EGFR.	58	9.7	19.3
		Platinum based doublets		15	5.2	19.5
SIGNAL	(Han et al., 2012)	Gefitinib	Korean never smokers with NSCL adenocarcinoma	84.6	8	27.2
		Cisplatin + gemcitabine		37.5	6.3	25.6

ORR: Objective response rate OS: overall survival PFS: progression free survival. Adapted from (Rossi et al., 2013)

1.3.3 Resistance to TKI treatment

There are two forms of resistance: Intrinsic resistance also called primary resistance, where resistance to the TKI is present in the patient before the start of TKI therapy, and acquired resistance, which arises following treatment.

1.3.3.1 Intrinsic resistance

In NSCLC exon 20 insertion EGFR mutants confer intrinsic resistance to TKI therapy. Patients harbouring EGFR with D770 (NPG) N771 insertion mutation do not respond to gefitinib treatment (Gazdar, 2009). Other forms of intrinsic resistance result from mutations to genes encoding other proteins within the major signalling pathways occurring in up to 50 % of NSCLC patients. These include KRAS, EML-ALK fusion, HER2 and PIK3CA (Pao and Hutchinson, 2012).

1.3.3.2 Acquired resistance

- T790M EGFR mutation

In 50 % of cases of acquired resistance, a single nucleotide substitution in exon 20 is detected which leads to the exchange of threonine at position 790 of the EGFR to a methionine amino acid (Gazdar, 2009). Two hypotheses as to how this mutation causes resistance to gefitinib treatment have been proposed. The first results from the location of amino acid 790 at the back of the ATP binding pocket of EGFR. This residue is called a “gate keeper residue”. The bulkier nature of methionine compared to threonine was hypothesized by several researchers to cause a steric hindrance blocking the access of gefitinib or erlotinib to the binding site (Pao and Miller, 2005, Kobayashi et al., 2005). However, X-ray crystallography structures of T790M mutant EGFR in lattice with erlotinib, have shown binding to the ATP pocket of the mutant EGFR despite the bulky methionine, suggesting that steric hindrance may not be an explanation for the developed resistance (Yun et al., 2008).

The second hypothesis attributes changes to the affinity of ATP, for the mutated EGFR, for the lack of response to TKI treatment. *In vitro* work on T790M mutant EGFR has shown that the binding affinity of ATP to T790M EGFR is increased compared to that measured in active mutant EGFR. TKIs no longer have higher binding affinity compared with ATP to bind in the pocket and inhibit the tyrosine kinase activity (Yun et al., 2008).

Understanding how and when this mutation occurs is important for early detection and patient selection. Inukai *et al* reported that the T790M mutation was found in a subpopulation of tumour

cells during the development of NSCLC prior to any treatment and that these clones would then be selected during gefitinib treatment (Inukai et al., 2006). A study in which resistance to second generation TKI drugs was developed in mutant T790M EGFR gefitinib resistant cells showed that this double resistance (to gefitinib and 2nd generation TKI) was the result of the amplification of the T790M EGFR encoding allele (Ercan et al., 2010). These results are in line with both *in vitro* and *in vivo* work which has demonstrated that T790M provides cells with a growth advantage (Yoshida et al., 2010). This is an important finding and highlights the need of efficient ways of detecting the presence of this mutation as early as possible.

- Other mechanisms of resistance

Other mechanisms of resistance include less frequent mutations to EGFR including D716Y (Balak et al., 2006) and T854A (Bean et al., 2008).

MET gene amplification is also responsible for resistance to TKI therapy. The role of *MET* gene in TKI resistance first became apparent following *in vitro* work in which the analysis of resistant cell lines, developed following months of exposure to gefitinib, was carried out. The cell lines expressed 5 to 10 times higher levels of *MET* oncogene and regained sensitivity to gefitinib after *MET* inhibition (Engelman et al., 2007). This led to the investigation of *MET* amplification in patient samples where it was found to represent an average of 5 to 10 % of cases of TKI resistance (Bean et al., 2008, Engelman et al., 2007, Kubo et al., 2009, Sequist et al., 2011).

Patients who possess activating mutations in their *KRAS* gene show less response to gefitinib and erlotinib treatment compared to patients who express non mutated *KRAS* (Pao et al., 2005). 15 to 25 % of adenocarcinoma patients have activating *KRAS* mutations that lead to TKI resistance (Massarelli et al., 2007).

It has also been suggested that mutations that result in loss of function of phosphatase and tensin homolog (PTEN) function could be a cause of resistance to gefitinib. This enzyme dephosphorylates Phosphatidylinositol (3,4,5)-triphosphate (PIP3) giving rise to Phosphatidylinositol 4,5-bisphosphate (PIP2). If this function is lost the excess of PIP3 will result in activation of AKT/ mammalian target of rapamycin (mTOR) pathway and this despite inhibition of the tyrosine kinase activity of EGFR by a TKI (Wheeler et al., 2010).

Owing to the onset of resistance in the majority of patients who undergo treatment with reversible TKI agents, a new approach to the inhibition of EGFR is needed. One of the possible ways of

overcoming the acquired resistance discussed above is thought to be achieved by treating patients with second generation also called irreversible TKIs.

1.3.4 Overcoming resistance

1.3.4.1 Second generation of TKI

This second generation of TKIs are characterised by the irreversible nature of their binding to the kinase domain of EGFR. This irreversible binding occurs via a Michael acceptor, an α,β -unsaturated carbonyl moiety, that covalently binds to cysteine 773 of EGFR (Figure 4).

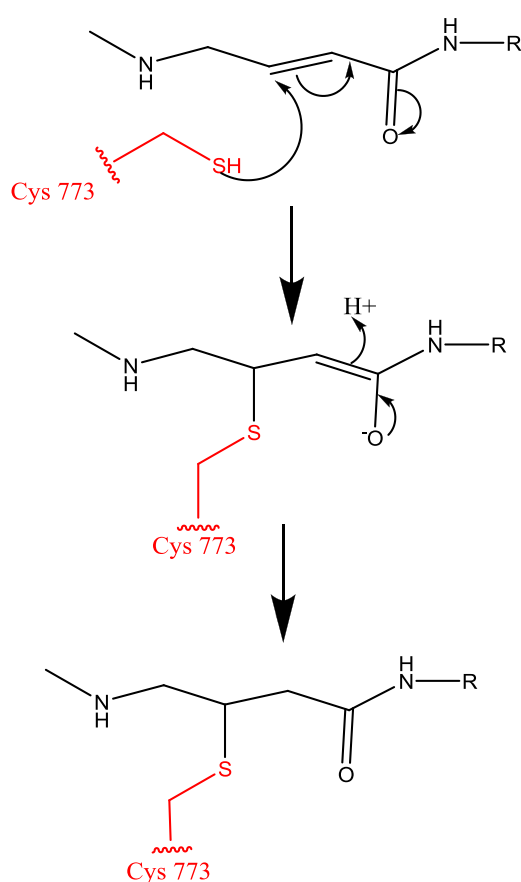


Figure 4: Covalent bond formation via Michael acceptor

Second generation TKI containing a Michael acceptor will form a covalent bond to cysteine 773 in the kinase domain of EGFR as described in this schematic.

The irreversible binding of these compounds leads to a sustained inhibition of EGFR activity in comparison to the reversible inhibitors. Many of the second generation drugs being developed inhibit other dimerisation partners of EGFR such as HER2 leading to a better blockade of EGFR signalling. These molecules have also been reported to overcome the resistance developed following

treatment with reversible TKI's such as erlotinib. Indeed, cell lines expressing resistant mutant EGFR show response to irreversible tyrosine kinase inhibitors (Li et al., 2008). Together it is thought that these drugs will delay or suppress the resistance seen in the clinic with gefitinib and erlotinib. Several of these second generation compounds are currently in clinical trials including EKB-569 and afatinib (BIBW-2992), which are reviewed below.

- EKB-569

EKB-569, pelitinib (Figure 5), was derived from a 6, 7-disubstituted-4-anilinoquinoline-3-carbonitrile core structure by scientists at Wyeth research. It is one of the first irreversible inhibitors of EGFR to be developed and demonstrated increased affinity *in vitro* compared to the 1st generation of TKIs (Wissner et al., 2003). Activity of the compound measured by tumour regression was seen in a Phase I trial in which EKB-569 was administered to NSCLC patients who had developed resistance to gefitinib treatment (Yoshimura et al., 2006). However, no further trials have been planned for EKB-569 as a single agent. Instead, it has been investigated in combination with several "classical" chemotherapeutic treatments (Folprecht et al., 2008, Laheru et al., 2008), and a Phase I trial investigating the combination of m-TOR inhibitor temsirolimus with EKB-569 demonstrated the tolerability of this drug combination (Bryce et al., 2012).

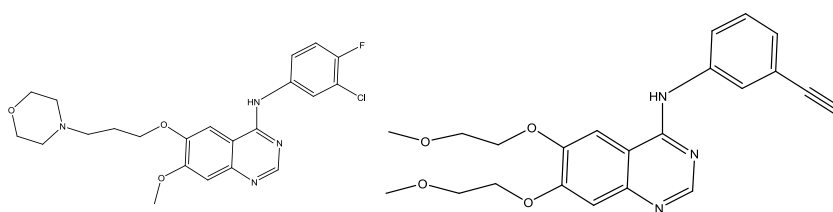
- Afatinib, BIBW2992

Afatinib (Figure 5) is an irreversible inhibitor with activity against, EGFR, HER2 and HER4. Preclinical studies including *in vitro* kinase activity; cellular receptor phosphorylation and *in vivo* activity in xenograft mouse models, demonstrated the potency of this TKI against both WT and mutant EGFR (Li et al., 2008). Furthermore, it was also shown to be active against T790M mutant EGFR harbouring cells, and inhibited the growth of mouse xenografts expressing T790M mutant EGFR (Spicer and Rudman, 2010). This promising preclinical data led to a series of clinical trials, the LUX-lung 1 to LUX-lung 8 trials, which investigated afatinib in first, second, third and fourth line therapy for NSCLC. The results from these trials, some of which are still ongoing, have recently been summarised by Chen *et al* (Chen et al., 2013b). LUX-Lung 3 in which afatinib was given in first line setting gave PFS of 11.1 months for patients receiving afatinib compared to 6.9 months for those on the chemotherapy arm. Due to the small number of patients in the trial, harbouring T790M mutation, LUX-Lung 3 did not allow any conclusions as to the efficacy of afatinib against resistant mutant EGFR to be drawn (C.-H. Yang, 2012). LUX-Lung 7 and 8, which are currently in the recruiting phase, will be two arm studies comparing afatinib in one arm of the study to gefitinib or erlotinib in the other arm. This will allow

direct comparison of this second generation TKI over clinically available gefitinib and erlotinib (Chen et al., 2013b).

Despite the above outcomes, disease progression following afatinib treatment does occur, and thus second generation TKIs do not seem to be spared of the development of acquired resistance. Resistance to second generation TKI has also been reported in *in vitro* studies. Others have demonstrated that irreversible inhibitors such as CL-387,785 can also cause drug resistance (Yamada et al., 2010, Ercan et al., 2010).

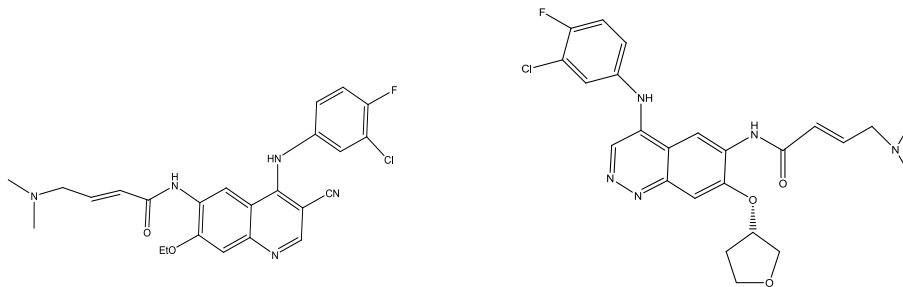
Reversible inhibitors



Gefitinib

Erlotinib

Irreversible inhibitors



EKB-569

Afatinib (BIBW 2992)

Figure 5: Epidermal growth factor receptor tyrosine kinase inhibitor structures.

The irreversible inhibitors, EKB-569 and afatinib contain the Michael acceptor, described above, which allows covalent bonding of these drugs to EGFR. Gefitinib and erlotinib which do not contain a Michael acceptor, bind reversibly to EGFR (Fry, 1999, Eskens et al., 2008).

1.3.4.2 Third generation of TKIs

Finally, drugs, which specifically target T790M mutant form of EGFR, are currently in development. These so called third generation TKIs, are hoped to be a potential therapeutic option for patients that acquire the T790M mutation. The first of these is WZ4002. It showed high levels of selectivity against T790M EGFR compared to WT EGFR as well as inhibitory efficacy in L858R/T790M EGFR

bearing mouse xenograft models (Zhou et al., 2009). The second compound is CO-1686 which is currently undergoing phase I-II dose escalation trial after showing efficacy at inhibiting the activity of T790M mutant EGFR *in vitro* and causing inhibition in growth of H1975 (L858R/T790M) Xenograft (A.O. Walter, 2011).

1.3.4.3 Multitarget TKI and combination studies

New approaches to inhibiting the activity of EGFR are needed due to the emergence of resistance following treatment with first generation TKI's such as gefitinib or erlotinib. One approach reviewed in section 1.3.4.2 is the use of irreversible inhibitors; another approach involves the development of compounds that target more than one type of receptor.

Several small molecular TKIs, currently in development, target other members of the HER family as well as EGFR (e.g. afatinib). EGFR signalling is brought about by receptor homo- or heterodimerisation with HER2, HER3 or HER4. Blocking such interactions is thought to lead to an improved biological effect of EGFR inhibition (Spicer and Rudman, 2010). Secondly, compounds such as ZD6474 (Vandetanib; Astra Zeneca), which target EGFR as well as pro angiogenic receptor VEGFR-2, increase the efficacy of slowing tumour proliferation (Flanigan et al., 2010).

Combination therapy is a further approach, which is taken. A number of clinical trials investigating the efficacy of combining EGFR targeted therapies with radiotherapy or "classic" cytotoxic chemotherapeutics have been and are being carried out (Milano et al., 2008, Nyati et al., 2006).

It is also thought that changes to the scheduling of cancer therapies will be an effective way to overcome the development of resistance and improve treatment outcome. Indeed, rather than waiting for a patient to develop resistance, occurring between 9 to 12 months after the start of therapy in NSCLC patients treated with gefitinib or erlotinib, to change their course of treatment, scheduled breaks in drug administration could prolong the time frame for which the patient responds to a particular therapy (Wheeler et al., 2010). Based on the concurrence of mutation to other proteins it is thought that combination treatment targeting two or more molecules from the same or different pathways could help prevent or overcome resistance. In this regard a study found synergistic effect of afatinib and MEK inhibitor SU11274, resulting in reduction of growth and increased induction of apoptosis (Chen et al., 2013a).

1.4 PET imaging of EGFR

Before describing the principles of PET in more detail it is important to place PET in the context of other available imaging modalities. Table 2 describes several features of the different imaging modalities, which are used pre-clinically and clinically.

Since the major role of EGFR in cancer was identified over 20 years ago several approaches to studying this protein and the gene which encodes it have been taken.

The majority of the techniques approved by the FDA and used in the clinic for diagnosis and prognostic studies are histology based and require tumour biopsies to be carried out. The measure of EGFR gene amplification can be carried out by fluorescence *in situ* hybridization using a gene specific probe. Measuring the expression level of EGFR at the protein level, which may be a better indicator of tumourogenicity, can be assessed by immunohistochemistry using anti EGFR antibodies (Petak et al., 2010, Maheswaran et al., 2008). One of the major drawbacks of the majority of methods listed above is the dependence on tissue biopsies from patients. This demands invasive surgery, which is unpleasant for the patient and depending on the location of the tumour not always a possibility. It is estimated that adequate tissue biopsies may not be possible in 1 out of 5 patients (Cobo et al., 2007). Recent advances in the detection of low frequency cells from blood samples, have allowed the use of circulating cancer cells as a tool to analyse EGFR status without the need to carry out tumour biopsies (Maheswaran et al., 2008, Goto et al., 2012, Akca et al., 2013). This method is still in the experimental stages and further studies involving larger sample sizes will be needed before this method can be validated for routine use. One of the drawbacks of using circulating cancer cells from blood samples is that one cannot distinguish between cells originating from the primary or metastatic lesions. For these reasons, the use of an imaging modality that can probe EGFR *in vivo* is of great interest. The advantages and disadvantages of these different methods have been summarised in Table 3.

Table 2: Summary of imaging modalities used pre-clinically and clinically.

Technique	Resolution	Depth	Time	Quantitative	Imaging agents	Targets	Cost	Clinical use
MRI	10-100 μ m	No limit	Minutes to hours	YES	Paramagnetic chelates, magnetic particles	Anatomical, physiological, molecular	> £200,000	YES
CT	50 μ m	No limit	Minutes	YES	Iodinated molecules	Anatomical, physiological	£60,000 to £200,000	YES
Ultrasound	50 μ m	cm	Seconds to minutes	YES	Microbubbles	Anatomical, physiological	£60,000 to £200,000	YES
PET	1-2 mm	No limit	Minutes to hours	YES	¹⁸ F, ⁶⁴ Cu, ¹¹ C- labelled compounds	Physiological, molecular	> £200,000	YES
SPECT	1-2 mm	No limit	Minutes to hours	YES	⁹⁹ Tc, ¹¹¹ In- labelled compounds	Physiological, molecular	£60,000 to £200,000	YES
Bioluminescence imaging	several mm	cm	Minutes	NO	Luciferins	Molecular	£60,000 to £200,000	NO

MRI: Magnetic resonance imaging, CT: Computerised tomography, PET: Positron emission tomography, SPECT: Single photon emission computed tomography. Adapted from (Weissleder and Pittet, 2008).

Table 3: Methods for assessing EGFR.

	Gene sequencing in circulating cancer cells	Immunohistochemistry	Fluorescence <i>in situ</i> hybridization	PET imaging
Advantages	<ul style="list-style-type: none"> -low cost - non invasive -objective analysis 	<ul style="list-style-type: none"> -low cost -Simple protocol 	<ul style="list-style-type: none"> -low cost -Accessible in all hospitals -Objective evaluation 	<ul style="list-style-type: none"> -Non invasive -Information from the whole tumour and possible metastasis - allows for the monitoring at different stages of treatment
Disadvantages	<ul style="list-style-type: none"> - complex protocol - cannot distinguish between primary tumour and metastasis. -High percentage of false negatives -experimental 	<ul style="list-style-type: none"> - requires tissue biopsies -results are subjective and can vary between laboratory protocols. -EGFR expression detected is not tumour specific. 	<ul style="list-style-type: none"> -Requires tissue biopsies, invasive surgery -Doesn't look at the whole of the tumour -gene number not always correlated with prognosis 	<ul style="list-style-type: none"> -Expensive -Access to specialist equipment.

This table indicates both the advantages and disadvantages of the various methods used for the assessment of EGFR (Petak et al., 2010) (Maheswaran et al., 2008, Goto et al., 2012).

1.4.1 Principles of Positron emission tomography imaging

Positron emission tomography (PET) is a highly sensitive, non-invasive, molecular imaging modality that can be used to produce images of physiological and pathological functions within the body. These features are important in oncology. Unlike some imaging modalities such as X-ray, which

measures features at the anatomical level, PET imaging allows the functional assessment of biological and biochemical processes *in vivo*. Functional changes within a tumour can occur rapidly after the start of therapy, without being associated with any anatomical changes.

Currently, clinical response in oncology is assessed using the response evaluation criteria in solid tumours (RECIST) (Therasse et al., 2000). These criteria were first described in 2000 and revised in 2009 (Eisenhauer et al., 2009). These criteria describe the assessment of tumour burden based on anatomical measurements, which can be assessed using different techniques including MRI and computed tomography (CT). PET can however be used to monitor functional changes that would otherwise be unnoticed with anatomical measurements.

PET imaging relies on the design of a radiotracer or probe. These radiotracers or probes are injected into the patient to allow visualisation of the process investigated. PET probes are varied in nature and may be analogues of molecules involved in metabolic pathways (e.g. [¹⁸F]FDG), analogues of nucleotides (e.g. [¹⁸F]FLT) or targets of receptors (e.g. [¹⁸F]erlotinib) (Phelps, 2000). One common feature of all radiotracers is that they contain a radioisotope. Several of the radioisotopes used in PET are summarised in Table 4. Carbon, oxygen and nitrogen are found in abundance in organic molecules and can therefore be replaced by their radioisotopes for the production of radiolabelled probes. Other atoms that are not found in biological compounds are substituted for other atoms with the resulting molecules used as analogues of biological molecules.

Table 4: Radioisotopes used in PET imaging.

Positron isotopes	¹¹ C	¹³ N	¹⁵ O	¹⁸ F	⁶⁴ Cu	⁸⁶ Y	⁸⁶ Z	⁶⁸ Ga
Half-life	20.4min	9.96min	2.07min	109.7min	12.7 h	14.7 h	14.7 h	68 min

Radioisotopes used in PET imaging with associated half-life (Wong, 2004).

The radioisotopes are characterised by unstable proton rich nuclei. In order to reach a more stable state the nuclei will reduce the number of protons. This is achieved through the decay of a proton into a neutron and a positively charged particle, a positron. The Positrons emitted from the radionuclide travel a short distance within the body, usually 0.2 to 2 mm, before undergoing an annihilation reaction upon interaction with an electron (Baghaei, 2003). This annihilation results in the simultaneous release of two γ rays (photons), with an energy of 511 KeV each, in opposite directions (approximately 180°). These two γ rays are detected by two scintillation detectors, which are positioned opposite each other on a ring within in the scanner. Only γ rays that are detected by

opposing detectors within a specific time frame are recorded as coincidence events. These coincidence events, are collected and using mathematical algorithms, which correct for scattering and attenuation are used to reconstruct images that depict the location of the biochemical or metabolic function which was probed by the radiotracer (Basu et al., 2011, Phelps, 2000, Hutchins GD, 2008). These different stages of PET imaging are summarised in Figure 6. The advantage of PET over other imaging modalities such as MRI is a high sensitivity in the nanomolar range of concentrations. Currently scanners that combine both PET and CT allow for both anatomical and molecular imaging in the same framework. This helps to overcome the lower resolution of PET scanners compared to the high resolution of MRI (Mishani et al., 2008). Furthermore, PET scanners that are used specifically for animals, small animal PET, have been developed to help in the discovery and assessment of PET radiotracers (Hutchins GD, 2008). More recently, PET/MR systems have also been designed for both pre-clinical and clinical imaging.

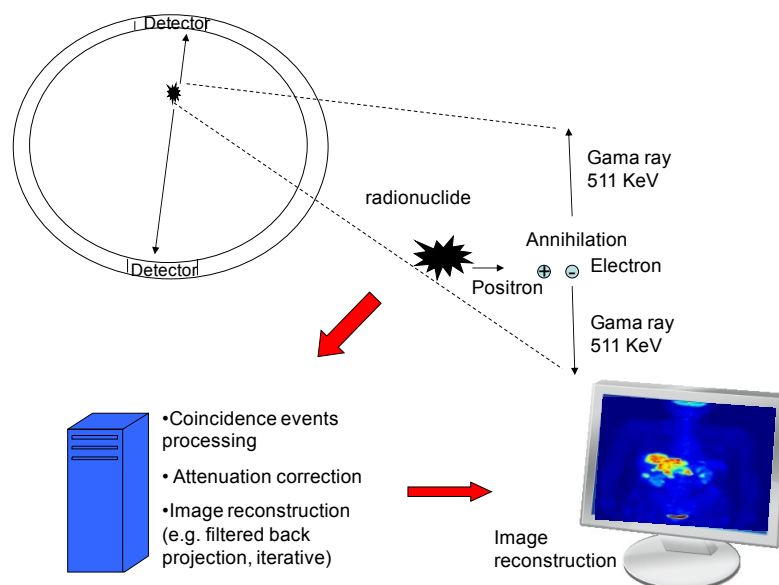


Figure 6: Principles of PET imaging.

The annihilation of a positron with an electron leads to the emission of two gamma rays which are detected by the PET scanner, coincidence events are registered and the data is then corrected for scatter and random events before an image is reconstructed.

1.4.2 Tracers used in the clinic

One of the characteristics of cancerous cells is an increased requirement for glucose, to support the higher levels of metabolism in these cells. This feature is the basis for the most widely used PET tracer in the clinic: [^{18}F]FDG. [^{18}F]FDG is an analogue of glucose in which the hydroxyl group at position C2 is replaced by an [^{18}F] fluorine isotope. This glucose analogue is taken up into the different tissues of the body from the blood via glucose transporter proteins (GLUT), GLUT1 is most

commonly overexpressed in tumours. Once [^{18}F]FDG has been taken up into the tumour it will be phosphorylated to [^{18}F]FDG-6-phosphate by hexokinase II protein. However, due to its modified structure, with a fluorine atom at position 2 in place of a hydroxyl group, [^{18}F]FDG cannot undergo further glycolysis and it is trapped in the cell (Wong, 2004, Phelps, 2000). The uptake and trapping of [^{18}F]FDG are summarised in Figure 7. In oncology [^{18}F]FDG is used for diagnosis but also for monitoring patients throughout their disease, assessing response to treatment and possible occurrence of metastasis (Haberkorn et al., 2011).

Another characteristic of cancerous cells, which has been exploited for imaging, is the high levels of proliferation in these cells. Indeed, tumour proliferation is one of the hallmarks of cancer. Increased proliferation implies increased DNA replication and therefore increased demand for nucleosides. An analogue of the nucleoside thymidine, [^{18}F]FLT has been used for PET imaging of the process of tumour proliferation. Like thymidine, [^{18}F]FLT is taken up into cells via equilibrative nucleoside transporter 1 (ENT1). Once in the cell it is phosphorylated by thymidine kinase (TK1). The uptake and trapping of [^{18}F]FLT are illustrated in Figure 7. This phosphorylated FLT cannot be incorporated into the DNA due to the lack of a hydroxyl group on position three of the ribose (Phelps, 2000, Shields et al., 1998). The uptake of [^{18}F]FLT within a tumour reflects the activity of TK1 which is increased in cells during proliferation (Shields, 2003). To what extent [^{18}F]FLT tumour uptake reflects the proliferation index of a tumour is still debated by many in the field and a recent study indicated that the proliferation index of a tumour and the levels of tumour uptake of [^{18}F]FLT were not necessarily correlated (McKinley et al., 2013).

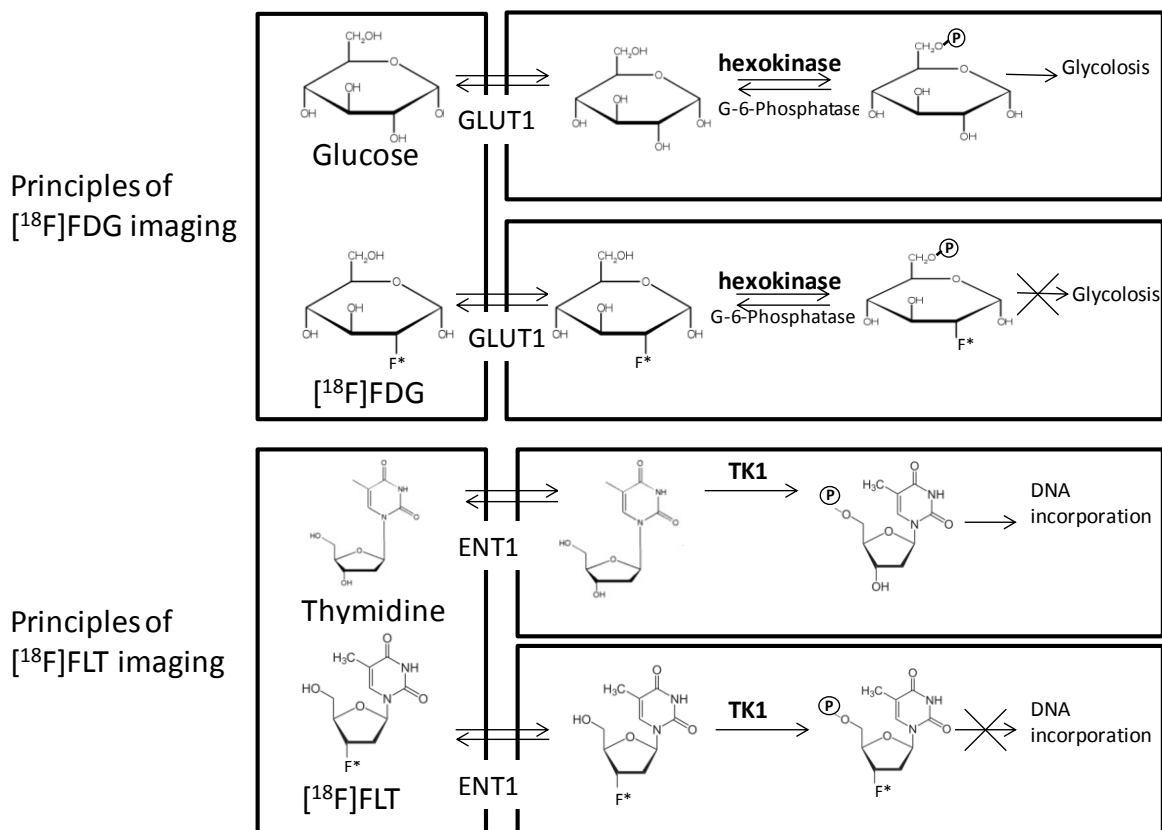


Figure 7: Principles of ^{18}F FDG and ^{18}F FLT metabolism.

GLUT1: Glucose transporter 1, ENT1: equilibrative nucleoside transporter 1, TK1: thymidine kinase 1. ^{18}F FDG is taken into cells as glucose by GLUT1 transporters and phosphorylated by hexokinase enzyme. ^{18}F FLT is taken up into the cell as thymidine via ENT1 transporters and phosphorylated by TK1. Adapted from (Rosen et al., 2007) and (McKinley et al., 2013)

1.4.3 PET Imaging and its application in the study of EGFR

PET imaging in oncology has a broad range of applications ranging from diagnosis to drug efficacy monitoring. As mentioned previously in this review changes to levels of EGFR expression occur in many cancers. Being able to monitor and measure these levels *in vivo*, could aid in patient selection for EGFR targeted mAb or TKI therapy. Identifying patients with active mutant forms of EGFR is important for selection for TKI therapy, and PET imaging of EGFR could also be used in this instance (Yeh et al., 2011).

The majority of tracers, which have been developed for the imaging of EGFR, have been based on EGFR targeting therapeutic agents, either antibodies or small molecular TKIs.

1.4.3.1 Tracers developed from antibody therapeutic agents

Several tracers based on cetuximab and panitumumab antibodies have been developed. In mouse xenograft models [⁶⁴Cu]DOTA-cetuximab showed higher levels of accumulation in high vs low EGFR expressing tumours (Cai et al., 2007, Ping Li et al., 2008). However, metabolism studies highlighted high levels of metabolism of [⁶⁴Cu]DOTA cetuximab in tumour tissue. Indeed, 4 h post injection only 15.65 % of authentic intact [⁶⁴Cu]DOTA cetuximab remained in A431 tumour. There was also high retention in the liver rendering this tracer unsuitable for imaging possible metastatic disease in this area (Ping Li et al., 2008).

The humanized mAb panitumumab has also been radiolabelled for use in PET imaging. [⁸⁶Y]Panitumumab showed high accumulation in high EGFR expressing tumour models. Pre-treatment with non radiolabelled antibody, which resulted in a decrease in tumour uptake of [⁸⁶Y]Panitumumab demonstrated the specificity of [⁸⁶Y]Panitumumab binding for EGFR (Nayak et al., 2010, Nayak et al., 2011). A comparative study demonstrated superior characteristics of [⁸⁶Y]Panitumumab over [⁸⁶Y]Cetuximab. These included lower liver uptake with [⁸⁶Y]Panitumumab than [⁸⁶Y]Cetuximab, leading to improved tumour to liver ratios for [⁸⁶Y]-Panitumumab (Nayak et al., 2011). Panitumumab has also been radiolabelled with other radionuclides such as zirconium, [⁸⁹Zr]DFO-panitumumab (Bhattacharyya et al., 2013).

Alongside the radiolabelling of antibodies, antibody fragments including Fab's and affibodies have been radiolabelled for the imaging of EGFR. These include, [¹¹¹In]DOTA-Z-EGFR:2377 affibody (Tolmachev et al., 2010), [⁶⁴Cu]DOTA-Z-EGFR:1907 (Miao et al., 2010).

Tracers developed from mAb or affibodies will enable *in vivo* monitoring of EGFR expression levels and the possibility to measure therapeutic mAb/receptor binding throughout the course of treatment. However, they will not give any information as to the mutational status of the tyrosine kinase domain of EGFR, and the effect of such mutations on response to treatment. This is where imaging tracers based on small molecular TKIs could play a key role.

1.4.3.2 Tracers developed from the first generation TKIs

Both gefitinib and erlotinib have been radiolabelled for the PET imaging of EGFR. [¹¹C] and [¹⁸F]gefitinib (Su et al., 2008, Zhang et al., 2010) gave mixed results. There were no differences in the uptake of [¹⁸F]gefitinib *in vitro* and *in vivo* in models that expressed differential levels of EGFR or mutant forms of EGFR (Su et al., 2008). On the other hand high levels of [¹¹C]gefitinib uptake correlated with high levels of EGFR expression both *in vitro* and *in vivo* (Zhang et al., 2010).

[¹¹C]erlotinib was initially investigated *in vitro* and *in vivo* mouse studies. High levels of [¹¹C]erlotinib uptake were measured in HCC827 cells that express high levels of EGFR (del E746-A750) but not in A549 or NC1358 cells, both expressing WT EGFR. Furthermore, this tracer showed higher uptake levels in HCC827 tumours, 3.7 % of injected dose per gram (% ID/g), compared to only 1.6 % in A549 tumours. These two findings, correlated with a decrease in HCC827 but not A549 or NCIH358 cell proliferation following erlotinib treatment, and made [¹¹C]erlotinib a promising tracer for the identification of tumours sensitive to erlotinib treatment (Memon et al., 2009). However, from this study one cannot confirm if the higher uptake of [¹¹C]erlotinib in the HCC827 tumours compared to the A549 or NCIH358 tumours was a result of the overexpression and or the mutational status of EGFR in the HCC827 tumours (Memon et al., 2009).

Recent results from a clinical trial evaluating the use of [¹¹C]erlotinib for the *in vivo* assessment of EGFR mutational status in NSCLC patients have been published (Bahce et al., 2013). This small trial of five patients with exon 19 deletion and five patients with WT EGFR involved two scans (test and retest) on the same day, with both [¹⁵O]H₂O, to assess blood perfusion of the tumour, and [¹¹C]erlotinib on the same day. Quantification of the uptake of [¹¹C]erlotinib in the tumour by kinetic modelling using arterial blood as an input function was carried out. From this, the volume of distribution (V_t) was worked out. It was found that V_t was on average two times greater in the exon 19 deletion EGFR than in the WT EGFR expressing tumours (Bahce et al., 2013). This study only looked at one mutant form of EGFR, further investigation of the other prevalent active mutant L858R EGFR will be necessary to conclude on the application of [¹¹C]erlotinib for the identification of mutant forms of EGFR *in vivo*.

1.4.3.3 Tracers developed from second generation of TKI's

Radiotracers are injected in picomolar concentrations and it is thought that at such doses, radiolabelled reversible binding TKIs such as erlotinib and gefitinib would be out competed for the kinase binding site of EGFR by high *in vivo* levels of ATP. For this reason inhibitors which bind irreversibly to EGFR are thought to be better suited for PET imaging of EGFR and this is the direction which was taken for the majority of TKI based tracers (Gelovani, 2008).

Several groups have investigated radiolabelled irreversible binding TKI for the imaging of EGFR. Many of the tracers developed showed disappointing results *in vivo*. One compound, ML04, showed strong but not exclusive selectivity for EGFR *in vitro*. Mishani *et al* were able to use ML04 to quantify the number of EGFR molecules *in vitro* in A431 cells. (Abourbeh et al., 2007). Furthermore, the stability of ML04 *in vivo* was significantly greater than that of ML03, a tracer that showed high levels

of metabolism, and was a previously developed tracer in the group. In fact, at 3 h post injection the tumour activity uptake was 18 times greater with [¹⁸F]ML04 compared to [¹¹C]ML03. However, the EGFR specific uptake of ML04 was poor. Firstly, the levels of uptake measured in EGFR negative U138MG human glioma tumours were elevated. Secondly, a blocking experiment in which non-radiolabelled ML04 was administered in the mouse 1 h before injection of the tracer showed no decrease in the uptake of the radiotracer in the tumour. Both these results led to the conclusion that the activity measured was not EGFR-specific and the use of this compound as a PET tracer was deemed unfavourable (Abourbeh et al., 2007).

An Iodine radiolabelled compound, [¹³¹I]IPQA, showed selective binding to active (phosphorylated) EGFR rather than inactive EGFR. *In vivo* PET imaging, demonstrated that the tracer showed higher levels of uptake in A431 (EGFR overexpressing) vs K562 tumour bearing mouse xenografts and also higher levels of uptake in U87 ΔWT (expressing EGFRIII mutant) vs U87WT mouse xenografts. This backs up the *in vitro* radiotracer accumulation finding in which [¹³¹I]IPQA bound to active but not inactive EGFR (Pal et al., 2006). Although this tracer demonstrated good tumour uptake and good specificity, there were high levels of liver and intestinal uptake, which would render imaging in these regions impossible. Furthermore, the tracer was highly metabolised.

In order to overcome the high levels of liver metabolism seen with previously mentioned anilinoquinazoline tracers such as ML03, ML04 and IPQA, compounds with a reduced log P and an increased solubility needed to be developed (Gelovani, 2008). One approach consisted of the addition of a polyethylene glycol (PEG) group at position 7 of the quinazoline moiety. Three such PEG-anilinoquinazoline-based radiotracers were developed. They were labelled with [¹²⁴I], [¹⁸F] or [¹¹C] and investigated for the imaging of EGFR by small animal PET, using mouse xenografts (Pantaleo et al., 2010). Two human glioblastoma cell lines were used including U138MG (which lacks EGFR expression) and U87MG WT EGFR (which overexpresses EGFR). The tumour uptake of these radiotracers was poor over time and no significant difference in uptake was seen between U138MG and U87MG masses. Enzyme linked immunosorbent assay was carried out to evaluate the levels of total and phosphor-EGFR in the two tumour types. The total levels of EGFR measured were significantly higher in the U87MG tissue (just under 0.25 ng/mg of protein) compared to that measured in U138MG (under 0.05 ng/mg of protein). However, there was no significant difference in the levels of phospho/total EGFR ratios between the two tumours and this was hypothesized as the reason for the similar levels of uptake in the two tumour models (Pantaleo et al., 2010).

To date, the most promising radiotracer for the imaging of mutant EGFR is a derivative from the PEG series of compounds discussed above. [^{18}F]F-PEG6-IPQA, was shown to bind with higher selectivity and specificity both *in vitro* and *in vivo* to the L858R activating mutant EGFR expressing cell line and tumour xenografts. Indeed, this tracer showed a 7.6 fold higher uptake in H3225 (L858R EGFR) xenograft compared to H1975 (L858R/T790M EGFR) xenograft (Figure 8). The fold changes in uptake of [^{18}F]F-PEG6-IPQA were however not as significant when comparing to wild type EGFR. There was only 1.4 fold increase in the uptake of the tracer in the H3255 compared to H441 (WT EGFR) xenografts. Furthermore, expression levels of EGFR were higher in H3255 compared to H1975, and this could be responsible, at least in part, for the increased uptake of [^{18}F]F-PEG6-IPQA in H3255 compared to H1975 xenografts (Yeh et al., 2011). One characteristic of this radiotracer was a rapid plasma clearance, by 30 min only 16.2 % (\pm 8.6 %) of the radiotracer present in the blood was [^{18}F]F-PEG6-IPQA, whilst the remaining radioactivity corresponded to [^{18}F]F-PEG6. As [^{18}F]F-PEG6 does not cross the cell membrane and is rapidly cleared by the kidneys it does not confound the imaging of [^{18}F]F-PEG6-IPQA (Yeh et al., 2011).

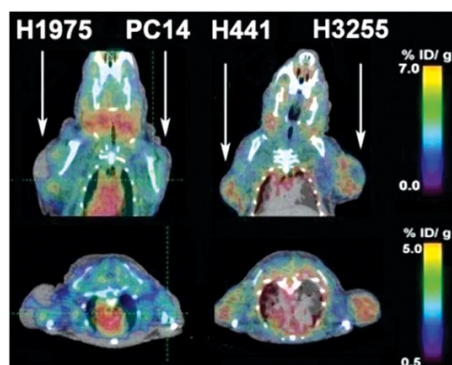


Figure 8: PET image of [^{18}F]F-PEG6-IPQA in mouse xenografts

Representative coronal and axial PET/CT images obtained 120 min post radiotracer injection of mice bearing H1975 (resistant mutant EGFR), PC14 (WT EGFR xenografts) or H441 (WT EGFR), H3255 (L858R EGFR) tumours (Yeh et al., 2011).

Biodistribution, metabolism and pharmacokinetics of [^{18}F]F-PEG6-IPQA have been carried out in non human primates. This study demonstrated acceptable radiation absorbed doses to vital organs including, heart, liver, kidney and gall bladder. They showed that the radiotracer was cleared from the body via both hepatobiliary and renal clearance. They concluded that this radiotracer would be safe for PET in human patients (Tian et al., 2011).

1.4.3.4 FED Compounds

A series of fluorine containing 3-cyanoquinoline derivatives based on the core structure of the irreversible TKI, EKB-569, were synthesized by a radiochemist within our centre. As with other

tracers based on irreversible compounds, the first aim for this series of molecules was to increase the binding of the compound to EGFR and reduce the washout by ATP, seen with reversible compounds. The second goal was to increase the metabolic stability compared to other probes previously designed for the imaging of EGFR (Pisaneschi et al., 2010).

Three key features characterized the cyanoquinoline compounds. First, an aniline moiety at C-4, which is thought to increase the occupancy of the hydrophobic pocket of the receptors active site. Second, a Michael acceptor at C-6, which leads to the covalent binding of the compound with cysteine residue 773 of EGFR. Third, a secondary amine as opposed to a tertiary amine as the Michael acceptor to increase metabolic stability. The Quinoline compound, FED6 (Figure 9) showed high *in vitro* affinity against isolated WT EGFR protein (IC_{50} 1.8 nM) and ease of radiolabeling via “click” chemistry (Kolb et al., 2001), a method that is characterised by simple reaction conditions. This chemistry method is especially important for radiochemistry where synthesis needs to be carried out in the shortest possible time and with the smallest number of reaction steps, so as to reduce the radiation exposure to the radiochemist and to maximise the radiochemistry yield. FED6 was selected as the lead compound to use for PET imaging. The metabolic stability of [^{18}F]FED6 was assessed by analysing plasma and liver extracts taken after 2, 30 and 60 min post radiotracer injection. At 60 min, the parent radiotracer was present at 50 % in the plasma and 75 % in the liver, which was indicative of relatively good stability. [^{18}F]FED6 showed high levels of uptake in A431, EGFR overexpressing tumours, compared to HCT116, low EGFR expressing tumours (Pisaneschi et al., 2010).

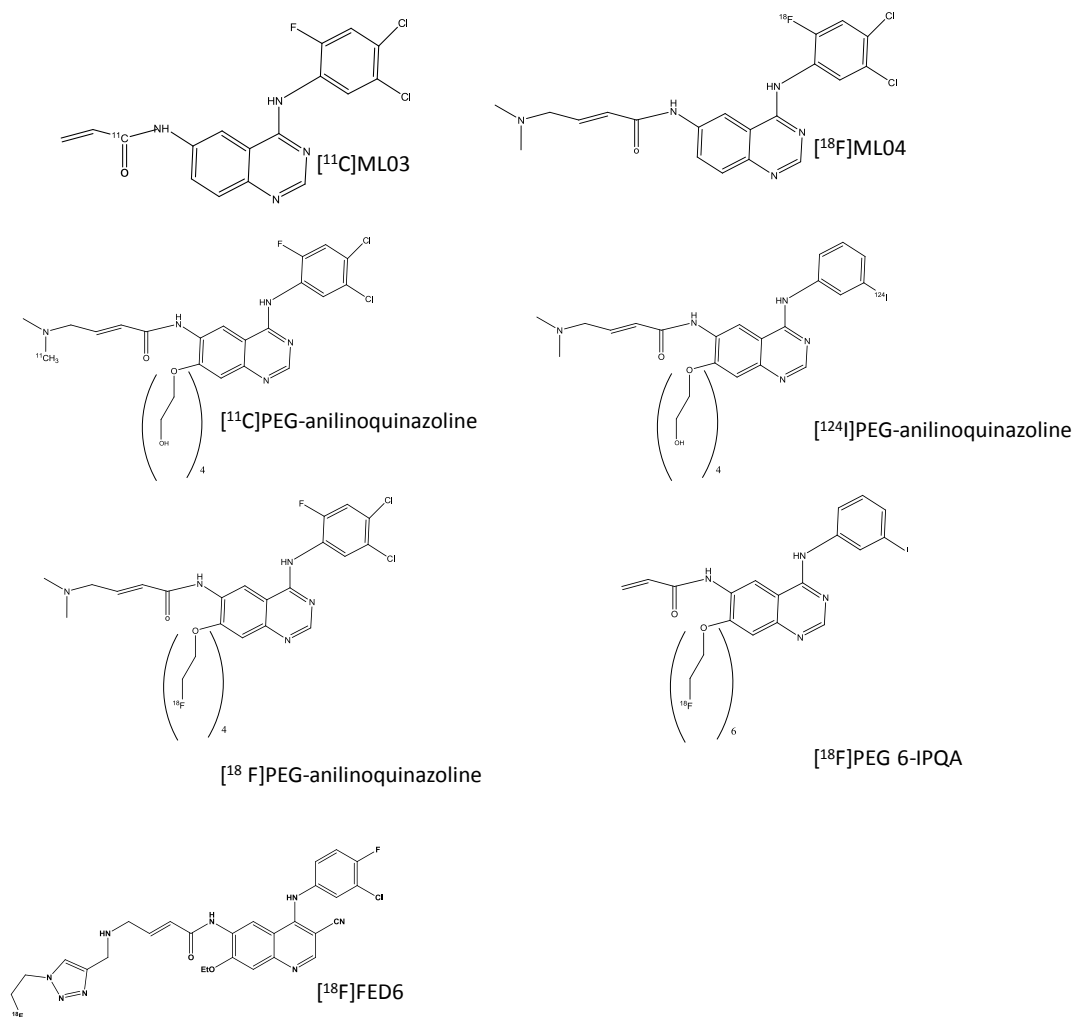


Figure 9: Radiolabelled irreversible inhibitors of EGFR.

Summary of the radiolabeled EGFR targeting tracers based on the structure of irreversible TKIs. Radiolabeling with [¹⁸F], [¹¹C] or [¹²⁴I]. Radiolabelling on the quinazoline core or on the side chain (Pal et al., 2006, Pantaleo et al., 2010, Abourbeh et al., 2007, Pisaneschi et al., 2010, Ortu et al., 2002).

1.4.4 Summary of EGFR PET imaging agents and future application in the clinic

As reviewed above research over the last decade has led to the development of a number of PET probes that target EGFR. These have included both mAb and TKI derived radiotracers. Radiolabelled Mab showed good specificity and sensitivity for EGFR. However, their long half life and large size result in slow excretion, which are a disadvantage for sequential scanning in a clinical setting. Smaller antibody fragments such as, the affibodies introduced above, could help to overcome this timing drawback.

In terms of TKI derived radiotracers, despite strong *in vitro* data, the first developed radiotracers based on reversible TKI showed poor results *in vivo*, due to competition with high levels of ATP. For

this reason the trend was to move toward irreversible TKI based radiotracers (e.g. ML04, FED6) (Pisaneschi et al., 2010, Abourbeh et al., 2007). These showed higher affinity for EGFR but often had high levels of non specific binding especially in liver and gastrointestinal tract. The next step in the field of EGFR radiotracer probes then involved lowering the lipophilicity of radiotracers by adding a PEG moiety to the structure. This led to improvement in stability and reduced non specific binding. The most recent radiotracer in this class being the [¹⁸F]F-PEG6-IPQA. Despite this progress, there are still no EGFR targeting PET probes available for clinical use. The transition of radiotracers from the pre-clinical to the clinical setting will come with a new set of challenges. These may include higher levels of tumour heterogeneity in terms of EGFR expression and activity in humans compared to mouse models, difficulties in understanding the significance of a “negative” PET scan for treatment selection, and overcoming high levels of uptake in organs involved in the clearance and metabolism of the radiotracers (Pantaleo et al., 2009).

1.5 Biomarkers of response, failure of response to TKI treatment in NSCLC

A biomarker can be defined as: “a characteristic that is objectively measured and evaluated as an indicator of normal biological processes, pathogenic processes or pharmacological responses to a therapeutic intervention” (Downing, 2001). This definition highlights the broad range of areas and applications in which biomarkers can be used. In the context of this thesis, the focus will be in predictive biomarkers of therapeutic response. These biomarkers are especially important for the selection of patients who will respond to treatment and more importantly identify those that will not.

In NSCLC many studies have investigated potential biomarkers of response to TKI, gefitinib and erlotinib. The majority of these biomarkers have been evaluated pre-treatment and correlated with response or failure of response to TKI treatment.

1.5.1 Biomarkers obtained from tissue samples.

EGFR copy numbers, mutational status and protein expression have been evaluated as potential biomarkers or therapeutic response.

A high EGFR gene copy number was shown to correspond to an increased response to EGFR TKI (Hirsch et al., 2005). A recent meta-analysis reviewing over 50 clinical trials in NSCLC patients looked into the correlation between somatic mutations and response to gefitinib or erlotinib. EGFR mutations were found to show both strong sensitivity and specificity as a predictive biomarker of response to TKI inhibitor treatment (Dahabreh et al., 2010). It has also been shown that EGFR

mutations are a better predictor of TKI response compared to EGFR expression levels as assessed by methods including immunohistochemistry (IHC) or fluorescence *in situ* hybridization (FISH) (Sholl et al., 2010). Other molecules have also been studied as biomarkers of response to TKI. It has been shown that patients whose tumours were positive for p-AKT showed increased response rate and progression free survival than those whose tumours were p-AKT negative. Thus, P-AKT assessment prior to TKI treatment could be used as a biomarker of response to therapy (Cappuzzo et al., 2004). KRAS has also been investigated as a negative biomarker of response to gefitinib treatment. Two meta-analysis studies showed that patients who had KRAS mutations showed an absence of response or decrease in overall response rates to TKI treatment (Linardou et al., 2008, Mao et al., 2010). Murray et al carried out a study looking at several of the above mentioned biomarkers in 59 NSCLC patients that underwent TKI treatment. They assessed several biomarkers including MET amplification, KRAS mutational status and EGFR expression and mutational analysis. They found EGFR mutations to predict response to TKI treatment. However, the small sample size made it impossible to draw any conclusions on the other tested biomarkers (Murray et al., 2012). The disadvantage with the above biomarkers is that they all require tumour biopsies. Furthermore, they are evaluated before the start of treatment and are not useful for detecting patients who may initially respond and then fail to respond to treatment.

Early prediction of response to treatment and particularly TKI treatment such as gefitinib and erlotinib is important for several reasons. First, If patients are not responding to treatment, rapid initiation of alternative approaches need to be taken so that patients do not continue a course of treatment, often associated with side effects, which is not benefitting them.

Biomarkers that can be assessed during the course of therapy would instead allow resistance to therapy to be detected. Increased serum levels of α 1 antitrypsin were shown in a small study to be predictive of disease progression following gefitinib treatment (Zhao et al., 2013).

In this regard PET imaging which allows non invasive detection and can be performed both before and during treatment can overcome the disadvantages of biopsy collections. The use of an *in vivo* PET imaging probe soon after the start of therapy could allow assessment of response to therapy.

1.5.2 Predicting response to TKI treatment: PET Imaging with [¹⁸F]FDG and [¹⁸F]FLT

[¹⁸F]FDG is commonly used for staging and detection of NSCLC (Weber et al., 2003), but has also been used to predict response in patients receiving chemotherapy or TKIs (see review by Hicks et al ,2009) (Hicks, 2009). [¹⁸F]FLT, which was developed as a marker to measure cellular proliferation *in vivo*, can also be used to determine drug-induced cell cycle inhibition *in vivo* (Shields et al., 1998).

Several preclinical and many clinical studies have been published in recent years investigating the use of both [¹⁸F]FDG and [¹⁸F]FLT as tools for the early detection of response or failure of response to TKI gefitinib and erlotinib in NSCLC.

1.5.2.1 Pre-clinical findings

The pre-clinical studies which investigated the use of early [¹⁸F]FDG and [¹⁸F]FLT PET imaging, to predict treatment outcome, have shown contradicting results. Ullrich *et al* showed a significant decrease in [¹⁸F]FLT uptake in sensitive but not T790M EGFR mutant resistant NSCLC tumour xenograft models, following 48 h erlotinib treatment. They found that the decrease in [¹⁸F]FLT uptake correlated with a decrease in proliferation marker Ki67 and G1 arrest of the tumour cells. They found no significant decrease in the uptake of [¹⁸F]FDG following gefitinib treatment in neither the sensitive nor the resistant NSCLC xenografts (Ullrich et al., 2008). Zannetti *et al* also found a significant decrease in [¹⁸F]FLT uptake (-45 %) following 3 days erlotinib treatment in a sensitive NSCLC xenograft model. They further showed an increase in uptake of [¹⁸F]FLT in the T790M resistant mutant EGFR xenografts following gefitinib treatment, and this as a result of tumour proliferation (Zannetti et al., 2012).

On the other hand Su et al demonstrated a decrease in [¹⁸F]FDG uptake after two days of gefitinib treatment in sensitive NSCLC xenografts (Su et al., 2006).

1.5.2.2 Clinical findings

As with the preclinical studies both early PET imaging with [¹⁸F]FDG and [¹⁸F]FLT PET have been investigated for the prediction of long term response to TKI treatment in NSCLC.

Several studies involving NSCLC patients showed that changes to [¹⁸F]FDG uptake correlated with response to TKI treatment.

Sunaga *et al* showed that a decrease in standard uptake values (SUV) of [¹⁸F]FDG, after two days of gefitinib treatment compared to baseline, correlated with patients with partial response or stable disease (Sunaga et al., 2008). Others correlated the decrease in SUV of [¹⁸F]FDG at two days post treatment with morphological changes, measured by decrease in tumour size by CT at 1 month after start of treatment (Takahashi et al., 2012). Zander *et al* investigated early response to erlotinib treatment independent of mutational status in NSCLC. Decreases in [¹⁸F]FDG uptake after 1 week treatment correlated with an increase in both PFS and OS as well as non progression after 6 weeks. Whereas, decreases in [¹⁸F]FLT uptake did not correlate with changes to OS and were not predictive

of non progression after 6 weeks (Zander et al., 2011). These findings did not correlate to the preclinical studies, which were carried out by the same group, where they found a decrease in [^{18}F]FLT but not [^{18}F]FDG following erlotinib treatment (Ullrich et al., 2008). In another study, low residual uptake of both [^{18}F]FDG and [^{18}F]FLT uptake at 1 week post treatment was associated with an increase in PFS (Kobe et al., 2012). Sohn *et al* also confirmed that [^{18}F]FLT predicted response to gefitinib (Sohn et al., 2008). A recent study looking at use of FDG and FLT to predict therapeutic outcome before the start of therapy showed that a low SUV max at baseline with [^{18}F]FDG and [^{18}F]FLT was associated with an increased response to erlotinib treatment but not with a PFS (Scheffler et al., 2013). The different findings as to the predictability of either radiotracer for measuring response to TKI treatment in NSCLC, emphasise the need for further clinical trials in this field before early routine scanning with [^{18}F]FLT or [^{18}F]FDG could be implemented.

The above section reviewed the potential biomarkers for the assessment of response to therapy in NSCLC. One metabolic pathway which has been extensively linked to an oncogenic phenotype is choline metabolism. The metabolism of choline in cancer is discussed in the following section.

1.6 Choline metabolism in Cancer

Choline is an essential nutrient and is a key precursor in several biochemical pathways within the cell. Choline metabolism involves several pathways including choline phosphorylation, oxidation and acetylation. The positively charged choline molecule relies on active transport into the cells via transporters, including organic cation transporters and choline transporter-like proteins. Once internalized choline will either be oxidized forming betaine or phosphorylated into phosphocholine (Glunde et al., 2011).

Changes to choline metabolism in malignant transformation, were first identified in the 1980's following the detection of increased levels of choline metabolites, including phosphocholine, from ^{31}P and ^1H magnetic resonance spectroscopy (MRS) studies in tumours (Griffiths et al., 1983, Leach et al., 1998). It was first hypothesized that the increase in choline metabolism was in line with a need for increased cell proliferation of the malignant cells. However, it was later shown that the changes in choline metabolism did not correlate with proliferation rates in malignant and non malignant cells but instead changes to choline metabolites were linked to malignant transformation. In breast cancer it was found that there was a gradual increase in levels of choline phospholipid metabolites as cells become more malignant (Aboagye and Bhujwalla, 1999).

Choline metabolism is an important mechanism for the production and maintenance of the cell membrane. Indeed, phosphatidylcholine, the most abundant phospholipid in the cell membrane is a

product of choline metabolism. The pathway that results in the *de novo* synthesis of phosphatidylcholine is the Kennedy pathway (Aboagye and Bhujwalla, 1999, Gibellini and Smith, 2010). This pathway is summarised in Figure 10.

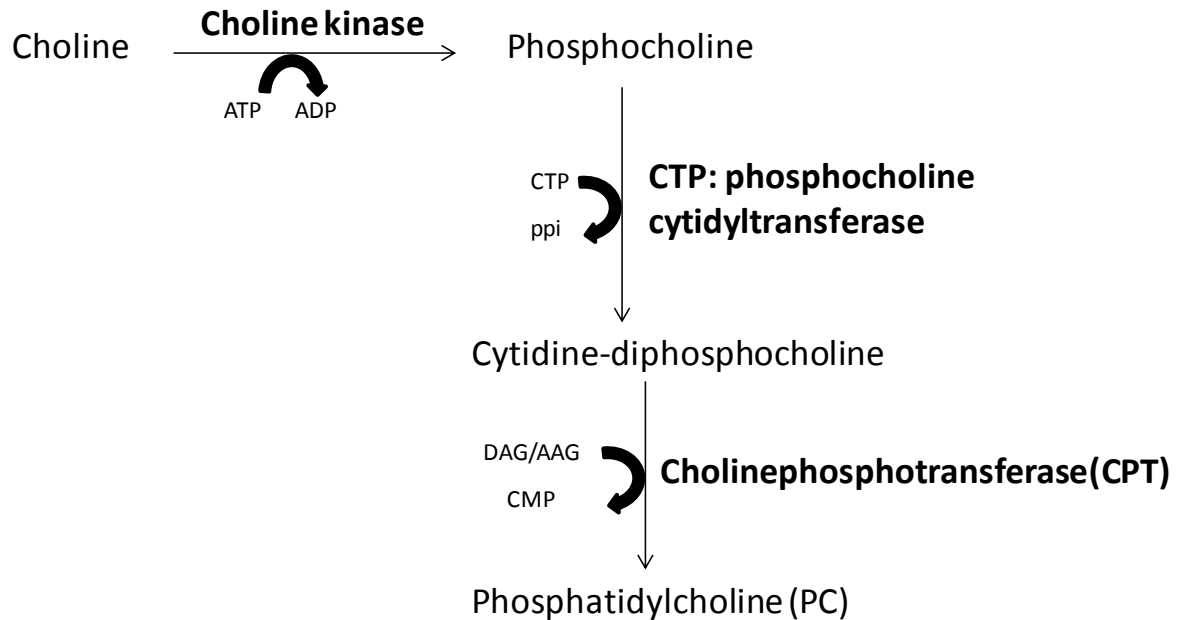


Figure 10: Kennedy pathway.

The phosphorylation of choline by ChK to form phosphocholine forms the initial step of the Kennedy pathway. Phosphocholine is then converted into phosphatidylcholine following two separate reactions. Adapted from (Aboagye and Bhujwalla, 1999) and (Gibellini and Smith, 2010).

The involvement of choline metabolites, including in a number of signalling pathways is illustrated in Figure 11. Phosphatidylcholine is a precursor of diacylglycerol (DAG), arachidonic acid and phosphatidic acid. These molecules have been shown to act as second messengers, activating mitogenic pathways such as the MAPK pathway, thus promoting cell proliferation in cancer. Furthermore, downstream metabolites of phosphatidylcholine, eicosanoids, play an important role in cell motility and metastatic dissemination of cancer cells (Ackerstaff et al., 2003).

1.6.1 Choline kinase

Choline kinase, which is the first enzyme in this pathway, consists of a dimer of the three isoforms of ChK. These are ChK α 1 and ChK α 2, and ChK β . ChK α 1 and ChK α 2 are a result of alternate splicing of the same ChK α 1 gene. The three isoforms combine as hetero or homodimers leading to functional ChK enzyme (Aoyama et al., 2004). ChK α but not ChK β has been associated with malignancy and has been the focus of the majority of research into ChK in cancer (Gallego-Ortega et al., 2009).

Overexpression and increased activity of ChK α have been shown in many cancers including, lung, breast, prostate, ovarian and colorectal cancer (Lenkinski et al., 2008, Iorio et al., 2010, Ramirez de Molina et al., 2002a). The overexpression of ChK α has been linked to increased tumour aggressiveness (Hernando et al., 2009) as well as increased invasiveness and drug resistance (Shah et al., 2010). In lung cancer, ChK α was found to be a valuable prognostic marker. A study, which looked at 167 NSCLC patients, showed a correlation between increased levels of ChK α and poor clinical outcome (Ramirez de Molina et al., 2007).

Regulation of choline metabolism and ChK α in cancer

The regulation of choline metabolism has been shown to involve several oncogenic pathways including MAPK and PI3K-AKT. It has been shown that the increases in phosphocholine that are measured in tumours result in part from the activation of ChK α by Rho GTPases as well as PI3K signalling (Ramirez de Molina et al., 2002b, Ramirez de Molina et al., 2005). Inhibition of ChK α results in a decrease in the MAPK and PI3K signalling pathways (Glunde et al., 2011).

A study in which microarrays were established following ChK α over expression showed an up regulation of over 280 genes (Ramirez de Molina et al., 2008). These were involved in mechanisms of metabolism, cell proliferation, cell cycle and apoptosis. ChK α led to increases in the expression of cyclin D1 and D3 as well as a decrease in expression of P21 and P27, defining ChK α as a key molecule in the regulation of the transition from G1 to S phase of the cell cycle (Ramirez de Molina et al., 2008).

ChK α has also been shown to form a complex with EGFR in the presence of c-SRC. In breast cancer models, Miyake *et al* showed that EGFR and ChK α immunoprecipitated together in the presence of kinase active but not kinase inactive c-SRC. EGFR kinase activity was however not necessary for the EGFR-ChK α interaction to occur. They further showed that this complex of EGFR-c-SRC and ChK α led to an increase in the activity of ChK α (Miyake and Parsons, 2012).

The oncogenic regulation of choline kinase and choline kinase metabolism are summarised in Figure 11.

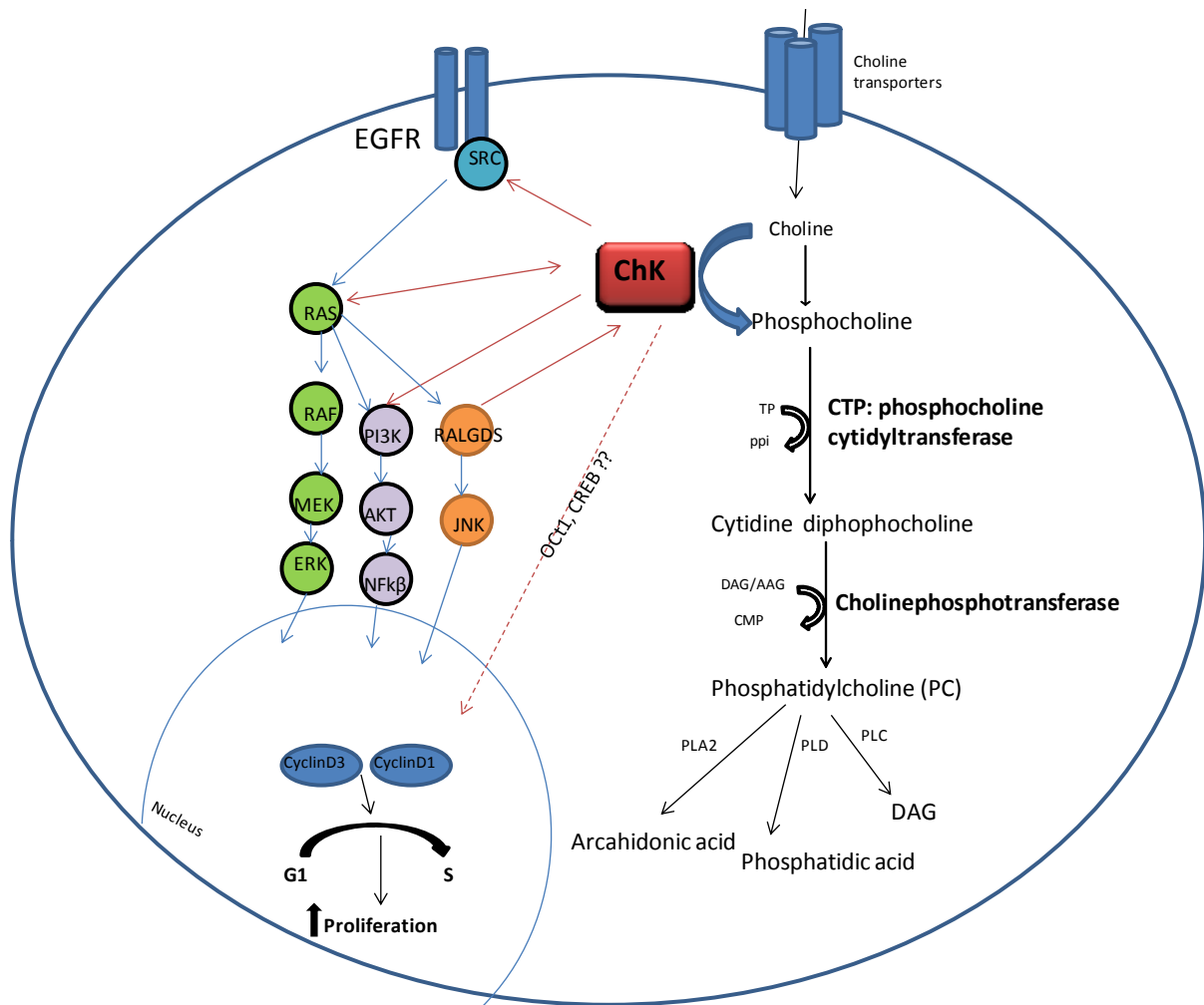


Figure 11: Schematic of ChK α and metabolic control.

Summary figure of the different oncogenic regulations of ChK α and choline metabolism pathway. ChK: choline kinase; DAG: Diacylglycerol; JNK: JUN N-terminal kinase; RALGDS: RAL GTPase guanine nucleotide dissociation stimulator; PLA2: phosphatidylcholine-specific phospholipase A2; PLC phosphatidylcholine-specific phospholipase C. PLD phosphatidylcholine-specific phospholipase D. Red arrows indicate interaction between ChK α and signalling pathways, these include the MAPK and PI3K pathways.

Since it was first discovered that choline metabolism played a crucial role in malignant transformation, assessing this in patients for detection, staging and measuring therapy response was pursued.

1.6.2 *In vivo* imaging of choline metabolism

In vivo imaging of choline metabolism allows for the non invasive assessment of changes to choline metabolism. Two main imaging modalities are used for the assessment of choline metabolism. These are MRS and PET imaging.

1.6.2.1 MRS imaging

MRS imaging exploits the differential resonance frequencies of atoms when placed in differential electric fields. The resonance frequencies reflect the chemical groups present in that particular tissue section. Therefore, measuring these different frequencies allows the collection of information on the specific metabolites present (Kauppinen and Peet, 2011). MRS can be used for the *in situ* measuring of total choline containing molecules, by detecting alteration to ^{31}P and ^1H MRS spectral profiles. MRS quantification of total choline metabolites has been used as part of the diagnostic and staging of cancers including brain (McKnight et al., 2007), breast (Katz-Brull et al., 2002) and prostate (Squillaci et al., 2005). Furthermore MRS has also been selected to monitor therapeutic response (Kurhanewicz et al., 2000, Leach et al., 1998). One disadvantage of this imaging modality is that *In vivo* MRS only provides information on total choline metabolites, as a result of reduced spectral and spatial resolution. This is in contrast to *in vitro* MRS, which is a high resolution NMR technique and provides spectral resolution of different choline components. With advances in clinical MR scanners this draw back could be improved (Glunde et al., 2011).

1.6.2.2 PET imaging of choline metabolism

To date several PET radiotracers have been developed for the imaging of choline metabolism. The first of these was [^{11}C]choline which has been used for the study of several cancers including breast cancer (Hara et al., 1998, Kitajima et al., 2013, Contractor et al., 2011a, Contractor et al., 2011b). Other tracers including [^{18}F]fluoromethylcholine (Kwee et al., 2004, DeGrado et al., 2001a), were designed to overcome the short half-life of [^{11}C]choline. [^{18}F]fluoromethylcholine has been used to detect tumours in brain, breast and prostate (DeGrado et al., 2001a, DeGrado et al., 2001b). [^{18}F]fluoromethylcholine shows high levels of systemic metabolism and this is especially problematic when longer scanning times are required as both parent and catabolites are detected.

To overcome this instability, Leyton *et al* developed a derivative of [^{18}F]fluoromethylcholine, [^{18}F]D4Choline. This radiotracer contains a deuterium moiety that had been shown to render the molecule more stable to oxidation. The authors showed an increase in tumour radiotracer levels and a reduction in oxidation with [^{18}F]D4Choline compared to [^{18}F]fluoromethylcholine (Leyton et al., 2009). A comparative study of [^{18}F]D4Choline, [^{11}C]choline and [^{11}C]D4choline showed that both fluorination and deuteration rendered the choline radiotracer more stable to oxidation (Witney et al., 2012).

As in MRS, PET imaging can also be used to monitor therapeutic response. Leyton et al showed a decrease in uptake of [^{18}F]D4Choline in mouse xenograft following MAPK inhibitor treatment (Leyton

et al., 2009). A clinical study investigated [^{11}C]Choline imaging in the context of measuring response to antibody therapy in breast cancer patients. Kenny *et al* showed a decrease in tumour uptake of [^{11}C]Choline following trastuzumab treatment (Kenny et al., 2010).

As discussed in section 1.3.3, the development of resistance to therapy is a common feature of cancer. One such mechanism of resistance, involves the overexpression of a member of a family of transporters called the ATP binding cassette (ABC) transporters. These transporter proteins and their interaction with TKI will be discussed in the following section.

1.7 ATP binding cassette (ABC) transporters and TKI interaction

1.7.1 ABC Transporters

ABC transporters form a large family of over 48 proteins, divided into seven subfamilies (Dean et al., 2001). These transporters are highly conserved from prokaryotes to humans, and are localised on both intra and extracellular membranes. They are expressed physiologically in a wide range of organs including, blood-brain barrier, lungs, liver and intestines. Their main function is one of protection, by actively excluding endogenous metabolites and xenobiotics from the different organs where they are expressed in conjunction with the hydrolysis of ATP (Figure 12) (Szakacs et al., 2008, Litman et al., 2001).

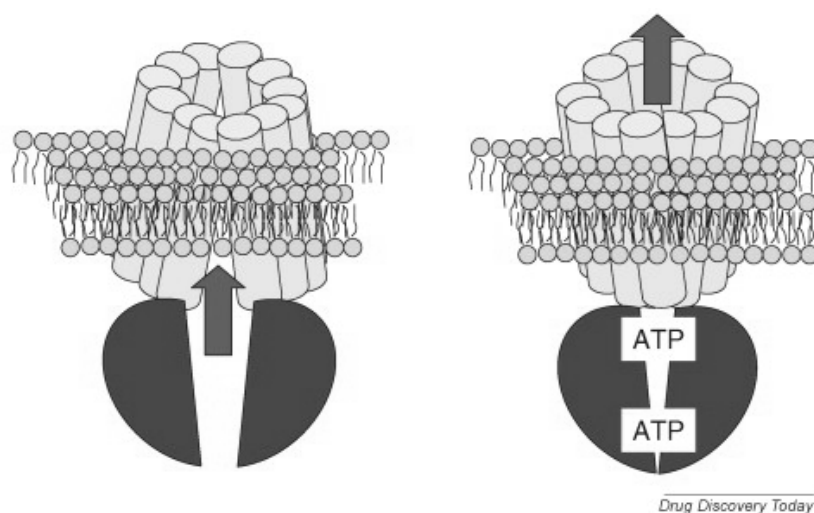


Figure 12: Topological and hypothetical schematic of typical ABC transporter in cellular membrane.

Representation of membrane spanning ABC transporter molecule indicating role of ATP in the efflux activity of these transporters, reproduced from (Szakacs et al., 2008).

The overexpression of ABC transporters has been shown to be a major cause of multidrug resistant phenotype, named MDR. MDR has been extensively studied in the context of cancer where prolonged exposure to a given chemotherapeutic agent often leads to the development of drug resistance. Indeed, upregulation of ABC transporters at the cell surface of a tumour result in lower accumulation of a given drug in the tumour, due to the active efflux of the drug via the transporters, this lower drug exposure, can lead to patients developing resistance to therapy.

Three members of the ABC transporter family which have been linked to MDR are ABCB1 also called permeability glycoprotein (Pgp), ABCG2 also called breast cancer resistance protein (BCRP) and ABCC1 also referred to as multidrug resistant protein 1 (MRP1) (Litman et al., 2001, Shi et al., 2007, Munoz et al., 2007).

ABCB1 is encoded by the MDR1 gene and is formed of two homologous subunits which are joined together by a linker (Ambudkar et al., 1999). A number of molecules have been shown to interact with the ABCB1 pump, from several therapeutic classes. These include anticancer drugs (e.g. paclitaxel), vinca alkaloids (e.g. vinblastine), Hiv-therapies (e.g. ritonavir), and fluorescent dyes (e.g. calcein AM) (Didziapetris et al., 2003). Several studies have investigated the potential characteristics of drugs that increase their substrate specificity for ABCB1. These parameters include (MW) > 400, hydrophobicity determined by $1 < \log P > 5$, sum of oxygen and nitrogen atoms > 8, polar surface area (PSA), defined as the sum of surfaces of polar atoms (usually oxygen, nitrogen, and attached hydrogen) > 85\AA^2 (Varma et al., 2005, Dellinger et al., 1992, Gottesman and Pastan, 1993, Kaliszczak et al., 2010, Didziapetris et al., 2003). Knowing what characteristics lead to recognition and efflux of a drug by ABCB1 is important for designing out any substrate specificity during the drug development process.

The second transporter linked with MDR is ABCG2. This half transporter was first discovered in breast cancer (Doyle et al., 1998), and has since been found to be overexpressed in a wide range of both hematopoietic and solid tumours (Mo and Zhang, 2012). As for ABCB1 the substrate specificity of drugs for ABCG2 encompass a wide variety of chemical structures. Substrates of ABCG2 include, anticancer drugs of the topoisomerase inhibitor class (e.g. mitoxantrone), anthracyclines (e.g. doxorubicin), tyrosine kinase inhibitors (e.g. gefitinib, erlotinib) (Doyle and Ross, 2003, Hegedus et al., 2012, Ozvegy-Laczka et al., 2004, Ozvegy et al., 2001). A planar structure has been shown to be an important feature for determining the substrate specificity of a drug for ABCG2 (Saito et al., 2006). The number of aromatic rings in a compound have also been shown to influence ABCG2 substrate specificity, with compounds containing greater than two aromatic rings showing increased substrate specificity for ABCG2 (Nakagawa et al., 2006).

Finally, ABCC1 also referred to as MRP1, is involved in MDR. This transporter was first identified in lung cancer and is overexpressed in a wide range of cancers (Cole et al., 1992, Deeley and Cole, 2006). Substrates of ABCC1 include anionic molecules as well as molecules that have been conjugated to either glutathione, sulphate or glucuronide (Munoz et al., 2007, Ozvegy-Laczka et al., 2004). As for the two previously mentioned transporters ABCC1 recognises a wide range of drugs including, antivirals (e.g. ritonavir), anthracycline (e.g. doxorubicin), fluorescent molecules (e.g. calcein AM) (Munoz et al., 2007, Hollo et al., 1994).

Some drugs are substrates for just one of the transporters whilst others may be substrate for two or all three. The overlapping substrate specificity of various drugs for these three ABC transporters have been summarised in Figure 13.

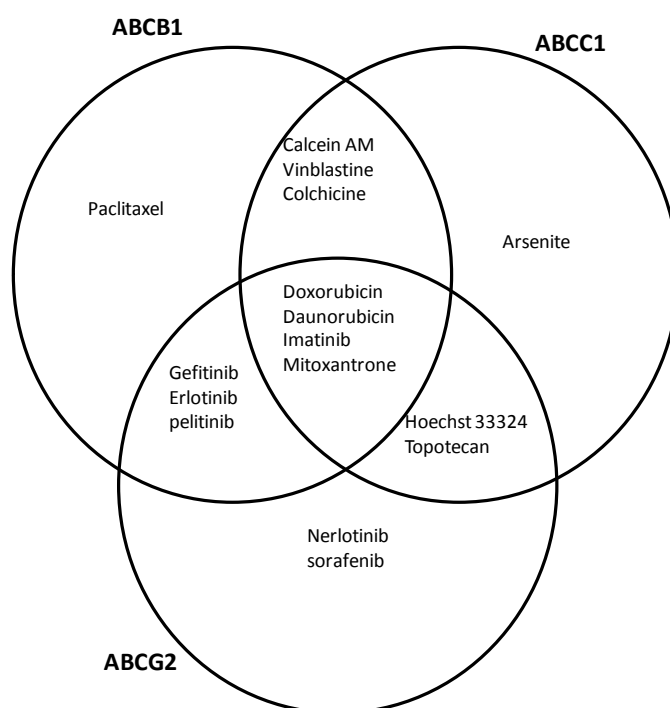


Figure 13: Diagram illustrating the overlapping substrate specificity for ABCB1, ABCG2 and ABCC1 transporters of a variety of drugs.

Molecules including anthracyclines, tyrosine kinase inhibitors, antivirals are listed. This figure highlights a few examples but is not exhaustive.

1.7.2 TKI and ABC transporter protein interaction.

Several groups have investigated the interactions between EGFR TKIs and ABC transporters involved in MDR. The nature of the interaction between EGFR TKIs and MDR transporters is at two levels. TKIs have been shown to be both substrates and inhibitors of MDR transporters.

- TKIs as substrates for ABC transporters

Both first and second generation TKIs have been shown to have substrate specificity for ABCG2 and ABCB1 including dasatinib, nilotinib, pelitinib, gefitinib and erlotinib (Hegedus et al., 2009, Shi et al., 2007, Hegedus et al., 2012). An *in vitro* study investigating the interaction of ABCG2 and gefitinib demonstrated an overexpression of ABCG2 following chronic exposure to gefitinib treatment which accounted for the subsequent acquired resistance to gefitinib (Chen et al., 2011). This finding is important as patients receiving TKIs as 2nd or third line treatments following pre-exposure to chemotherapeutic drugs that lead to MDR could explain the reduced action of TKI in these patients (Hegedus et al., 2012).

- TKIs as inhibitors of ABC transporters

In addition to being a substrate for ABCB1 and ABCG2, both gefitinib and erlotinib have been shown to inhibit ABCG2 and ABCB1 activity (Kitazaki et al., 2005, Ozvegy-Laczka et al., 2004, Nakamura et al., 2005, Shi et al., 2007). In these studies gefitinib reversed resistance to chemotherapeutic drugs by acting as an inhibitor of ABCG2 and ABCB1. In these studies when gefitinib was given in combination with mitoxantrone, a known substrate for both ABCB1 and ABCG2, an increase in cell cytotoxicity in cell lines which overexpressed the MDR proteins was found. A recent study demonstrated the involvement of the PI3K/AKT pathway in the modulation of expression levels of ABCG2. It was found that combination treatment of gefitinib with LY294002 (AKT inhibitor) led to a decrease in expression of ABCG2. This combination treatment could be promising for the potential reversal of MDR caused by overexpression of ABCG2 (Pick and Wiese, 2012, Huang et al., 2011).

Second generation TKI have also been shown to exhibit inhibitory activity against ABCG2, these include EKB-569 (pelitinib), neratinib and vandetanib (Hegedus et al., 2012).

A recent review summarised the various tyrosine kinase inhibitors which have been shown to reverse MDR (He and Wei, 2012).

1.7.3 Tracers and ABC transporter interaction

As the majority of radiotracers for the imaging of EGFR have been designed on core structures of TKIs used in therapy, it is fair to assume that interactions that have been reported for TKI with the ABC transporters also exist between TKI based EGFR radiotracers and the ABC transporters.

The interaction of the radiolabelled tracer with ABC transporters can have a significant impact on the biodistribution of the tracer *in vivo* especially if the tumour to be imaged expresses high levels of these transporters. As radiotracers are injected in pM to nM concentrations, the lack of accumulation due to efflux via the ABC transporters will render the tracer unsuitable in the clinic. Mishani *et al* carried out two experiments to investigate the possible interaction between ML04 radiotracer they developed and the ABCB1 efflux pump (Abourbeh et al., 2007). To find out if ML04 was a substrate of ABCB1 they investigated the uptake of [¹¹C] radiolabelled ML04 in two cell lines, the CEM wild type cell line and its isogenic CEM col1000 cell line which expressed multi drug resistant phenotype following sustained colchicine treatment. They found that the uptake of radiolabelled ML04 in CEM col1000 cells increased with increasing concentrations of ABCB1 inhibitor, verapamil. Furthermore, following ABCB1 inhibition, the uptake of ML04 in the CEMcol1000 cell line approached that of the wild type CEM cells (Abourbeh et al., 2007).

These findings are important as they can help in the design of new tracers that have reduced ABCB1 substrate properties. This would limit the confounding effect of ABC transporters on the *in vivo* biodistribution of the radiotracers.

Aims

Since the cyanoquinoline series of compounds, which were designed for the PET imaging of EGFR, were developed, the importance of mutant forms of EGFR and the role these mutations play in therapeutic response in NSCLC have emerged.

1- The first aim of this project was to investigate the previously characterised cyanoquinoline compound, FED6, for the imaging of mutant EGFR. Could [¹⁸F]FED6 be used to discriminate between mutant and WT EGFR ? The ability to image mutant vs WT EGFR could be used alongside histological tests to select patients suitable for TKI therapy.

The cyanoquinoline compounds shared structural similarities with drugs, which have been shown to interact with MDR ABC transporters.

2- The Second aim of this project was to investigate, the substrate specificity of FED6, and other members of the cyanoquinoline series (Pisaneschi et al., 2010), for ABC transporters. Is FED6 a substrate for the ABC transporters? If so how will this affect PET imaging with [¹⁸F]FED6 and can this be modulated by inhibiting these transporters?

One of the most important decisions in oncology therapy is choosing when to change the course of treatment of a patient, in order for them to be given the most suitable drugs to which they will respond. To help with these decisions, being able to predict the response to therapy at an early stage can be crucial.

3- The third aim of this project was to investigate ChK α as a potential biomarker of response, failure of response to gefitinib treatment in NSCLC. Can PET imaging of choline kinase metabolism be used to predict early response to TKI treatment in NSCLC? How does [¹⁸F]D4Choline compare to other radiotracers, [¹⁸F]FDG and [¹⁸F]FLT for this purpose?

Chapter 2: Methods

2.1 Chemical structure analysis

The chemical structures of compounds investigated in this work were drawn using the Chemdraw pro 11.0 software (PerkinElmer informatics, Waltham, USA). The hydrophobicity (Log P) and Polar surface area (PSA) and pKa: logarithmic value of acid dissociation constants were calculated by importing Chemdraw structures into MarvinSketch/Chemaxon online software.

2.2 Cell culture

Cell lines used to investigate the ABC transporter substrate specificity included: the breast cancer cell line MCF7 and a mitoxantrone drug resistant subclone MCF7MX, which were donated by Dr E. Schneider, University of Maryland, USA. Murine fibroblast cell line 3T3, transfected with non targeting scramble cDNA and the 3T3 cell line stably transfected with human MDR1 gene (referred to as 3T3-MDR1 hereafter) were donated by Dr E. Schietz, St Jude's Children Research Hospital Memphis, TN USA. Caco2 cells used in the transwell assay were purchased from ATCC (Rockville USA). Cell lines utilised to investigate the mutational status of EGFR included, NSCLC A549, H1650, H358, H1975 and H3255 from ATCC. Dr O. Pardo, Imperial College London, donated PC9 cells, and erlotinib resistant derivative PC9ER cells. Cell lines: A549, A431, MCF7, MCF7MX, 3T3 and 3T3-MDR1 cells, were grown in DMEM growth media (Invitrogen, Carlsbad, USA), supplemented with 1 % penicillin/streptomycin and 10 % foetal bovine serum (FBS) (all purchased from Invitrogen). High glucose DMEM supplemented with 20 % FBS 1 % penicillin streptomycin was used for the Caco2 cell line. Lung cancer cell lines H358, H1650, H1975, H3255, PC9 and PC9ER were grown in RPMI1640 (Invitrogen), supplemented with 1 % L-glutamine 1 % penicillin streptomycin and 10 % foetal bovine serum (FBS). All cells were grown in a humidified atmosphere, at 37 °C and 5 % CO₂. When confluency of 80 to 90 % was reached, cells were passaged upon addition of trypsin EDTA (Invitrogen). The cell lines utilised, along with their EGFR mutation status are summarised in Table 5.

Table 5: Summary of cell lines used.

Cell line	Source	EGFR mutation status	Other genes	Growth media
H1650	ATCC	Del 746-750	PTEN null	RPMI
H358	ATCC	WT		RPMI
A549	ATCC	WT	k-RAS mutant	RPMI
H3255	ATCC	L858R		RPMI
H1975	ATCC	L858R/T790M		RPMI
PC9	Dr Olivier Pardo	Del 746-750		RPMI
PC9ER	Dr Olivier Pardo	Del 746-750/T790M		RPMI
A431	ATCC	WT		DMEM
MCF-7	Dr E. Schneider, University of Maryland, USA	WT		DMEM
MCF-7 MX	Dr E. Schneider, University of Maryland, USA	WT	ABCG2	DMEM
3T3	Dr E. Schietz, TN USA	WT		DMEM
3T3- MDR1	Dr E. Schietz, TN USA	WT	MDR1	DMEM

2.3 siRNA transfection

SiRNA transfections were carried out using ON TARGET plus-SMARTpool siRNA or non targeting siRNA (Dharmacon, Lafayette, USA). Lipofectamine RNAiMAX (Invitrogen) was the transfection reagent used and was prepared as indicated on product protocol. A list of siRNAs used are summarised in Table 6.

Table 6: List of Dharmacon ON TARGET plus- SMARTpool siRNA used

siRNA	product code
ABCG2	L-009924-00-0005
SRC	L-003175-00-0005
EGFR	L-003114-00-0005
Scramble (Non-targeting)	D-001810-10-05

2.3.1. siRNA transfection in 6-well plates

siRNA transfections were carried out using the reverse transfection method. siRNA was diluted first in 1 x siRNA buffer (Invitrogen) then in FCS and antibiotic free opti-MEM media. Lipofectamine RNAiMAX (Invitrogen) was separately diluted in FCS and antibiotic free opti-MEM media. The siRNA and Lipofectamine were then mixed in a one to one ratio and incubated at room temperature for 20 min.

Cells prepared in antibiotic free, L-glutamine and 10 %FCS supplemented DMEM or RPMI were then added to the siRNA and Lipofectamine complexes and seeded into 6 well plates. A final concentration of siRNA of 25 nM was used for all siRNA's unless otherwise stated.

After 24 h media were removed and replaced with DMEM or RPMI containing L-glutamine, 10 % FCS and 1 % penicillin streptomycin. Cells were lysed for RNA extraction or protein lysis after 72 h unless otherwise stated.

2.3.2. siRNA in 96-well plates

Cells were seeded in antibiotic free media in black 96 well plates. On the day of transfection siRNA and Lipofectamine were separately diluted in opti-MEM media and then mixed in a 1 to 1 ratio and incubated at room temperature for 20 min. The siRNA-Lipofectamine complexes were then added to the cells in the 96-well plate. After 24 h, fresh media containing 1 % penicillin streptomycin were added to the cells. After 72 h transfection, Hoechst 33324 fluorescent assays were carried out on cells as described below (section 2.10).

2.4 RNA quantification

2.4.1 RNA extraction

Cells were seeded in 6 well plates to a confluency of 60 to 80 %. Cells were washed twice, with room temperature phosphate buffered saline (PBS). Cells were then lysed, by addition of RLT cell lysis reagent, from the RNeasy mini kit (Qiagen, Hilden, Germany). Cells were then scraped and transferred into RNase and DNase free tubes. RNA extraction was then performed using the RNeasy mini kit (Qiagen), following the product protocol. The concentration of the eluted RNA was assessed by measuring the absorbance at 260 nm on the nanodrop ND1000 spectrophotometer (Labtech International, UK). Extracted RNA was stored at -80°C .

2.4.2 cDNA synthesis

Five hundred nanograms of RNA were retrotranscribed into cDNA using the QuantiTech reverse transcription kit (Qiagen) following the product protocol. cDNA was diluted 1 in 5 with RNase and DNase free water and was stored at -20°C .

2.4.3 RT-PCR

Real time PCR was carried out using SYBR green rox reagent (Invitrogen). A master mix was prepared for each set of primers used as follows:

10 μL SYBR green buffer

0.8 μL ROX reagent

1 μL forward + reverse Primer (10 μM)

3.2 μL RNase and DNase free H_2O

5 μL of cDNA sample was pipetted into 96 well Microamp, fast optical plate (Applied Biosystems, Foster City, USA), to which 15 μL of the master mix was added. Plates were sealed using Optical adhesive film (Applied Biosystems). Plates were analysed using ABI 7900 fast real-time PCR machine (Applied Biosystems).

The thermal cycle profile was:

Steps	Temperature	Time
Carry over prevention	50°C	2 min
PCR activation step	95°C	2 min
Denaturation step	95°C	3 sec
Combined annealing and extension step	60°C	30 sec

40 x (

Samples were run in duplicate. mRNA of interest was normalised to GAPDH mRNA levels and was expressed relative to a control sample using the ddCT value (Schmittgen and Livak, 2008). The primers used for Q-PCR are summarised in Table 7.

Table 7: Primers used for Q-PCR

Gene	Compagny	Product code
ABCB1	Qiagen(Quantitect primer assay)	QT00081928
ABCG2	Qiagen(Quantitect primer assay)	QT00073206
ABCC1	Qiagen(Quantitect primer assay)	QT00061159
SRC	Qiagen(Quantitect primer assay)	QT00039326
ChKα	Invitrogen	for 5' CGGAAGTATCCCACCAAGAA 3' rev 5' TCCCCAGAGGAAATGAGATG 3'
GAPDH	Invitrogen	for 5' ATCACCATCTTCCAGGAGCG 3' rev 5' CTGCTTCACCACCTTCTTG 3'

2.5 Inhibition of EGFR activation

Inhibition of EGFR activation via FED6 (Dr Pisaneschi, CCIC Imperial college), FED20 (Dr Pisaneschi, CCIC Imperial college), and gefitinib (selleck chemicals, Houston, USA) were assessed by measuring changes to p-EGFR Y1068 via western blot.

On day one, cells were seeded in 6 well plates. Cells were serum starved overnight on day two. On day three, cells were treated with increasing concentrations of either FED6, FED20 or gefitinib prepared in serum-free growth media from a DMSO stock, for 3 h at 37 °C. Cells were stimulated by addition of 100 ng/mL of EGF for the last 15 minutes of drug incubation. After 3 h, cells were placed on ice. Media were removed and cells were washed twice with ice cold PBS. Cell lysates were prepared and analysed as described in 2.6.

2.6 Western blotting

2.6.1 Cell lysate preparation

Cells were grown to 70-80% confluence. Cells were then washed twice in ice cold PBS. Cells were lysed by addition of radioimmunoprecipitation assay (RIPA) (Thermo Fisher scientific, Waltham, USA) buffer (50 mM Tris-HCl pH 7.2, 150 mM NaCl, 1 % NP40, 1 % sodium deoxycholate, 0.1 % sodium dodecyl sulphate). In order to preserve protein phosphorylation and to protect the cell lysates from protein degradation, the RIPA buffer was supplemented with 1 X protease and phosphatase inhibitor cocktail (1 mM 4-(2-Aminoethyl) benzenesulfonyl fluoride hydrochloride, 800 nM aprotinin, 50 μ M bestatin, 15 μ M E-64, 5 μ M EDTA, 20 μ M leupeptin, 10 μ M pepstatin A; Thermo scientific). Cells were detached using a cell scraper, collected into an eppendorf and placed on ice. Samples were then sonicated for 30 seconds on ice. Levels of protein were assessed by carrying out a bicinchonidic acid (BCA) protein assay as indicated in user's manual(Thermo Fisher scientific).

2.6.2 Sample processing

Protein lysates were prepared by addition of 10 x reducing agent (Invitrogen) and 4x NuPAGE® LDS Sample Buffer (4X) (lithium dodecyl sulphate) (Invitrogen) to give a final volume of 200 μ L. The protein lysates were then denatured by heating for 10 minutes at 70 °C. Unless otherwise stated 15 μ g of the protein samples were separated using SDS-polyacrylamide gel electrophoresis (SDS-PAGE). For this 4/15 % polyacrylamid Mini-PROTEAN TGX precast gels (Bio-Rad, Hercules, USA) were used. Samples were transferred to polyvinylidene difluoride (PVDF) membrane using Trans-Blot Turbo system from BIO-RAD. Membranes were blocked with 5 % milk or 5 % bovine serum albumin (BSA) (Sigma-Aldrich, St Louis, USA) in tris-buffered saline tween 20 (TBST, 50 mM Tris, 150 mM NaCl, 0.05 % tween 20) according to manufacturers guidance for each antibody utilised, for 1 h at room temperature. The membranes were then incubated overnight with primary antibody prepared in 1 % milk or 1 % BSA in TBST. Table 8 summarises the antibodies used. After overnight incubation, membranes were washed three times for 10 minutes with TBST before incubating with secondary goat anti-rabbit or goat anti-mouse antibody at 1/2000 dilution for 1 h at room temperature. Membranes were washed a further three times for 10 minutes with TBST. Blots were visualized using chemoluminescence ECL (GE Healthcare, Little Chalfont, UK) and exposed on Amersham Hyperfilm ECL (GE healthcare). Unless otherwise specified, β -Actin was used as a loading control.

Densitometry

Intensity of the protein bands were obtained using GS-800 calibrated densitometer (BioRad).

To evaluate EGFR inhibition via FED6, FED20 or gefitinib densitometry values of p-EGFR (Y1068) were obtained, normalised for levels of EGFR then plotted against the concentration of compound using the sigmoid curve fit with variable slope in GraphPad prism (version 5.01, La Jolla, USA).

The concentration of compound causing 50 % inhibition of p-EGFR (Y1068) (IC_{50}) were obtained for each experiment.

Table 8: Source and working dilutions of antibodies used.

Antibody	Source	Blocking agent	Dilution
EGFR	Cell signalling	5 % milk TBST	1 in 2000
p-EGFR Y1068	Cell signalling	5 % BSA TBST	1 in 1000
SRC	Cell signalling	5 % milk TBST	1 in 5000
p-SRC Y416	Cell signalling	5 % BSA TBST	1 in 3000
Chk α	Sigma	5 % milk TBST	1 in 1000
p-AKT	Cell signalling	5 % BSA TBST	1 in 2000
AKT	Cell signalling	5 % milk TBST	1 in 2000
p-ERK	Cell signalling	5 % BSA TBST	1 in 2000
ERK	Cell signalling	5 % milk TBST	1 in 2000
GLUT1	Cell signalling	5 % milk TBST	1 in 1000
TK1	Abcam	5 % milk TBST	1 in 1000
Na ⁺ /k ⁺ ATPase	Abcam	5 % milk TBST	1 in 5000
ABCG2	Abcam	5 % milk TBST	1 in1000
ABCB1	Abcam	5 % milk TBST	1 in 1000
β -Actin	Sigma	5 % milk TBST	1 in 5000

Cell-signalling, Ipswich, USA; Abcam, Cambridge, UK

2.7 Cell viability assay

2.7.1 General protocol

A sulforhodamine B (SRB) assay was carried out to assess cell growth and cytotoxicity of tested compounds on cells (Skehan et al., 1990). This assay was carried out in 96 well plates. Cells were

seeded at densities of 3500 to 5000 cells per well for 24 h. Cells were then treated with drugs for 72 h, at 37 °C unless otherwise specified. After drug treatment, cells were fixed by addition of 50 % trichloroacetic acid (TCA) for 1 h at 4 °C. Plates were washed ten times with tap water and left to dry on the bench. Cells were then stained with a 0.4 % solution of sulforhodamine B (Sigma) in 1 % acetic acid for 30 minutes. Excess dye was removed upon washing with 1 % acetic acid (Sigma) solution four times. Plates were dried and bound protein was solubilised upon addition of 150 µL of 10 mM Tris base buffer. Absorbance was measured at 540 nm using Thermo Multiskan-Ex plate reader.

2.7.2 Cell viability assay with drug pre-treatment

Cells were seeded on 96 well plates. 1 h prior to drug treatment, MCF7MX and MCF7 cells were pre-treated or not with 10 µM fumitremorgin C (FTC) (Sigma), 3T3 and 3T3-MDR1 with or without 0.3 µM of zosuquidar (Selleck Chemicals) and A549 with or without 50 µM of MK-571 (Enzo life science). Cells were then treated with drug for 72 h. After 72 h, the SRB assay protocol was carried out as described above.

2.7.3 Data analysis

Cell viability vs compound concentration curves were plotted as a percentage of control cells. The concentration of drug that gave 50 % inhibition in cell growth (GI_{50}) was extrapolated from these curves using the sigmoid curve fit with variable slope in GraphPad prism (version 5.01, La Jolla California, USA). Three to six replicate wells were used for each drug concentration and experiments were carried out on three separate occasions for each compound.

For the SRB assays carried out to investigate the ABC transporter substrate specificity, ratios of GI_{50} of the paired cell lines were carried out. A ratio of the GI_{50} 's was carried out for each experiment and used to compute the mean ratio.

2.8 EGFR tyrosine kinase enzyme inhibition assay

The inhibitory activity of FED20 against EGFR kinase activity was measured using a fluorescence assay (DELFI, Perkin–Elmer Life Sciences, Boston, MA, USA). FED20 was serially diluted in DMSO. FED20 was incubated with EGFR protein (E-3641, Sigma) and a kinase buffer for 15 min at room temperature in accordance with manufacturer's instructions (DELFI Tyrosine kinase kit; Perkin–Elmer). The kinase reaction was started by addition of 25 µM ATP, 25 mM MgCl₂, and 0.25 µM/L of biotinylated poly (Glu, Ala, Tyr) in 10 mM HEPES buffer, pH 7.4. The samples were kept at room

temperature for 1 h. The reaction was stopped by addition of 100 mM EDTA. The enzyme reaction solution was diluted 1 in 20 in assay buffer (provided in the kit) and 200 μ L were added to 96-well ELISA streptavidin coated plates. The plates were washed three times with washing buffer. Europium labelled antiphosphotyrosine antibody (PT66; Perkin–Elmer) was added at a concentration of 50 ng per well. Plates were washed six times with washing buffer. 200 μ L of enhancement solution was added per well and fluorescence measured on Victor3 multi-label counter (Perkin–Elmer) using the Europium protocol. Percentage inhibition of receptor phosphorylation activity over concentration of FED20 curve was plotted. The concentration of compound that inhibited 50 % of receptor phosphorylation activity (IC_{50}) was estimated by non-linear regression analysis using GraphPad Prism. IC_{50} of other cyanoquinoline compounds have previously been determined (Pisaneschi et al., 2010).

2.9 Calcein-AM assay

Cells were seeded in black 96 well plates. On day two cells were treated with an increasing concentration range of zosuquidar (Selleckchem) (up to 3 μ M) or MK-571 (Enzo life science) (up to 100 μ M) in 3T3-MDR1 or A549 cells, respectively. DMSO was used as a control. After 1 h incubation at 37 °C cells were treated by addition of Calcein-AM (Sigma) at a final concentration of 250 nM per well and incubated for 30 minutes at 37 °C. Calcein-AM is taken up by the cells and hydrolyzed by esterases into a green-fluorescent molecule: Calcein. Calcein is cell membrane impermeable and therefore trapped in the cell. One of the properties of Calcein AM is its substrate specificity to ABCB1 and ABCC1 (Hollo et al., 1994, Limtrakul et al., 2007). Reaction was stopped by placing cells on ice. Cells were washed twice by addition of 100 μ L per well of cold PBS. Finally, 150 μ L PBS was added per well and fluorescence measured at an excitation wavelength of 485 nm and an emission of 535 nm using the Victor3 multi-label counter plate reader.

2.10 Hoechst 33324 uptake assay.

Cells were seeded in black 96 well plates. On day two cells were pre-treated with either gefitinib, FTC or FED6 and DMSO as control for 1 h or at 37 °C. Cells were then treated by addition of Hoechst 33324 (Sigma, UK) at a final concentration of 3 μ M per well and incubated for 30 minutes at 37 °C. One of the properties of Hoechst 33324 is its substrate specificity for ABCG2. Hoechst 33324 dye will therefore be effluxed out of cells that overexpress ABCG2 (Scharenberg et al., 2002).

The reaction was stopped by placing cells on ice. Cells were washed twice by addition of 100 μ L per well of cold PBS. Finally, 150 μ L PBS was added per well and fluorescence measured at an excitation wavelength of 355 nm and an emission of 460 nm using the Victor plate reader. Cells were then

fixed by addition of 50 % TCA (Sigma). An SRB assay was then carried out. Fluorescent values were normalised to protein levels using the absorbance values from the SRB assay.

2.11 Caco2 transwell assay.

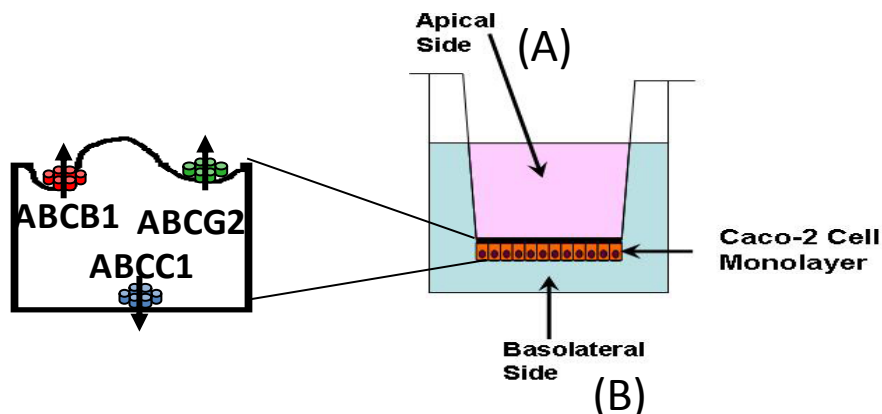


Figure 14: Schematic of transwell and transporter localisation on a Caco2 cell.

Following differentiation Caco2 cells will express ABCB1 and ABCG2 transporters on the apical side and ABCC1 on the basal side of the cell.

2.11.1 Transwell preparation.

Caco2 cells were seeded at a density of 60,000 cells per well in a 24 well transwell plate (Millipore, Billerica, USA), and maintained in DMEM supplemented with 4.5 g/mL glucose (20 % FBS, 1 % Penicillin streptomycin, 1 % glutamine) for 21 days at 37 °C in 5 % CO₂. After 21 days the cells differentiate into enterocytes and express all three MDR proteins, ABCB1 and ABCG2 at the apical side and ABCC1 on the basal side (Figure 14). The caco-2 monolayer and the orientation of the transporters resemble that of the intestinal epithelial layer where the transporters have a protective role, effluxing xenobiotics into the gut lumen for excretion (Sarkadi et al., 2006).

On day 21, cells were washed three times with Hank's Balanced Salt Solution (HBSS) (Thermo-Fisher scientific) and the trans-epithelial electric resistance (TERR) was measured using an Epithelial Voltohmmeter (EVOM) (World Precision Instruments, Sarasota, USA); only transwells with TERR of 400 Ω/cm^2 or above were used for the experiment.

Cells were treated either at the apical (n = 3) or basal (n = 3) side of the transwell by addition of 10 μM of cyanoquinoline compound or 50 μM vinblastine prepared in a volume of 400 μL HBSS (compound added to apical well) or 800 μL of HBSS (added to basal well).

When transport inhibitors FTC (10 μM) and zosuquidar (0.3 μM) were utilised they were added to both the apical and basal wells 1 h prior to drug treatment. After 1 h pre-treatment media was removed from the wells and cells were treated with the compounds prepared in HBSS containing FTC or Zosuquidar.

Plates were then incubated in a shaker incubator at 37 °C and 60 rpm for 120 minutes. After incubation, 400 μL samples from the apical and the basal wells were collected and analysed using high protein liquid chromatography (HPLC).

2.11.2 HPLC analysis

In order to determine the amount of compound in the apical and the basal side of the transwell plates, high protein liquid chromatography (HPLC) was used. Samples were run on a Millipore Waters HPLC system which included a 717 plus autosampler and 2487 dual wavelength absorbance detector system. The stationary phase comprised a Phenomenex Luna C₁₈ (2) reverse phase column (150 X 4.6 mm; 5 μm particle size.) The mobile phase comprised 0.1 % trifluoroacetic acid (TFA) and acetonitrile 0.1 % TFA (80:20 v/v) at a flow rate of 1 mL/min for all compounds except vinblastine.

For vinblastine, the stationary phase comprised a Supelcosil LC-ABZ reverse phase column (5 X 4.6 mm; 5 μm particle size). The mobile phase comprised 0.1 % formic acid and methanol. (90:10 to 10:90 v/v gradient).

2.11.3 Data analysis

Peak areas corresponding to the compounds of interest were recorded. Using a standard curve, peak areas under the curve were converted into concentrations of compound. The permeability coefficient (P_{app}) was calculated using the following equation (Artursson and Karlsson, 1991):

$$P_{app} = (dQ/dt)/A C_0$$

Where A is the surface area of the transwell membrane in cm^2 (= 0.33 cm^2), C_0 is the drug concentration in the donor chamber at time $t = 0$ and dQ/dt is the rate of transfer of the compound to the receiver chamber, determined from the slope of the graph of concentration (dQ) versus time (dt). dQ/dt can also be expressed as :

$$\frac{dQ}{dt} = \frac{B - C}{T}$$

Where B is the concentration of compound in the receiver chamber at time $t = 7200$ sec (120 minutes) and C is the concentration of compound in the receiver chamber at time $t = 0$. T is the time of transfer $T = 7200$ sec. As no compound is added to the receiver chamber at $t = 0$ $C = 0$. The equation then becomes

$$\frac{dQ}{dt} = \frac{B}{T}$$

Papp values corresponding to absorption and secretion were calculated and used to calculate efflux ratios.

$$\text{Efflux ratio} = \frac{(\text{Papp B} - \text{A})}{(\text{Papp A} - \text{B})}$$

Where $\text{Papp B-A} = \text{Papp secretion}$ and $\text{Papp A-B} = \text{Papp absorption}$.

2.11.4 Membrane integrity

The integrity of the Caco2 cell membrane was assessed for each well following the experiment by addition of a 100 μM solution of luciferase yellow (sigma) in HBSS to the apical side of the plate. The plates were placed in a shaker incubator for 1 h at 37 °C and 60 rpm. Samples from the basal wells were transferred into a 96 well plate and the levels of luciferase yellow were assessed by measuring with an excitation of 450 nm and an absorbance of 540 nm using the PerkinElmer Wallac 1420 multilabel counter. The membrane was considered intact if levels of fluorescence in the basal side were inferior to 2 % of levels measured in the apical side.

2.12 Caspase glow assay

Levels of apoptosis, following drug treatment were established by carrying out a Caspase 3/7-Glo assay (Promega, Fitchburg, USA). This luminescence assay kit, measures levels of activity of caspase 3 and 7, both of which play a key role in apoptosis (Taylor et al., 2008).

The kit includes a proluminescent substrate, which contains a DEVD peptide and an ultraGlow luciferase enzyme. Upon cleavage of the substrate via cellular caspases amnioluciferin is released and reacts with luciferase to emit light. The light emitted is proportional to the activity of caspase 3 and 7. Cells were seeded in white 96-well plates. Following drug treatment, levels of apoptosis were measured by carrying out a caspase 3/7glow assay. Caspase Glow reagent (Promega) was added to cells in a 1:3 (v/v) ratio, and incubated at room temperature for 1 h. The luminescence was then measured using a luminometer (TopCount NXT, Packard Instruments, Meriden, USA). Media alone

plus caspase reagent was used to correct for background luminescence. Luminescence values were normalised to protein levels by undertaking an SRB cell viability assay, in parallel to the caspase glow assay. Four to six replicates were carried out for each condition and experiments were repeated twice.

2.13 Cell cycle analysis via flow cytometry using propidium iodide

The distribution of cells within the different phases of the cell cycle, were assessed by performing DNA staining with propidium iodide (PI). Stained cells were then analysed via Flow cytometry.

Cells were seeded in 6 well plates. On day two, cells were treated with gefitinib or DMSO as control. After 6, 24 or 48 h treatment the supernatant was collected. Adherent cells were trypsinised and combined to the supernatant before centrifugation to obtain a cell pellet. Cells were resuspended in 1 mL of ice cold PBS, which was then added drop by drop to 9 mL of 70 % ethanol, in order to fix the cells. Samples were then incubated at -20 °C overnight. Cells were centrifuged at 600 g and the supernatant was discarded. The cell pellet was rehydrated in PBS for 15 minutes before being stained with PI staining buffer containing: 100 mM Tris (pH 7.4), 150 mM NaCl, 1 mM CaCl₂, 0.5 mM Mg Cl₂, 0.1 % Triton-X, 0.1 mg/mL RNase A and 25 µg/mL PI. Cells were incubated in staining buffer for 3 h at 37 °C. Cells were then analysed using a BD FACS Canto cytometer (BD, Oxford, UK). Cell debris and doublets were excluded by performing gating of the samples. For each condition 10,000 cells were counted.

Data analysis was performed using FlowJo software version 7.6.5 (Treestar, Ashland,.USA)

2.14 Radiopharmaceuticals

[¹⁸F]FDG and [¹⁸F]FLT were both purchased from PETNET solutions (Nottingham, UK). [³H]Choline was purchased from PerkinElmer (Waltham, USA).

[¹⁸F]FED6 was produced by Dr. Pisaneschi from the Comprehensive Cancer Imaging Centre, Imperial College London, as described in (Pisaneschi et al., 2010). [¹⁸F]FED20 was synthesised by Dr.Pisaneschi using “Click” radiochemistry using a method adapted from Maschauer *et al* (Maschauer and Prante, 2009).

2.15 Cell uptake assay

2.15.1 [³H]choline

In order to assess the activity of ChK, [³H]choline uptake experiments were carried out in PC9 and PC9ER cells. These assays measure the transport and phosphorylation of choline in whole cells.

- Whole cell [³H] choline uptake

Cells were seeded in 6 well plates. Following drug or siRNA treatment the [³H]choline uptake experiment was carried out. A volume of 100 μL of media, containing 3.7 KBq of [³H]choline (Perkin-Elmer), was added per well and cells were incubated at 37 °C for 1 h. Supernatant containing floating cells was collected and a cell pellet was obtained via centrifugation. Cells in plates were washed twice with room temperature PBS. Cells were then trypsinised and collected. Cells were centrifuged for 3 minutes at 2000 RPM to obtain a cell pellet. The cell pellet was washed once with PBS and then resuspended in 200 μL of RIPA buffer. One hundred and fifty microliters of cell lysate was then transferred to a scintillation tube to which 4 mL of Ultima Gold™ XR scintillation cocktail (Perkin Elmer) was added. Scintillation counts were acquired on a LS6500 multipurpose scintillation counter (Beckman Coulter, Pasadena, USA) using a 5 minute accession. Scintillation values in counts per minute (CPM) were then normalized to total protein using Pierce® BCA Protein Assay Kit (Thermo Scientific) which was carried out on the remaining 50 μL of cell lysate.

Experiments were carried out at least three times using triplicates of samples for each experiment.

- [³H]Phosphocholine extraction

Phosphocholine formation was assessed using a modified Bligh and Dyer extraction as described in (Sebastian Trousil, 2013). Cells were seeded in 6 well plates. Following drug treatment [³H]choline uptake experiment was carried out. A volume of 100 μL of media, containing 37 KBq of [³H]choline, was added per well and cells were incubated at 37 °C for 1 h. Supernatant and any floating cells were collected and cell pellet obtained via centrifugation. Cells were washed twice with room temperature PBS. Cells were then trypsinised and collected. Any further reaction was stopped by addition of 750 μL of a 2:1 ratio of methanol/chloroform. After 10 minutes, incubation at room temperature cells were transferred to a microcentrifuge tube and 200 μL of H₂O was added. Cells were centrifuged at 200 g for 10 minutes. The aqueous upper phase, 750 μL, was transferred to a new tube to which 250 μL of chloroform and 250 μL of H₂O were added and samples vortexed and centrifuged. 650 μL of the upper aqueous phase was transferred to a fresh microcentrifuge tube to

which 500 μL of 12 mM sodium phosphate (pH 7.0) and 750 μL 5 mg/mL tetraphenylborate (TPB) (Sigma) in heptan-4-one (Sigma) was added. Samples were vortexed and centrifuged. The upper phase, containing the choline was discarded. Residual choline was re-extracted from the lower phosphocholine phase with 500 μL TPB. After vortexing and centrifugation, 200 μL of the lower aqueous phase was added to 4 mL of Ultima Gold™ XR scintillation cocktail and scintillation measured on scintillation counter. Scintillation values were then normalised to total protein using Pierce® BCA Protein Assay Kit (Thermo Scientific) which was carried out on parallel processed samples. Experiments were carried out a minimum of three times using triplicates of samples for each experiment. Method summarised in Figure 15.

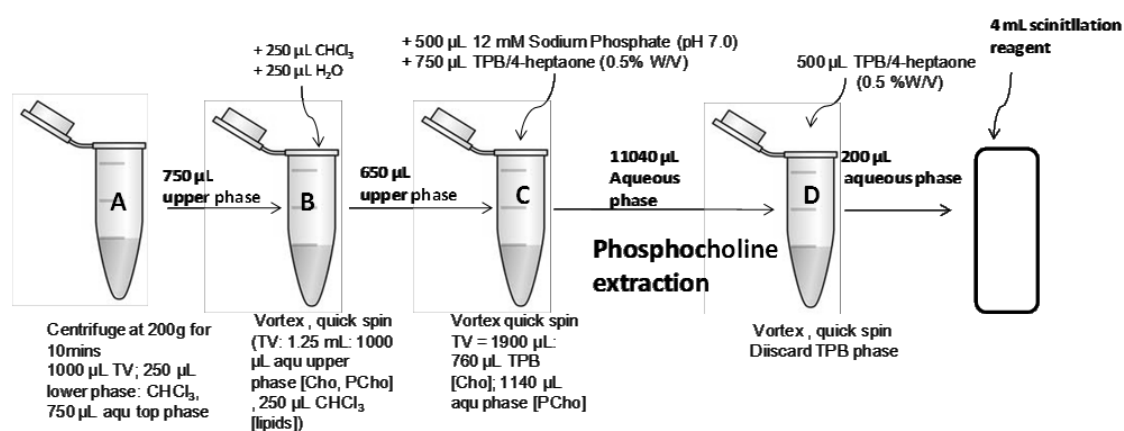


Figure 15: Schematic of phosphocholine extraction.

Following 1 h incubation with [^3H]Choline the phosphocholine component was extracted as described in this diagram. TPB: Tetraphenylborate; Pcho: phosphocholine; Cho: Choline Aqu: Aqueous

2.15.2 [^{18}F] uptake experiments

Cells were seeded in 6 well plates. Cells were seeded in complete medium with the exception of the FED20 blocking experiment and the uptake assays in the NSCLC using [^{18}F]FED6 and [^{18}F]FED20, for which cells were serum starved overnight and stimulated upon addition of 100 ng/mL of EGF 15 minutes before incubation with radiotracer. On the day of the cell uptake, cells which had been pre-treated or not, were incubated for 1 h at 37 °C upon addition of [^{18}F]FED6 (Imanova, London, UK), [^{18}F]FDG (PETNET, Nottingham, UK) or [^{18}F]FLT (PETNET, Nottingham, UK) or [^{18}F]FED20 (Imanova, London, UK), at 0.37 MBq well (unless otherwise stated). Following incubation, the medium was removed and cells were washed twice by addition of 500 μL of room temperature PBS. Cells were then trypsinised and collected. Cells were centrifuged for 3 minutes at 2000 RPM to obtain a cell pellet. The cell pellet was washed once with PBS. The cell pellet was then resuspended in 200 μL of

RIPA buffer. Cell lysates were transferred to gamma counting tubes. The radioactivity in the pellet was measured on a (Packard 109 cobra II gamma counter, Perkin-Elmer).

Following radioactive decay, protein concentrations of the samples were evaluated using Pierce® BCA Protein Assay Kit (Thermo Fisher Scientific). Data were decay corrected and expressed in corrected counts per minute acquired (CCPMA) per µg of protein.

2.16 *In vivo*

2.16.1 Tumour inoculation

Cells were grown as described in 3.1. Fresh media were added to the cells the night before tumour inoculation. Cells were trypsinised, then centrifuged and resuspended in PBS. 6 to 8 week old BALB/c nu/nu female mice from (Harlan UK Ltd, Bicester, United Kingdom) were injected with 5×10^6 A431, H1650 or A549 Cells, 2×10^6 PC9 cells or 3.5×10^6 PC9ER cells. Cells were injected as a suspension in 100 µl of PBS subcutaneously on the back of the neck. Tumour volumes were assessed by caliper measurement every other day. Volume was calculated using the following equation

$$volume = w \times l \times h \times \frac{\pi}{6}$$

Where w is the width, l the length, and h the height of the tumour.

2.16.2 Positron emission tomography imaging

The different schematics of drug treatment for the different PET studies which were carried out are shown in Figure 16. Vehicle was 0.4 % tween 20 PBS. Gefitinib was prepared by diluting powdered gefitinib (selleck Chemicals) in 0.4 % tween 20 PBS and homogenised by vortexing and sonicating briefly.

A

[¹⁸F]FED6 blocking study

Pre-treatment with
I.P. Injection of
gefitinib 100 mg/kg

60 min dynamic
[¹⁸F]FED6 PET
scan

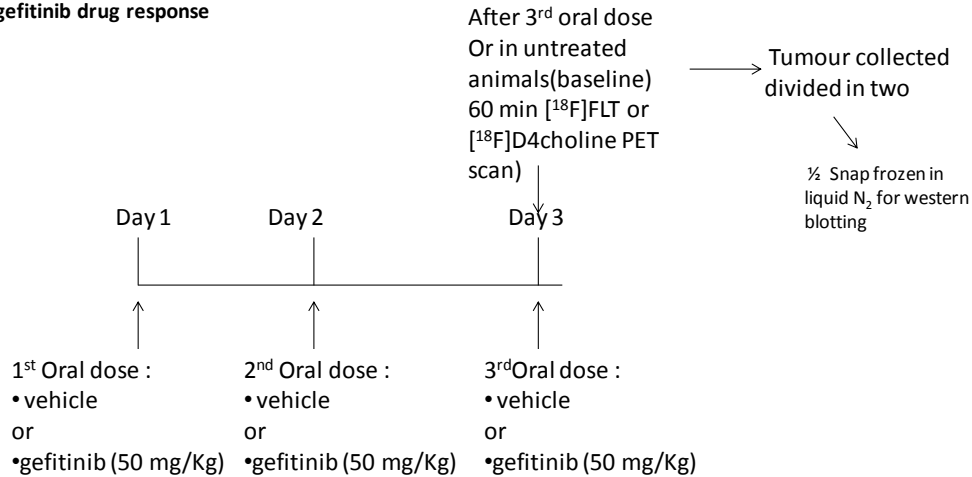
Tumour collected
divided in two

½ Snap frozen in
liquid N₂ for western
blotting



B

**[¹⁸F]FLT or [¹⁸F]D4choline assessment
of gefitinib drug response**



C

**[¹⁸F]FDG assesment of gefitinib drug
response**

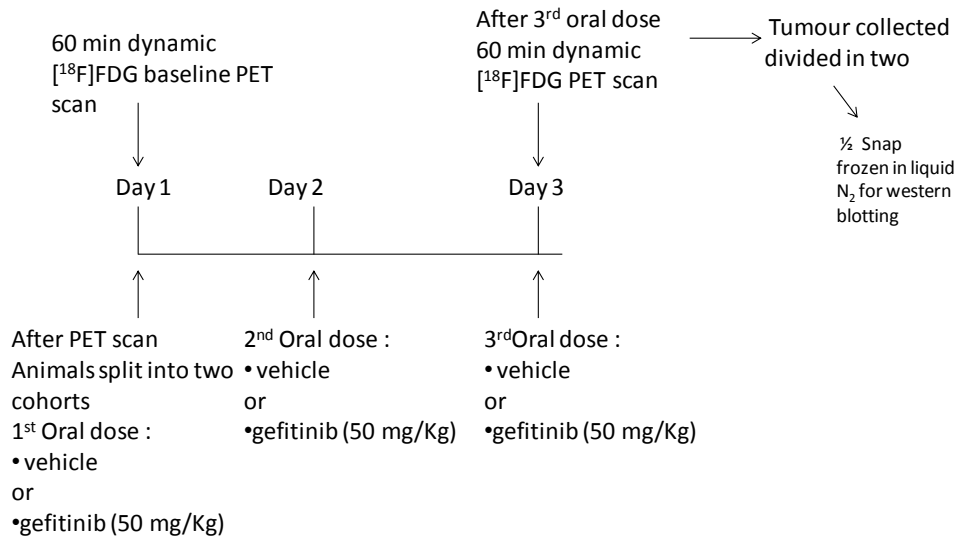


Figure 16: Schematic of drug treatments before PET scan

A- Scheme used for A431 xenografts which were pre-treated with gefitinib 1 h prior to performing [¹⁸F]FED6 PET scan. B- Scheme used for PC9 and PC9ER xenografts scanned before treatment or after 48 h of vehicle or 50 mg/kg of gefitinib with [¹⁸F]FLT or after 48 h of vehicle or 50 mg/kg of gefitinib with [¹⁸F]D4choline. C- Scheme used for PC9 and PC9ER xenografts scanned with [¹⁸F]FDG at baseline then again following 48 h vehicle of gefitinib treatment.

Female BALB/c nu/nu mice bearing xenografts with tumours of an average size of 100 mm³ were imaged by positron emission tomography. All animals were scanned on a small animal CT/PET scanner (Siemens Multimodality Inveon, Siemens Molecular Imaging Inc., Knoxville, USA). During this procedure, mice were anesthetized using 2.5 % isoflurane. A CT scan was first carried out and these data were later used to correct for attenuation of the PET data; 3.7 MBq of [¹⁸F]FED6, [¹⁸F]FDG, [¹⁸F]FLT or [¹⁸F]D4choline was injected as a bolus solution in PBS via a cannular to the tail vein. Dynamic emission scans were acquired in list-mode format over 60 minutes.

Cumulative images of the dynamic data were reconstructed by an iterative (OSEMD3D) method and used for visualization of radiotracer uptake to define the regions of interest (ROIs) with the Siemens Inveon Research Workplace software (IRW; Siemens, Frimley, UK). Three-dimensional ROIs were defined for each tumour. Time-activity curves (TACs) were obtained from these ROI. Tumour TACs were then normalized to the total injected dose (ID) to obtain the normalized uptake value expressed as % ID/mL. Area under the curve (AUC) measurements were calculated. These corresponded to the area under the curve of the TAC of the tumour. Normalised uptake values at 60 min (NUV₆₀) were also determined and corresponded to the uptake of radiotracer in the tumour at time t = 60 min after the start of the PET acquisition. Two other parameters were determined. These were, the highest mean quartile of tracer uptake in the tumour and the fractional retention of the tracer (FRT). The highest quartile of tracer uptake was determined by selecting values corresponding to the tumour voxels, from the 30 to 60 min time frames, then ordering them and calculating the average of the highest quartile for each tumour. The FRT was calculated as the uptake of the tracer in the tumour at 60 min over the uptake of the tracer at 3.5 min. A minimum of n = 3 mice per cohort for [¹⁸F]FED6 studies and n = 4 mice per cohort for [¹⁸F]FDG, [¹⁸F]FLT or [¹⁸F]D4choline studies were imaged. These numbers of animals were used to obtain initial estimates of drug effect on radiotracer tumour location.

All animal work was performed according to the United Kingdom's "Animals (scientific Procedures) Act 1986"(Workman et al., 2010).

2.16.3 Biodistribution

A biodistribution was carried out for the A431 xenograft study. At the end of the PET scan, animals were sacrificed; blood was obtained via cardiac puncture. Tissues (21 in total), were collected from the animal and the radioactivity of each tissue was measured in a gamma counter. Tissues were weighed and radioactivity in each tissue was expressed as CCPMA/μg tissue.

2.16.4 Tumour lysate preparation

Following PET imaging tumours were collected and divided in two sections. One section was preserved in 10 % formalin for immunohistochemistry processing, while the other was snap frozen in liquid nitrogen and stored at - 80° C.

The snap frozen tumour sections were used to prepare protein lysates for western blot analysis. Briefly, tumour sections were transferred to Precellys® CK14 ceramic bead containing tubes (Bertin Technology, Toulouse, France) along with RIPA buffer supplemented with 1 X protease and phosphatase inhibitor (Thermo scientific). Tumour samples were homogenised using the Precellys® 24 tissue homogeniser (Bertin Technology) at 5000 RPM for 2 x 30 sec. Samples were then centrifuged for 5 min at 4 °C to obtain a supernatant. The supernatant was then sonicated for 2 x 30 sec and protein concentration was assessed by carrying out a BCA assay. Samples were then processed for western blot analysis as described in section 2.6.2 and 2.6.3.

2.17 Statistics

Unless otherwise specified data were expressed as mean \pm standard error. After testing that the data were normally distributed, data were compared using an unpaired, two tail Student's t-test (Prism 3.03 software, GraphPad). Data that showed statistical significant differences, were indicated with one (p value \leq 0.05) or two (p value \leq 0.01) stars. The *in vivo* work consisted of pilot studies, power tests estimating the number of animals to be used in the PET studies would be carried out for complete studies.

Chapter 3: Imaging mutant EGFR with [¹⁸F]FED6

As described in chapter 1, a series of cyanoquinoline compounds have previously been developed in the group for the imaging of EGFR. One member of this family of compounds, FED6, has been radiolabelled and was shown to give rise to higher levels of uptake in A431 (EGFR overexpressing) xenografts compared to HCT116 (low EGFR) xenografts (Pisaneschi et al., 2010). Before examining the potential of labelled FED6 to discriminate mutant forms of EGFR the interaction of FED6 for WT EGFR was further confirmed.

3.1 Binding of [¹⁸F]FED6 to EGFR overexpressing cells

To verify the results of the initial FED6 study indicated above, we first asked the question, can FED6 discriminate cells with differing levels of EGFR. To address this, the uptake of [¹⁸F]FED6 was measured in EGFR overexpressing A431, and low EGFR expressing MCF7 cells (Figure 17A). The uptake of [¹⁸F]FED6 was 3.5 fold higher in A431 cells than in MCF7 cells (Figure 17 A). Higher expression of both p-EGFR (Y1068), which corresponds to active EGFR and EGFR in A431 compared to MCF7 cells was confirmed by western blot (Figure 17B). To verify if the difference in [¹⁸F]FED6 uptake between A431 and MCF7 cells was EGFR related, the protein was silenced by siRNA. There was a 50 % decrease in the uptake of [¹⁸F]FED6 at 72 h after treatment with EGFR siRNA compared to scramble treated A431 cells (Figure 17C). Finally, specificity of the radiotracer was further assessed with a blocking study, which involved pre-treatment of A431 cells with 10 µM of non-radiolabelled FED6. Rather than an expected decrease, a 4.5 fold increase in uptake of [¹⁸F]FED6 was measured (Figure 17C). Western blot analysis confirmed a decrease in p-EGFR (Y1068) expression following both FED6 and EGFR siRNA pre-treatment, and a knock down of EGFR following siRNA treatment (Figure 17D).

These uptake experiments suggested that [¹⁸F]FED6 was sensitive for EGFR expression, binding with higher affinity to EGFR overexpressing cells than to low EGFR expressing cells. Transfection with EGFR siRNA also confirmed the sensitivity of FED6 for EGFR. There appeared to be a component of non specific binding, as indicated by relatively high residual uptake of [¹⁸F]FED6 in the A431 cells after EGFR siRNA transfection, although the outcome could be explained in part by the incomplete knockdown of EGFR in this cell line. However, the increase in tracer uptake following pre-treatment with non radiolabelled FED6 goes against the other findings and warrants further investigation.

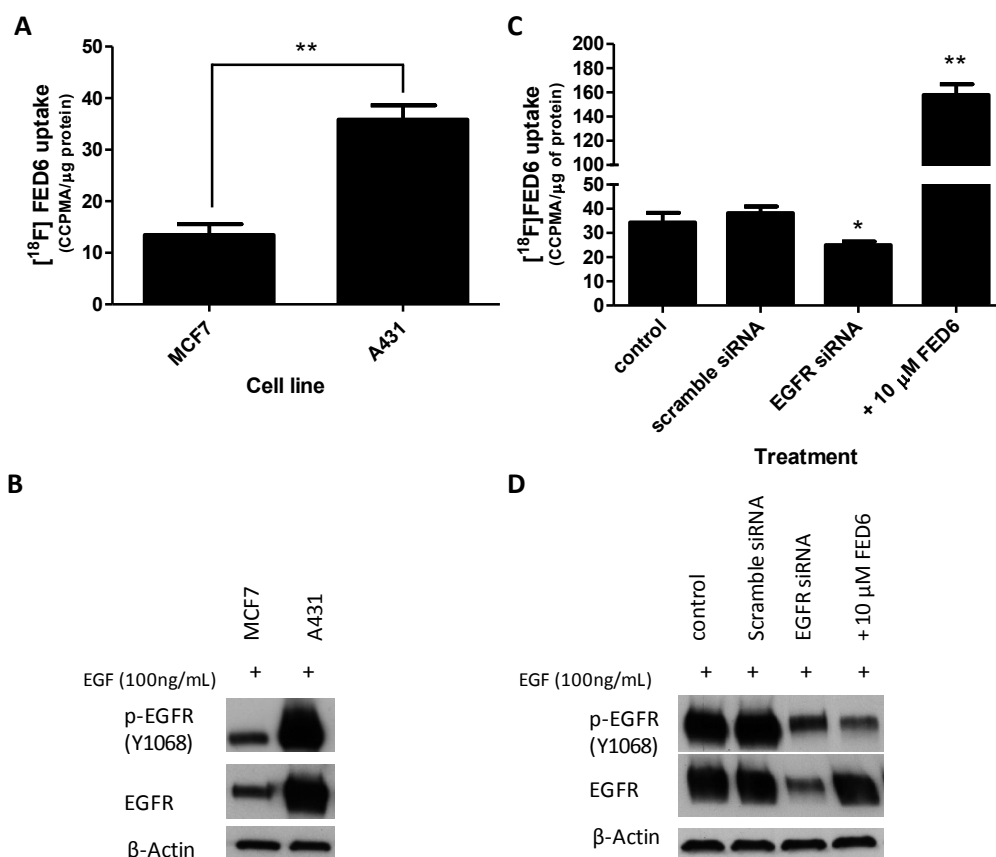


Figure 17: *In vitro* uptake of [¹⁸F]FED6 following EGFR siRNA treatment.

A- Protein normalised uptake of [¹⁸F]FED6 in MCF7 and A431 cells following 1 h incubation with 0.37 MBq [¹⁸F]FED6. B- Protein expression of p-EGFR (Y1068) and EGFR in MCF7 and A431 cells. C- Protein normalised uptake of [¹⁸F]FED6 in A431 cells following 1 h incubation with 0.37 MBq [¹⁸F]FED6 after 72 h transfection with 25 nM EGFR or scramble siRNA or 1 h pre-treatment with 10 μM FED6. D- p-EGFR (Y1068) and EGFR protein expression in A431 cells following EGFR or scramble siRNA treatment. Data show mean ± SE of triplicate from one representative experiment carried out twice. Stars indicate statistical difference between values of two-tailed unpaired t-test (* p ≤ 0.05 **p ≤ 0.01).

Since the cyanoquinoline compounds were designed, the significance of the mutational status of EGFR, particularly in NSCLC, has emerged. In fact, mutational status has been shown to play an important role in the therapeutic response of NSCLC patient (Mok et al., 2009). Patients expressing active mutant forms of EGFR show greater response to TKI treatment compared to patients expressing wild type EGFR. With this in mind, having confirmed the sensitivity of FED6 for EGFR, FED6 was investigated in the context of binding to mutant EGFR.

3.2 Sensitivity of wild type and active mutant EGFR expressing NSCLC to FED6

In order to assess the cyanoquinoline molecule, FED6, as a probe for the imaging of mutant vs WT EGFR, the affinity of FED6 for WT and del 746-750 active mutant EGFR, was measured and compared with the affinity of gefitinib in a cell based setting. As a proxy for receptor affinity, the inhibitory potential of the compounds were assessed in H358 and A549, two adenocarcinoma NSCLC cell lines,

which both expressed WT EGFR and H1650 that expressed del 746-750 EGFR. The inhibition of EGFR activation was measured following 3 h of gefitinib or FED6 treatment by measuring the phosphorylation of tyrosine 1068 which is involved in the autophosphorylation and activation of EGFR (Downward et al., 1984a).

The active mutant EGFR, H1650 cell line, constitutively expressed activated EGFR, as indicated by the presence of p-EGFR (Y1068) in unstimulated conditions (Figure 18A). This was in opposition to wild type expressing EGFR cell lines, A549 and H358, which only expressed p-EGFR (Y1068) upon EGF stimulation. The densitometry measurements from the blots were used to determine the percentage inhibition of p-EGFR (Y1068) (Figure 18B). The IC_{50} values obtained from these plots were tabulated in Figure 18C. The IC_{50} value of gefitinib was highest in the A549 cells at 0.4 μ M compared to 0.08 and 0.1 in H358 and H1650 cells, respectively (Figure 18C1). The IC_{50} value of gefitinib in the H1650 cells expressing del 746-750 mutant EGFR, was not significantly different to the IC_{50} values measured in WT EGFR cells lines. As previously reported in the literature despite expressing del 746-750 mutant EGFR, H1650 cells were resistant to gefitinib (Sos et al., 2009). In contrast, the IC_{50} of FED6 was over 10 fold lower in the del746-750 mutant EGFR expressing H1650 cell line with a value of 0.04 μ M compared to 0.72 μ M and 0.65 μ M in WT EGFR expressing A549 and H358 cell lines, respectively (Figure 18C2).

In summary, gefitinib appeared more active at inhibiting EGFR compared to FED6 in WT EGFR expressing cells lines, and this was illustrated with lower IC_{50} values. However, FED6 appeared more selective for mutant EGFR.

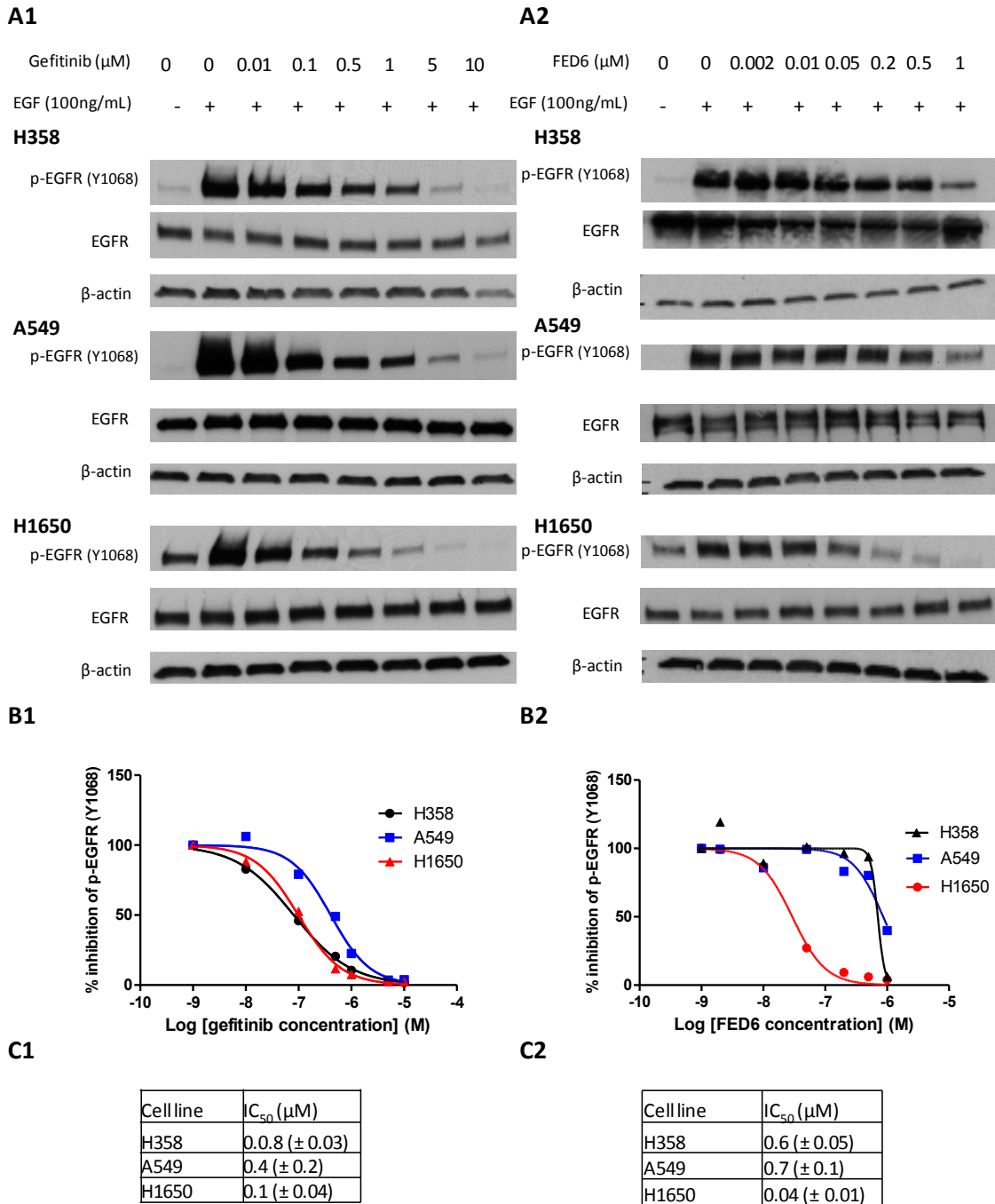


Figure 18: Inhibition of EGFR activation in WT and del 746-750 mutant EGFR expressing cells following gefitinib and FED6 treatment.

A- Western blots showing the changes in phosphorylation of EGFR at tyrosine 1068 following gefitinib (A1) or FED6 (A2) treatment. B- Percentage inhibition of p-EGFR (Y1068) normalised to EGFR levels following gefitinib (B1) or FED6 (B2) treatment determined from densitometry of western blots. C- Table summarising the average IC_{50} values \pm SE, obtained from the percentage inhibition of p-EGFR plots, of gefitinib (C1) or FED6 (C2). Data show mean \pm SE from three separate experiments.

To investigate whether the increased affinity of FED6, for del 746-750 EGFR, compared to WT EGFR, would translate into preferential binding of [¹⁸F] radiolabelled FED6 in active mutant EGFR expressing cells, the uptake of [¹⁸F]FED6 was measured in these cells.

3.3 [¹⁸F]FED6 *in vitro* and *in vivo* uptake in A549 vs H1650

In order to assess the binding of [¹⁸F]FED6 to mutant and WT EGFR, a cell uptake assay in A549, H358 and H1650 cells was carried out. After 1 h incubation with [¹⁸F]FED6, H358 cells showed the highest levels of uptake of [¹⁸F]FED6, over 80 CCPMA/μg of protein. The uptake in the A549 cells was 25 CCPMA/μg of protein, 2.5 times higher than the uptake in the H1650 cells which was 10 CCPMA/μg of protein (Figure 19A). The expression of both p-EGFR (Y1068) and EGFR were highest in the A549 cells compared to H1650 and H358 cells, as indicated by the western blot and corresponding densitometry in Figure 19BC. Therefore, the higher uptake of [¹⁸F]FED6 in the H358 cells was not related the level of expression of EGFR.

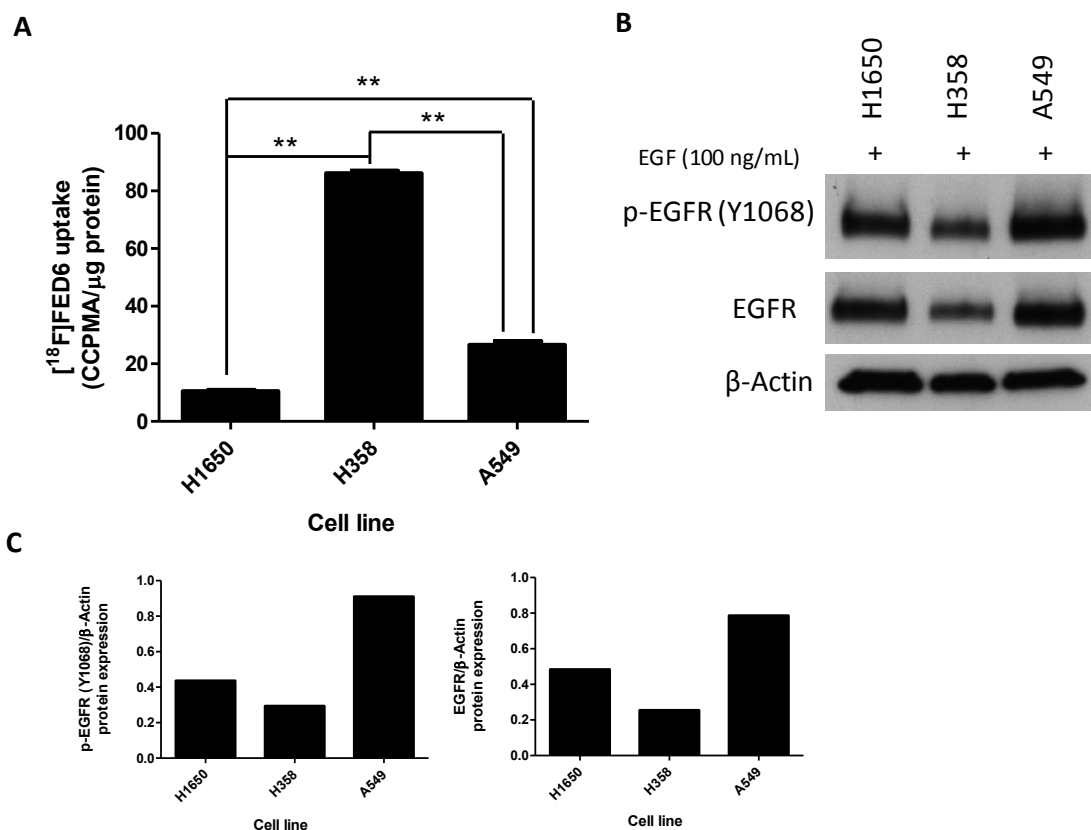


Figure 19: *In vitro* uptake of [¹⁸F]FED6 in H1650, H358 and A549 cells.

A- [¹⁸F]FED6 uptake in H358, A549 and H1650 cells following 1 h incubation with 0.37 MBq of [¹⁸F]FED6. Data show mean values of corrected counts per minute acquired per μg of protein ± SE of triplicate samples from one representative experiment carried out three times. Stars indicate statistical difference between values of two-tailed unpaired t-test (**p<0.01). B- Differential protein expression of p-EGFR (Y1068) and EGFR in H358, A549 and H1650 cells. C- Densitometry values of p-EGFR (Y1068) and EGFR expression corrected for β-actin expression.

Furthermore, higher affinity of FED6 for del 746-750 EGFR (Figure 18C2) did not correspond to higher uptake of [¹⁸F]FED6 in del 746-750 EGFR expressing H1650 cells (Figure 19A).

Following the *in vitro* uptake of [¹⁸F]FED6 and to establish that the effects seen were not simply due to an *in vitro* artefact, the uptake of [¹⁸F]FED6 in xenograft models of the cell lines studied was undertaken via PET imaging. Imaging studies of the H358 xenografts could not be completed, as these tumours became extensively angiogenic, and formed pockets of blood, as soon as the tumour volumes reached 30 to 40 mm³. PET imaging of A549 and H1650 xenografts was therefore carried out. Both H1650 and A549 mouse xenograft were injected intravenously via the tail vein with 3.7 MBq of [¹⁸F]FED6 and underwent a 60 min dynamic PET scan. The result of the PET scan are summarised in Figure 20. The sagittal images indicated that the uptake of [¹⁸F]FED6 in the tumours, marked by white arrows, was relatively low compared with a high uptake in the gastrointestinal tract (Figure 20A). The time activity curves of [¹⁸F]FED6 in the tumours, which were plotted in Figure 20B, showed an initial uptake of the radiotracer in the tumour followed by washout and decrease in [¹⁸F]FED6 with time. There was no statistical significant difference between the normalised uptake value at 60 min (NUV₆₀) post [¹⁸F]FED6 injection in the A549 and the H1650 xenografts (Figure 20C). The NUV₆₀ values were 0.32 and 0.39 % ID/mL in A549 and H1650 tumours, respectively. The area under the time activity curves (AUC), were the same in both models with an average value of 25 %ID/mL*min.

The protein expression analysis of the tumour lysates showed that p-EGFR (Y1068) and total EGFR were slightly higher in the A549 tumours than in the H1650 tumours (Figure 21).

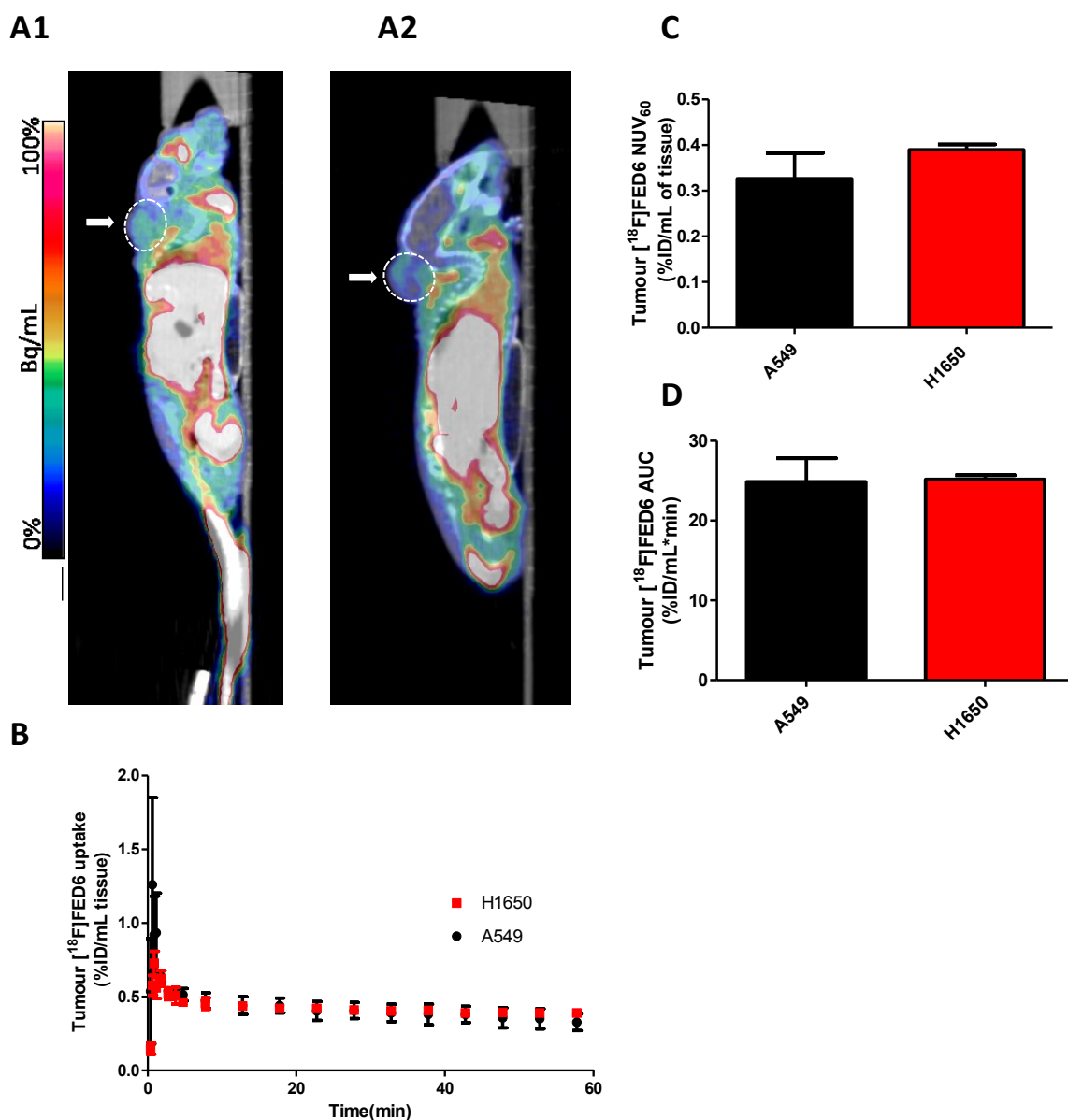


Figure 20: *In vivo* PET imaging of A549 and H1650 xenografts with [^{18}F]FED6.

A- Sagittal merged CT/PET image of a BALB/c nu/nu mouse obtained at 60 min following an i.v. injection of 3.7 MBq of [^{18}F]FED6 with the scanning of. A1- H1650 xenograft. A2- A549 xenograft. Tumour position indicated by white arrow. Data show images collected from one representative mouse from each group B- Time activity curves, corresponding to the uptake of [^{18}F]FED6 in the tumour against time. C- Uptake of [^{18}F]FED6 at 60 min post tracer injection normalised to injected dose. D- Area under the tumour time activity curve values. For B-D- Data represent mean \pm SE of n=3 per group. No statistical difference was found between values after carrying out a two-tailed unpaired t-test.

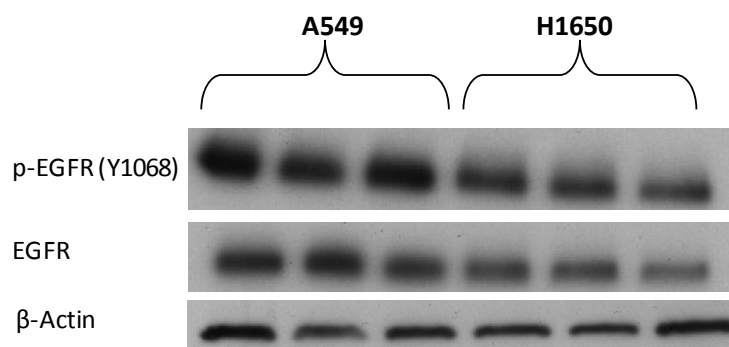


Figure 21: p-EGFR and EGFR levels of A549 and H1650 tumours.

Expression of p-EGFR (Y1068) and EGFR in tumour lysates of A549 and H1650 xenografts previously imaged via PET. Each column represents one lysed tumour sample.

In summary, the *in vivo* PET imaging data did not correlate with the *in vitro* cell uptake experiment that showed a 2.5 fold higher uptake of [¹⁸F]FED6 in A549 cells compared to H1650 cells.

3.4 Testing FED6 in active and resistant mutant NSCLC cell lines

3.4.1 Western blot analysis of gefitinib and FED6 Inhibition of p-EGFR.

To further investigate FED6 in the context of imaging mutant EGFR, cell lines expressing mutant forms of EGFR, including L858R active mutant and T790M resistant mutant EGFR were used. First, the inhibition of EGFR activation following 3 h treatment with gefitinib or FED6 was determined. PC9 (del 746-750), PC9ER (del 746-750/T790M), H3255 (L858R) and H1975 (L858R/T790M) all showed constitutive activation of EGFR as indicated by the presence of the p-EGFR (Y1068) band in unstimulated conditions (Figure 22A). Both gefitinib and FED6 treatment led to higher levels of p-EGFR Y1068 inhibition in active mutant EGFR expressing cells, H3255 and PC9 compared to resistant mutant expressing H1975 and PC9ER, as depicted in Figure 22.

The densitometry measurements from the blots were used to determine the percentage inhibition of p-EGFR (Y1068) (Figure 22B). The IC₅₀ values obtained from these plots were tabulated in Figure 22C. The IC₅₀ values for gefitinib were lowest in PC9 and H3255 cells at 0.014 and 0.15 μM, respectively compared to 1.1 and > 10 μM in PC9ER and H1975 cells, respectively.

The IC₅₀ of FED6 was lowest in the H3255 cells, at 0.008 μM, compared with 0.02 μM in PC9 and 0.045 μM in PC9ER cells. At the concentrations selected, the IC₅₀ of FED6 was not reached in the resistant mutant EGFR expressing H1975 cells. In addition, FED6 showed a stronger affinity for EGFR in H3255 and PC9ER cells compared to gefitinib. The IC₅₀ of FED6 was 24 fold lower than the IC₅₀ of gefitinib in PC9ER cells. The irreversible nature of FED6 binding could explain the increased affinity of this compound in PC9ER cells compared to gefitinib.

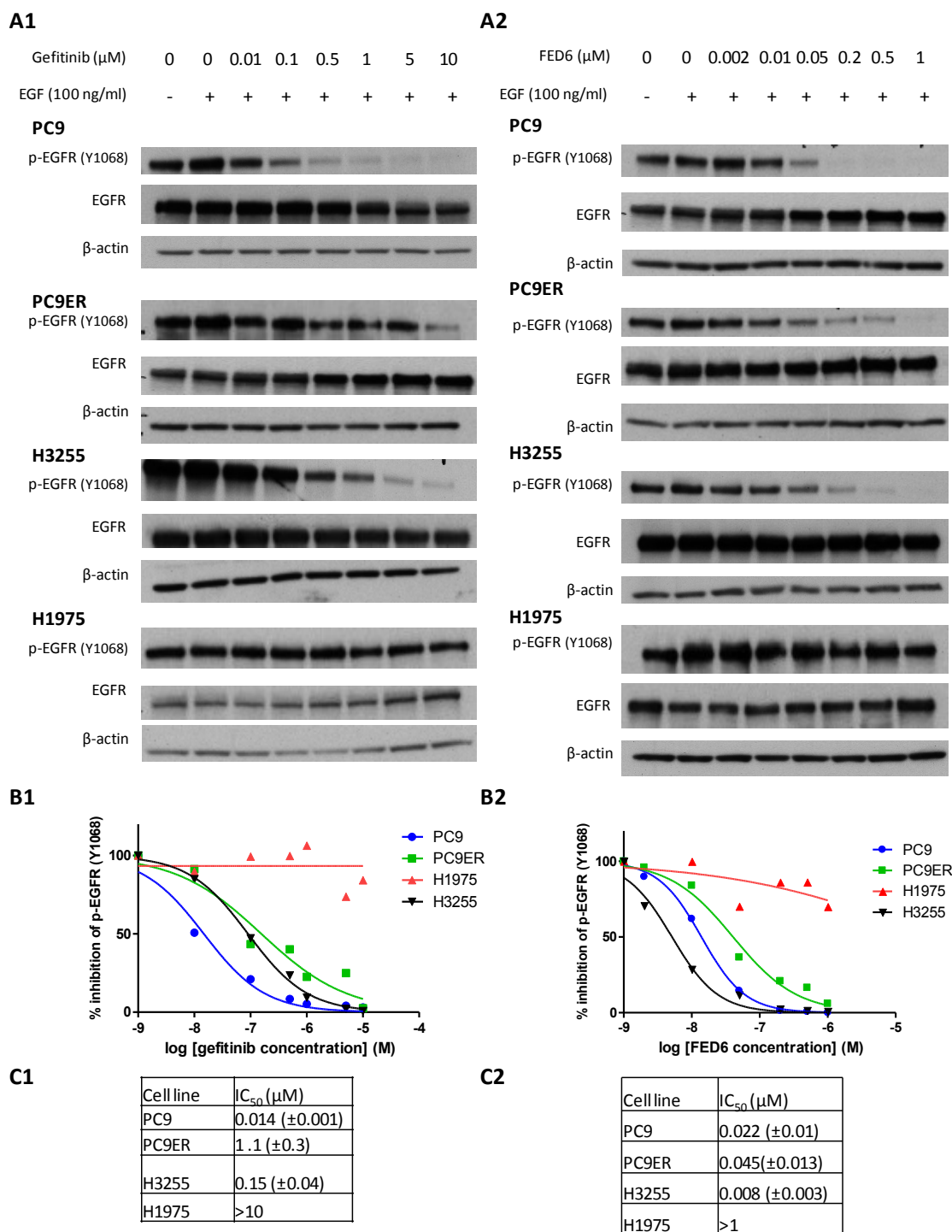


Figure 22: Inhibition of EGFR activation in NSCLC following gefitinib and FED6 treatment.

A- Western blots showing changes in phosphorylation of EGFR at tyrosine 1068 following gefitinib (A1) or FED6 (A2) treatment of PC9, PC9ER, H3255 and H1975 cells. B- Percentage inhibition of p-EGFR (Y1068) normalised to EGFR levels following gefitinib (B1) or FED6 (B2) treatment determined from densitometry of western blots. C- Table summarising the average IC_{50} values \pm SE, obtained from the percentage inhibition of p-EGFR plots, of gefitinib (C1) or FED6 (C2). Data show mean \pm SE from three separate experiments.

3.4.2 [¹⁸F]FED6 *in vitro* uptake in active and resistant mutant NSCLC cells.

A cell uptake assay was performed in the different NSCLC cells, to investigate whether the higher affinity of FED6 for active mutant EGFR and lower affinity of FED6 for resistant mutant EGFR, was translated into differential binding of [¹⁸F]FED6 (Figure 23A). H3255 cells showed the highest uptake of [¹⁸F]FED6 with a value of 130 CCPMA/μg of protein and the lowest level of tracer uptake was measured in H1975 cells with a value of 12 CCPMA/μg of protein. Finally, the uptake of [¹⁸F]FED6 was higher in the active mutant PC9 compared to resistant mutant PC9ER cells, with values of 88, and 72 CCPMA/μg of protein, respectively. This difference was however not statistically significant.

H3255 cells which had the highest uptake of [¹⁸F]FED6 also expressed the highest levels of p-EGFR (Y1068) and total EGFR (Figure 23BC). Furthermore, H1975 cells which had the lowest uptake of [¹⁸F]FED6 also expressed the lowest levels of both p-EGFR (Y1068) and total EGFR (Figure 23BC). Thus, the difference in uptake could also be a result of the levels of expression of EGFR rather than differential binding to active and resistant mutant EGFR. The levels of expression of p-EGFR (Y1068) and EGFR were similar in PC9 and PC9ER cells.

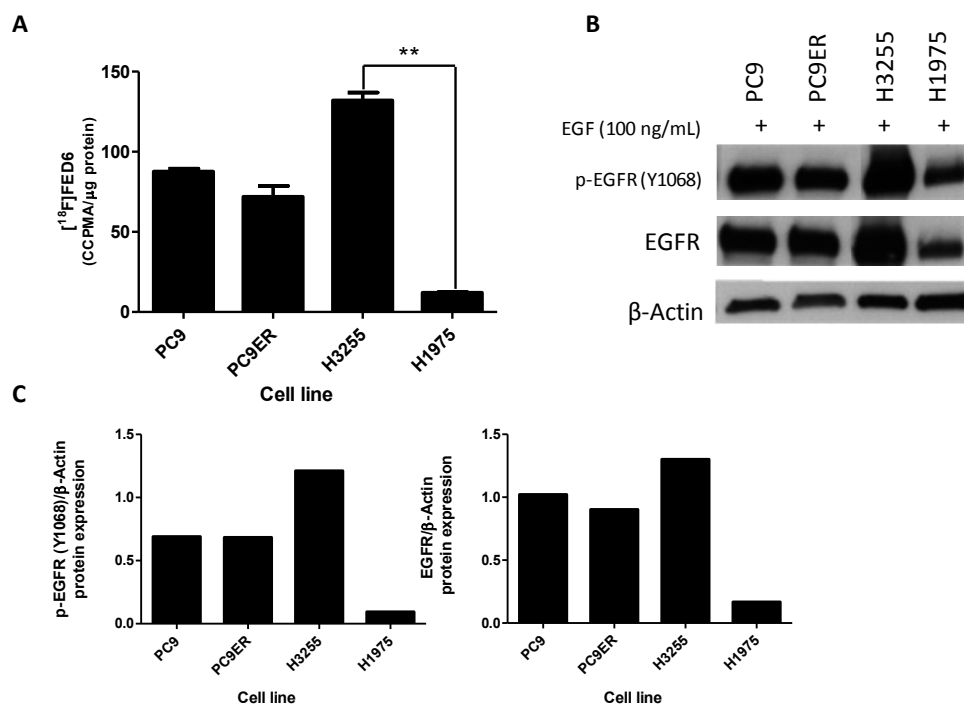


Figure 23: *In vitro* uptake of [¹⁸F]FED6 in NSCLC.

A- Protein normalised uptake of [¹⁸F]FED6 in NSCLC cells following 1 h incubation with 0.22 MBq [¹⁸F]FED6. Data show mean ± SE of triplicates from one representative experiment performed two times. Stars indicate statistical difference between values of two-tailed unpaired t-test (**p≤0.01) B- Differential protein expression of p-EGFR (Y1068) and EGFR in NSCLC cell lines. C- Densitometry values of p-EGFR (Y1068) and EGFR protein expression normalised for β-actin protein expression.

In order to better understand whether the differential uptake of [¹⁸F]FED6 in the NSCLC studied was linked to p-EGFR (Y1068) protein expression, EGFR protein expression and or FED6 affinity in these different cell lines, correlation graphs were plotted (Figure 24). With the exception of the H358 cells there was a strong correlation between levels of p-EGFR (Y1068) and EGFR protein expression and [¹⁸F]FED6 uptake. With the highest levels of [¹⁸F]FED6 uptake corresponding to the highest expression of p-EGFR (Y1068) or EGFR (Figure 24AB). There didn't seem to be a direct correlation between the uptake of [¹⁸F]FED6 and the IC₅₀ of FED6 which were obtained from the western blots and plotted in Figure 18 and Figure 22. The higher affinity of FED6 in active mutant EGFR expressing cell lines did not always correlate with a higher uptake of [¹⁸F]FED6 as is illustrated with the H1650 cell line (Figure 24C).

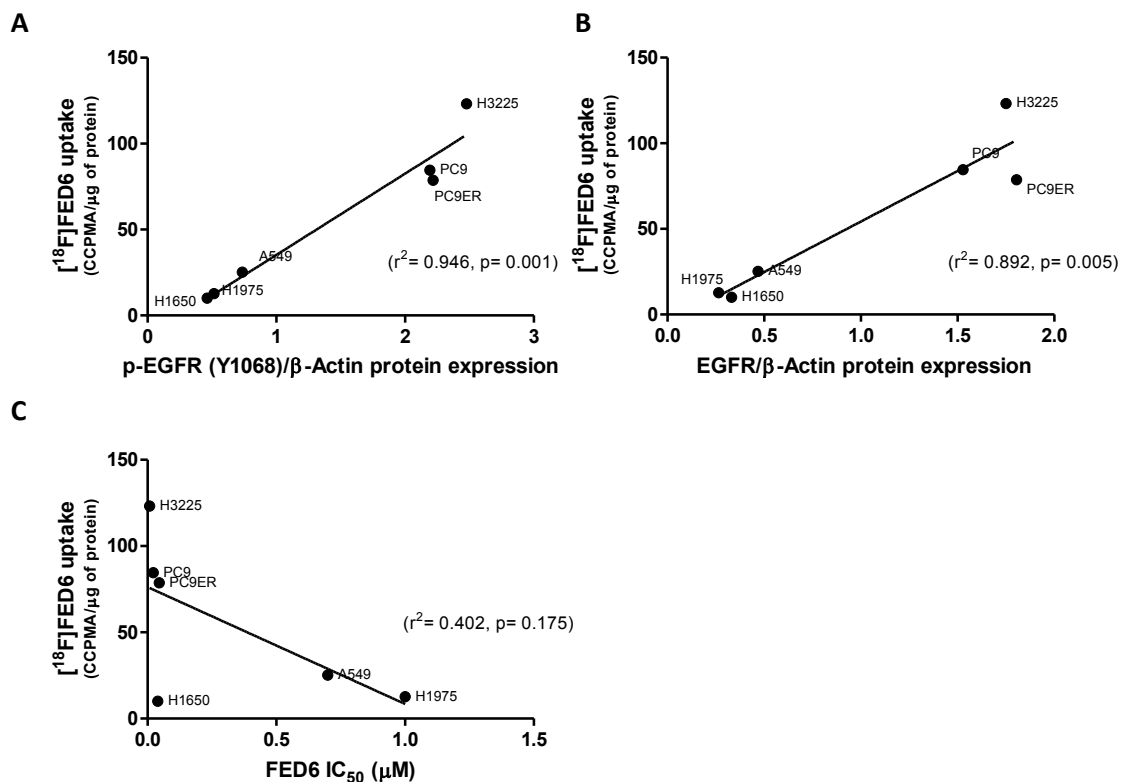


Figure 24: Correlation between [¹⁸F]FED6 uptake, EGFR protein expression and FED6 IC₅₀.

A- [¹⁸F]FED6 uptake over protein expression of p-EGFR (Y1068) normalised to β-Actin. B- [¹⁸F]FED6 uptake over protein expression of EGFR normalised to β-Actin. Protein expression values obtained from densitometry reading of western blots. Data show values from one representative experiment carried out in triplicate. C- [¹⁸F]FED6 uptake over IC₅₀ of FED6. IC₅₀ values expressed as mean of IC₅₀ values obtained from p-EGFR (Y1068) inhibition plots following FED6 treatment from three separate experiments. r^2 correlation values indicated in brackets, statistically significant correlation indicated by $p < 0.05$.

In conclusion, higher levels of binding of [¹⁸F]FED6 in EGFR overexpressing vs low EGFR expressing cells were confirmed. Then, FED6 showed higher affinity for inhibiting EGFR activity in active mutant EGFR vs WT or resistant mutant expressing NSCLC cells. The *in vitro* uptake of [¹⁸F]FED6 in the different mutant expressing cell lines gave mixed results, with the uptake of the radiotracer not consistently correlating with the previously measured affinity of FED6 in these different cells. Furthermore, the *in vivo* PET imaging of A549 and H1650 xenografts showed no differential tumour uptake of [¹⁸F]FED6 in these two models. The tumour uptake was low and the TAC indicated a gradual washout of the tracer over time.

The inconclusive results of the *in vitro* uptake experiments and the low tumour uptake *in vivo* led us to further investigate the properties of FED6. This suggests that other factors could affect the relationship between affinity of FED6 to active mutant or resistant mutant EGFR and the cell uptake of [¹⁸F]FED6. Indeed, other quinoline based molecules have been demonstrated to be substrates of the ABC transporters. Abourbeh *et al* showed that the EGFR tracer they had developed, ML04, was a substrate for ABCB1 and that low tumour uptake of this tracer was a result of efflux via ABCB1 transporter (Abourbeh et al., 2007).

The possible substrate specificity of FED6 for the ABC transporters was investigated, to establish whether this could explain some of the results discussed above.

Chapter 4: Interaction of FED6 with ABC transporters

MDR, which can result in the overexpression of members of the ABC transporters has been reported in several cancers (Litman et al., 2001). The expression of these transporters in tumours is an important factor to take into account when designing a radiotracer. Indeed, if a radiotracer is a substrate of the ABC transporter, it will be actively extruded from the tumour, especially if the tumour expresses high levels of transporters. This will result in poor accumulation of the radiotracer in the tumour. Several EGFR targeting TKIs have been shown to interact with the ABC transporters, this includes EKB-569 from which the cyanoquinoline series of compounds were designed (Kitazaki et al., 2005, Ozvegy-Laczka et al., 2004, Nakamura et al., 2005, Hegedus et al., 2012). It was therefore important to investigate the possible substrate specificity of FED6 and other members of the cyanoquinoline family for ABC transporters, and determine how this may impact the PET imaging of EGFR with [^{18}F]FED6.

4.1 Physico-chemical properties of compounds can help predict ABC transporter substrate specificity.

It has been reported in the literature that substrates of the ABC transporters share common physico-chemical properties. For instance substrates for ABCB1 are characterised by one or more of the following: a molecular weight (MW) > 400, hydrophobicity determined by $1 < \log P > 5$, sum of oxygen and nitrogen atoms > 8, polar surface area (PSA), defined as the sum of surfaces of polar atoms (usually oxygen, nitrogen, and attached hydrogen) > 85\AA^2 (Varma et al., 2005, Dellinger et al., 1992, Gottesman and Pastan, 1993, Kaliszczak et al., 2010). The number of aromatic rings in a compound have been reported to influence ABCG2 substrate specificity with compounds containing greater than two aromatic rings showing increased substrate specificity for ABCG2 (Nakagawa et al., 2006). Finally the pKa of a molecule has also been reported to play a role in ABC transporter substrate specificity, and this by modifying the thresholds listed above (Didziapetris et al., 2003, Varma et al., 2005).

In order to predict the substrate specificity of FED6 and other closely related members of the cyanoquinoline family of molecules for the different transporters and to use this information to design future compounds, the relevant physico-chemical properties of the series of compounds were tabulated (Table 9).

The cyanoquinoline series of compounds possess several of the physico-chemical properties, which are associated with ABCB1 substrate specificity. With the exception of FED14 (precursor molecule in the series), all the compounds in the series had MW > 400, PSA > 85\AA^2 , and $1 < \log P > 5$.

Table 9: Physico-chemical properties of the FED series in relation to prediction of ABC transporter substrate specificity

Compounds	Structures	MW	Log P*	PSA	(N+O)	Aromatic rings	pKa
EKB-569		468	4.18	90	7	3	8.8
FED2		454	3.8	100	7	3	9.6
FED3		500	4.38	90	7	3	7.2
FED6		567	3.85	130	10	3	7.4
FED9		500	3.73	100	7	3	8.4
FED14		357	3.54	84	5	3	4.6

MW: Molecular weight and the sum of oxygen and nitrogen atoms (N+O) calculated Log P and polar surface area (PSA) were determined as described in materials and methods. pKa : logarithmic value of acid dissociation constant. Values in red indicate properties characteristic of substrate specificity to ABC transporters.

4.2 Testing for ABCB1, ABCG2, ABCC1 substrate specificity.

ABC transporters form a large family of over 48 proteins, divided into seven subfamilies (Dean et al., 2001). Three members of this large family which have been most commonly involved in MDR; ABCB1, ABCG2 and ABCC1 will be investigated in this report (Fletcher et al., 2010).

4.2.1 Substrate specificity for ABCB1

With a MW > 400, log P > 3 and a PSA > 85 Å², the physicochemical determinants of FED6 would predict its interaction with ABCB1. To verify its interaction with the transporter, an isogenic model was used: 3T3 cells (transfected with an empty vector) and 3T3-MDR1 cells (transfected with the

human MDR1 gene which encodes for ABCB1), with a differential expression of the transporter (Figure 25), and investigated the impact of FED6 treatment on cell viability. If a drug is a substrate for ABCB1, it will be actively transported out of the cell. Thus, higher concentrations of the drug will be required to cause cytotoxicity in the cell line that overexpresses ABCB1 compared to the cell line expressing no transporter.

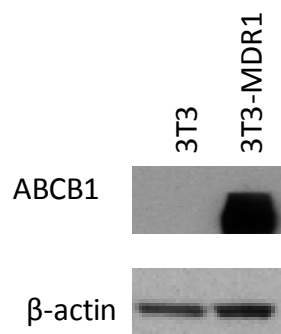


Figure 25: ABCB1 protein expression in 3T3 and 3T3-MDR1.

Levels of ABCB1 (MDR1) protein expression as determined by western blotting.

The cyanoquinoline series have been designed based on the structure of TKI, EKB-569 that is associated with anti-proliferative activity. FED6 and other derivatives could also induce cytotoxicity and this characteristic could be exploited to assess ABCB1 substrate specificity.

As well as comparing the levels of cytotoxicity in 3T3 and 3T3-MDR1 cells the impact of a specific inhibitor of ABCB1, zosuquidar (Shepard et al., 2003) on the cytotoxicity of FED6 in 3T3 and 3T3-MDR1 cells was assessed.

The optimal concentration of zosuquidar required to inhibit ABCB1 was assessed by measuring the change in fluorescence levels of calcein by performing a calcein acetomethoxy (calcein AM) assay. Traditionally used to monitor cell viability, calcein AM, a known substrate of ABCB1 (Varma et al., 2005), has also been used to monitor active efflux. In live cells, the non-fluorescent calcein AM is converted to a green-fluorescent calcein after acetoxymethyl ester hydrolysis by intracellular esterases. In cells expressing ABCB1, calcein AM will be extruded out the cells, leading to low levels of fluorescent calcein. At baseline, the levels of fluorescence in untreated control 3T3-MDR1 cells were equal to background levels due to high levels of efflux of calcein AM. This was in opposition to the high fluorescence measured in the 3T3 cells (Figure 26). Levels of fluorescence increased dose dependently with zosuquidar in the 3T3-MDR1 cells, with levels plateauing off at 0.3 μ M. Higher

concentrations of zosuquidar did not lead to increased fluorescence. At 0.3 μM of zosuquidar, the activity of ABCB1 was completely inhibited and it no longer extruded calcein AM. This resulted in levels of fluorescence in the 3T3-MDR1 reaching those measured in the 3T3 cells. The optimal concentration of zosuquidar was found to be 0.3 μM for further experiments.

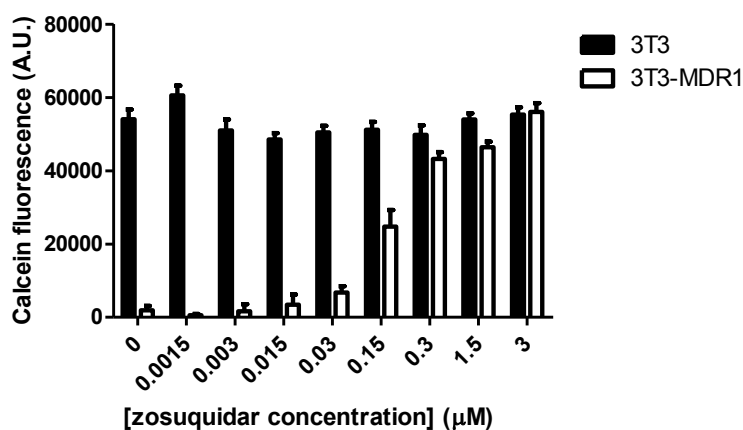


Figure 26: Calcein fluorescence in 3T3 and 3T3-MDR1 cells following zosuquidar treatment.

Levels of calcein, in 3T3 or 3T3-MDR1 cells following 1 h pre-treatment with increasing concentrations of zosuquidar. Data show means \pm SE of quadruplet from one representative experiment. A.U.: Arbitrary unit of fluorescence.

Vinblastine is a known substrate of ABCB1 and was used as a positive control (Ambudkar et al., 1999). Growth inhibitory effect of vinblastine was tested in 3T3 and 3T3-MDR1 cells with or without pre-treatment with zosuquidar at 0.3 μM . 3T3-MDR1 cells were more resistant to vinblastine than 3T3 cells (Figure 27A). Following zosuquidar pre-treatment the sensitivity of 3T3-MDR1 cells was the same as that of 3T3 cells (Figure 27B). The GI_{50} (i.e: 50 % reduction in cell growth) of vinblastine decreased from 220 nM, without pre-treatment, to 1.1 nM, with zosuquidar pre-treatment, in the 3T3-MDR1 cells. This represented a 200 fold increase in the cytotoxicity of vinblastine following zosuquidar pre-treatment. In the 3T3 cells, the GI_{50} was 1.8 nM without pre-treatment and 1.5 nM with pre-treatment.

Inhibition of ABCB1 efflux of vinblastine via zosuquidar, led to an increase in the cytotoxicity of vinblastine in the 3T3-MDR1 cells.

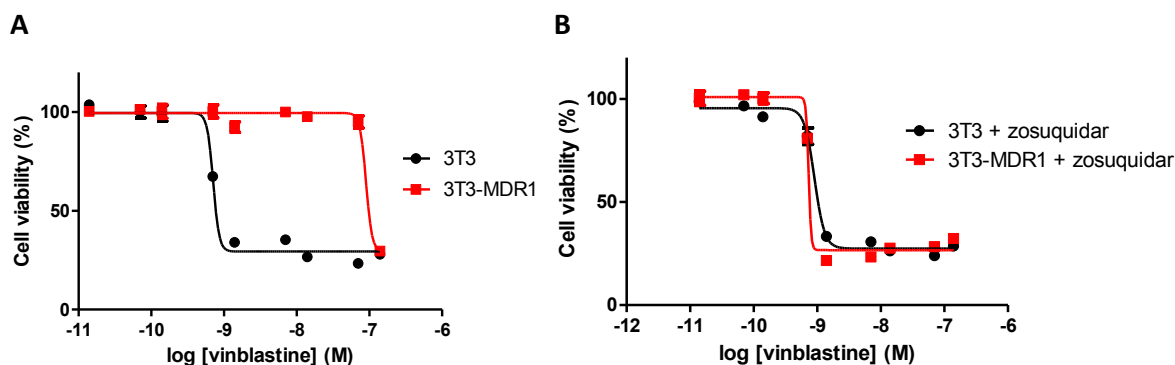


Figure 27: Cell viability curves showing reversal of resistance to vinblastine in 3T3-MDR1 following zosuquidar treatment.

A-B- Cell viability plots of 3T3 and 3T3-MDR1 cells following vinblastine treatment with (B) or without (A) pre-treatment with 0.3 μM of zosuquidar. Data show mean \pm SE of $n = 3$ replicates from one experiment carried out three times.

Having characterised the cells with known inhibitors, further testing of the growth inhibitory effect of the cyanoquinoline series was performed. FED6 and FED2 were associated with a GI_{50} of > 100 and $37 \mu\text{M}$ in the 3T3-MDR1 cells, respectively, and with a GI_{50} of 10 and $7 \mu\text{M}$ in the 3T3 cells. This represents a 10- and 5-fold increase in GI_{50} values, for FED6 and FED2, respectively, in the ABCB1 overexpressing cell line (Table 9). This suggested that both compounds were being effluxed via ABCB1. The GI_{50} values of FED14, the core cyanoquinoline moiety, from which other cyanoquinoline molecules were synthesised, were similar in both cell lines. Following zosuquidar pre-treatment of the 3T3-MDR1 cells, the GI_{50} value decreased over 7-fold for FED6, 6.1-fold for FED2, and 2.1-fold for EKB-569 (Table 10). This confirmed that the lower cytotoxicity of EKB-569, FED2 and FED6 in the 3T3-MDR1 cells was a result of efflux via ABCB1.

Table 10: Growth inhibitory effect associated with the series of cyanoquinoline molecules in 3T3 and 3T3-MDR1 cells.

		3T3		3T3-MDR1	
		control	+ zosuquidar	control	+ zosuquidar
EKB-569	GI ₅₀ (μM)	1.1	1.2	5.8	2.7
	SE	0.6	0.6	0.7	0.8
FED2	GI ₅₀ (μM)	7	4.5	36	5.9
	SE	1.2	0.8	1.1	0.6
FED6	GI ₅₀ (μM)	11	7.8	>100	14
	SE	1	0.7		0.6
FED14	GI ₅₀ (μM)	15	15	8.7	12
	SE	0.7	0.7	0.7	0.6
Vinblastine	GI ₅₀ (nM)	1.8	1.5	220	1.1
	SE	1	1.2	0.8	1.1

GI₅₀ values were obtained for each experiment. Data represents mean GI₅₀ and SE obtained from three separate experiments.

Ratios of the GI₅₀ in 3T3-MDR1 to GI₅₀ in 3T3, in the presence and absence of zosuquidar, were plotted in Figure 28. Compounds associated with a ratio > 2 were considered to be actively effluxed by the ABC transporters. This in turn limited their growth inhibitory effect. In the absence of ABCB1 inhibitor, zosuquidar, EKB-569, FED2 and FED6 had ratios of GI₅₀ of 4.4, 5.4 and > 20, respectively. In the presence of zosuquidar all ratios were below the threshold of 2, further indicating substrate specificity for ABCB1.

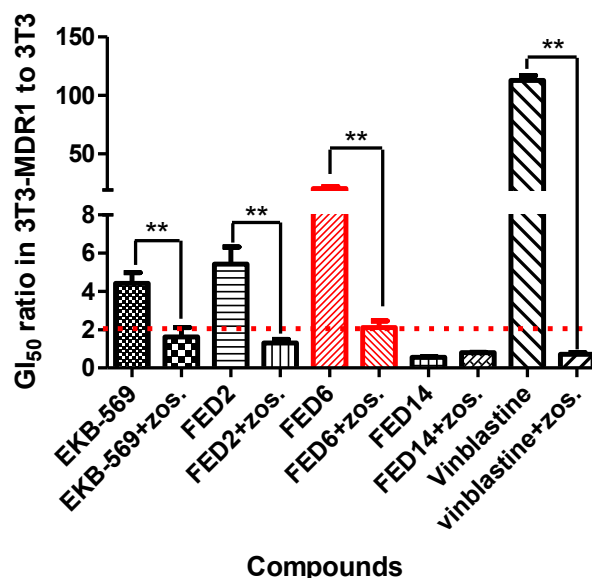


Figure 28: Impact of zosuquidar on the cytotoxicity of cyanoquinoline derivatives.

Ratios of GI₅₀ in 3T3-MDR1 and GI₅₀ in 3T3 were determined for each experiment. Data show mean ± SE of ratios from three experiments. Vinblastine was used as a positive control. Red dashed line indicates threshold for ABCB1 substrate specificity. FED6 indicated in red. Zos: zosuquidar. Stars indicate statistical difference between values of two-tailed unpaired t-test (**p ≤ 0.01).

4.2.2 Substrate specificity for ABCG2

FED6 is associated with physicochemical features that would predict its interaction with ABCG2: It contains three aromatic rings and has a sum of nitrogen and oxygen atoms above ten. To verify its interaction with the transporter, MCF7 and a mitoxantrone resistant, MCF7MX cell line, which overexpresses ABCG2 were used to investigate the impact of FED6 treatment on cell viability (Figure 29).

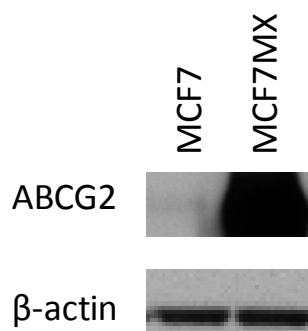


Figure 29: Protein expression of ABCG2 in MCF7 and MCF7MX.

Levels of ABCG2 protein expression as determined by western blot.

To investigate the ABCG2 substrate specificity of the cyanoquinoline derivatives, cells were pre-treated with or without the ABCG2 specific inhibitor fumitremorgin C (FTC) (Rabindran et al., 2000). A concentration of 10 μ M was previously shown to inhibit ABCG2 without causing toxicity (Robey et al., 2001) and was used in subsequent studies.

The growth inhibitory effect of mitoxantrone, a known substrate of ABCG2 was evaluated in MCF7 and MCF7-MX cells (Doyle and Ross, 2003). The GI_{50} was 11 μ M in MCF7 cells and 2500 μ M in MCF7MX cells without pre-treatment, representing a 234 fold decrease in cytotoxicity in the ABCG2 expressing cells. Following FTC pre-treatment the sensitivity of MCF7MX cells was increased and was similar to that of MCF7 cells (Figure 30). The GI_{50} was 23 μ M in MCF7MX cells after pre-treatment with FTC, representing a 110 fold increase in cytotoxicity of mitoxantrone. This was indicative of an efflux of mitoxantrone via ABCG2 in the MCF7MX cells resulting in reduced toxicity.

The impact of ABCG2 on the growth inhibitory effect of the cyanoquinoline derivatives was evaluated in MCF7 and MCF7MX. Vinblastine is not a substrate of ABCG2 and was chosen as a negative control. The GI_{50} values are summarised in

Table 11. EKB-569, FED2 and FED6 were associated with GI_{50} values of 4.3, 28 and 76 μ M in MCF7MX without pre-treatment, compared to 2.6, 8.6 and 12 μ M in MCF7 without pre-treatment. Following FTC pre-treatment, the GI_{50} values of EKB-569, FED2 and FED6 decreased to 1.5, 10, and 38 μ M in

the MCF7MX whereas the GI_{50} values were unchanged in the MCF7 cells. The GI_{50} value of FED14 was higher in the MCF7 (12 μ M) than in the MCF7MX (6.5 μ M) (Table 11).

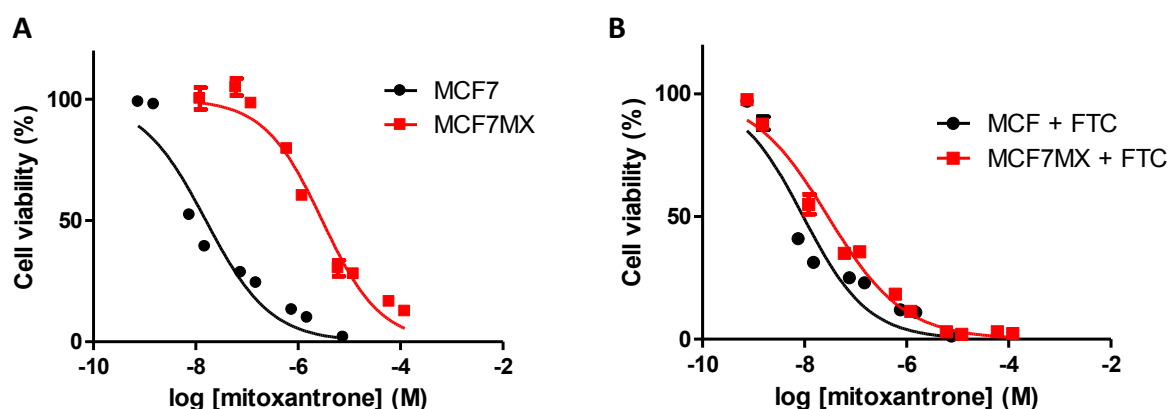


Figure 30: Cell viability assays showing reversal of resistance to mitoxantrone in MCF7MX following FTC treatment.

A- Cell viability plots of MCF7 and MCF7MX cells following mitoxantrone treatment with (B) or without (A) pre-treatment with 10 μ M FTC. Data show mean \pm SE of $n = 3$ replicates from one experiment carried out three times.

Table 11: Growth inhibitory effect associated with the series of cyanoquinoline molecules in MCF7 and MCF7MX cells.

		MCF7		MCF7MX	
		-ftc	+ftc	-ftc	+ftc
EKB-569	GI_{50} (μ M)	2.61	2.55	4.28	1.54
	SE	0.07	0.04	0.23	0.06
FED2	GI_{50} (μ M)	14.93	14.77	27.55	10.29
	SE	1.8	1.78	1.11	1.47
FED6	GI_{50} (μ M)	11.98	12.29	75.92	37.85
	SE	0.03	0.83	4.92	17.18
FED14	GI_{50} (μ M)	11.41	11.18	6.53	10.09
	SE	1.36	1.11	0.34	0.73
vinblastine	GI_{50} (nM)	5.12	5.36	2.08	2.66
	SE	0.74	0.63	0.41	0.66
Mitoxantrone	GI_{50} (nM)	10.73	6.62	2503.50	22.75
	SE	0.50	0.74	316.50	2.35

GI_{50} values were obtained for each experiment. Data represent mean GI_{50} and SE obtained from three separate experiments.

The impact of ABCG2 was plotted as a ratio between the GI_{50} of the compound in MCF7MX over the GI_{50} of the compound in MCF7 cells (Figure 31). Compounds associated with a ratio >2 were considered to be actively effluxed by the ABC transporters (Szakacs et al., 2006). In the absence of ABCG2 inhibitor, FTC, EKB-569, FED2, FED6 and FED14 have GI_{50} ratios of 1.6, 1.9, 6.3 and 0.6, respectively. In the presence of FTC these ratios decreased to 0.6, 0.7, 3.1 and 0.9 for EKB-569, FED2, FED6 and FED14, respectively. FED6 was associated with a ratio > 2 suggesting its substrate specificity towards ABCG2. Following FTC pre-treatment the ratio of GI_{50} 's for FED6 remained >2 , which could be due to an inability of FTC to completely block the efflux of FED6 via ABCG2 or other non-related factors that led to lower cytotoxicity of FED6 in the MCF7MX cells.

Taken together, these results indicate that FED6 is a substrate of ABCG2.

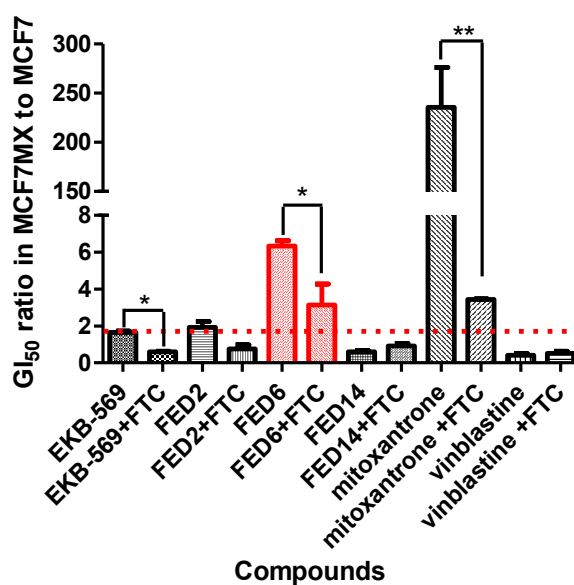


Figure 31. Impact of FTC on the cytotoxicity of cyanoquinoline derivatives.

Data show ratio between GI_{50} in MCF7MX and GI_{50} in MCF7 cells expressed as mean \pm SE of ratios from three experiments. Mitoxantrone was used as a positive control. Red dashed line indicates threshold for ABCB1 substrate specificity. FED6 indicated in red. Stars indicate statistical difference between values of two-tailed unpaired t-test (* $p \leq 0.05$, ** $p \leq 0.01$).

4.2.3 Substrate specificity for ABCC1

Substrate specificity of the cyanoquinoline derivatives for ABCC1 was investigated in A549 cells, which overexpress ABCC1; the impact of MK-571, a specific inhibitor of ABCC1 was also evaluated (Regina et al., 1998, Pham et al., 2009).

Calcein-AM is a substrate of ABCC1 and could be used to monitor the active efflux mediated by the transporter. To determine the optimal concentration of MK-571 to inhibit ABCC1 cells, the impact of increasing concentration of the inhibitor on intracellular levels of calcein in A549 cells was evaluated. Fifty micro molar of MK-571 led to a 1.5 fold increase in fluorescence compared to baseline (Figure 32). An optimal concentration of the inhibitor (100 μM) led to a higher level of fluorescence. However, this concentration also led to a decrease in cell viability when A549 cells were incubated with MK-571 for more than 24 h. The lower concentration of 50 μM of MK-571 was therefore selected in further experiments.

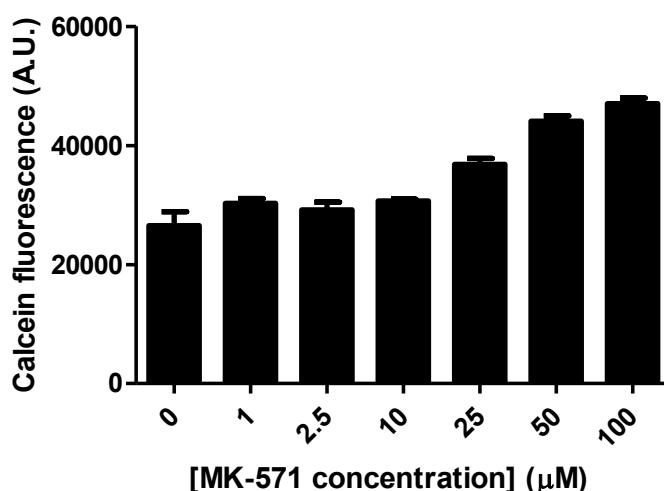


Figure 32: Calcein fluorescence in A549 cells following MK-571 treatment.

Fluorescence of calcein in A549 cells following a calcein AM assay performed after pre-treatment with or without increasing concentrations of ABCC1 inhibitor MK-571 for 1 h. Data show means \pm SE of quadruplet of calcein fluorescence. A.U.: Arbitrary unit

The impact of MK-571 on the growth inhibitory effect of the cyanoquinoline derivatives was further evaluated in Figure 33. The GI_{50} values are summarised in Table 12. EKB-569, FED2, FED6 and FED14 were associated with GI_{50} values of 1.6, 28, 35 and 6.5 μM , respectively in A549, compared to 1.4, 25, 21, and 6.9 μM in A549 when the cells were pre-treated with MK-571 (Table 12).

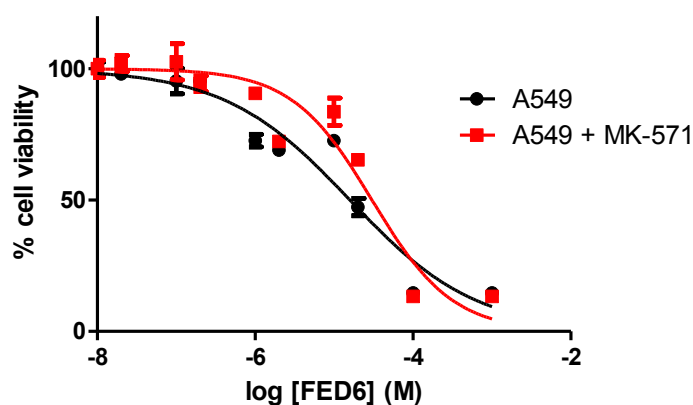


Figure 33: Cell viability assays in A549 cells with and without pre-treatment with ABCC1 inhibitor MK-571.

Cell viability plots of A549 cells following FED6 treatment with (B) or without (A) pre-treatment with 50 μ M MK-571. Data show mean \pm SE of n = 3 replicates from one experiment carried out three times.

Table 12: Growth inhibitory effect associated with the series of cyanoquinoline molecules in A549 and A549 cells treated with MK-571

		A549	A549 + MK-571
EKB-569	GI ₅₀ (μ M)	1.6	1.4
	SE	0.3	0.1
FED2	GI ₅₀ (μ M)	28	25
	SE	5.7	5.6
FED6	GI ₅₀ (μ M)	35	21
	SE	2.5	1.7
FED14	GI ₅₀ (μ M)	6.5	6.9
	SE	1.2	1.7

GI₅₀ values were obtained for each experiment. Data represent mean GI₅₀ and SE obtained from three separate experiments.

GI₅₀ ratio in A549 to A549 + MK-571 were plotted in Figure 34. Compounds associated with a ratio > 2 were considered to be actively effluxed by ABCC1. EKB-569, FED2, FED6 and FED14 have GI₅₀ ratios of 1.1, 1.2, 1.8, 1.1 μ M, respectively (Figure 34).

None of the tested compounds had ratios > 2 and were therefore not considered as substrates for ABCC1.

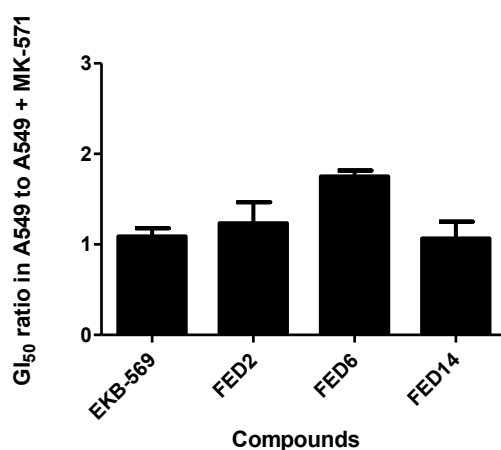


Figure 34: Impact of MK-571 on the cytotoxicity of cynanoquinolines derivatives in A549 cells.

Data show ratio between GI₅₀ in A549 cells and GI₅₀ in A549 pre-treated with MK-571 expressed as mean \pm SE of ratios from three experiments.

4.2.4 ABC transporters and uptake of [¹⁸F]FED6 *in vitro*.

The preceding section highlighted FED6 as a potential substrate of ABCB1 and ABCG2. To verify that radiolabelled FED6 (used in tracer amount) could also be substrate of ABCB1 and ABCG2, the differential uptake of [¹⁸F] radiolabelled FED6 was investigated in ABCB1 and ABCG2 overexpressing cell lines, and by using specific inhibitors.

The uptake of [¹⁸F]FED6 was more than 20 times greater in 3T3 cells (22 CCPMA/ μ g of protein) than in 3T3-MDR1 cells (0.74 CCPMA/ μ g) (Figure 35A). The uptake of [¹⁸F]FED6 increased to over 12 CCPMA/ μ g of protein in the 3T3-MDR1 cells, following pre-treatment with zosuquidar. The latter did not have any effect in 3T3 cells (Figure 35A). These results indicate that [¹⁸F]FED6 is a substrate for ABCB1.

MCF7MX cells also showed low levels of uptake of [¹⁸F]FED6; 7 CCPMA/ μ g of protein compared to 80 CCPMA/ μ g of protein in MCF7 cells (Figure 35B). When cells were pre-treated with 10 μ M of FTC, 1 h prior to incubation with the radiotracer, the uptake of [¹⁸F]FED6 increased to 31 CCPMA/ μ g of protein in MCF7MX cells. There was a small increase in the uptake in the MCF7 cells following pre-treatment with FTC, but this was not statistically significant. These results indicate that [¹⁸F]FED6 is a substrate for ABCG2.

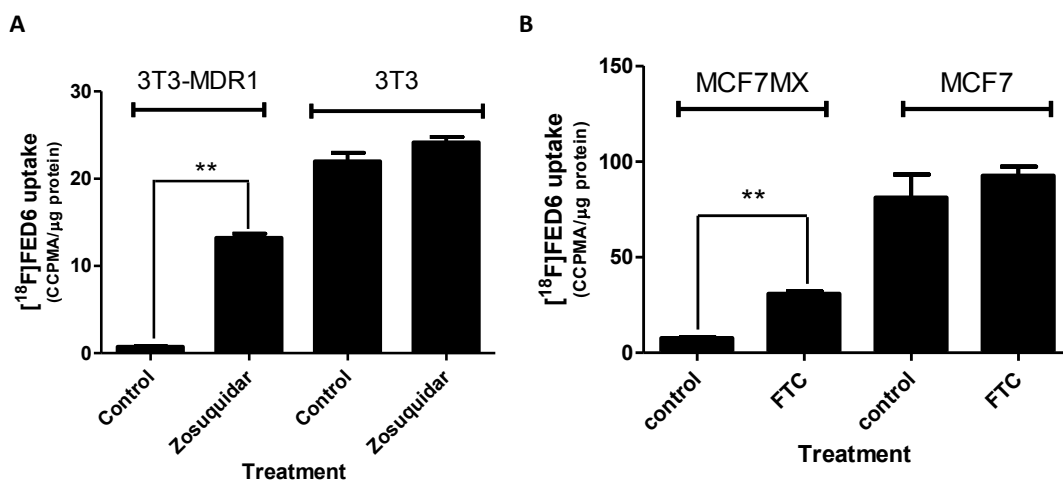


Figure 35: [¹⁸F]FED6 uptake in ABC transporter expressing cells.

Protein normalised uptake of [¹⁸F]FED6 in 3T3, 3T3-MDR1 cells, following 1 h incubation with 0.22 MBq of [¹⁸F]FED6, with or without pre-treatment with zosuquidar at 0.3 μM for 1 h. B- Protein normalised uptake of [¹⁸F]FED6 in MCF7 and MCF7MX cells, following 1 h incubation with 0.22 MBq of [¹⁸F]FED6, with or without pre-treatment with 10 μM FTC for 1 h. All data show mean ± SE of triplicates of one representative experiment carried out in duplicate. Statistical difference between data indicated on graph. Stars indicate statistical difference between values of two-tailed unpaired t-test (**p < 0.01).

4.2.5 Caco2 cell permeability assay.

The Caco2 model of permeability has been widely used to investigate the absorption properties and the active transport of drugs (Szakacs et al., 2006). Here, the transporter expression profile of these cells was used, as an alternative model to further investigate the active efflux of the cyanoquinoline compounds by ABCB1 and ABCG2.

It has been reported that a ratio between the secretion ($P_{app\ B-A}$) and absorption ($P_{app\ A-B}$), referred to as the efflux ratio, with values greater than 2 corresponds to molecules which are actively extruded by the cell via the ABC transporters (ABCB1 and/or ABCG2) (Szakacs et al., 2006).

The efflux ratios of EKB-569, FED2, FED6, and FED14 are summarised in Figure 36. EKB-569, FED2 and FED6 were actively effluxed as indicated by efflux ratios ($P_{app\ B-A} / P_{app\ A-B}$) of 3.4, 6.6 and 6.9, respectively (Figure 36). The efflux ratio for FED14 was below 1 indicating a lack of active Transport. Vinblastine was chosen as a control compound and has an efflux ratio above 2 due to the substrate specificity for ABCB1 (Figure 36).

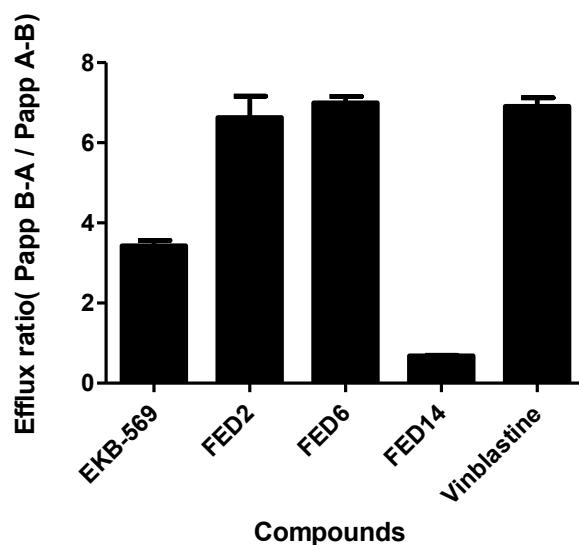


Figure 36: Active efflux of cyanonquinoline derivatives across Caco2 cells.

Data are expressed as ratios between permeability of secretion and permeability of absorption. Positive control vinblastine, is shown for comparison. Data show mean \pm SE of efflux ratios obtained from triplicates of one representative experiment

We further evaluated the impact of inhibitors of the ABC transporters on the permeability of FED6 (Figure 37). Following FTC pre-treatment, the active efflux of FED6 was partially inhibited. This was indicated by a decrease in the efflux ratio of FED6 from 6.9 without pre-treatment to 5 with FTC (Figure 37A). Pre-treatment with FTC did not completely reverse the efflux ratio suggesting that FED6 may also be extruded via ABCB1. Zosuquidar pre-treatment did not inhibit the active efflux of FED6, suggesting that ABCG2 participated in the active efflux of FED6 (Figure 37B). The efflux ratio for FED6 decreased significantly following pre-treatment with verapamil, a non-specific inhibitor of ABCB1 which also shows inhibitory potential against ABCG2 (Rogan et al., 1984), from 6.9 without pre-treatment to 1.2 with verapamil.

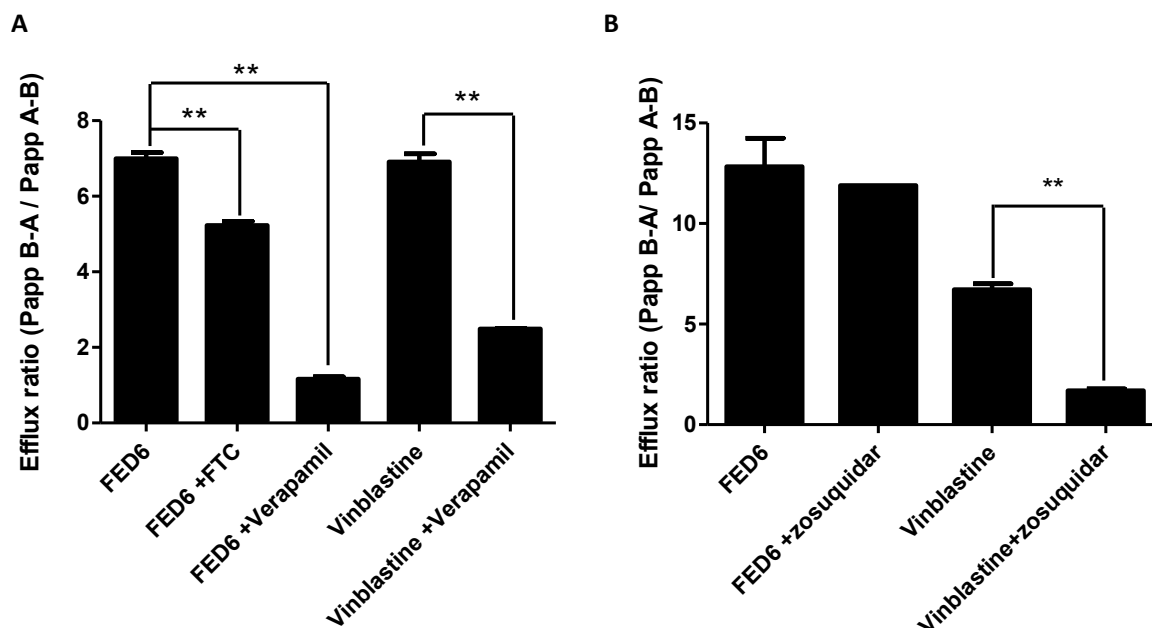


Figure 37: Efflux ratio of cyanoquinoline compounds in the presence of ABC transporter inhibitors.

Efflux ratios of FED6 and vinblastine with or without 1 h pre-treatment with 10 mg/ml of verapamil or FTC (A) or 0.3 μ M zosuquidar (B) obtained from a Caco2 transwell assay. Data show mean efflux ratios \pm SE of n = 3 of one representative experiment. Stars indicate statistical difference between values of two-tailed unpaired t-test (**p \leq 0.01).

These results show that FED6, FED2 and EKB-569 were actively effluxed out of the cell via the ABC transporters, and that pre-treatment with verapamil led to a significant decrease in the efflux ratio of FED6. These experiments further confirmed the substrate specificity of FED6 for the ABC transporters.

4.3 Impact of ABC transporter substrate specificity of FED6 for imaging EGFR.

4.3.1 Levels of ABC transporters across a panel of cell lines

A panel of cell lines was previously used to study the affinity of FED6 for EGFR (Cf chapter 3). To further investigate the impact of ABC transporters, on the uptake of [18 F]FED6, across the different cell lines, levels of mRNA and protein expression were determined for both transporters (Figure 38).

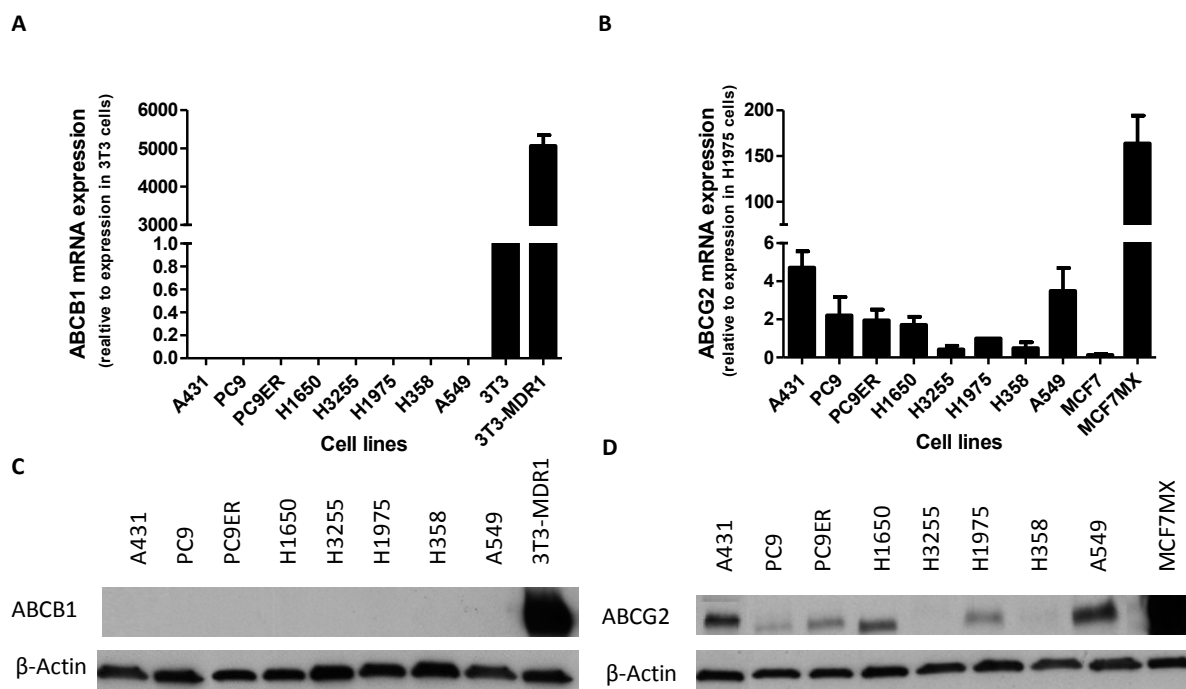


Figure 38: mRNA and protein expression of ABCB1 and ABCG2 in cell lines studied.

A-B- mRNA levels of ABCB1 (A) and ABCG2 (B) in different cell lines studied, assessed by RT-PCR. Data show mean \pm SE values of relative levels of ABCB1 and ABCG2 normalised for GAPDH from three experiments. C-D- Protein expression of ABCB1 (C) and ABCG2 (D) in different cell lines studied.

ABCB1 expression was below the levels of detection in all cell lines. ABCG2 was expressed to a variable but appreciable extent in all cell lines assessed. The MCF7MX cells expressed levels of ABCG2 mRNA 130 fold higher than the other cell lines tested. A431 and A549 cells showed more physiological levels of mRNA and protein expression of ABCG2. H3255 and H358 were the only cell lines that expressed ABCG2 below the limit of detection by western blot. As ABCB1 was not detected in the cell lines studied, the interaction between FED6 and ABCG2 was the focus for the rest of this work.

4.3.2 Overcoming ABCG2 efflux.

4.3.2.1 Inhibition of ABCG2 in MCF7MX cells.

FED6 was previously shown to be a substrate for ABCG2. Furthermore, low to moderate levels of this transporter were expressed in the cell lines which were chosen to study the imaging characteristics of EGFR with [18 F]FED6. The aim was to investigate whether or not the efflux via ABCG2 could be inhibited by pharmacological means and whether the blocking of ABCG2 efflux would lead to an increase in the uptake of [18 F]FED6.

Hoechst 33324 dye, is a known substrate for ABCG2 and its accumulation in cells overexpressing the transporter is significantly reduced (Kim et al., 2002). Using the fluorescence properties of Hoechst 33324, the accumulation of this dye in MCF7 and in MCF7MX cells following pre-treatment with ABCG2 specific inhibitor FTC and gefitinib was determined. Gefitinib has been reported by several groups to act as an inhibitor of ABCG2 (Nakamura et al., 2005, Hegedus et al., 2012). Following drug inhibition, the ABCG2 transporter will no longer be expected to efflux the Hoechst dye. This dye will accumulate in the cells giving a rise in fluorescence.

At baseline the fluorescence values recorded in MCF7MX (350 A.U.) were 16 fold lower than the fluorescence recorded in MCF7 cells (5500 A.U.) (Figure 39). This reflected the efflux of Hoechst 33324 dye via the ABCG2 transporter in the MCF7MX cells. FTC pre-treatment lead to a dose dependent increase in fluorescence in the MCF7MX cells, reaching 2700 A.U. at 10 μ M FTC (8-fold increase in fluorescence from baseline), whilst no change was measured in MCF7 cells (Figure 39A, B). Gefitinib pre-treatment led to a concentration dependent increase in fluorescence with concentrations above 6 μ M gefitinib in MCF7MX, reaching 4800 A.U. at 100 μ M gefitinib (Figure 39C), whilst no changes in fluorescence were measured in the MCF7 cells (Figure 39D). Pre-treatment of MCF7MX cells with concentrations of FED6 as high as 100 μ M, did not lead to a significant increase in the fluorescence of Hoechst 33324 (Figure 39E).

In conclusion, FTC and gefitinib but not FED6 inhibited ABCG2, causing a decrease in efflux of Hoechst 3334 from the cells and a subsequential increase in measured fluorescence. For further experiments, concentrations of 100 μ M gefitinib and 10 μ M FTC were selected.

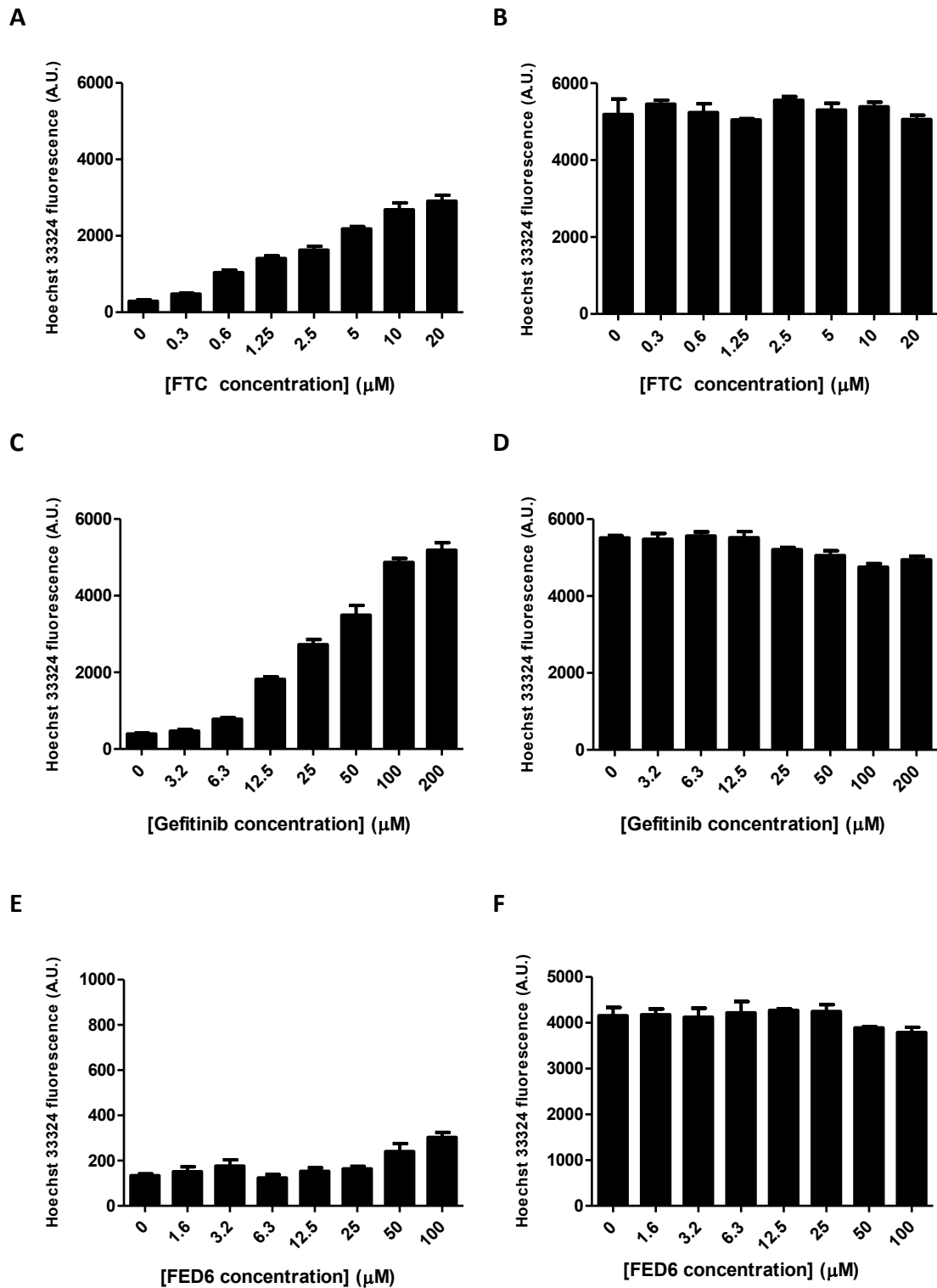


Figure 39: Hoechst 33324 uptake in MCF7 and MCF7MX cells following FTC or gefitinib pre-treatment

A-B- Hoechst 33324 fluorescence in MCF7MX (A) and MCF7 (B) cells following 1h pre-treatment with FTC. C-D- Hoechst 33324 fluorescence in MCF7MX (C) and MCF7 (D) cells following 1 h pre-treatment with gefitinib. E.-F- Hoechst 33324 fluorescence in MCF7MX (E) and MCF7 (F) cells following 1 h pre-treatment with FED6. Fluorescence values were normalised for protein levels by carrying out an SRB assay. Data show mean \pm SE of minimum of n = 4 replicates from one representative experiment carried out three times. A.U.: Arbitrary unit

To demonstrate the specific role of ABCG2 in relation to the changes to Hoechst 33324 uptake, ABCG2 protein expression was knocked down via ABCG2 siRNA transfection in MCF7MX cells. Fluorescence levels increased 4.2-fold to 562 A.U., following treatment of MCF7MX cells, with ABCG2 siRNA compared to 135 A.U. in scramble siRNA treated cells. The increase in Hoechst 33324 fluorescence was the greatest following 1 h pre-treatment with either 10 μ M FTC or 100 μ M gefitinib, where the fluorescence increased fourfold (Figure 40A). Hoechst 33324 fluorescence values did not reach the levels measured in MCF7 cells. There was no change in the fluorescence of Hoechst in MCF7 cells following drug treatment (Figure 40B).

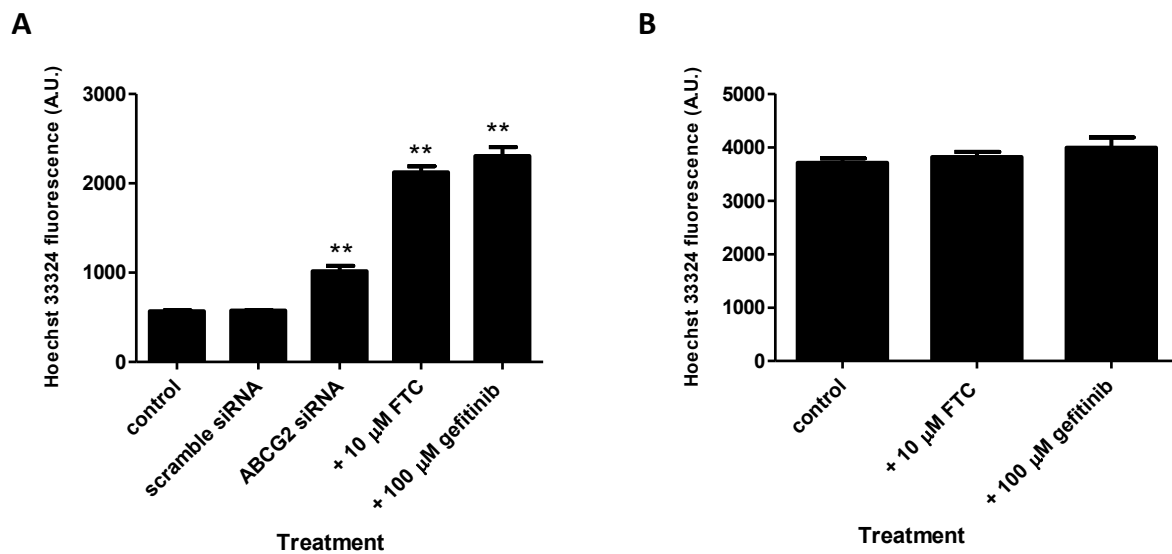


Figure 40: Hoechst 33324 uptake in MCF7MX and MCF7 following siRNA and drug inhibition of ABCG2.

A- Normalised fluorescence values in MCF7MX cells after ABCG2 siRNA transfection or drug pre-treatment. B- Normalised fluorescence values in MCF7 cells after drug pre-treatment. Data show means \pm SE of minimum of n = 4 replicates from one experiment carried out 3 times. A.U.: Arbitrary Unit. Statistical differences from two-tailed unpaired t-test performed between treatments and control (untreated cells) indicated on graph by stars. (**= P \leq 0.01). C-D- ABCG2, p-EGFR (Y1068) and EGFR protein expression in MCF7MX (C) and MCF7 (D) cells following siRNA or drug treatment.

Knock down of ABCG2 in the MCF7MX cells was confirmed by western blot. Levels of ABCG2 were significantly decreased in the ABCG2 siRNA treated MCF7MX cells. However, knock down of ABCG2 was incomplete (Figure 41A). Levels of p-EGFR (Y1068) were completely knocked down following gefitinib treatment, levels of EGFR were unchanged following both FTC and gefitinib treatment in both MCF7MX and MCF7 cells (Figure 41).

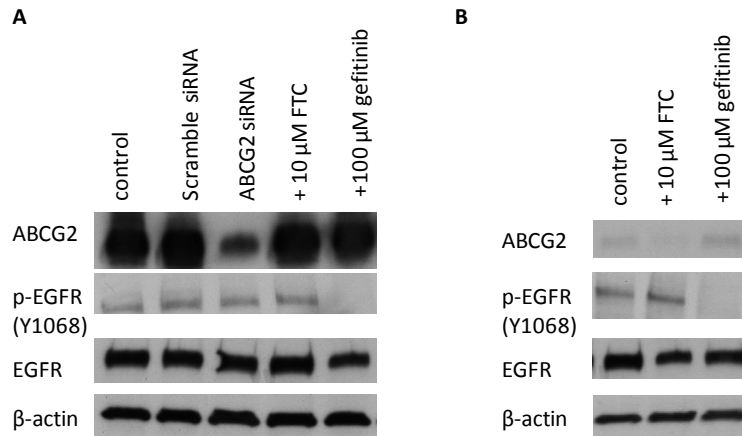


Figure 41: ABCG2 knock down in MCF7MX cells.

Protein expression of ABCG2, p-EGFR (Y1068) and EGFR in MCF7MX (A) and MCF7 (B) cells following pre-treatment with ABCG2 or scramble siRNA for 72h and FTC or gefitinib for 1 h.

After showing that both gefitinib and FTC led to an increase in fluorescence, as a result of a reduction of the efflux of the Hoechst dye, a substrate of ABCG2, the role of these two drugs at inhibiting the efflux of [¹⁸F]FED6 by ABCG2 was assessed. To investigate whether ABCG2 mediated efflux of [¹⁸F]FED6 could be overcome the impact of ABCG2 was evaluated by genetic means and using ABCG2 inhibitors. [¹⁸F]FED6 uptake was 10 fold higher in ABCG2 siRNA transfected MCF7MX cells (3.5 CCPMA/μg of protein) compared to scramble siRNA transfected cells (0.6 CCPMA/μg of protein), but did not reach the values of uptake measured in the MCF7 cells (17 CCPMA/μg of protein) (Figure 42AB). Pre-treatment with either gefitinib or FTC led to uptake values of [¹⁸F]FED6 of 6.3 and 6 CCPMA/μg of protein compared to 0.4 CCPMA/μg of protein in the control sample in MCF7MX but no changes in MCF7 cells (Figure 42A).

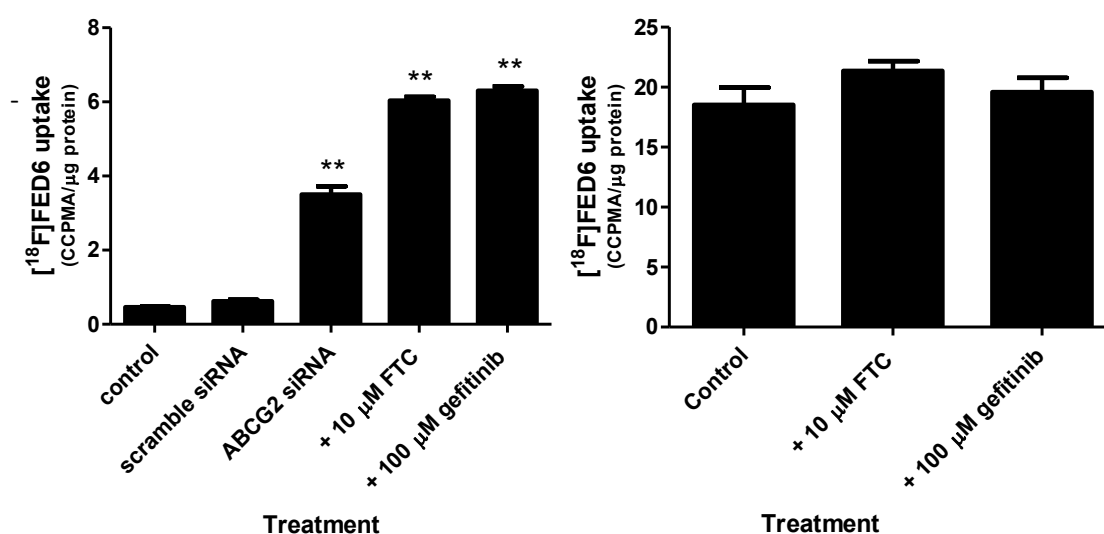


Figure 42: [¹⁸F] FED6 uptake in MCF7MX cells following ABCG2 knock down or drug inhibition.

A- Uptake of [¹⁸F] FED6 in MCF7MX cells after 1 h incubation with 0.22MBq of [¹⁸F]FED6 following ABCG2 siRNA transfection or drug pre-treatment. B- Uptake of [¹⁸F] FED6 in MCF7 cells with or without drug pre-treatment. Data show means ± SE of triplicate of one representative experiment carried out three times. Statistical differences from two-tailed unpaired t-test performed between treatments and control (untreated cells) indicated on graph by stars (**= P ≤ 0.01).

4.3.2.2 Inhibition of ABCG2 in A431 cells *in vitro* and *in vivo*

We have previously investigated the impact of ABCG2 inhibition using a cell line that overexpressed the transporter (i.e. MCF7MX). To translate these findings into more physiological conditions, A431 that expressed intermediate levels of ABCG2 and were previously chosen to assess the specificity of [¹⁸F]FED6 for EGFR were investigated (Figure 38).

4.3.2.2.1 Inhibition of ABCG2 in A431 cells.

The modulation of the uptake of, Hoechst 33324, in A431 cells following ABCG2 siRNA transfection or drug pre-treatment was first measured. There were no differences between the fluorescence of scramble and ABCG2 siRNA treated A431 cells, using conditions optimised for in the MCF7MX cells. Fluorescence values increased from 3900 A.U. in untreated control cells to 5600 and 5100 A.U. following FTC and gefitinib pre-treatment. This corresponded to a 1.5 and 1.3-fold increase in fluorescence after FTC and gefitinib treatment, respectively (Figure 43). These results suggested that the increase in fluorescence following FTC or gefitinib pre-treatment involved other factors than ABCG2. In addition, the baseline levels of fluorescence measured in the A431 cells were similar to those measured in MCF7 cells. It is possible that, the lack of increase in fluorescence following

ABCG2 siRNA treatment in A431 cells could be due to an already near maximal uptake of Hoechst 33324 in these cells.

ABCG2 siRNA knock down was confirmed by western blot (Figure 44). Levels of ABCG2 were unchanged following both gefitinib and FTC treatment. Expression of p-EGFR (Y1068) was unchanged following pre-treatment with siRNA or FTC, whereas gefitinib treatment led to a complete knock down of p-EGFR (Y1068). Levels of EGFR were the same under all conditions (Figure 44).

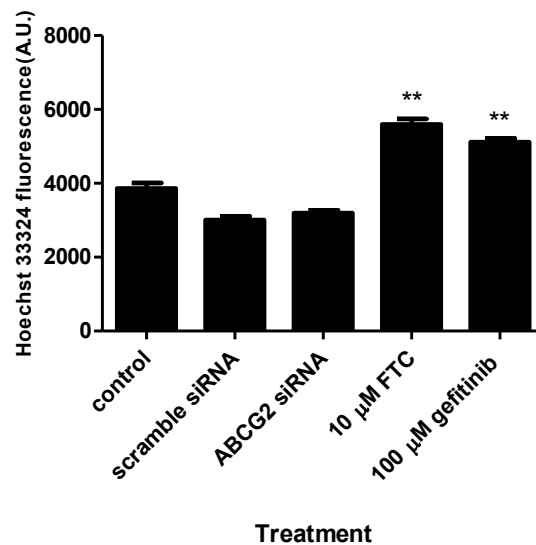


Figure 43: Hoechst 33324 uptake in A431 cells following ABCG2 siRNA transfection and drug treatment.

A- Hoechst fluorescence in A431 cells following ABCG2 siRNA or drug pre-treatment. Data shows mean fluorescence values normalised for protein \pm SE of minimum of n = 6 replicates from one experiment carried out 3 times. A.U.: arbitrary unit. Statistical differences between treatments and control (untreated cells) indicated on graph. (**= $P \leq 0.01$) of two-tailed unpaired t-test

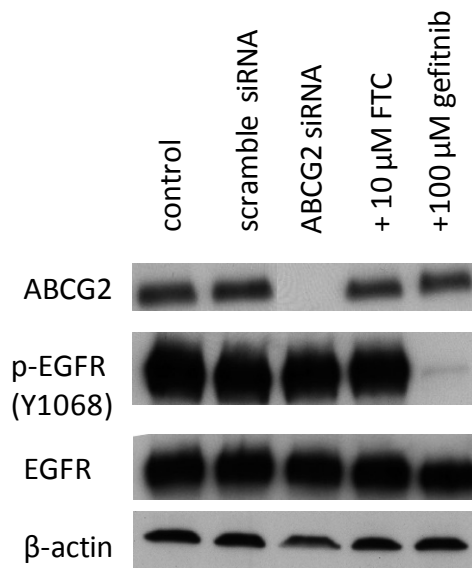


Figure 44: ABCG2 knock down in A431 cells.

Protein expression of ABCG2, p-EGFR (Y1068) and EGFR in A431 cells following pre-treatment with ABCG2 or scramble siRNA for 72h and FTC or gefitinib for 1 h.

The effect of blocking ABCG2 on the uptake of [¹⁸F]FED6 in A431 cells was then assessed. The uptake of [¹⁸F]FED6 increased 1.5-fold from 34 CCPMA/μg of protein in scramble treated cells to 49 CCPMA/μg of protein in ABCG2 siRNA treated cells. There was a 1.8 and 2.3 fold increase in radiotracer uptake following FTC and gefitinib treatment, respectively (

Figure 45). The higher levels of uptake of [¹⁸F]FED6 following gefitinib pre-treatment compared to ABCG2 siRNA or FTC pre-treatment would indicate that the effect of gefitinib is not solely related to the inhibition of ABCG2.

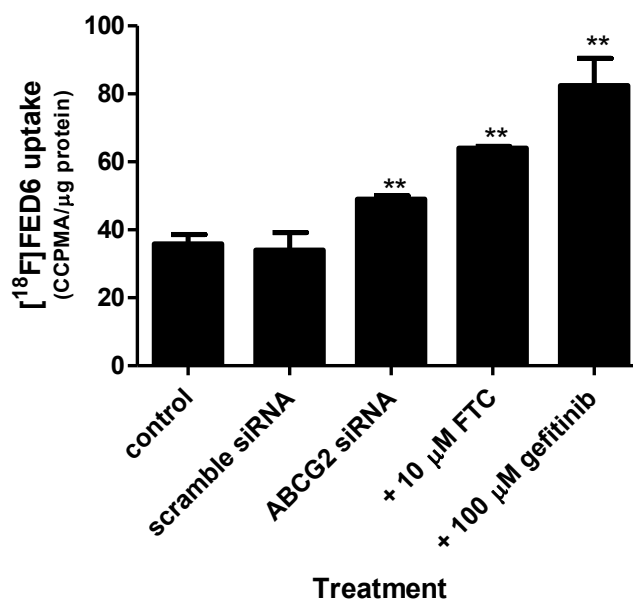


Figure 45: [¹⁸F]FED6 uptake in A431 cells following inhibition of ABCG2.

Uptake of [¹⁸F] FED6 in A431 cells after 1 h incubation with 0.22 MBq of [¹⁸F]FED6, following ABCG2 siRNA transfection or drug pre-treatment. Data show means ± SE of triplicate of one representative experiment carried out three times. Statistical differences from two-tailed unpaired t-test performed between treatments and control (untreated or scramble treated cells) indicated on graph by stars (**= P ≤ 0.01).

In conclusion, the *in vitro* data from the Hoechst 33324 fluorescence assay and the [¹⁸F]FED6 uptake experiments indicated that efflux via ABCG2 could be reduced following pre-treatment with FTC or gefitinib. Furthermore, the inhibition of ABCG2 efflux led to an increase in uptake of [¹⁸F]FED6.

4.3.2.3 *In vivo* modulation of ABCG2 efflux of [¹⁸F]FED6.

FTC could not be used *in vivo* due to high levels of neurotoxicity (Rabindran et al., 2000). Therefore, in order to translate the impact of ABCG2 inhibition on [¹⁸F]FED6 uptake measured *in vitro* to an *in vivo* setting, the effects of gefitinib at inhibiting the efflux of [¹⁸F]FED6 via ABCG2 was assessed. A CT/PET scan was performed in female BALB/c nu/nu A431 xenograft bearing mice to assess the uptake of [¹⁸F]FED6 following pre-treatment with gefitinib. There was a 2-fold increase in [¹⁸F]FED6 uptake in the A431 tumours, which were pre-treated with gefitinib: From 3.5 % I.D / mL of tissue in the untreated control group to 0.7 % I.D / mL of tissue in gefitinib treated mice (Figure 46).

We hypothesized that pre-treatment with gefitinib would not lead to significant changes in the uptake of [¹⁸F]FED6 in tissues other than the tumour. The biodistribution of the tracer has previously been reported (Pisaneschi et al., 2010). Similar to the previous findings, there was a high level of uptake in the gastrointestinal system. The uptake of [¹⁸F]FED6 was unchanged in the majority of tissues following pre-treatment with gefitinib with the exception of tumour and muscle tissues. In muscle, gefitinib pre-treatment led to a decrease in [¹⁸F]FED6 uptake. The uptake in the tumour increased in the gefitinib pre-treated group.

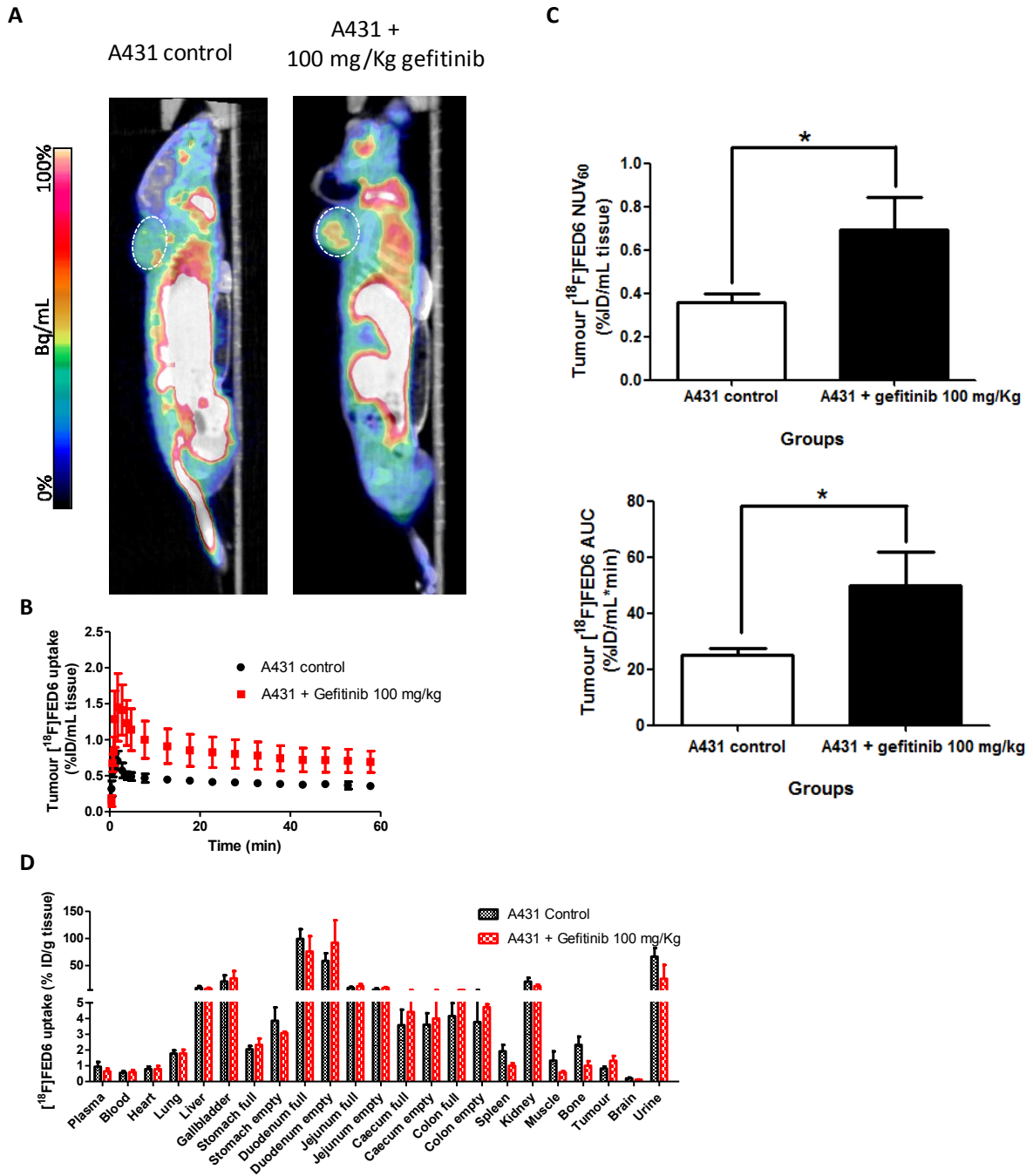


Figure 46: *In vivo* uptake of [¹⁸F]FED6 in A431 xenograft after gefitinib pre-treatment.

A- Merged PET/CT image of representative sagittal cross section of a female nude mouse expressing A431 xenograft following 1 h dynamic scan post i.v. injection of 3.7 MBq of [¹⁸F]FED6, with (right) or without (left) 1 h pre-treatment of 100 mg/Kg of gefitinib *via* i.p. injection. Tumour delineated by white dotted line. B- Tumour time activity curves of A431 xenografts with or without pre-treatment. C- Normalised uptake value (NUV₆₀) in the tumour and area under the curve (AUC) values. D- Biodistribution data showing the uptake of [¹⁸F]FED6 in different organs of A431 mouse xenograft with or without pre-treatment with gefitinib. Data represent average of n = 3 mice per group ± SE. Stars indicate statistical difference between values of two-tailed unpaired t-test (* p < 0.05).

As well as inhibiting ABCG2 gefitinib will be binding to an inhibiting EGFR. To measure the inhibition of EGFR autophosphorylation by gefitinib levels of p-EGFR (Y1068) and EGFR were determined in A431 tumour lysates. A decrease in levels of p-EGFR in tumours acquired from mice pre-treated with 100 mg/Kg of gefitinib was measured (Figure 47).

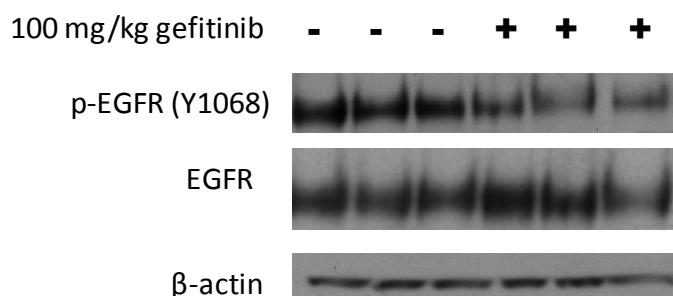


Figure 47: p-EGFR and EGFR protein expression of A431 tumours following gefitinib treatment.

Protein expression in A431 xenograft tumour lysates. Each column represents one lysed tumour sample.

In summary, the *in vivo* data correlated with the *in vitro* findings showing an increase [¹⁸F]FED6 uptake of in the A431 xenografts following gefitinib pre-treatment. FED6 was shown to be a substrate for both ABCB1 and ABCG2, with a preferential binding affinity for the latter. Although a relative increase in [¹⁸F]FED6 uptake was demonstrated both *in vitro* and *in vivo*, following inhibition of ABCG2, the overall levels of uptake in the tumour were below 2 % of ID/mL of tissue. Furthermore, there were high levels of non-specific binding or elimination in other organs.

Rather than employing pharmacological inhibition of ABC transporter activity to overcome ABC transporter efflux, which can be associated with toxicity, the optimal radiotracer should lack substrate specificity to ABC transporters.

Therefore, it is crucial to design derivatives that are non-substrates of the ABC transporters.

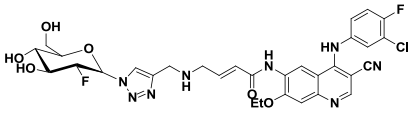
4.4 Investigation of an alternative cyanoquinoline molecule

4.4.1 Affinity of FED20 for EGFR

The main aim in the design of FED20, was to have a compound that maintained specificity and strong affinity for EGFR but lacked substrate specificity for the ABC transporters. As lowering the lipophilicity of other compounds of the aniloquinolines family had been reported to improve the

specificity of the radiotracer, this aspect was the focus in the design of FED20. The physico-chemical properties of FED20 are summarised in Table 13.

Table 13: Physico-chemical properties of FED20.

Compound	Structures	MW	Log P*	PSA	(N+O)	Aromatic rings	pKa
FED20		685.08	2.13	199.7	14	3	7.2

Measures of hydrophobicity, LogP and polar surface area (PSA) Mw: Molecular weight and the sum of oxygen and nitrogen atoms (N+O), were determined as described in methods. pKa : logarithmic value of acid dissociation constant. Values in red indicate characteristics favourable for substrate specificity to ABC transporters.

In comparison to FED6 which has a log p of 3.85 (Table 9), the log P of FED20 is significantly lower at 2.13; this is below the log P threshold of 3 which is associated with substrate specificity for ABC transporters. The MW of FED20 is relatively high at 685.08 g/mol. This property may play a role in the substrate specificity of this molecule for the ABC transporters, in particular ABCB1 as it is > 400 which has been shown to be a defining characteristic of substrates (Varma et al., 2005, Dellinger et al., 1992, Gottesman and Pastan, 1993, Kaliszczak et al., 2010).

In order to investigate the affinity of FED20 for EGFR, the sensitivity of FED20 for the EGFR enzyme was investigated, both in a cell free, and then in a cell based setting. First, the IC₅₀ of FED20 against purified EGFR enzyme was evaluated using a DELFIA tyrosine kinase assay. The IC₅₀ of FED20 against EGFR was determined at 4.46 (±0.7) nM, which was over 2 fold higher than the IC₅₀ for FED6 (1.81 nM) (Pisaneschi et al., 2010).

The activity of FED20 against EGFR was assessed *in vitro*. In EGFR overexpressing A431 cells, FED20 treatment led to a dose dependent decrease in the autophosphorylation of EGFR as measured by a decrease in p-EGFR at tyrosine 1068 (Figure 48).

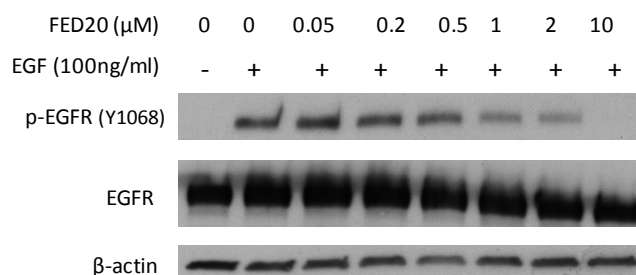


Figure 48: Inhibition of p-EGFR *via* FED20.

Expression of p-EGFR (Y1068) and EGFR in A431 cells following FED20 treatment.

4.4.2 Specificity of FED20 for EGFR

To further evaluate the specificity of FED20 for EGFR, an uptake assay measuring levels of [¹⁸F]FED20 uptake in high (A431) versus low (MCF7) EGFR expressing cells was carried out. Furthermore, a blocking study in which A431 and MCF7 cells were pre-treated with 10 μM of none-radiolabelled FED20 for 1 h before adding the radiotracer to the cells were assessed (Figure 49). The uptake of [¹⁸F]FED20 was 2.8 fold higher in the A431 cells compared to the MCF7 cells. Pre-treatment with FED20 led to a decrease in [¹⁸F]FED20 uptake in the A431 cells compared to untreated cells. However, this decrease was not statistically significant. There was no change in the tracer uptake following pre-treatment in the MCF7 cells. Overall, the uptake values of [¹⁸F]FED20 were significantly lower than those of [¹⁸F]FED6 with values under 2 CCPMA/μg of protein. Western blot analysis confirmed the high expression of EGFR in the A431 compared to low EGFR in the MCF7 cells. P-EGFR (Y1068) was lower in both cell lines following pre-treatment with FED20 (Figure 49B) suggesting that despite the inhibition of EGFR activity the uptake of [¹⁸F]FED20 did not decrease significantly.

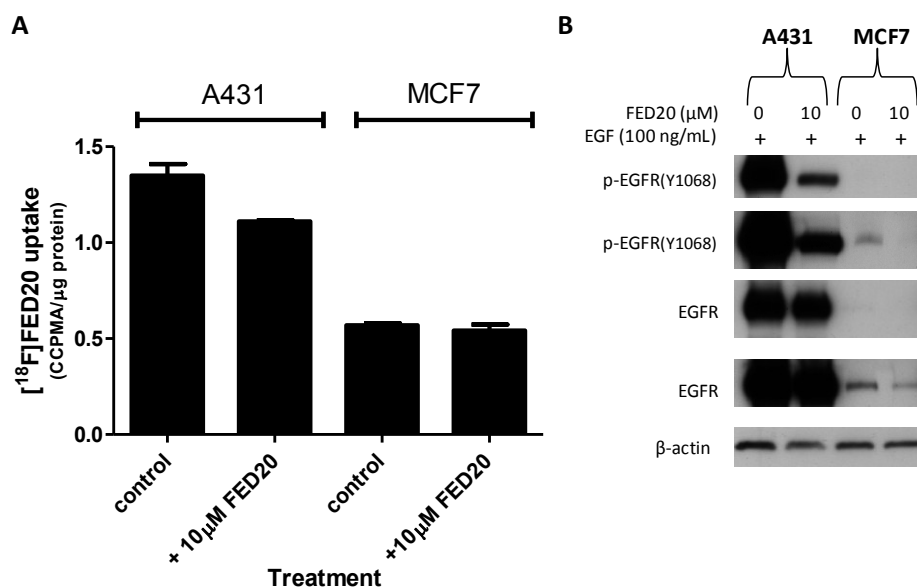


Figure 49: [¹⁸F]FED20 uptake in high vs low EGFR expressing cells.

A- [¹⁸F]FED20 uptake values in A431 and MCF7 cells treated with 0.55 MBq of [¹⁸F]FED20 for 1 h following pre-treatment with or without 10 μM of FED20 for 1 h. Data show mean ± SE of triplicates from one representative experiment carried out twice. B- Protein expression of p-EGFR (Y1068) and EGFR in A431 and MCF7 cells after pre-treatment with or without 10 μM of FED20. Short and long exposures of the blot are shown.

4.4.3 Substrate specificity of FED20 for the ABC transporters.

The cytotoxic assays, which were carried out in the paired cell lines in order to indirectly assess the substrate specificity of the cyanoquinoline compounds for the ABC transporters (see section 4.2.) were also performed with FED20. However, under the conditions used FED20 did not lead to high levels of cytotoxicity and assays based on cellular toxicity of FED20 could therefore not be utilised to assess the substrate specificity of FED20 for the ABC transporters.

To test the ABCG2 substrate specificity of FED20, the efflux ratios of FED20 were measured using the Caco2 transwell model. FED20 was associated with an efflux ratio < 2, indicating that it was not actively effluxed by the ABC transporters. Furthermore, pre-treatment with verapamil had no effect on efflux ratios of FED20 (Figure 50). Vinblastine was chosen as a positive control.

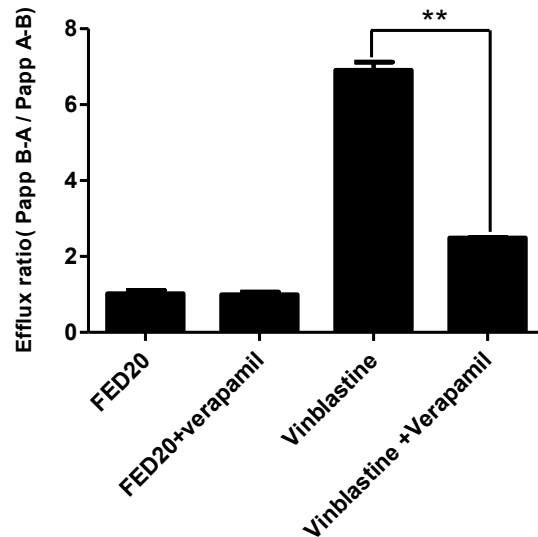


Figure 50: Efflux ratio of FED20 in Caco2 cells with and without pre-treatment with verapamil.

Efflux ratios of FED20 and vinblastine with or without 1 h pre-treatment with 10 mg/ml of verapamil obtained from a Caco2 transwell assay. Data show mean efflux ratios \pm SE of $n = 3$ of one representative experiment. Stars indicate statistical difference between values of two-tailed unpaired t-test (** $p \leq 0.01$).

The substrate specificity of FED20 for the ABC transporter was assessed by determining the uptake of [18 F]FED20 in cell lines with differential expression of the transporters: ABCG2 overexpressing cell lines MCF7MX and MCF7 and ABCB1 overexpressing cell lines 3T3-MDR1 and 3T3 using concentrations of pharmacological modulators optimised for FED6 (Figure 51).

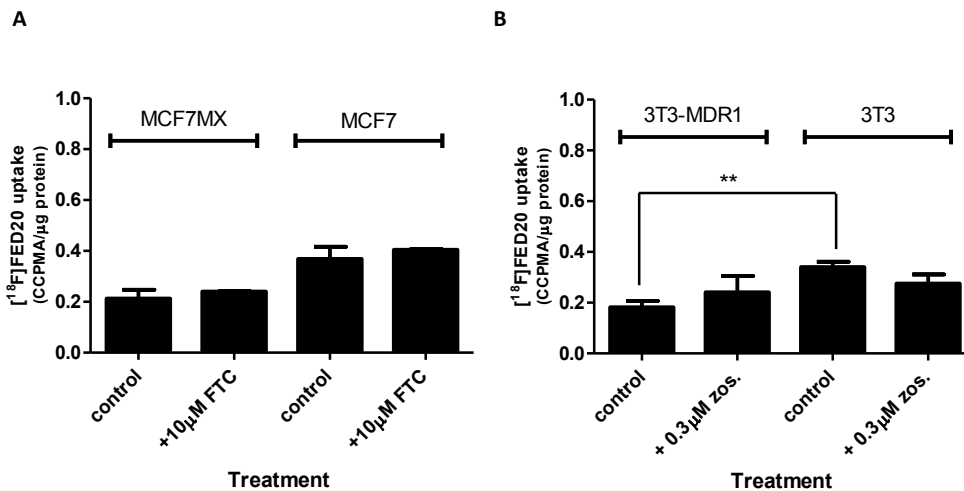


Figure 51: [18 F]FED20 uptake in ABC transporter expressing cells.

A- Protein normalised uptake of [18 F]FED20 in MCF7 and MCF7MX cells after 1 h incubation with 0.55 MBq [18 F]FED20 with or without pre-treatment with FTC. B- Protein normalised uptake of [18 F]FED20 in 3T3, 3T3-MDR1 cells after 1 h incubation with 0.55MBq [18 F]FED20 with or without pre-treatment with zosuquidar. Zos.: zosuquidar All data show mean \pm SE of triplicates of one representative experiment carried out in duplicate. Stars indicate statistical difference between values of two-tailed unpaired t-test (** $p \leq 0.01$).

The uptake of [¹⁸F]FED20 was higher in MCF7 (0.4 CCPM/μg of protein) compared to MCF7MX cells (0.2 CCPM/μg of protein). However, there was no increase in the uptake of [¹⁸F]FED20 following inhibition of ABCG2 by FTC (Figure 51A). These results suggest that the difference in uptake of [¹⁸F]FED20 between MCF7 and MCF7MX cells was not related to ABCG2 efflux of the radiotracer.

Similarly, the uptake of [¹⁸F]FED20 was higher in 3T3 (0.3 CCPMA/μg protein) compared to 3T3-MDR1 cells (0.2 CCPMA/μg of protein). There was no statistically significant difference in the uptake values of [¹⁸F]FED20 following zosuquidar pre-treatment (Figure 51B) suggesting that the difference in uptake of [¹⁸F]FED20 between 3T3 and 3T3-MDR1 cells was not related to ABCB1 efflux of the radiotracer.

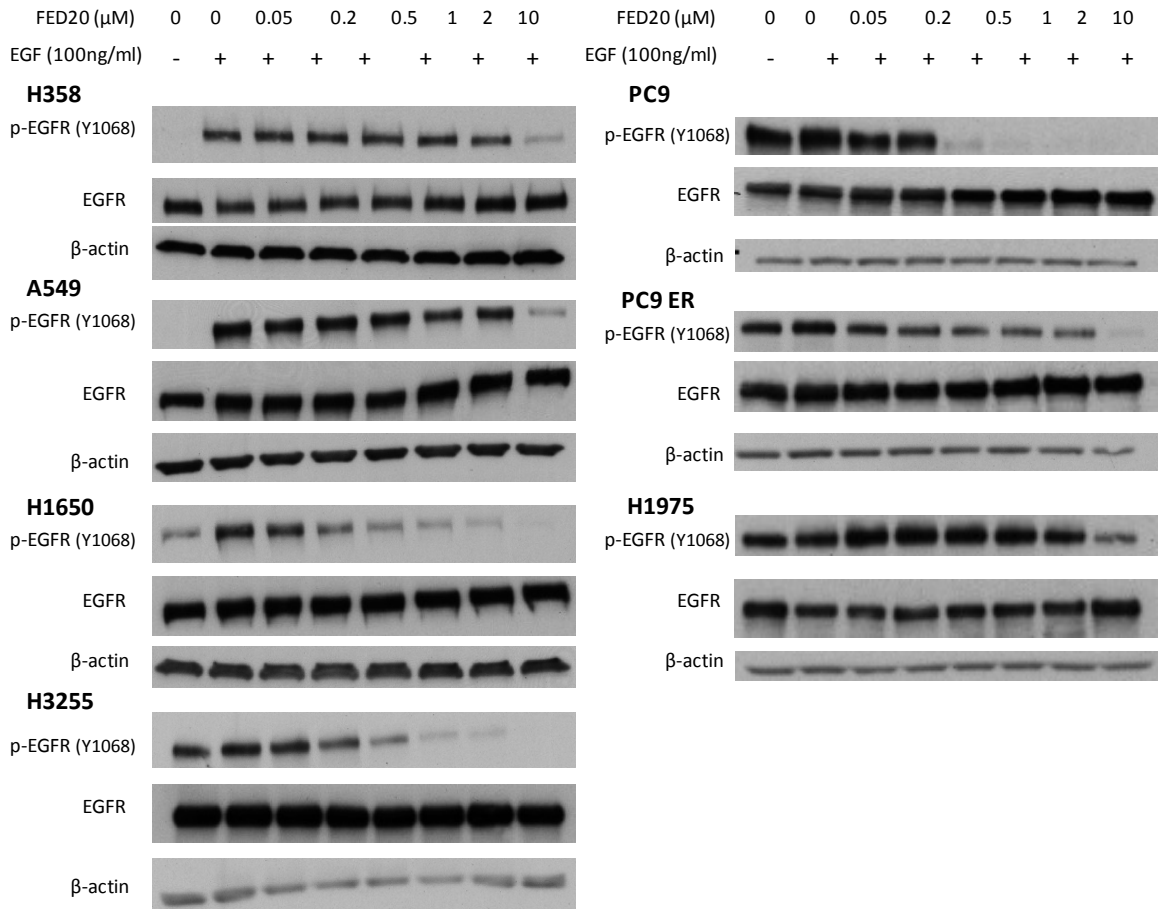
The lack of increase in uptake of [¹⁸F]FED20 following FTC treatment in MCF7MX and zosuquidar treatment in 3T3-MDR1 indicate that FED20 is not a substrate for ABCB1 nor ABCG2.

4.4.4 FED20 in the context of mutant EGFR in NSCLC

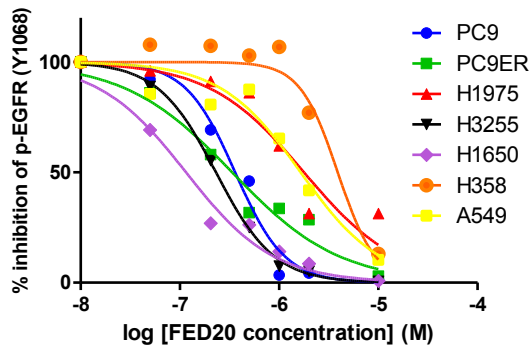
The affinity of FED20 for EGFR was in the nanomolar range and caused inhibition of p-EGFR (Y1068) as did FED6. Furthermore, FED20 was not found to be a substrate for either ABCB1 or ABCG2. Then, the affinity of FED20 to different mutant forms of EGFR was investigated. The inhibition of EGFR autophosphorylation following FED20 treatment in a series of NSCLC expressing either wild type, active or resistant mutant forms of EGFR (Figure 52) was determined. FED20 showed the strongest levels of inhibition of p-EGFR in the cells lines that express active mutant forms of EGFR, PC9, H3255 and H1650. Only the highest concentration of 10 μM of FED20 led to changes in p-EGFR in wild type EGFR expressing A549 and H358 cells and resistant mutant expressing H1975 cells. The IC₅₀ values of FED20 were 0.3 μM in the PC9 and H3255 compared to 7.1 μM in the H1975 cells (Figure 52 B2).

[FED20] μ M 0 0 0.05 0.2 0.5 1 2 10

A



B1



B2

Cell line	IC ₅₀ (μ M)
PC9	0.3 (\pm 0.08)
PC9ER	0.7 (\pm 0.3)
H3255	0.3 (\pm 0.02)
H1975	7.1 (\pm 0.8)
H358	3.3 (\pm 0.6)
A549	1.8 (\pm 0.3)
H1650	0.2 (\pm 0.04)

Figure 52: Differential FED20 inhibition of p-EGFR in NSCLC cell lines expressing mutant or wild type EGFR.

A- Protein expression of p-EGFR (Y1068) and EGFR in NSCLC cells, treated with increasing concentrations of FED20. B1- Percentage inhibition of p-EGFR (Y1068) normalised to EGFR levels following FED20 treatment determined from the densitometry of the western blots. B2- Table summarising the average IC₅₀ values \pm SE, obtained from the percentage inhibition of p-EGFR plots. Data show mean \pm SE from three separate experiments.

To investigate a potential relationship between the differential inhibition of EGFR autophosphorylation in mutant EGFR by FED20, and the binding of radiolabeled [¹⁸F]FED20 to the different mutant forms of EGFR, the uptake of [¹⁸F]FED20 in wild type and mutant EGFR expressing NSCLC cell lines was carried out (Figure 53).

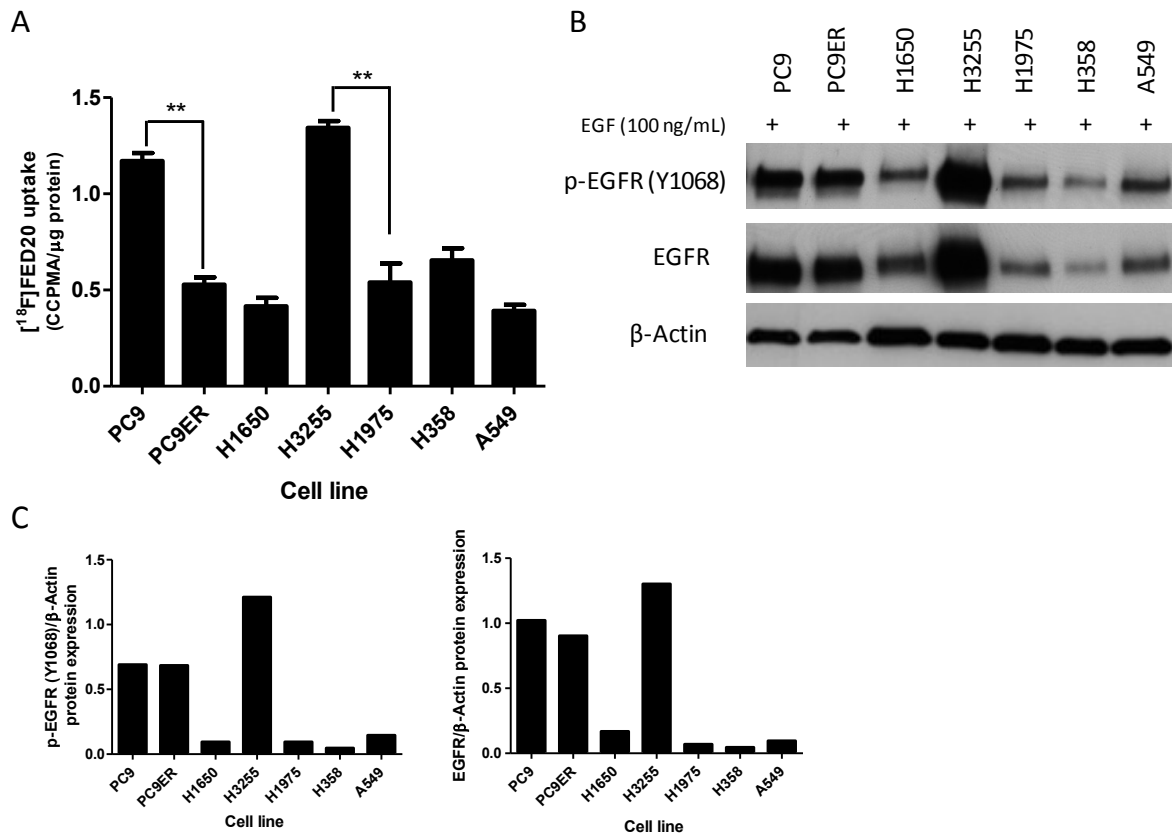


Figure 53: Differential uptake of [¹⁸F]FED20 in active and resistant mutant EGFR.

A- Protein normalised uptake of [¹⁸F]FED20 in NSCLC cells expressing mutant or WT EGFR following 1 h incubation with 0.55 MBq of [¹⁸F]FED20. Data show mean of triplicate ± SE from one representative experiment performed twice. Stars indicate statistical difference between values of two-tailed unpaired t-test (**p ≤ 0.01). B- Differential protein expression of p-EGFR (Y1068) and EGFR in NSCLC cell lines. C- Densitometry values of p-EGFR (Y1068) and EGFR protein expression normalised for β-actin protein expression.

Cell lines expressing active mutant forms of EGFR, showed the highest levels of uptake of the tracer, with values of 1.2 and 1.3 CCPMA/μg of protein in PC9 and H3255 cells, respectively (Figure 53A). However, the uptake of [¹⁸F]FED20 in H1650 cells, which also express active mutant EGFR, was low at 0.41 CCPMA/μg of protein. Wild type EGFR expressing A549 and resistant mutant expressing H1975 and PC9ER showed the lowest levels of uptake, with values of 0.4, 0.5 and 0.5 CCPMA/μg of protein, respectively (Figure 53A). H358 cells which also expressed wild type EGFR showed slightly higher uptake of [¹⁸F]FED20 (0.6 CCPMA/μg of protein). As discussed previously as well as expressing

different mutant forms of EGFR the different NSCLC studied also expressed differential levels of both p-EGFR (Y1068) and EGFR (Figure 53B). The densitometry measures obtained from the western blots indicated that H3255 cells expressed the highest levels of p-EGFR (Y1068) and EGFR whilst H1650, H1975 and H358 expressed the lowest levels of p-EGFR (Y1068) and EGFR (Figure 53C).

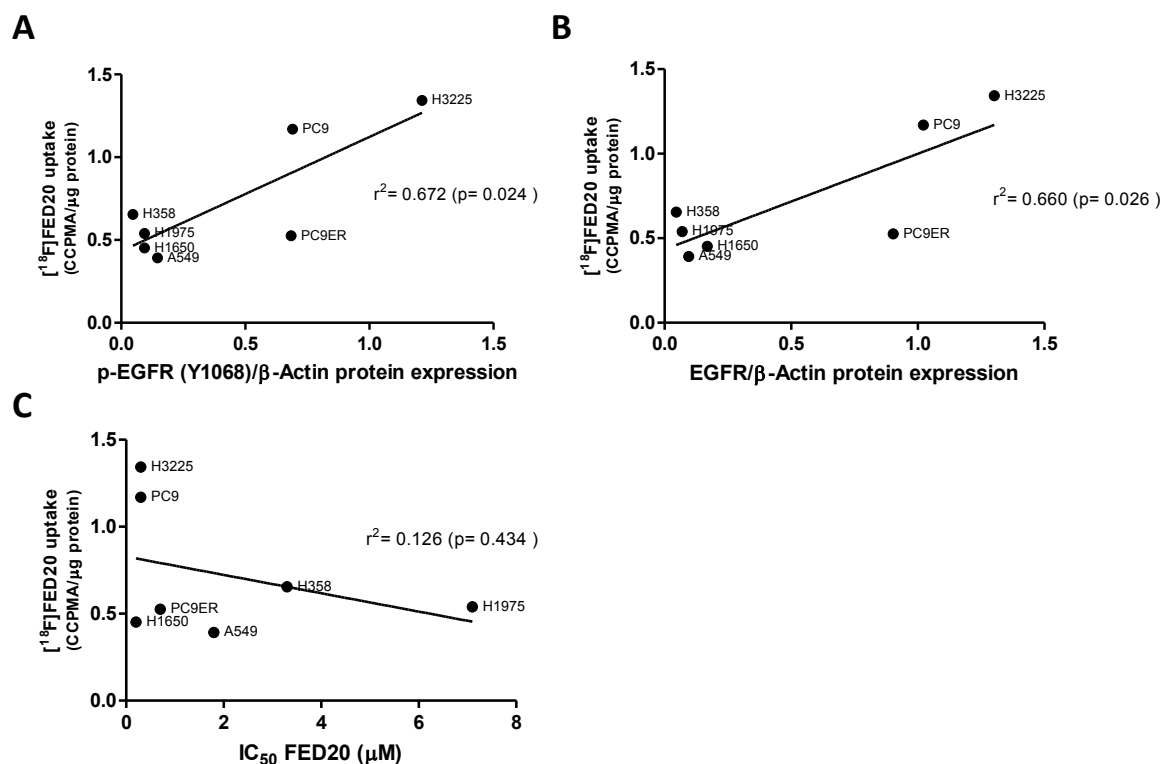


Figure 54: Correlation between ^{18}F FED20 uptake, EGFR protein expression and FED20 IC_{50} status.

A- ^{18}F FED20 uptake over protein expression of p-EGFR (Y1068) normalised to β -Actin. B- ^{18}F FED20 uptake over protein expression of EGFR normalised to β -Actin. Protein expression values obtained from densitometry reading of western blots. Data show values from one representative carried out in triplicate. C- ^{18}F FED20 uptake over IC_{50} of FED20. IC_{50} values expressed as mean of IC_{50} values obtained from p-EGFR (Y1068) inhibition plots following FED20 treatment from three separate experiments. r^2 correlation values indicated on the plots, statistically significant correlation indicated by $p \leq 0.05$.

In order to better understand whether the differential uptake of ^{18}F FED20 in the NSCLC studied was linked to p-EGFR (Y1068) protein expression, EGFR protein expression and or FED20 affinity in these different cell lines, correlation graphs were plotted (Figure 54). The higher expression of p-EGFR (Y1068) and EGFR in H3255 correlated to a high uptake of ^{18}F FED20, whilst the low expression of p-EGFR (Y1068) and EGFR in H1975, H1650 and A549 correlated with low cell uptake of ^{18}F FED20 (Figure 54A,B). The levels of uptake of ^{18}F FED20 did not seem to correlate to p-EGFR (Y1068) or EGFR levels in the H358, PC9 or PC9ER cells (Figure 54A,B). The low IC_{50} of FED20 in H3255 and PC9 corresponded to higher uptake of ^{18}F FED20 whilst the high IC_{50} of FED20 in H1975

correlated with a low tracer uptake in these cells. However, there wasn't a clear correlation between the affinity of FED20 in the other NSCLC studied and the uptake of [¹⁸F]FED20 as indicated by a lack of statistical correlation and r^2 correlation values of 0.672 and 0.660 (Figure 54). The direct correlation of the affinity of FED20 in these different cells lines, which reflected the mutational status of EGFR, with the uptake of [¹⁸F]FED20 is confounded by differential levels of expression of both p-EGFR (Y1068) and EGFR in the majority of the cell line investigated. In this regard, the differential uptake of [¹⁸F]FED20 in PC9 and PC9ER cells, which express identical levels of EGFR, could be attributed to the differential affinity of FED20 in these two cell lines.

In conclusion, FED20 was sensitive to EGFR expression and as for FED6, FED20 also showed higher affinity against active mutant EGFR compared to WT or resistant mutant EGFR. There was also a better correlation between the uptake of [¹⁸F]FED20 in the NSCLC and the affinity of FED20 for the different mutant forms of EGFR than was the case for [¹⁸F]FED6, despite a lack of correlation in several of the NSCLC cell lines tested. We hypothesize that this is a consequence of the lack of substrate specificity of FED20 for ABCG2 or ABCB1. Indeed, the substrate specificity of FED6 for ABCG2 confounded the results of the uptake of [¹⁸F]FED6 in the NSCLC that were shown to express ABCG2.

Chapter 5: Monitoring response to gefitinib treatment in NSCLC

As well as investigating EGFR directly by PET imaging for potential therapy evaluation, another approach is to measure changes in other molecules, known to interact with EGFR as a surrogate of response to treatment. One such molecule, which will be investigated hereafter, is ChK α .

5.1 Choline kinase alpha as a biomarker of response to gefitinib

5.1.1 *In vitro* assessment of choline kinase alpha as a biomarker of response to gefitinib treatment in PC9 and PC9ER cells

Choline kinase plays a key role in the metabolism of choline (see Figure 11), it is the first enzyme in the Kennedy pathway and leads to the conversion of choline to phosphocholine (Gibellini and Smith, 2010). The role of ChK α as a component in the regulation of the activity of EGFR has been elucidated in breast cancer and was shown to involve the interaction of ChK α with EGFR and SRC. The mechanistic involvement of ChK α as part of this complex makes it an important molecule to investigate for the assessment of response to therapies directed against EGFR. As well as the mechanistic link between ChK α and EGFR, the biological relevance of studying ChK α in the context of lung cancer is also significant. Overexpression and or increased activity of ChK α have been reported in many cancers including, brain, breast, lung and colorectal (Glunde et al., 2011). It has also been shown to act as a prognostic biomarker of survival in lung cancer. (Ramirez de Molina et al., 2007). Based on these findings, the aim was to investigate whether choline kinase could be used as a biomarker of response/resistance to gefitinib treatment in lung cancer.

The effect of gefitinib treatment was measured *in vitro* in the sensitive PC9 and resistant PC9ER cells. The differential sensitivity of these two cell lines to gefitinib was confirmed by performing cell viability assays after 6, 24, 48 and 72 h treatment. The GI₅₀ values determined are plotted in Table 14.

For the rest of the experiments, three time points were assessed, 6, 24 and 48 h treatment. The 6 and 24 h time points would be predictors of pharmacodynamic interactions whereas the 48 h time point focused on response to treatment. The same concentrations of gefitinib were chosen for the 6 and 24 h time points. However, these concentrations were too toxic to the gefitinib sensitive PC9 cells when treating for 48 h. Therefore, lower concentrations of gefitinib were selected for the 48 h time point. As a prelude to measurement of ChK α function (expression and activity, linked to upstream and downstream signalling), changes in the cell cycle and apoptosis were determined.

Table 14: GI₅₀ of gefitinib in PC9 and PC9ER cells.

	PC9	PC9ER
GI₅₀ at 6 h	>100	>100
GI₅₀ at 24 h	42 (± 6)	62 (± 2)
GI₅₀ at 48 h	0.060 (± 0.01)	6.7 (± 0.3)
GI₅₀ at 72 h	0.036 (± 0.011)	5.8 (± 0.1)

GI₅₀ values were determined by performing a cell viability SRB assay following, 6, 24, 48, and 72 h gefitinib treatment of PC9 and PC9ER cells. Data represent means ± SE of GI₅₀ values obtained from three separate experiments. GI₅₀ Values expressed in µM.

5.1.1.1 Cell cycle profile following 6, 24 and 48 h gefitinib treatment.

Choline kinase has been shown to play an important role in the regulation of cell proliferation and appears to be involved in the regulating the G1 to S phase transition (Ramirez de Molina et al., 2008). Therefore, as well as investigating the changes to choline kinase activity and expression the effect of gefitinib treatment on the cell cycle profile was assessed in order to correlate any changes with changes to ChKα. For this, PI staining of the DNA obtained from gefitinib treated cells was performed, and the stained samples were analysed by FACS flow cytometry.

The cell cycle profile of the PC9 cells after 6, 24 and 48 h gefitinib treatment are illustrated in Figure 55A. The peak at 50K was characteristic of cells in G1 phase of the cycle and the peak at 100K was characteristic of cells in G2/M phase. There were no changes in the cell cycle profile after 6 h gefitinib treatment. Over 40 % of the PC9 cells were in G1 phase. After both 24 and 48 h treatment there was a significant increase in the number of cells in sub-G1 phase illustrated by appearance of a peak at 25K, and a reduction of the number of cells in G1 and G2/M phases of the cell cycle. After 24 h treatment, 40 % of PC9 cells were in sub-G1 at 3 and 10 µM gefitinib and 55 % of cells were in sub-G1 at 20 µM gefitinib compared to 3% in untreated control cells. The percentage of cells in G1 and G2/M phase of the cell cycle were also decreased following treatment from 59 and 17% in control cells to 26 and 3 % at 20 µM gefitinib. After 48 h treatment, 0.001 and 0.01 µM of gefitinib did not lead to significant changes to the cell cycle distribution compared to 1 and 3 µM of gefitinib which led to significant changes to the percentage distribution of cells in the cell cycle. The percentage of cells in sub-G1 increased from 5 % in control cells to 78 % at 1 µM gefitinib, whilst the percentage of cells in G1 and G2/M phases decreased from 66 and 14 % in the control sample to 14 and 1 % at

1 μM gefitinib. The reduction of cells in G1, S and G2/M and the increase in cells in sub-G1 were indicative of cell death.

As with the PC9 cells there was no change to the cell cycle profile of the PC9ER cells after 6 h gefitinib treatment, with over 40 and 30 % of the cells in G1 and G2M phase, respectively. After 24 h treatment, only the two highest concentrations of gefitinib led to a change in the cell cycle profile compared to the untreated cells. The percentage of cells in sub-G1 increased from 7 % in the untreated control cells to 25 % after 10 and 20 μM of gefitinib treatment (Figure 55B). After 48 h treatment, only the highest concentration of gefitinib of 3 μM led to any changes to the cell cycle profile of the PC9ER cells compared to the untreated control cells. Indeed, 12 % of cells were in sub-G1 compared to 4 % in the untreated control cells (Figure 55B).

In conclusion, the cell cycle profile analysis showed high levels of cell death in PC9 cells compared to PC9ER cells following gefitinib treatment for 24 and 48 h. The highest concentrations of gefitinib of 10 and 20 μM also caused an increase in cell death in the resistant PC9ER cells.

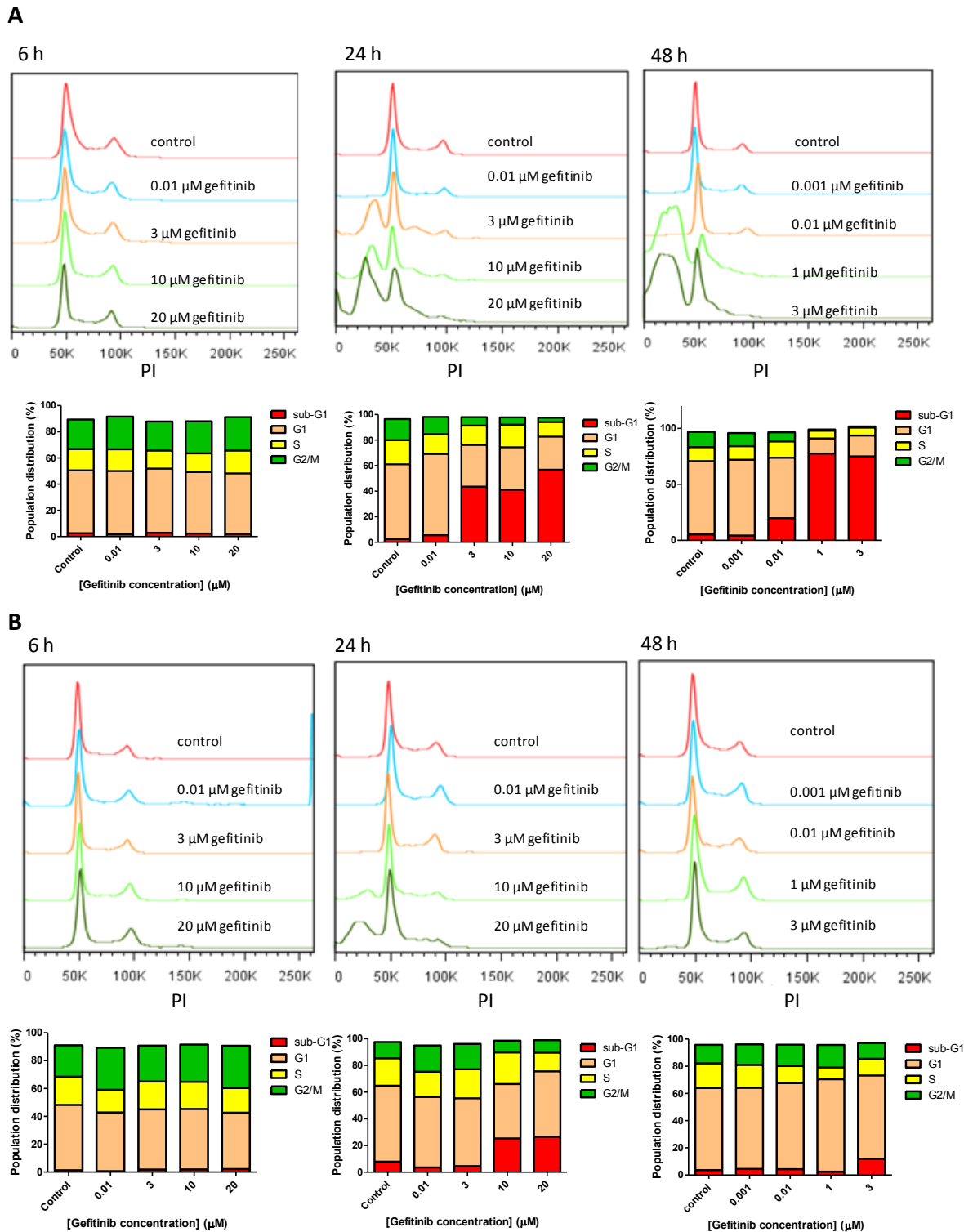


Figure 55: Cell cycle profile of PC9 or PC9ER cells following 6, 24 and 48 h gefitinib treatment.

Cell cycle profile (top panels) and cell cycle phase distribution (bottom panels) indicating DNA content of PC9 (A) and PC9ER (B) cells following 6 h (left hand panel), 24 h (middle panel) and 48 h (right hand panel) of gefitinib treatment. Data from one representative experiment carried out in triplicate.

5.1.1.2 Apoptosis levels following 6, 24 and 48 h gefitinib treatment

Gefitinib treatment especially at concentrations above 10 μM and after 24 h treatment led to significant increases in the number of cells in sub-G1 phase of the cell cycle. An accumulation of cells in sub-G1 was characteristic of an increase in cell death. To further investigate whether cell death was due to caspase 3/7-induced apoptosis, a caspase glow 3/7 assay was carried out in both cell lines following gefitinib treatment (Figure 56). In PC9 cells, after 6 h treatment, there were no changes to levels of apoptosis at concentrations below 10 μM of gefitinib. A 1.8 and 2.4 fold increase in apoptosis were measured at 10 and 20 μM of gefitinib, respectively. After 24 h treatment, there was a 4, 8 and 17 fold increase in apoptosis in the PC9 cells treated with 3, 10 and 20 μM of gefitinib, respectively. After 48 h treatment, there were no changes to the levels of apoptosis at gefitinib concentrations below 0.1 μM . There was a 13 and 15 fold increase in apoptosis following 0.1 and 1 and 3 μM gefitinib, respectively compared to untreated cells (Figure 56A). In PC9ER cells, levels of apoptosis were unchanged after 6 h gefitinib. After 24 h treatment, no apoptosis was measured at concentrations of gefitinib below 10 μM . However, there was a 6 and 20 fold increase in apoptosis levels after 10 and 20 μM gefitinib. After 48 h treatment, only 1 and 3 μM gefitinib led to an increase in levels of apoptosis. These increased by just under two-fold compared to control untreated cells (Figure 56B).

In conclusion, the caspase glow3/7 assay showed high levels of apoptosis in PC9 cells at 10 and 20 μM gefitinib after 6 and 24 h treatment and at 0.1, 1 and 3 μM gefitinib after 48 h treatment. High levels of apoptosis were only measured after 24 h treatment at 10 and 20 μM gefitinib in PC9ER cells. The high levels of apoptosis measured in the caspase glow 3/7 assay correlated with the high levels of cell death associated with high levels of sub-G1 measured in the cell cycle analysis of PC9 and PC9ER cells following gefitinib treatment.

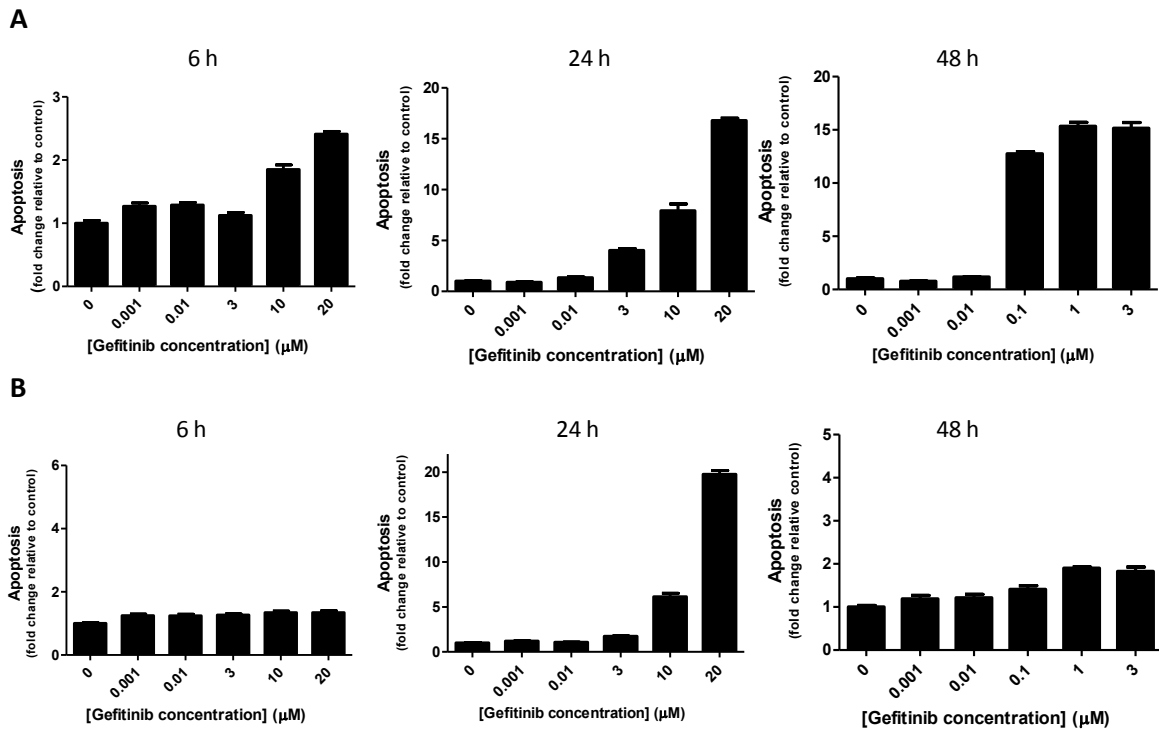


Figure 56: Apoptosis levels in PC9 and PC9ER cells following 6, 24 and 48 h gefitinib treatment.

Fold change in apoptosis in PC9 (A) and PC9ER (B) cells following 6, 24 and 48 h gefitinib treatment assessed by carrying out a caspase 3/7 assay. Data show mean fold changes in apoptosis following protein normalisation of $n = 4$ samples \pm SE from one representative experiment carried out two times.

5.1.1.3 Changes to ChK α protein expression following 6, 24 and 48 h gefitinib treatment.

The differential sensitivity of PC9 and PC9ER cells for gefitinib in particular after 48 h treatment were demonstrated above. The role of ChK α as a potential biomarker for the differential response to gefitinib treatment was then addressed. First, the protein expression profile of p-EGFR (Y1068), EGFR, p-ERK, ERK as well as ChK α following 6, 24 and 48 h gefitinib treatment of PC9 and PC9ER cells were investigated. p-EGFR (Y1068), EGFR, p-ERK and ERK showed similar patterns of expression after 6, 24 and 48 h gefitinib treatment (Figure 57). In the gefitinib sensitive PC9 cells, p-EGFR (Y1068) and p-ERK were completely inhibited at all concentrations of gefitinib while EGFR and ERK were unchanged. In the resistant PC9ER cells, there was a dose dependant decrease in p-EGFR (Y1068) and p-ERK with increasing concentrations of gefitinib, only the highest concentration of 20 μ M at 6 and 24 h, and 3 μ M at 48 h, of gefitinib led to complete inhibition of protein expression. EGFR and ERK protein levels were unchanged with treatment (Figure 57). ChK α expression was unchanged in both cell lines after 6 h gefitinib treatment. After 24 h treatment, the protein expression of ChK α decreased by 30 % at all concentrations of gefitinib in PC9 cells measured by a decrease in

densitometry values for ChK α (Figure 57B right panel) whereas a concentration dependant increase in levels of ChK α were measured in PC9ER cells. After the longer incubation of 48 h, there was a concentration dependant decrease in the protein expression of ChK α in the PC9 cells. A decrease of over 40 % was measured at 1 and 3 μ M gefitinib, whereas an increase in the protein expression of ChK α was measured in the PC9ER cells (Figure 57C right panel).

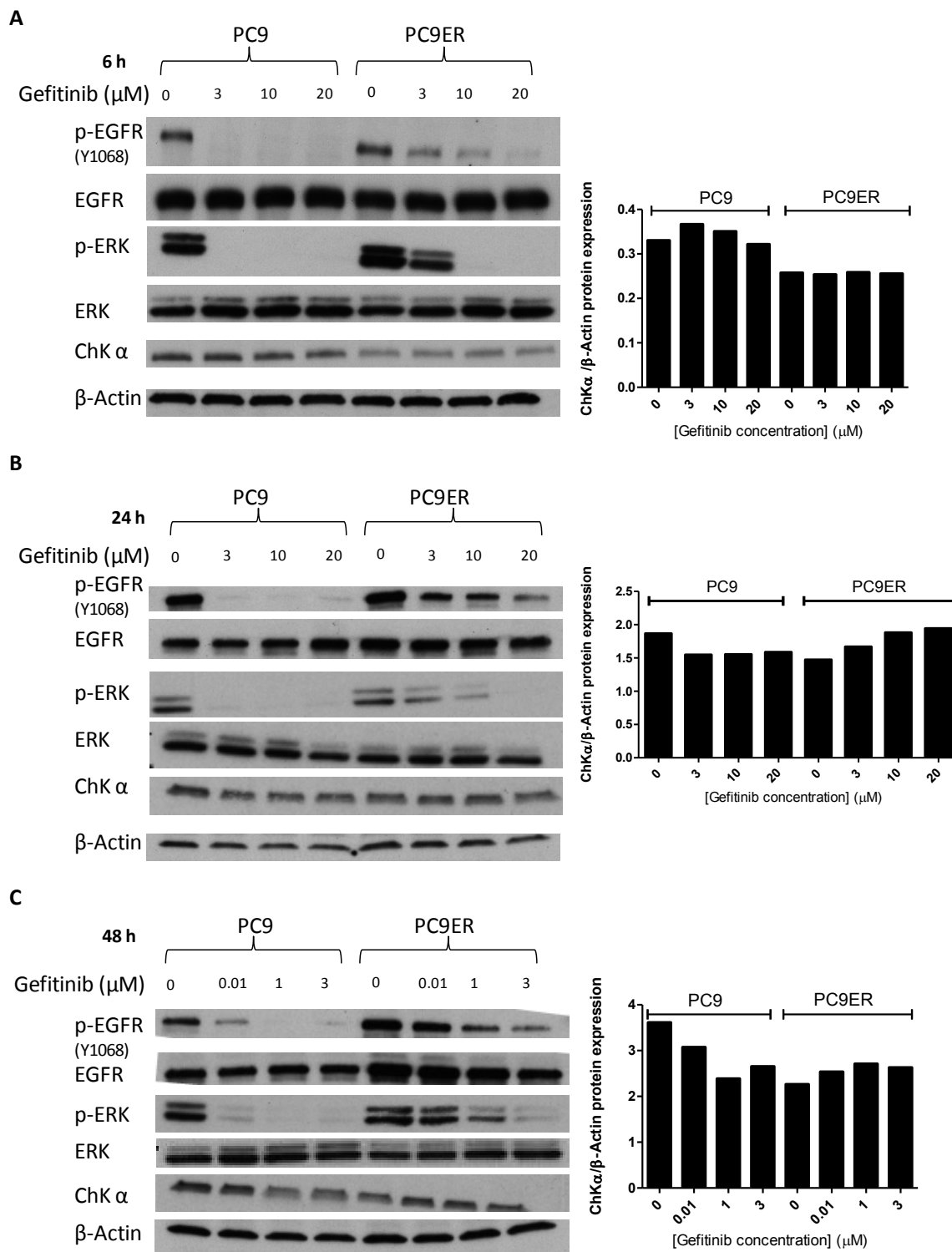


Figure 57: Changes in choline kinase alpha protein expression following 6, 24 and 48 h gefitinib treatment in PC9 and PC9ER cells.

A-C- Protein expression of P-EGFR Y1068, EGFR, p-ERK, ERK and ChK α (left panel) of PC9 and PC9ER cells following gefitinib treatment for 6 h (A), 24 h (B) and 48 h (C). Right panel indicates densitometry values of ChK α expression corrected for β -actin levels. Data show results from one representative experiment carried out three times.

To further investigate changes to ChK α expression, mRNA levels of ChK α were assessed following gefitinib treatment.

5.1.1.4 Levels of ChK α mRNA following 6, 24 and 48 h gefitinib treatment.

There was no significant change in the mRNA levels of ChK α in the PC9 cells at all three time points. In PC9ER cells, mRNA levels of ChK α increased following gefitinib treatment at 6, 24 and 48 h treatment. This increase was not always concentration dependant; after 6 h treatment, all three concentrations of the drug led to the same increase in expression of ChK α mRNA, just under 2 fold compared to control. There was a 2.8 and 3.1 fold increase in levels of ChK α mRNA after 1 and 3 μ M gefitinib treatment, respectively (Figure 58B).

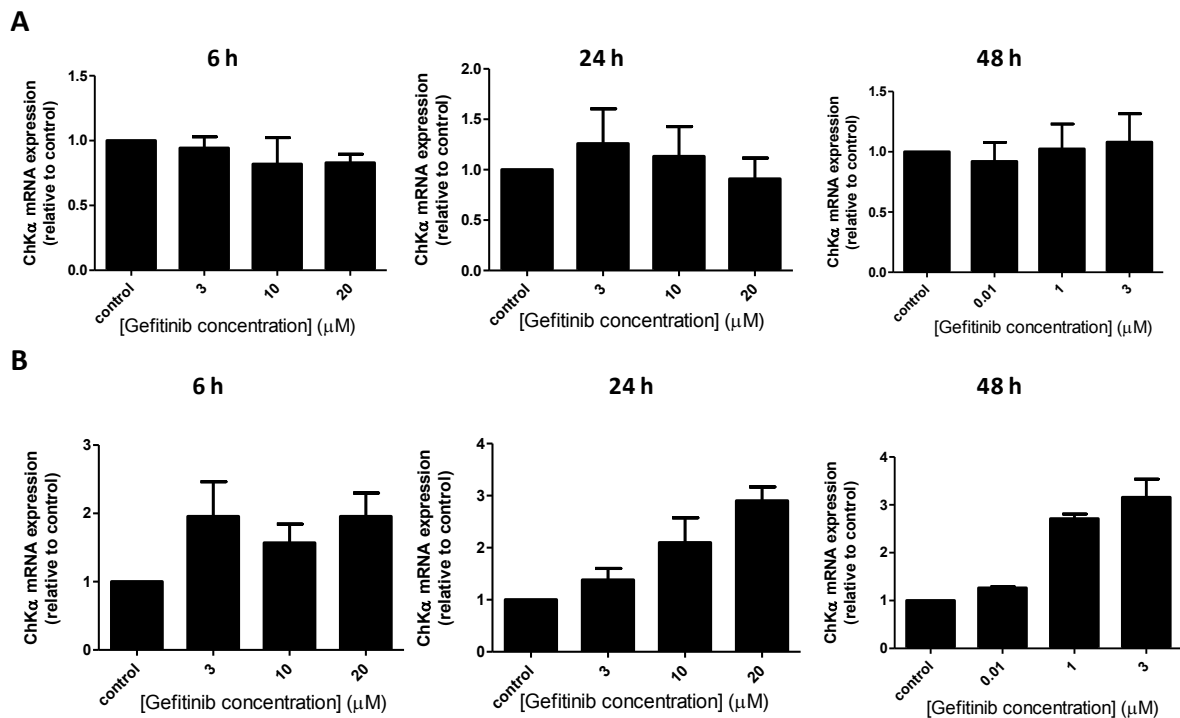


Figure 58: Changes to ChK α mRNA levels following 6, 24 and 48 h gefitinib treatment.

mRNA expression of ChK α of PC9 (A) and PC9ER (B) cells following 6, 24 and 48 h gefitinib treatment. Data represent mean levels of ChK α mRNA normalised to GAPDH and expressed relatively to control DMSO treated sample \pm SE of duplicates from three separate experiments

Despite a decrease in protein expression measured following 24 and 48 h gefitinib treatment in PC9 cells no decrease in ChK α mRNA was measured. Protein and mRNA expression of ChK α were also

uncorrelated in PC9ER cells, in which an increase in mRNA levels of ChK α were measured at all three time points whereas an increase in the protein expression was only measured after 48 h treatment.

Having measured differential expression levels of ChK α in PC9 and PC9ER cells following gefitinib treatment, the role of ChK α as a biomarker of response to gefitinib treatment was further assessed by measuring changes to the activity of ChK α .

5.1.1.5 [3 H]choline uptake following 6, 24 and 48 h gefitinib treatment.

In order to assess the activity of ChK α following gefitinib treatment in the PC9 and PC9ER cells [3 H]Choline uptake experiments were carried out.

Choline kinase is responsible for the phosphorylation of choline to phosphocholine. Once choline is phosphorylated it is trapped within the cell. Therefore, the retention of [3 H]phosphocholine in the cell can be used as a surrogate measure of the activity of ChK α (Nimmagadda et al., 2009).

[3 H]choline uptake experiments in which the retention of the radioactivity was measured in the whole cell lysate were first carried out (Figure 59). This uptake reflected both the transport and phosphorylation of [3 H]choline.

The basal levels of [3 H]choline uptake, measured in untreated cells, were 2 to 3 fold higher in PC9 than in PC9ER cells (Figure 59). In PC9 cells, the uptake of [3 H]choline decreased by 50 % after both 6 and 24 h treatment with gefitinib at 3 and 10 μ M. At the highest concentration of 20 μ M the uptake of the radiotracer decreased by 70 % after 6 h and 84 % after 24 h treatment. (Figure 59A,B). After 48 h treatment, both 1 and 3 μ M of gefitinib led to a 74 % decrease in the uptake of [3 H]choline (Figure 59C).

In PCER cells, at 6 h, in contrast to the PC9 cells, only the highest concentration of 20 μ M gefitinib led to a decrease in [3 H]choline uptake, over 50 % compared to untreated cells (Figure 59A). After 24 h treatment, both 10 and 20 μ M gefitinib led to a decrease in [3 H]choline uptake (Figure 59B). Finally, following 48 h gefitinib treatment no change in the uptake of [3 H]choline were measured in the PC9ER cells compared to control (Figure 59B,C).

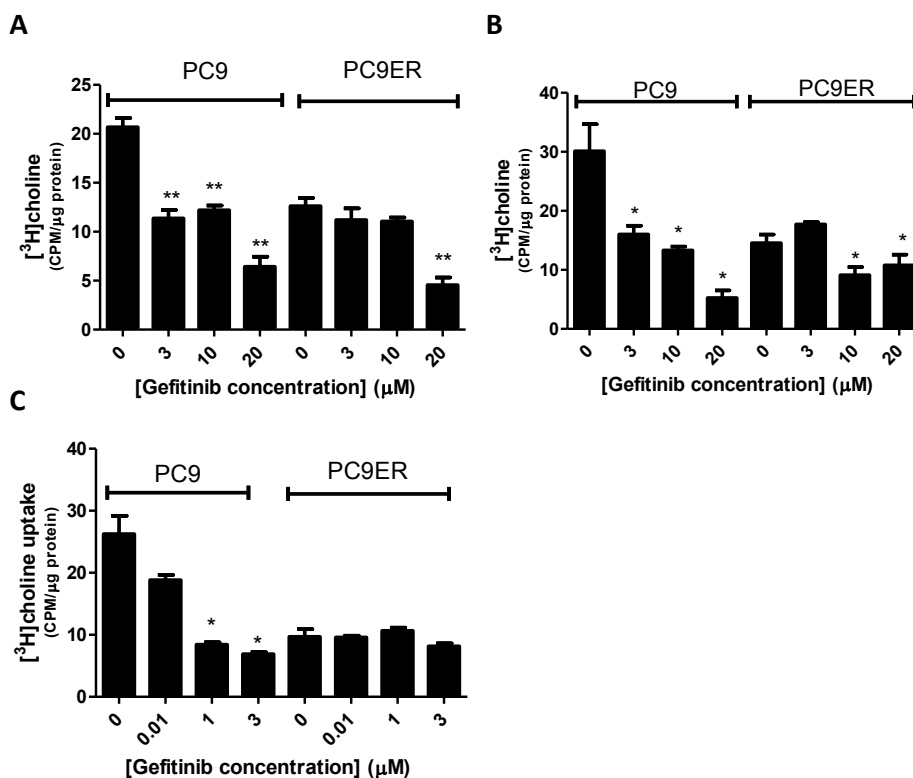


Figure 59: Whole cell [³H]choline uptake in PC9 and PC9ER cells following 6, 24 and 48 h gefitinib treatment.

Corrected counts per minute per μg of protein of [³H]choline in whole cell lysate of PC9 and PC9ER cells following 6 h (A), 24 h (B) and 48 h (C) gefitinib treatment. Data show mean values ± SE of triplicates from one representative experiment carried out three times. Stars indicate statistical difference between tested value and control of two-tailed unpaired t-test (* p ≤ 0.05 **p ≤ 0.01).

Following [³H]choline incubation, cells were washed before being collected and lysed. Any untrapped [³H]choline should therefore have been removed during the washing step. Hence only the [³H]phosphocholine component which would have been trapped in the cell would be measured in the whole cell lysate. In order to further investigate that the radioactivity measured in the whole cell lysate reflected the formation of [³H]phosphocholine, a [³H]Choline uptake assay in which the [³H]phosphocholine component was isolated from the whole cell lysate was performed (Figure 60).

As for the whole cell lysate uptake, the basal levels of [³H]phosphocholine were 2 to 3 fold higher in PC9 than in PC9ER cells (Figure 60A). In PC9 cells, there was a differential effect of gefitinib treatment at different time points. After 6h treatment, levels of [³H]phosphocholine decreased by 20 % at 10 μM gefitinib and by 40 % at 20 μM gefitinib compared to untreated cells (Figure 60A). After 24 h treatment, 3 μM gefitinib caused a 60 % decrease in levels of [³H]phosphocholine whilst the highest concentration of 20 μM caused a 90 % decrease in [³H]phosphocholine (Figure 60B). At

48 h, there was a significant decrease in [³H]phosphocholine at all concentrations of gefitinib. Both 1 and 3 μM of the drug led to a 67 % decrease in levels of [³H]phosphocholine compared to untreated cells.

In PC9ER cells, after 6 h treatment, levels of [³H]phosphocholine decreased by 30 and 60 % at 10 and 20 μM gefitinib, respectively. After 24 h treatment, only 20 μM gefitinib caused a significant decrease in [³H]phosphocholine levels (Figure 60A,B). At 48 h, in contrast to PC9 cells, levels of [³H]phosphocholine were unchanged following 48 h gefitinib treatment in PC9ER cells (Figure 60C).

With the exception of 6 h treatment in the PC9 cell, the values of [³H]phosphocholine measured following phosphocholine isolation were in line with the uptake values obtained from whole cell lysate. Therefore, the radioactivity measured in the whole cell lysate corresponded to the phosphocholine component. The initial washes which were carried out to remove the excess [³H]choline at the end of the tracer incubation, removed any untrapped choline. Incomplete recovery of [³H] phosphocholine, during the extraction process, could account for some of the discrepancies between the uptake values measured using both methods. We therefore concluded that isolation of [³H]phosphocholine was not necessary and that measuring the uptake of [³H]choline in the whole cell was indicative of the levels of phosphocholine formed as a result of ChKα activity.

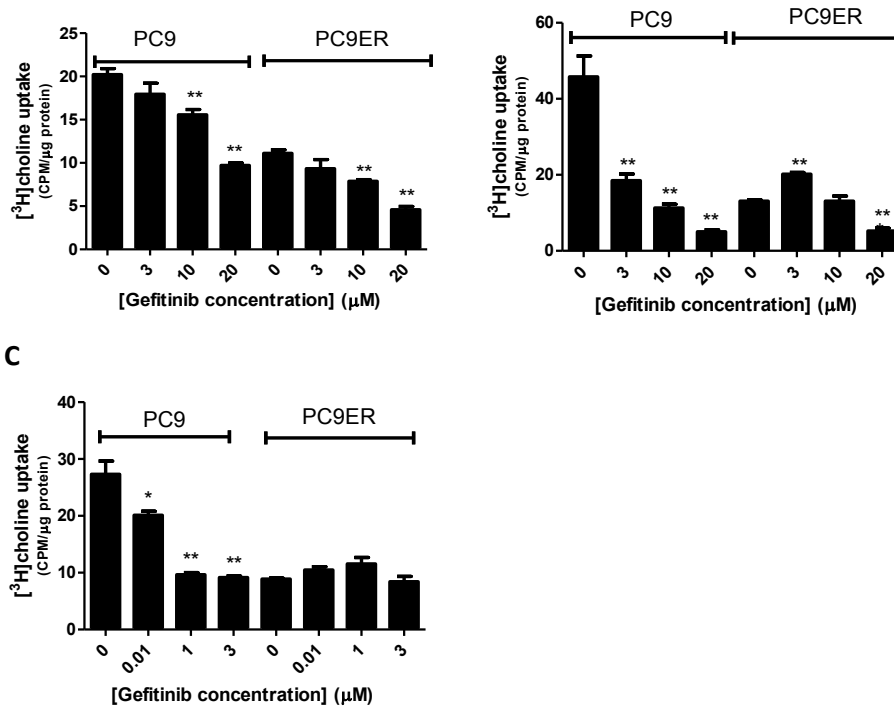


Figure 60: [³H]phosphocholine levels in PC9 and PC9ER cells following 6, 24 and 48 h gefitinib treatment.

Counts per minute acquired per μg of protein of the [³H]phosphocholine fraction from PC9 and PC9ER cells following gefitinib treatment for 6 h (A), 24 h (B) and 48 h (C). Data show mean values ± SE of triplicates of one representative experiment carried out three times. Statistically significant changes compared to untreated control from two-tailed unpaired t-test are marked with star (* = P ≤ 0.05 and ** = p ≤ 0.01).

In conclusion both [³H]phosphocholine isolation and whole cell lyaste [³H]choline uptake, indicated a differential effect of gefitinib on ChKα activity in the sensitive PC9 and resistant PC9ER cell line. At the earlier time points of 6 and 24 h, the activity of ChKα was decrease at all concentrations of gefitinib in the sensitive PC9 cells, whereas only the highest concentrations of 10 and 20 μM led to a decrease in ChKα activity in PC9ER cells. After 48 h treatment, there was a differential effect of gefitinib on ChKα activity as measured by a decrease in [³H]phosphocholine in PC9 cells but no change in PC9ER cells.

5.1.2 *In vivo* [¹⁸F]D4choline uptake in PC9 and PC9ER xenografts.

As discussed in section 5.1.1 a differential effect of both ChK α protein expression and activity were measured in PC9 and PC9ER cells treated with gefitinib. After 48 h treatment there was a significant decrease in ChK α activity and protein expression in gefitinib sensitive PC9 cells whereas there was no change in PC9ER cells. Based on the findings, the aim was to investigate whether ChK α could be used as a biomarker of early response, failure of response to gefitinib treatment *in vivo*.

Several radiotracers based on choline, including [¹¹C]choline (Contractor et al., 2011a) and [¹⁸F]fluoromethylcholine (DeGrado et al., 2001a) discussed in chapter 1 have been developed for PET imaging of choline metabolism. In these studies, a deuterium derivative of [¹⁸F]fluoromethylcholine, [¹⁸F]D4choline (Leyton et al., 2009, Witney et al., 2012), was used to investigate changes to choline metabolism of PC9 and PC9ER xenografts, following 48 h oral treatment of either 50 mg/kg of gefitinib or vehicle.

The merged CT/PET sagittal and transverse cross sections of PC9 xenografts (Figure 61A) indicated a low tumour uptake of [¹⁸F]D4choline. There was a high level of background uptake in the GI tract. Furthermore, there was a visibly lower uptake of the tracer at the very centre of the tumour. This was especially noticeable in the vehicle treated mouse (Figure 61A left panel) and could be caused by necrosis at the core of the tumour. The time activity curves (Figure 61B), indicated a higher uptake of [¹⁸F]D4choline in the gefitinib treated group compared to the vehicle treated group. The TACs were characterised by an initial phase from 0 to 3.5 minutes, in which the uptake of [¹⁸F]D4choline in the tumour increased in both groups. Following this initial perfusion of the tumour the uptake in the gefitinib treated group then decreased until 60 minutes, whereas the uptake in the vehicle treated group remained unchanged.

The sagittal and transverse cross section of the PC9ER xenografts showed similar levels of uptake in the vehicle (Figure 61B, left panel) and gefitinib treated (Figure 61B, right panel) xenografts. The TACs for both the vehicle (n = 6) and gefitinib (n = 4) treated PC9ER xenografts indicated an initial increase in [¹⁸F]D4choline uptake from 0 to 3.5 min followed by a small decrease in radiotracer uptake in the tumour until 60 min (Figure 61D). The TAC of the gefitinib treated group highlighted a significant intragroup variability in the uptake of [¹⁸F]D4choline compared to the vehicle treated group. The lower n number of mice scanned in the gefitinib group could account for this variability compared to the vehicle treated mice.

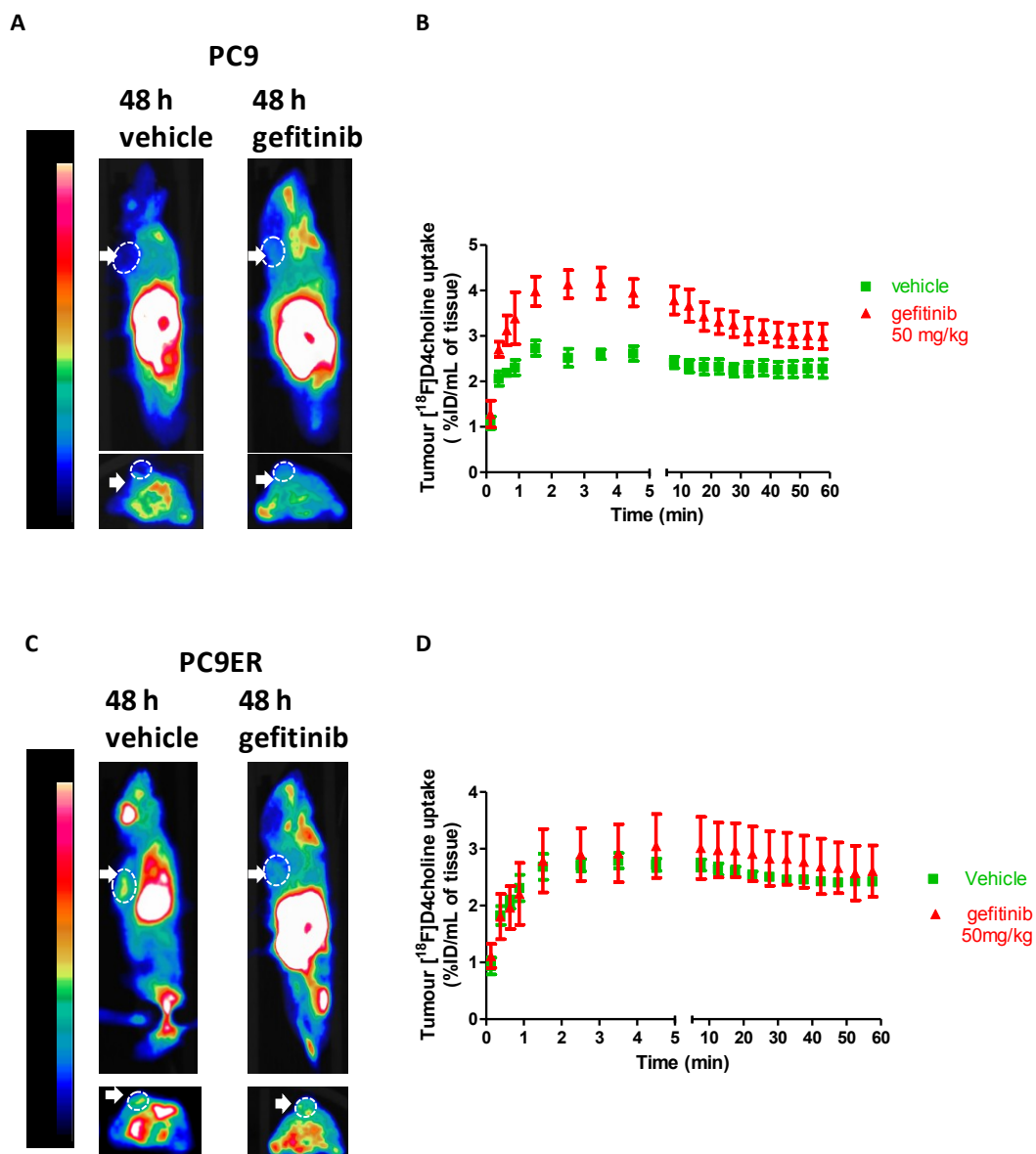


Figure 61: [¹⁸F]D4choline PET imaging of PC9 and PC9ER xenografts following 48 h gefitinib treatment.

A,C- Merged PET/CT image of representative sagittal (top) and frontal (bottom) cross section of PC9 (A) and PC9ER (C) xenograft mouse at baseline and following 48 h vehicle treatment or 48 h gefitinib treatment at 50 mg/Kg at 60 min post i.v. injection of 3.7 MBq of [¹⁸F]D4choline Tumours indicated by white arrow. B, D- Tumour time activity curves of PC9 (B) and PC9ER (D) xenografts. Values show mean ± SE of n = 4 mice per group.

Other parameters were determined to compare the vehicle and gefitinib treatments in both tumour models. First, the normalised uptake value at t = 60 min, which indicated the uptake of the tracer in the tumour 1 h post radiotracer injection was calculated There were no differences in the average NUV₆₀ of both vehicle and gefitinib treated PC9 and PC9ER xenografts (Figure 62A). The AUC value was significantly higher in the gefitinib treated group at 197 %ID/mL* min compared to 138 %ID/mL* min in the vehicle treated group in the PC9 xenografts. This can be explained by a

significantly higher initial uptake of [¹⁸F]D4choline in the tumour of the gefitinib compared to the vehicle treated PC9 xenografts. In the PC9ER xenografts, there was no difference in the AUC of the gefitinib and vehicle treated groups. (Figure 62B).

As described above the tumour models investigated were characterised by a tendency to develop necrotic cores, as illustrated in the H&E staining of sectioned tumours in Figure 63. One way of addressing this confounding feature was to determine the uptake of the radiotracer that corresponded to the highest quartile of radiotracer uptake in the tumour. These values were plotted in Figure 62C. These values indicated higher uptake as illustrated by higher % ID/mL values compared to the NUV₆₀. The uptake in the gefitinib treated group was no longer higher than that of the vehicle treated group for both the PC9 and PC9ER xenografts. This could indicate that potential higher levels of necrosis in the vehicle treated groups led to lower levels of uptake of [¹⁸F]D4choline than in the gefitinib treated groups.

Finally another potential confound to the tumour uptake of [¹⁸F]D4choline was differential perfusion of the tumours. One way of expressing the retention of the radiotracer in the tumour whilst discarding the initial uptake phase was to calculate the fractional retention of the tracer (FRT). Here the FRT was measured between 3.5 and 60 min. In the PC9 xenografts the FRT decreased from 0.9 in the vehicle treated group to 0.7 in the gefitinib treated group, this represented a 20 % decrease in FRT (Figure 62D). There was no change in the fractional retention values measured in the PC9ER xenografts (Figure 62D).

In conclusion, the confounds of tumour perfusion and necrosis may in part explain why no difference in tumour uptake were measured between the vehicle and gefitinib treated PC9 or PC9ER xenografts, when measuring the NUV₆₀. The FRT value was significantly lower following gefitinib treatment than vehicle treatment in the PC9 xenografts and based on the FRT values [¹⁸F]D4choline could be used to assess early response to gefitinib treatment in NSCLC.

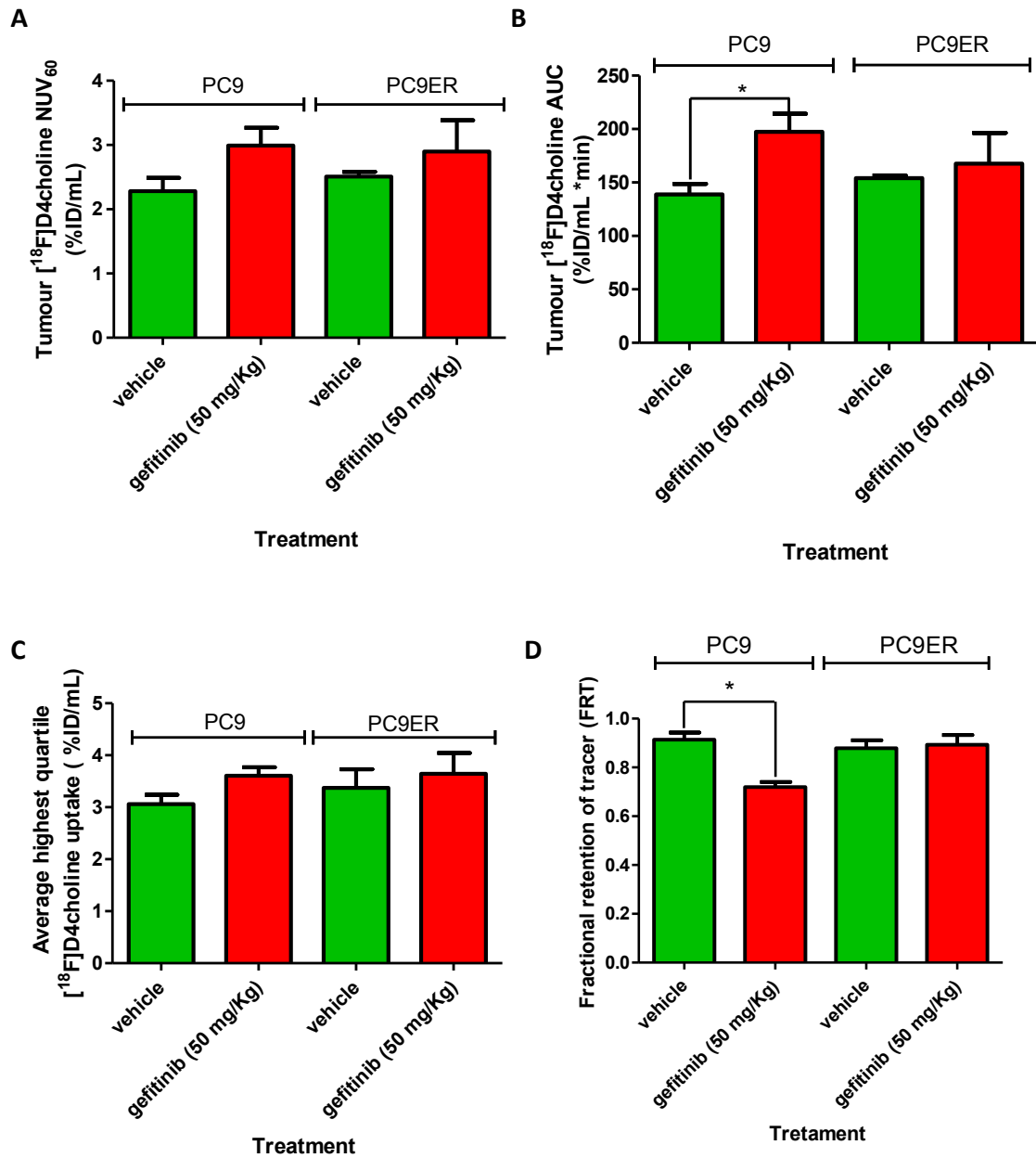


Figure 62: Tumour uptake parameters from [¹⁸F]D4choline PET imaging of PC9 and PC9ER xenografts following 48 h gefitinib or vehicle treatment.

Parameters determined after PET imaging of PC9 and PC9ER xenografts following 48 h gefitinib or vehicle treatment. A- Average tumour Uptake value of [¹⁸F]D4choline in PC9 and PC9ER tumours at t=60 min after tracer injection. B- Area under the curve values for PC9 and PC9ER tumours. C- Average highest quartile [¹⁸F]D4choline tumour uptake. D- Fractional retention of [¹⁸F]D4choline in PC9 and PC9ER tumours between 3.5 and 60 min post tracer injection. Data show mean ± SE of n = 4 mice per group. Statistically significant differences from two tailed unpaired t-test are marked with a star (* = P ≤ 0.05).

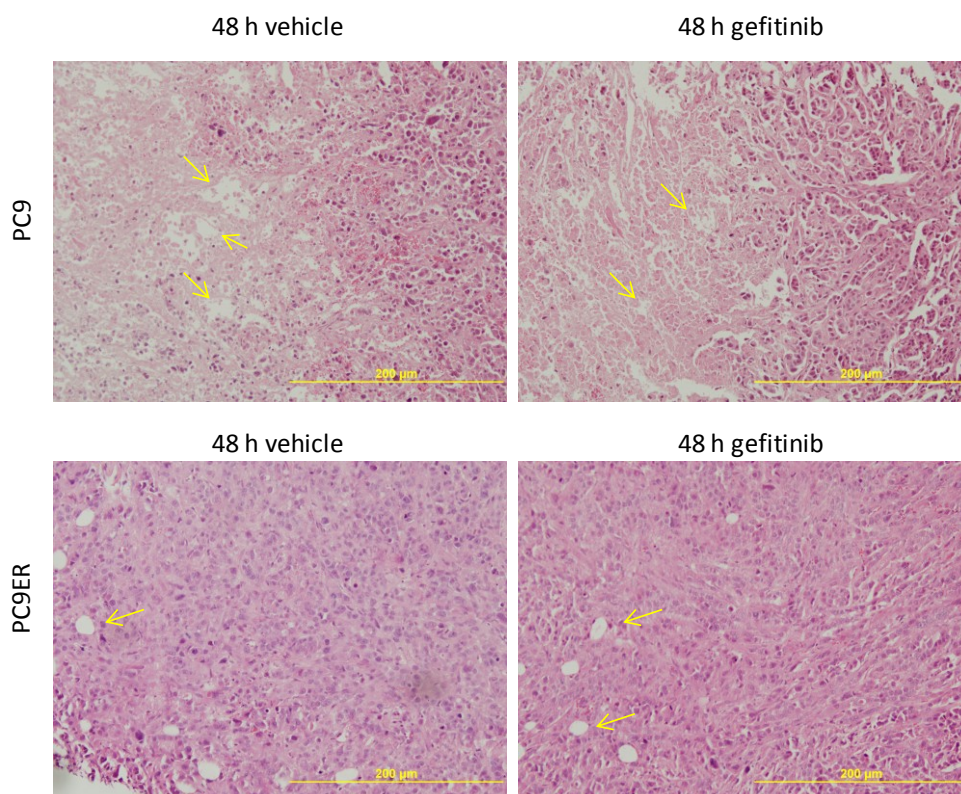


Figure 63: Representative immunohistochemistry analysis of PC9 and PC9ER tumour samples from [¹⁸F]D4choline PET imaging.

Tumours were extracted and fixed in formalin at the end of the PET scan. Tumours were then sectioned and stained for haematoxylin and eosin (H&E). Sample necrotic regions are indicated by yellow arrows.

The tumours from the PET study were collected, processed and analysed by gel electrophoresis (Figure 64). In the PC9 tumours a complete inhibition of p-EGFR (Y1068) in the tumours obtained from the gefitinib treated xenografts was measured, compared to tumour lysates from the vehicle group. Gefitinib treatment also led to a decrease in p-SRC Y416, Chk α , p-AKT and p-ERK. Levels of total EGFR were also decrease compared to vehicle treated xenografts. Total levels of AKT and ERK were the same as in vehicle treated tumours. In the PC9ER tumour lysates there was a decrease in the expression of p-EGFR Y1068 following gefitinib treatment. However, this decrease was y less than that of the PC9 tumours. There was also a decrease in the levels of p-SRC Y416 in the gefitinib treated group. Levels of Chk α , p-AKT, AKT, p-ERK and ERK were unchanged between vehicle and gefitinib treated tumours.

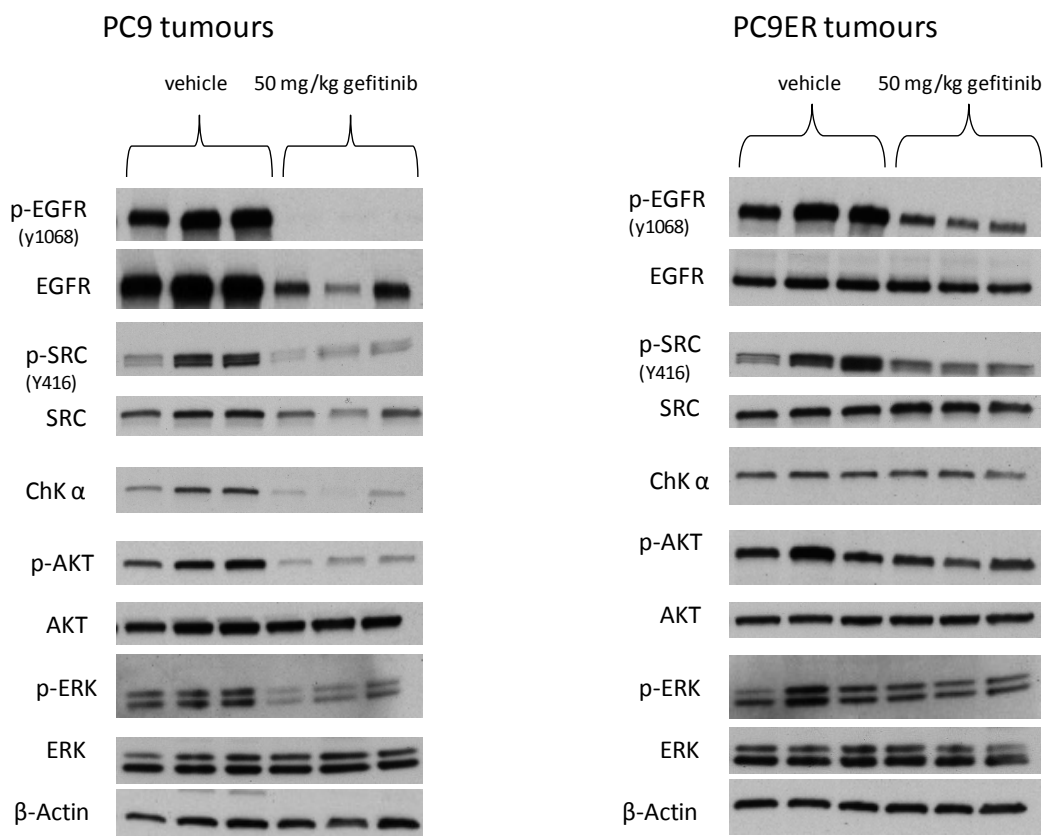


Figure 64: Protein expression analysis from PC9 and PC9ER tumour lysates following [¹⁸F]D4choline PET imaging.

Protein expression of p-EGFR Y1068, EGFR, ChK α , p-SRC Y416, SRC, p-AKT, AKT, p-ERK, ERK in tumour lysates from PC9 and PC9ER xenograft from 48 h vehicle or 50 mg/kg gefitinib treated groups. Each column represents a lysate from one tumour.

The changes to protein levels of ChK α that were measured from the analysis of the tumour lysates did not correlate with the values of [¹⁸F]D4choline which were measured in the different treatment groups of both the PC9 and PC9ER xenografts (when the measure was NUV₆₀ or AUC). The western blots indicated a decrease in levels of ChK α in the PC9 gefitinib treated group, the same group that showed the highest uptake of radiotracer in the PET imaging.

The FRT values for [¹⁸F]D4choline were the only parameters that appeared to correlate with the changes in ChK α expression. Indeed, no change in FRT values or ChK α expression were measured between the PC9ER groups and both the FRT and ChK α expression were decreased in the PC9 gefitinib treated group compared to vehicle.

5.1.3 Investigating the EGFR-ChK α -SRC complex.

In order to understand if the changes seen could be attributed in part to EGFR–SRC–ChK α complex, the involvement of ChK α in this complex was further assessed. It has been reported in breast cancer

models that SRC protein is involved in the interaction between EGFR and ChK α . Here, the interaction of EGFR, SRC and ChK α was studied in the sensitive and resistant lung cancer models used previously.

The effect of inhibiting EGFR or SRC on ChK α expression and activity were assessed. Protein expression of p-EGFR Y1068, p-SRC Y416, SRC and ChK α were measured and [3 H]choline uptake and changes in levels of apoptosis following both gefitinib and dasatinib were determined. Concentrations based on the GI $_{50}$ of each drug in the cell line investigated were used. PC9 and PC9ER cells were therefore treated with different concentrations of drug. In order to focus mainly on the pharmacodynamic effect of the drugs on the complex changes, 1, 6 and 24 h treatment were assessed.

5.1.3.1 Changes in protein expression, [3 H]choline uptake and apoptosis following 1, 6 and 24 h gefitinib treatment.

PC9 and PC9ER cells were treated with different concentrations of gefitinib based on the GI $_{50}$ of this drug in each cell line. The concentrations used are summarised in Table 15. Hereafter the concentrations will be referred to as 0.5* GI $_{50}$, GI $_{50}$ and 5* GI $_{50}$.

Table 15: GI $_{50}$ values of PC9 and PC9ER cells treated with gefitinib for 72 h.

	PC9	PC9ER
0.5*GI $_{50}$ (μ M)	0.018	2.9
GI $_{50}$ (μ M)	0.036(+/-0.011)	5.8(+/-0.1)
5*GI $_{50}$ (μ M)	0.18	29

PC9 and PC9ER cells seeded in 96 well plates were treated with gefitinib for 72 h. After drug incubation, an SRB assay was carried out. GI $_{50}$ values represents mean values \pm SE from n = 6 replicates of three separate experiments.

After 1, 6 and 24 h gefitinib treatment there was a concentration dependant decrease in p-EGFR (Y1068) but no changes to levels of total EGFR in both the PC9 and PC9ER cells. Expression of ChK α was unchanged at 1 and 6 h following gefitinib treatment but decreased at 5*GI $_{50}$ concentration of gefitinib in both cell lines at 24 h. P-SRC Y416 was unchanged at 1 and 6 h treatment. However, there was a concentration dependant decrease in levels of P-SRC Y416 in the PC9 cells and a decrease at 5* GI $_{50}$ concentration of gefitinib in the PC9ER cells after 24 h gefitinib treatment (Figure 65).

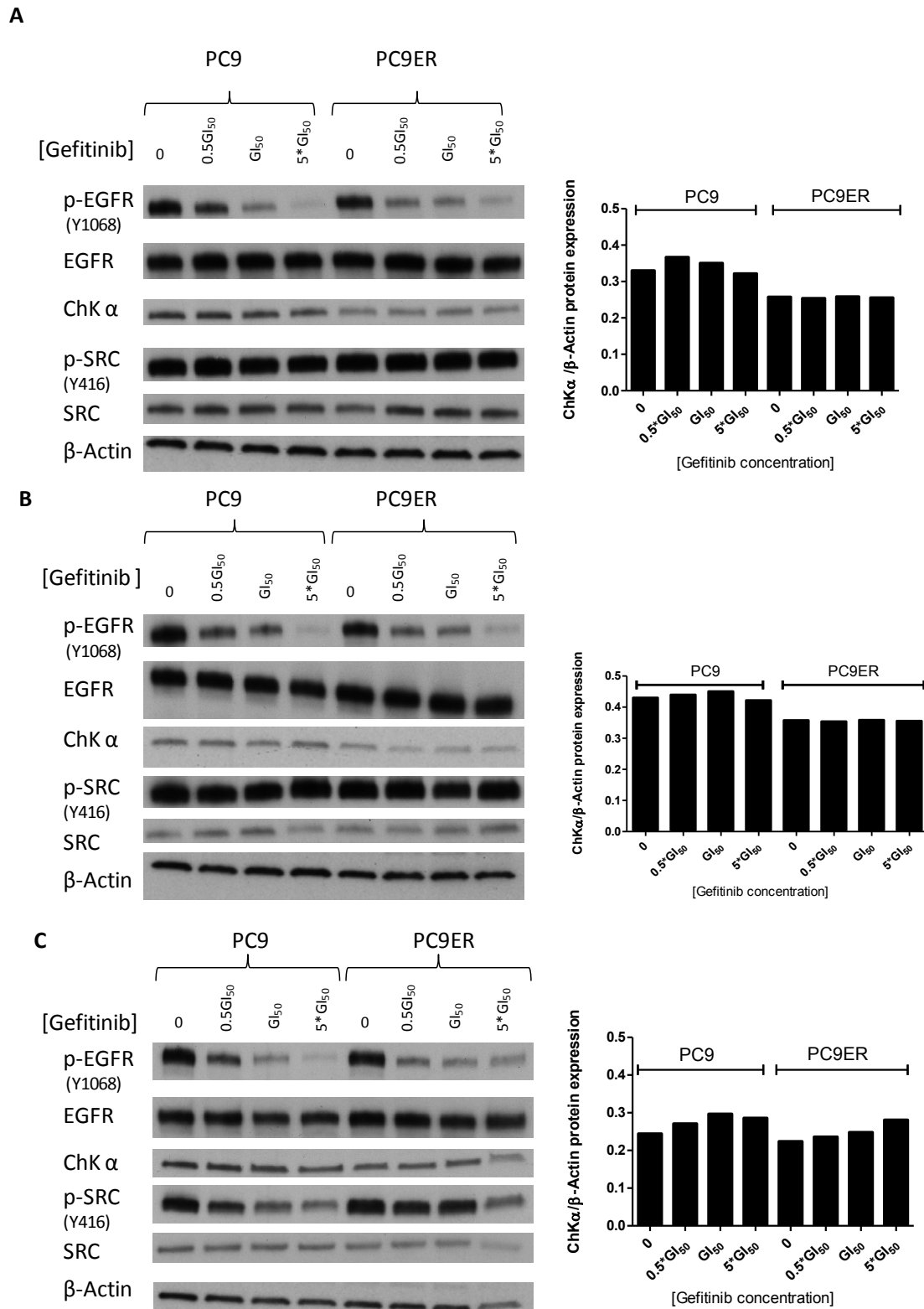


Figure 65: Effect of 1, 6 and 24 h gefitinib treatment on protein expression in PC9 and PC9ER cells.

Protein expression of p-EGFR (Y1068), EGFR, ChKα p-SRC (Y416) and SRC in PC9 and PC9ER cells treated with gefitinib for 1 h (A), 6 h (B), and 24 h (C). GI₅₀, 0.5 and 5* GI₅₀ concentration values are indicated in Table 15. Right panel represents the densitometry values of ChKα protein expression normalised for β-Actin. Data show results from one representative experiment carried out three times.

After examining changes in the protein expression of EGFR, SRC and ChK α changes to the activity of ChK α were indirectly assessed by carrying out [3 H]choline uptake experiments

The values of [3 H]choline uptake were expressed as percentage of untreated control cells for each cell line. After both 1 and 6 h gefitinib treatment there were no changes in levels of [3 H]choline uptake in the PC9 cells. After 24 h treatment, the uptake of [3 H]choline was decreased by 20 % at 0.5* and 1* GI $_{50}$ and by 45 % at 5* GI $_{50}$ concentration of gefitinib (Figure 66).

In the PC9ER cells at 1 h, only the 5* GI $_{50}$ concentration of gefitinib led to a decrease in the uptake of [3 H]choline compared to that in untreated control cells; the uptake was decreased by 40 % (Figure 66A). After 6 h treatment, there was a dose dependant decrease in the uptake of [3 H]choline in the PC9ER cells; there was a 25 % decrease in uptake at the GI $_{50}$ concentration of gefitinib and a 75 % decrease in the uptake at the 5* GI $_{50}$ concentration of gefitinib. Finally, after 24 h treatment, 0.5 and 1* GI $_{50}$ concentrations of gefitinib led to a 45 % decrease in [3 H]choline, whereas 5* GI $_{50}$ led to 85 % decrease in [3 H]choline uptake. The decrease in ChK α activity measured following 1 h treatment at 5* GI $_{50}$ concentration of gefitinib in the PC9ER cells could be caused by the direct inhibition of ChK α by gefitinib.

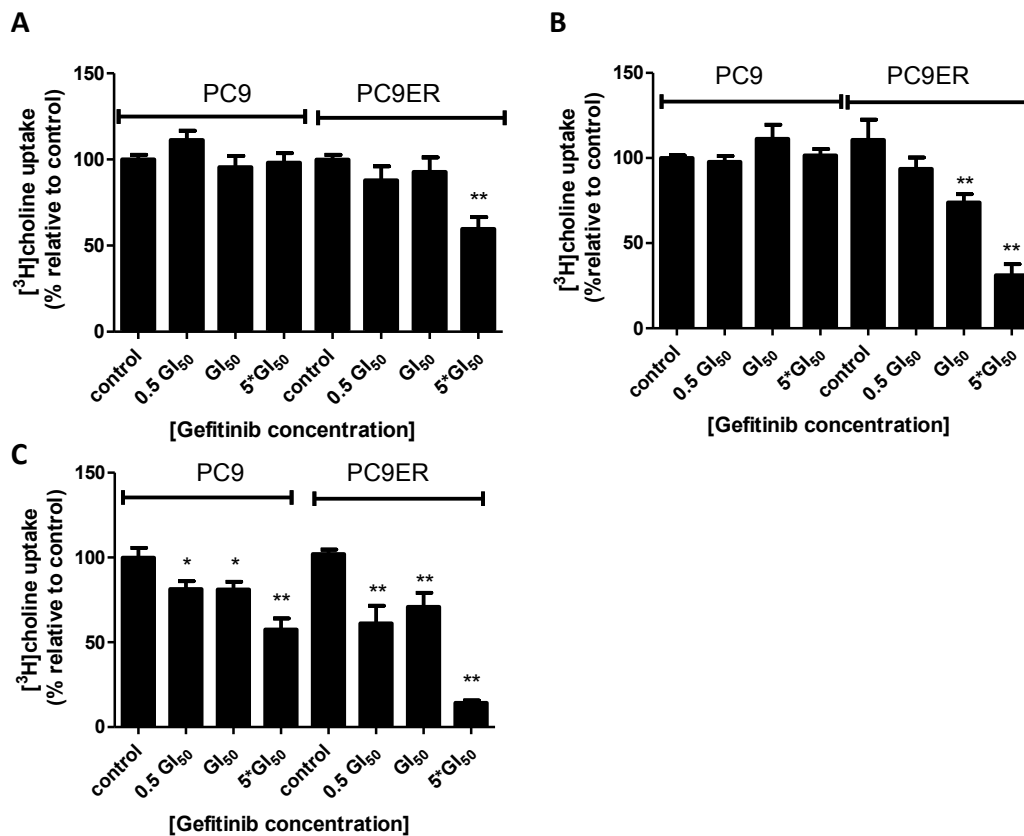


Figure 66: Changes in ChK α activity following 1, 6 and 24 h treatment with gefitinib.

Percentage of [³H]choline uptake compared to control in PC9 and PC9ER cells treated with gefitinib for 1 h (A), 6 h (B) and 24 h (C). Data show mean values \pm SE from three experiments each using triplicate samples per concentration. Statistically significant differences compared to control from two-tailed unpaired t-test are marked with a star (* = $P \leq 0.05$ and ** = $P \leq 0.01$).

Having treated cells with concentrations of up to 5* GI₅₀ of gefitinib, levels of apoptosis were also accessed via caspase glow 3/7 assay. Changes to levels of cell death especially at the 24 h time point needed to be taken into consideration when drawing any conclusions from changes to expression and activity of ChK α .

After 1 and 6 h drug treatment there was a small but insignificant increase in apoptosis in the PC9 cells with the exception of the 6 h treatment at 5* GI₅₀ concentration which was associated with a 1.8 fold increase in apoptosis (Figure 67). No significant changes in apoptosis levels were measured in the PC9ER cells at both 1 and 6 h treatment with the exception of 5* GI₅₀ concentration of gefitinib which led to a 1.6 fold increase in apoptosis (Figure 67). At 24 h treatment, levels of apoptosis increased in a dose dependant manner in the PC9 cells. At 5*GI₅₀ they were 4.8 fold higher

than at control. In PC9ER cells there was a very high increase in levels of apoptosis at 5* GI₅₀ value of gefitinib, increasing to over 11 fold from control (Figure 67C).

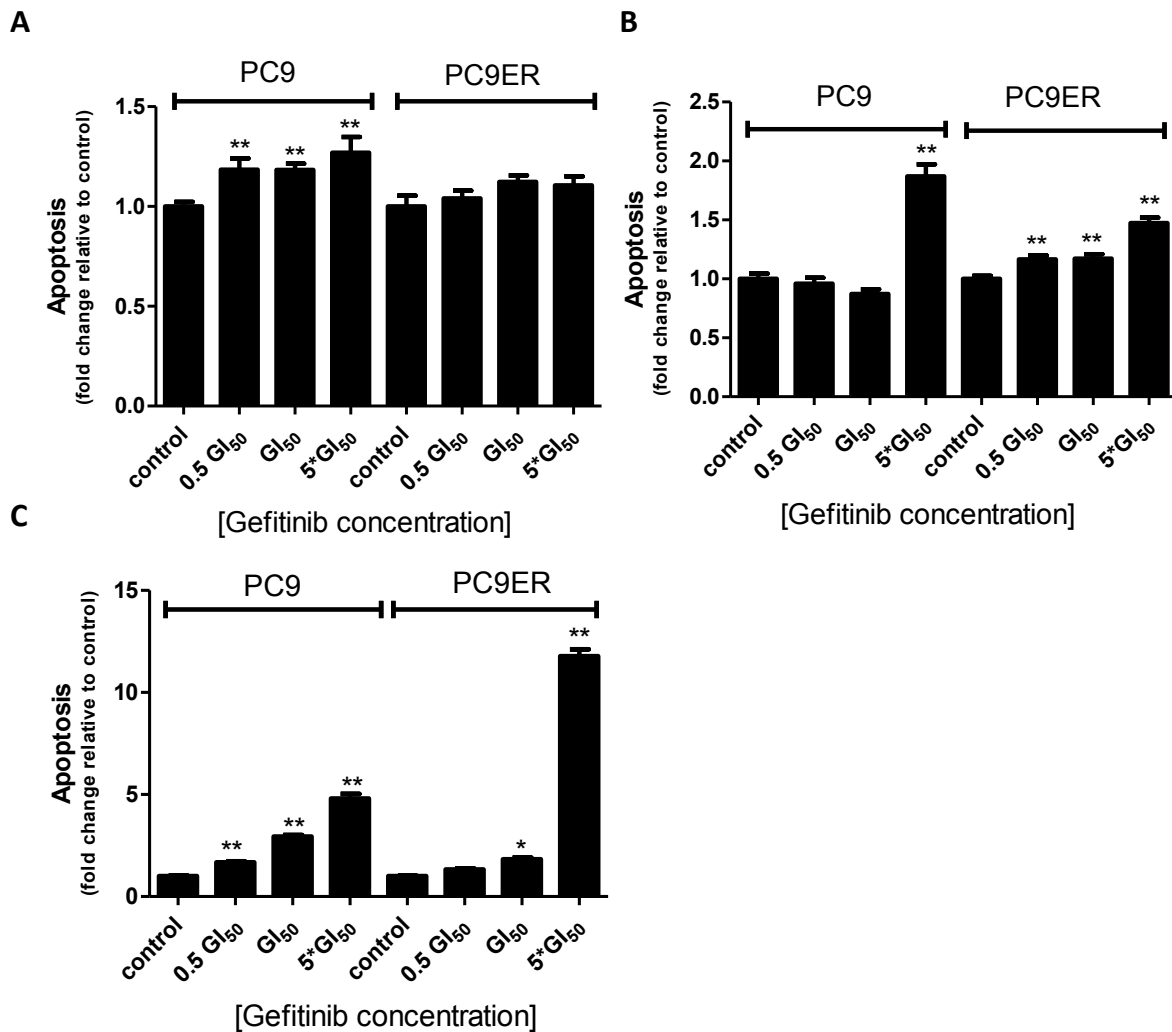


Figure 67: Effect of 1, 6 and 24 h gefitinib treatment on apoptosis in PC9 and PC9ER cells.

Fold increase in apoptosis in PC9 and PC9ER cells following 1 h (A), 6 h (B) and 24 h (C) gefitinib treatment assessed by carrying out a Caspase 3/7 assay. Data show mean values of fold increase in apoptosis normalised to protein levels \pm SE of n = 4 samples per concentration from one representative experiment carried out twice. Statistically significant differences compared to control from two-tailed unpaired t-test are marked with a star (* = $P \leq 0.05$ and ** = $p \leq 0.01$).

In summary, gefitinib dependant loss of EGFR activity occurred rapidly and in a dose dependant manner in both cell lines. However, after 1 and 6 h treatment, ChK α activity was not decreased in the PC9 cells and only the highest concentrations of gefitinib led to a decrease in ChK α in the PC9ER cells. As discussed above the decreased measured in ChK α at these concentrations of gefitinib could result from a direct inhibition of ChK α activity by gefitinib. The elevated levels of apoptosis at 24 h made understanding the regulation of ChK α activity by EGFR complicated. This suggested that EGFR activity would not be necessary for ChK α activity.

5.1.3.2 Changes in protein expression, [³H]choline uptake and apoptosis following 1, 6 and 24 h dasatinib treatment

The second molecule in the EGFR-SRC-ChK α complex, which was investigated, was SRC. In order to determine whether active SRC was key to the activity of ChK α , PC9 and PC9ER cells were treated with SRC inhibitor dasatinib. Following dasatinib treatment, changes in protein expression [³H]choline uptake and apoptosis were measured.

One, 6 and 24 h dasatinib treatment were assessed. The concentrations of drug were determined for each cell line based on the GI₅₀ of dasatinib. These concentrations are summarised in Table 16. Hereafter the concentrations will be referred to as 0.5* GI₅₀, GI₅₀ and 5* GI₅₀.

Table 16: GI₅₀ values of PC9 and PC9ER cells treated with dasatinib for 72 h

	PC9	PC9ER
0.5*GI ₅₀ (μ M)	0.33	2.8
GI ₅₀ (μ M)	0.66(\pm 0.03)	5.69(\pm 0.8)
5*GI ₅₀ (μ M)	3.3	28

PC9 and PC9ER cells seeded in 96 well plates were treated with dasatinib for 72 h. After drug incubation cytotoxicity was assessed via an SRB assay. GI₅₀ represents mean values \pm SE from n = 6 replicates of three separate experiments.

After 1, 6 and 24 h of dasatinib treatment there was complete inhibition of p-SRC Y416 and an increase in total SRC protein expression in both cell lines at all three concentrations tested compared to untreated cells (Figure 68). Dasatinib also caused an inhibition of p-EGFR Y1068 expression; this occurred at the 5*GI₅₀ concentration of dasatinib in the PC9 cells at 1 and 6 h treatment and at all three dasatinib concentration at 24 h treatment. There was a dose dependant decrease in p-EGFR Y1068 expression in the PC9ER cells at all-time points. Total EGFR levels were unchanged with drug treatment in both cell lines at all-time points. ChK α levels were unchanged in both cell lines after 1 h drug treatment. At 6 h, there was a dose dependant decrease in ChK α expression in the PC9ER cells following dasatinib treatment, whereas levels were unchanged in the PC9 cells (Figure 68B). At 24 h, there was a dose dependant decrease in ChK α in both cell lines (Figure 68C).

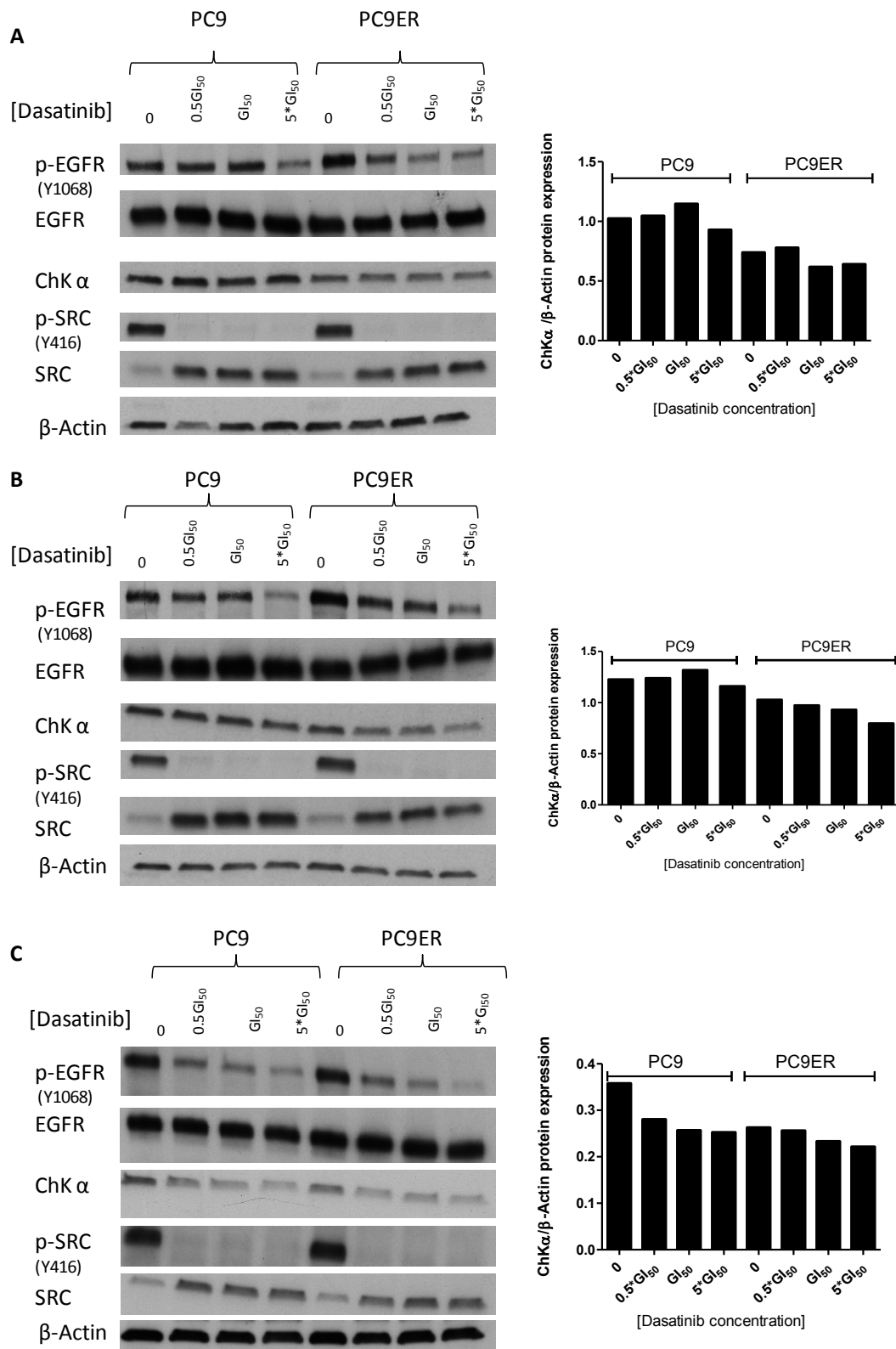


Figure 68: Effect of 1, 6 and 24 h dasatinib treatment on protein expression in PC9 and PC9ER cells.

Protein expression of p-EGFR (Y1068), EGFR, ChKα p-SRC (Y416), SRC in PC9 and PC9ER cells treated with dasatinib for 1 h (A), 6 h (B), and 24 h (C). GI₅₀, 0.5 and 5*GI₅₀ concentration values are indicated in Table 15. Right panel represents the densitometry values of ChKα protein expression normalised for β-Actin. Data show results from one representative experiment carried out three times.

The effect of dasatinib on ChK α activity was then assessed. After 1 h dasatinib treatment, there was no change in the uptake of [3 H]choline in PC9 cells. In PC9ER cells there was an 18 % decrease in [3 H]choline uptake at 0.5*GI $_{50}$ and GI $_{50}$ concentrations of dasatinib and a 40 % decrease at 5*GI $_{50}$ concentration of dasatinib (Figure 68A). There was a significant decrease in [3 H]choline uptake in both PC9 and PC9ER cells following dasatinib treatment for 6h. In PC9 cells at 0.5*GI $_{50}$, GI $_{50}$ and 5*GI $_{50}$ concentrations there was a 40 % decrease in uptake compared to control. In PC9ER cells, the uptake of [3 H]choline decreased the most at 5*GI $_{50}$, and was 56 % less than the uptake in the control untreated cells (Figure 69B). At 24 h there was a significant decrease in the uptake of [3 H]choline, of over 50 %, in the PC9 cells at GI $_{50}$ and 5*GI $_{50}$ concentrations of dasatinib. In the PC9ER cells 0.5*GI $_{50}$ and GI $_{50}$ concentrations of dasatinib led to a 35 and 25 % decrease in [3 H]choline uptake, respectively. The highest concentration of dasatinib led to a 72 % decrease in [3 H]choline uptake.

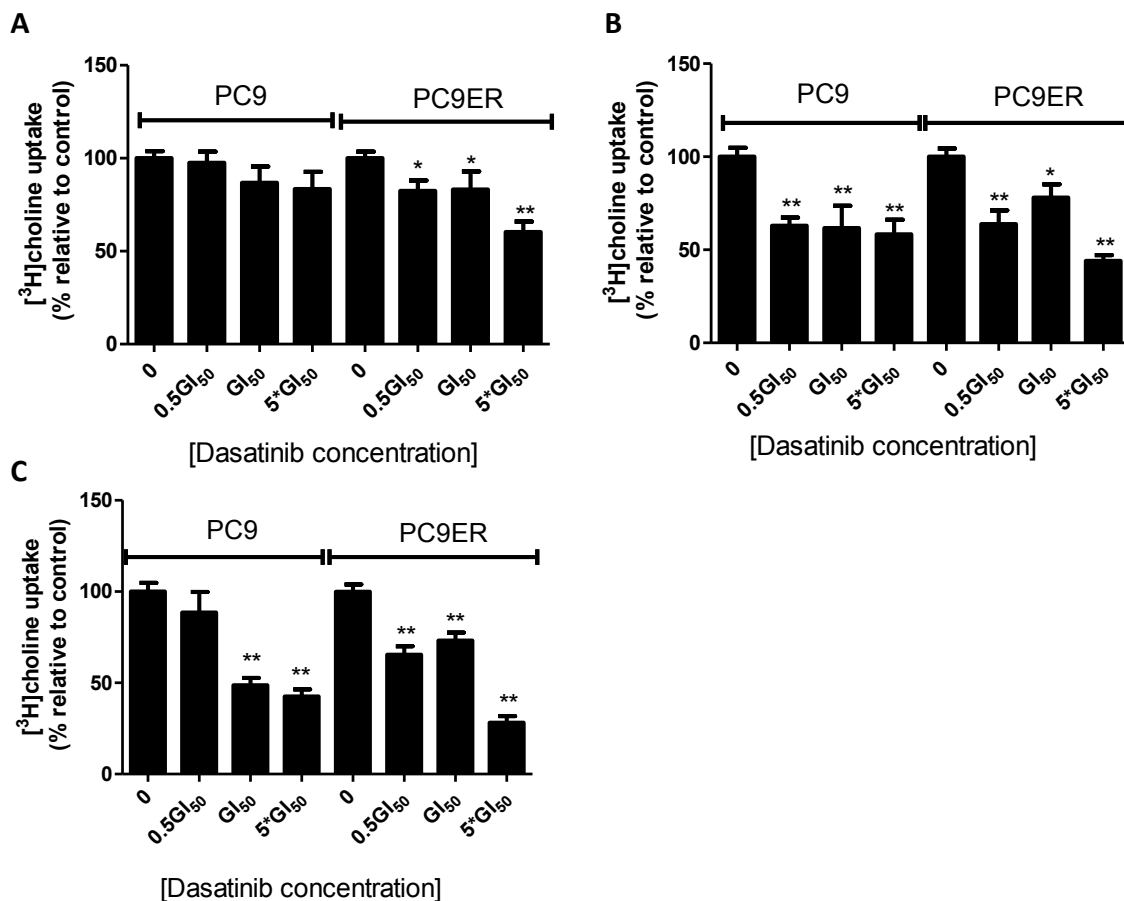


Figure 69: Changes in ChK α activity in PC9 and PC9ER cells following 1, 6 and 24 h dasatinib treatment.

Percentage of [3 H]choline uptake compared to untreated control in PC9 and PC9ER cells treated with dasatinib for 1 h (A), 6 h (B) and 24 h (C). Data show mean values \pm SE from three experiments each using triplicate samples per concentration. Statistically significant changes compared to control of an unpaired t-test are marked with a star (* = $P \leq 0.05$ and ** = $p \leq 0.01$).

There were no marked changes in levels of apoptosis in PC9 and PC9ER cells after both 1 and 6 h treatment (Figure 70A,B). Levels of apoptosis were significantly higher after 24 h treatment. In PC9 cells, there was a dose dependant increase in apoptosis. The highest concentration of dasatinib led to a 2.7 fold increase in apoptosis compared to control. In PC9ER cells, there was a slight increase in the levels of apoptosis at 0.5*GI₅₀ and GI₅₀ concentrations of dasatinib. However, at 5*GI₅₀ concentration of dasatinib there was an over 9.3 fold increase in apoptosis (Figure 70C).

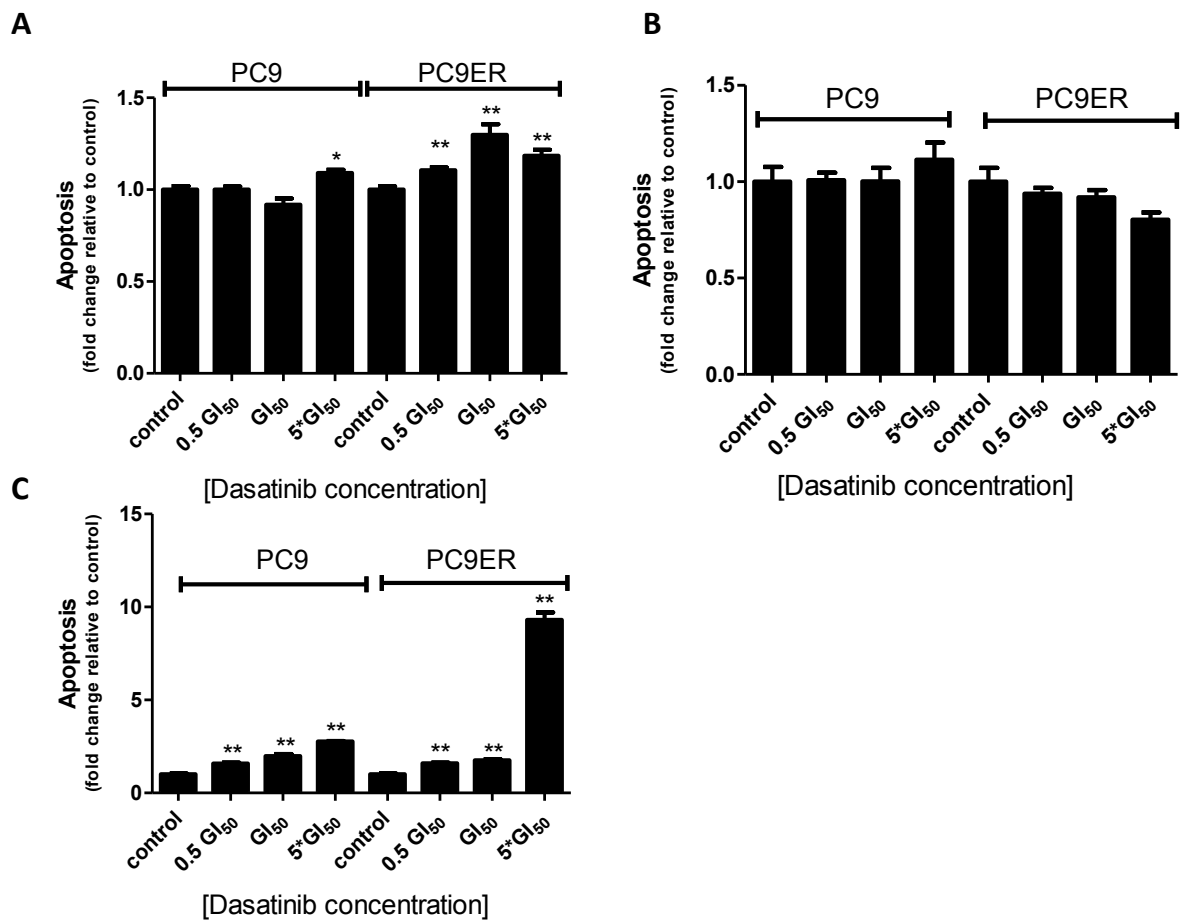


Figure 70: Apoptosis levels in PC9 and PC9ER cells following 1, 6 and 24 h dasatinib treatment.

Fold increase in apoptosis relative to control in PC9 and PC9ER cells following 1 h (A), 6 h (B) and 24 h (C) dasatinib treatment assessed by carrying out a Caspase 3/7 assay. Data show mean values of fold increase in apoptosis normalised to protein levels \pm SE of $n = 4$ samples per concentration from one representative experiment carried out twice. Statistically significant changes compared to control of an unpaired t-test are marked with a star (* = $P \leq 0.05$ and ** = $p \leq 0.01$).

In summary, dasatinib dependant loss of SRC activity occurred rapidly and at all dose levels used. In contrast ChK α activity had a longer latency and changes were measured at 6 and 24 h treatment

Increase levels of apoptosis at 24 h acted as a confound to the assessment of the effect of SRC activity of on the regulation of ChK α activity.

5.1.3.3 siRNA knock down of EGFR or SRC.

At the earlier time points of 1 and 6 h, only the highest concentration of gefitinib led to changes in [³H]choline uptake despite a decrease in p-EGFR Y1068, and thus activity of EGFR, at all concentrations of drug used. Similarly, dasatinib caused inhibition of p-SRC Y416, and thus activity of SRC, at all concentrations of drug used, but changes to ChK α activity were only measured following treatment with the highest concentrations of dasatinib. One possible explanation was that at the highest concentrations, both gefitinib and dasatinib were inhibiting other targets, these could include ChK α itself. Furthermore, after 24 h treatment there were high levels of apoptosis in cells treated at the highest concentrations of both drugs. Therefore, the changes in uptake of [³H]choline, ChK α activity, could be caused by the above rather than simple inhibition of either EGFR or SRC.

In view of the above limitations, a more direct approach was employed to assess the roles of SRC and EGFR in the regulation of ChK α in lung cancer cells, appreciating that loss of protein will perhaps give a different outcome compared to drug induced loss of EGFR/SRC activity.

Cells were transfected with either EGFR or SRC siRNA at 25 nM for 72 h. Following the siRNA transfection a [³H]choline uptake was carried out. In Both the PC9 and PC9ER cells only the EGFR siRNA treatment led to a decrease in [³H]choline uptake (Figure 71A). EGFR knock down was confirmed by western blot analysis (Figure 71BC). SRC knock down, was only achieved partially and this could explain the lack of change ChK α activity following SRC siRNA transfection (Figure 71A). Expression of ChK α was decreased in siRNA EGFR treated PC9 and PC9ER cells (Figure 71B).

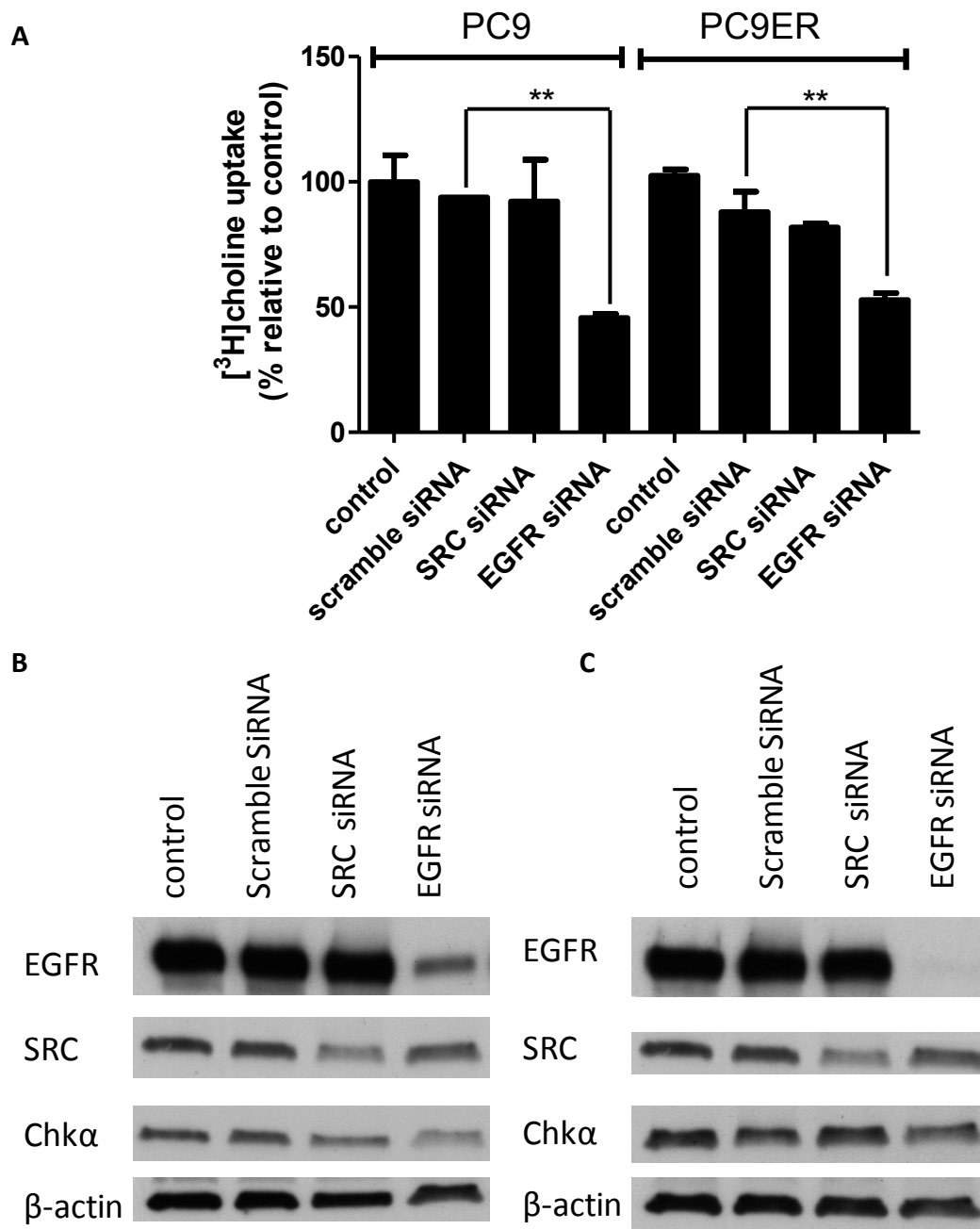


Figure 71: [³H]choline uptake following SRC and EGFR siRNA transfection of PC9 and PC9ER cells.

A- Percentage uptake of [³H]choline in PC9 and PC9ER cells following 72 h transfection with 25 nM of SRC, EGFR or scramble siRNA. Data show mean values \pm SE of percentage [³H]choline uptake relative to control, from three experiments each using triplicate samples per concentration. Statistically significant differences compared to scramble treated cells are indicated by a star (** = $p \leq 0.01$). B- Protein expression of EGFR, SRC and Chk α in PC9 (B) and PC9ER (C) cells following 72 h transfection with 25 nM of SRC, EGFR or scramble siRNA.

5.2. Other clinically available tracers and their role for imaging early response to gefitinib treatment.

Both [^{18}F]FDG and [^{18}F]FLT have been investigated for the monitoring of response to TKI treatment in lung cancer. These two radiotracers were used here, as means of comparison with the [^{18}F]D4choline study.

5.2.1 [^{18}F]FDG

5.2.1.1 *In vitro* assessment of the role of [^{18}F]FDG as a biomarker of response to gefitinib treatment.

In order to assess the potential role of [^{18}F]FDG as a biomarker of response to gefitinib treatment, the uptake of [^{18}F]FDG was measured in PC9 and PC9ER cells following 48 h gefitinib treatment (Figure 72). In untreated cells, the uptake of [^{18}F]FDG was 2.5 times higher in PC9ER cells at 25 CCPMA/ μg of protein compared to 10.5 CCPMA/ μg of protein in PC9 cells. There was up to 30 % decrease in the uptake of [^{18}F]FDG in the PC9 cells treated with 0.01, 1 and 3 μM of gefitinib. There was no statistically significant difference in the uptake of [^{18}F]FDG in PC9ER cells following drug treatment. The higher levels of uptake of [^{18}F]FDG at baseline in PC9ER cells, compared to PC9 cells, could result from higher levels of expression of the GLUT1 transporter in the PC9ER cells (Figure 72B).

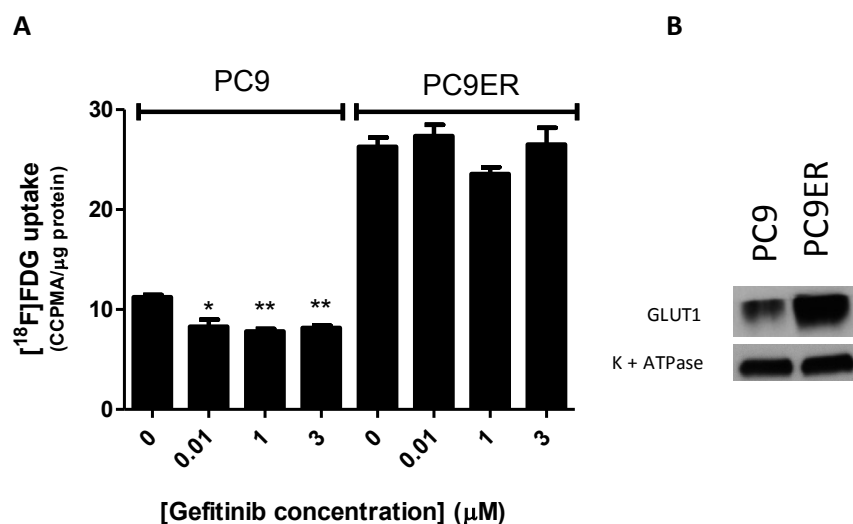


Figure 72: [^{18}F]FDG uptake in PC9 and PC9ER cells following gefitinib treatment for 1, 6 and 24 h.

A- Corrected counts per minute acquired per μg of protein of [^{18}F]FDG uptake in PC9 and PC9ER cells following 1 h incubation with 0.37 MBq of [^{18}F]FDG after 48 h gefitinib treatment. Data show mean values \pm SE of triplicates from one representative experiment carried out three times. Statistically significant changes compared to untreated control are marked with a star (* = $P \leq 0.05$ and ** = $p \leq 0.01$). B- Membrane GLUT1 expression in PC9 and PC9ER cells. K+ ATPase: potassium ATPase protein was used as a loading control.

5.2.1.2 *In vivo* uptake of [¹⁸F]FDG in PC9 and PC9ER xenograft

[¹⁸F]FDG is currently the “gold standard” radiotracer in oncology and is used by clinicians for diagnosis but also monitoring of patients during a course of drug treatment. Here, [¹⁸F]FDG was used as a means of comparison to the previously performed [¹⁸F]D4choline PET imaging for the early prediction of response or failure of response to gefitinib treatment.

CT/PET imaging of PC9 and PC9ER xenografts were investigated at baseline and following 48 h vehicle or 50 mg/Kg of gefitinib. The sagittal and transverse cross sections showed high levels of accumulation of [¹⁸F]FDG at baseline and following 48 h vehicle treatment in the PC9 xenografts (Figure 73A). There was a reduction in the accumulation of radiotracer in the tumour in the gefitinib treated group (Figure 73A). In the sagittal cross section of the vehicle treated mouse, the uptake was lower at the centre of the tumour. This could be a result of necrosis within the tumour tissue. The tumour time activity curves (TACs) at baseline and following vehicle treatment overlapped in the PC9 xenografts, following the same pattern, with a gradual increase and accumulation in the tumour with time. The TAC of the gefitinib treated group showed initial delivery and accumulation of [¹⁸F]FDG in the tumour for the first 10 min post tracer injection, followed by a washout from 10 to 60min (Figure 73B). In the PC9ER xenografts there was a high uptake of [¹⁸F]FDG at baseline and in both gefitinib and vehicle treated groups as shown by the sagittal and transverse cross sections (Figure 73C). The TAC's obtained from the PC9ER xenografts showed a small decrease in the uptake of the radiotracer in the gefitinib group compared to baseline and vehicle treated groups (Figure 73D).

NUV₆₀, AUC, highest quartile tumour uptake and FRT values were plotted in Figure 74. The NUV₆₀ was higher at baseline in the PC9ER tumours with a mean value of 5 %ID/mL of tissue compared to 4.3 %ID/mL of tissue in the PC9 xenografts. This higher uptake is in line with the *in vitro* uptake in which PC9ER showed higher baseline uptake of [¹⁸F]FDG than PC9 cells. In the PC9 xenografts, all four parameters were unchanged between baseline and vehicle treated mice but decreased following 48 h treatment with 50 mg/kg of gefitinib. The NUV₆₀ decreased from 4.3 %ID/mL of tissue at baseline to 2.9 %ID/mL of tissue after 48 h gefitinib treatment (Figure 53A). The AUC decreased from 250 at baseline to 190 %ID/ml *min following 48 h gefitinib treatment (Figure 53B). Finally, there was a 25 % decrease in the FRT in the gefitinib treated PC9 group (Figure 53D).

In the PC9ER xenografts there was no statistically significant changes in the different parameters measured between all three groups, despite a decrease in the parameters following gefitinib treatment (Figure 74B). High intra variability could account for the lack of statistical significance.

In summary, following 48 h gefitinib treatment a decrease in [¹⁸F]FDG uptake in gefitinib sensitive PC9 xenografts but not in resistant PC9ER xenografts was measured.

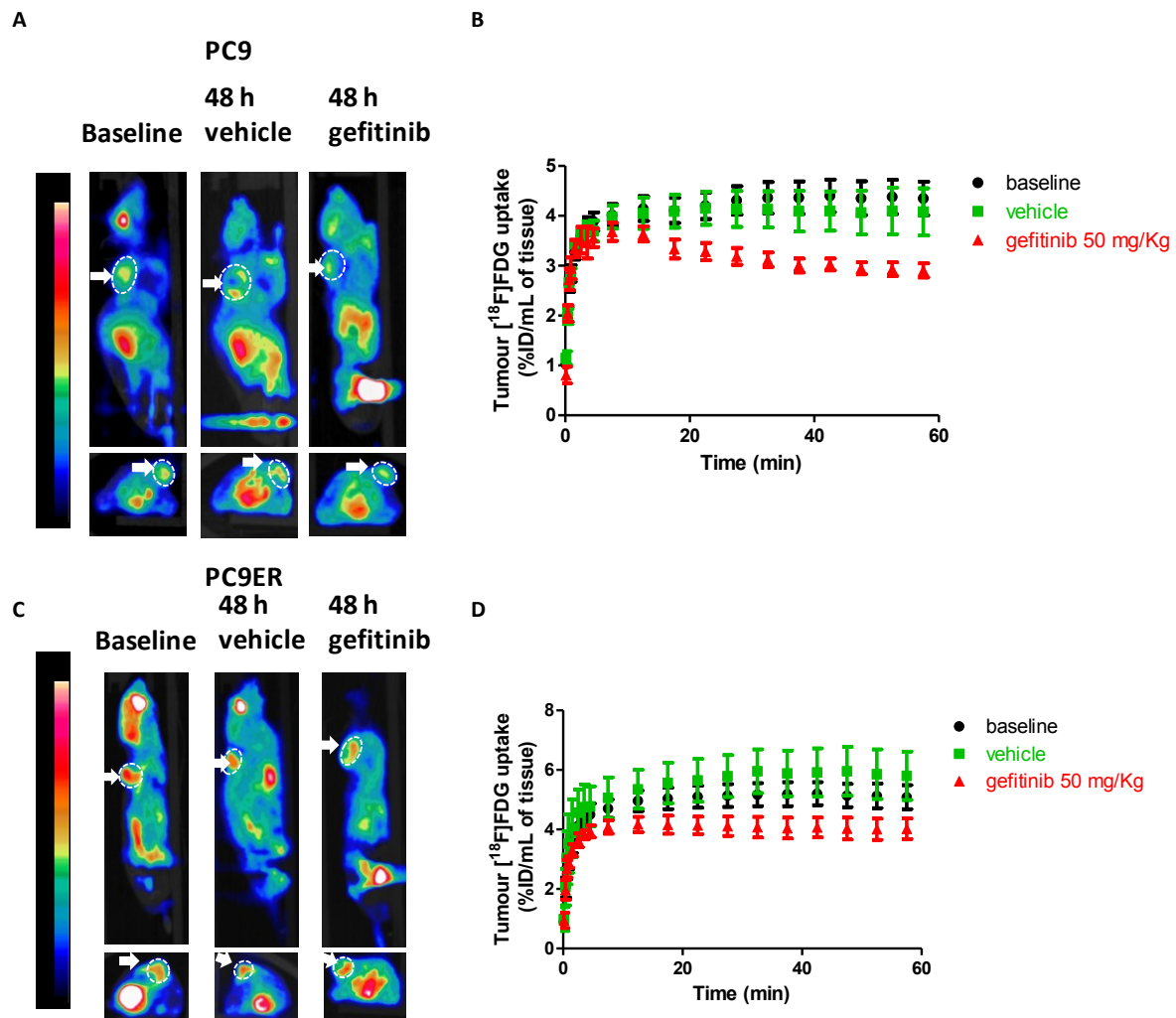


Figure 73: [¹⁸F]FDG PET imaging of PC9 and PC9ER xenografts following 48 h gefitinib treatment.

A, C- Merged PET/CT image of representative sagittal (top) and transverse (bottom) cross section of PC9 (A) and PC9ER (C) xenograft mouse at baseline and following 48 h vehicle treatment or 48 h gefitinib treatment at 50 mg/Kg at 60 min post i.v. injection of 3.7 MBq of [¹⁸F]FDG. Tumours indicated by white arrow. B, D- Tumour time activity curves of PC9 (B) and PC9ER (D) xenografts. Values show mean ± SE of n = 4 mice per group.

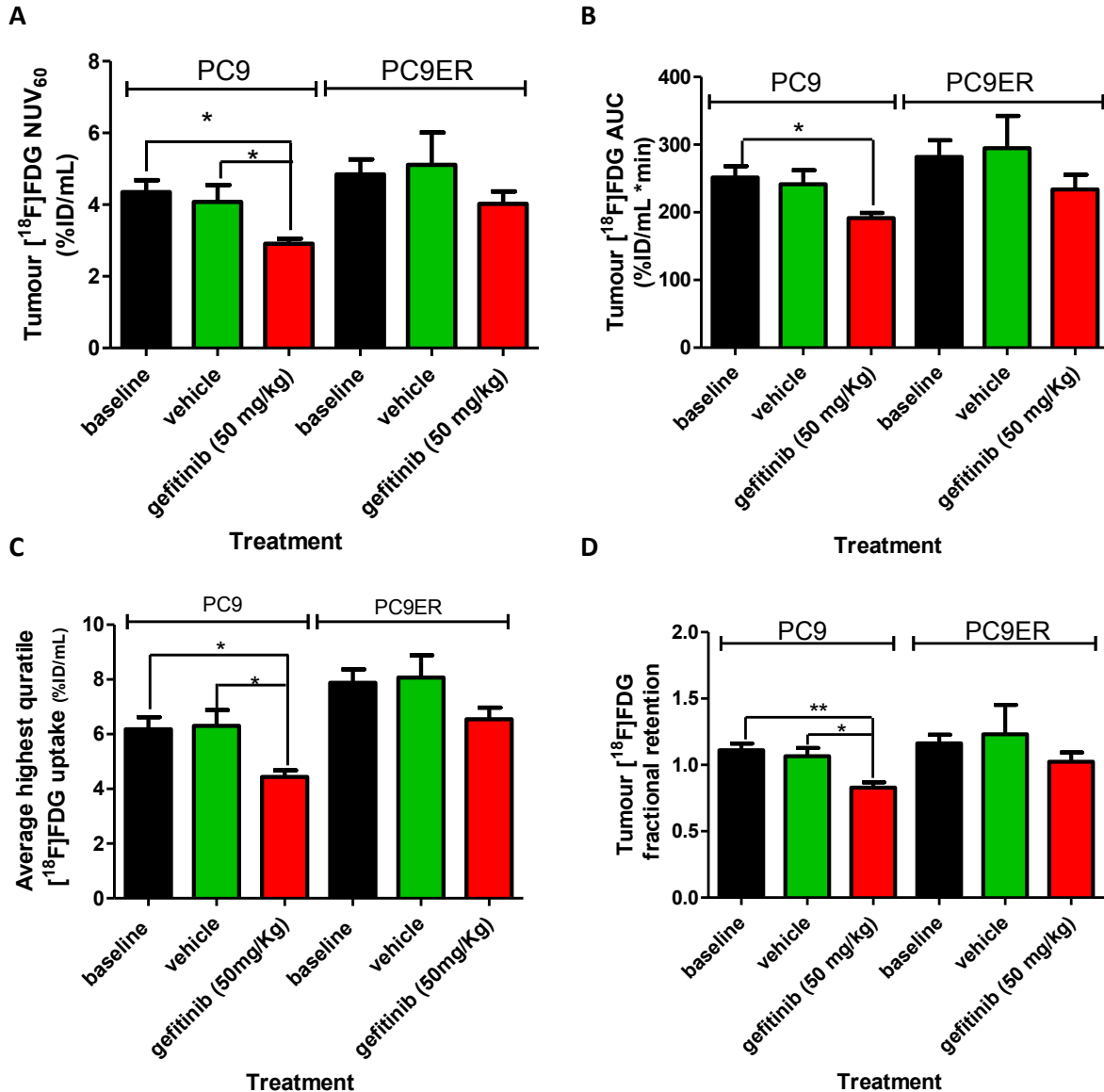


Figure 74: Tumour uptake parameters from [¹⁸F]FDG PET imaging of PC9 and PC9ER xenografts following 48 h gefitinib treatment.

A- Normalised uptake value of [¹⁸F]FDG in PC9 and PC9ER tumours at t = 60 min after tracer injection. B- Area under the curve plot D- Average highest quartile tumour [¹⁸F]FDG uptake. C- Fractional retention of [¹⁸F]FDG in PC9 and PC9ER tumours between 3.5 and 60 min post tracer injection. Data show means ± SE of n = 4 mice per group. Statistically significant difference between data sets are indicated on the graphs (* = P ≤ 0.05 and ** = P ≤ 0.01).

Tumours from the mouse xenografts used in the [¹⁸F]FDG PET study were collected and protein levels assessed. The [¹⁸F]FDG study was carried out longitudinally, therefore only tumours corresponding to vehicle and gefitinib treated mice were available to carry out the protein expression analysis. In the PC9 tumours, there was complete knock down of levels of p-EGFR (Y1068) and a decrease in total EGFR following gefitinib treatment. p-ERK, p-AKT and p-SRC Y416 expression were also decreased in the gefitinib treated group compared to vehicle treated. Total AKT, SRC and

ERK were unchanged. Levels of ChK α were decreased in 2 out of the 3 tumour samples from the gefitinib treated group. Finally there was also a small decrease in levels of GLUT1 (Figure 75 left column).

In the PC9ER tumours, there was no decrease in p-EGFR (Y1068) in the gefitinib treated group. Levels of EGFR, SRC, p-SRC Y416, p-AKT, AKT, p-ERK, and ERK were the same in both vehicle and gefitinib treated groups. Levels of GLUT1 were decreased in two out of three of the gefitinib treated samples compared to the tumours from the vehicle treated group (Figure 75 right column).

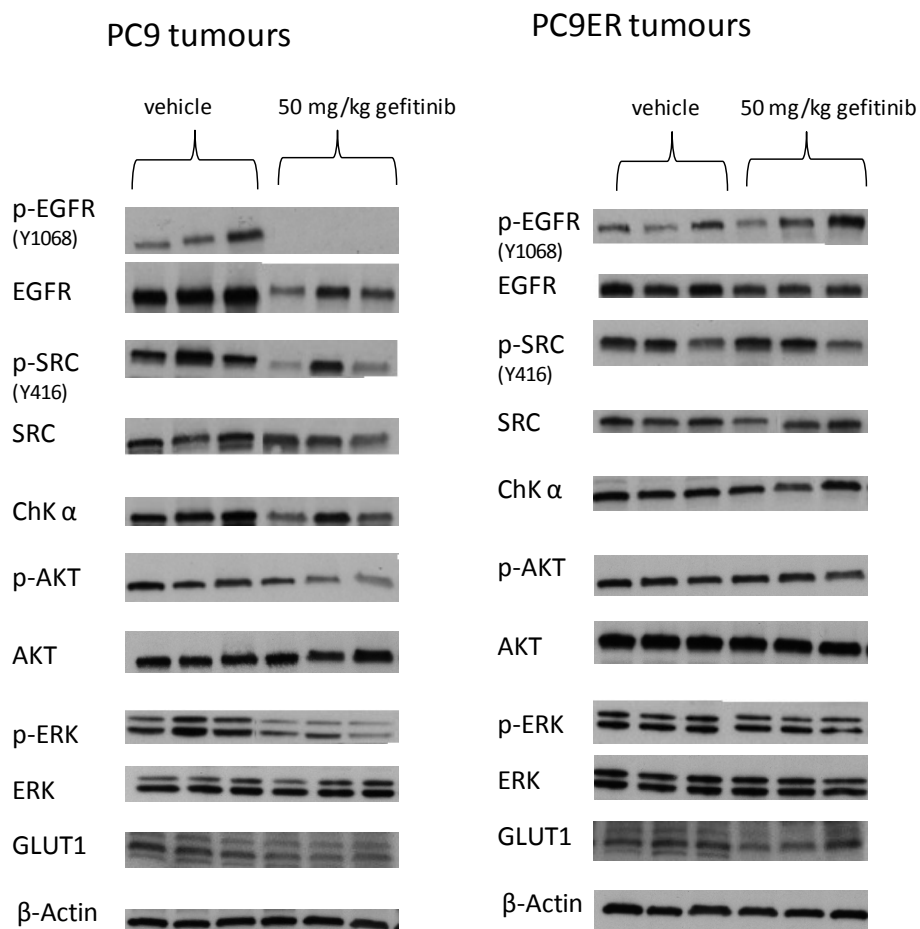


Figure 75: PC9 and PC9ER tumour lysate protein expression analysis from [¹⁸F]FDG PET imaging.

Protein expression of p-EGFR (Y1068), EGFR, ChK α , p-SRC (Y416), SRC, p-AKT, AKT, p-ERK, ERK and total cellular GLUT1 in tumour lysates from PC9 and PC9ER xenograft from 48 h vehicle or 50 mg/kg gefitinib treated groups. Each column represents a lysate from one tumour.

In summary, a decrease in [^{18}F]FDG uptake at 48 h gefitinib treatment was measured in NSCLC sensitive but not resistant xenograft model, indicating the opportunity of assessing early response to treatment with this tracer.

5.2.2 [^{18}F]FLT

5.2.2.1 *In vitro* assessment of the role of [^{18}F]FLT as a biomarker of response to gefitinib treatment.

In order to assess the potential role of [^{18}F]FLT as a biomarker of response to gefitinib treatment, the uptake of [^{18}F]FLT in PC9 and PC9ER cells was determined after 48 h treatment with gefitinib. The uptake of [^{18}F]FLT at baseline was higher in PC9ER cells, 135 CCPMA/ μg of protein, compared to the PC9 cells, 103 CCPMA/ μg of protein. After 48 h gefitinib treatment, the uptake of [^{18}F]FLT in PC9 cells, decreased from 105 CCPMA/ μg of protein in the untreated control cells to 5 CCPMA/ μg of protein following 1 and 3 μM gefitinib treatment, corresponding to a 95 % decrease in [^{18}F]FLT uptake (Figure 76). In PC9ER cells, only the highest concentration of gefitinib (3 μM), led to a statistically significant decrease in the uptake of [^{18}F]FLT from 135 in untreated cells to 110 CCPMA/ μg of protein; this represented a 19 % decrease in [^{18}F]FLT uptake.

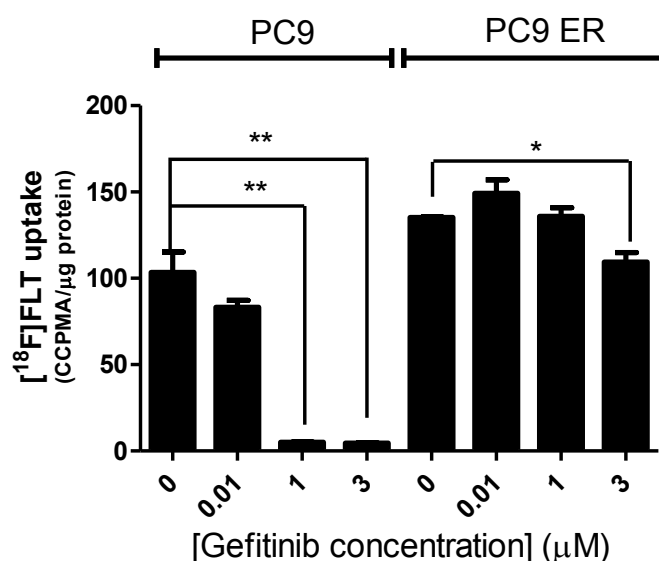


Figure 76: [^{18}F]FLT uptake in PC9 and PC9ER cells following 48 h gefitinib treatment.

Corrected counts per minute acquired per μg of [^{18}F]FLT uptake in PC9 and PC9ER cells after 1 h incubation with 0.37 MBq of [^{18}F]FLT following 48 h gefitinib treatment. Data show mean values \pm SE of triplicates from one representative experiment carried out three times. Statistically significant changes compared to untreated control from an unpaired t-test are marked with a star (* = $P \leq 0.05$ and ** = $p \leq 0.01$).

In conclusion, a differential effect of gefitinib treatment, on [^{18}F]FLT uptake was measured in sensitive, PC9, and resistant, PC9ER, cells. There was a strong decrease in uptake of [^{18}F]FLT in PC9

cells which was not measured in PC9ER cells following drug treatment. These results suggested [¹⁸F]FLT to be a good biomarker of response to gefitinib treatment in sensitive and resistant NSCLC.

5.2.2.2 *In vivo* uptake of [¹⁸F]FLT in PC9 and PC9ER xenograft.

Having demonstrated the differential uptake of [¹⁸F]FLT in PC9 and PC9ER cells following gefitinib treatment *in vitro*, [¹⁸F]FLT was investigated for the early prediction of response or failure of response to gefitinib treatment *in vivo*. [¹⁸F]FLT is currently a tracer used in the clinical trial setting and has shown efficacy in detection of tumour and monitoring patients during the course of treatment (Contractor et al., 2011c).

As for [¹⁸F]FDG and [¹⁸F]D4choline, PET/CT scans of PC9 and PC9ER xenograft bearing mice were performed at baseline and following 48 h vehicle or 50 mg/Kg gefitinib treatment. The sagittal merged CT/PET images in Figure 77A showed a low uptake of the tracer in PC9 tumours in all three groups. In the baseline and gefitinib group there was a lack of accumulation of [¹⁸F]FLT at the very centre of the tumour, indicated by dark blue colour on the PET scan. This lack of uptake is due to central necrosis of the tumour. The TAC's showed similar patterns of uptake of the radiotracer in both baseline and vehicle treated groups, characterised by a gradual increase in the uptake of [¹⁸F]FLT in the tumour from 0 to 10 min after which the uptake of [¹⁸F]FLT was unchanged until 60 min. However, the uptake in the gefitinib treated group was different with an initial increase in the uptake up to 5 min followed by a decrease in the uptake of the tracer until 60 min (Figure 77B).

In PC9ER xenografts (Figure 77C), a higher accumulation of [¹⁸F]FLT compared to PC9 xenografts was measured. The accumulation of tracer was highest in the gefitinib treated group. A high level of intra group [¹⁸F]FLT uptake variability was measured. The TAC's showed that in all three groups there was a gradual increase in the uptake of the tracer throughout the scanning time frame. The TAC of the gefitinib group showed overall higher uptake of the tracer compared to baseline or vehicle groups (Figure 77D).

By determining various tumour uptake parameters, further comparisons between the two xenograft models could be carried out. Both the NUV₆₀ and AUC values were significantly higher in PC9ER, 5.8 %ID/mL of tissue and 327 %ID/mL of tissue *min compared to 4.5 %ID/mL of tissue and 266 %ID/mL of tissue *min in PC9 tumours.

The NUV₆₀ and the AUC were the same in all three PC9 xenograft groups with values of 4.2 %ID/mL of tissue and 250 %ID/mL of tissue *min, respectively. The radiotracer uptake was therefore

unchanged with treatment when the imaging variable was NUV_{60} or AUC. The average highest quartile of [^{18}F]FLT uptake in the tumour was similar in all three groups of PC9 xenografts. There was a statistically significant decrease (27 %) in the FRT of the gefitinib treated PC9 group compared to both baseline and vehicle groups.

In PC9ER xenografts, the NUV_{60} was higher in the gefitinib treated group, at 7 %ID/mL of tissue, compared to 5.7 and 5 %ID/mL of tissue in baseline and vehicle groups, respectively. Due to high intra-group variability the differences in NUV_{60} 's measured were not statistically significant. There was a statistically significant increase in AUC from 275 %ID/mL of tissue * min in the vehicle treated group, to 400 %ID/mL of tissue * min in the gefitinib treated group. Both FRT values and highest quartile [^{18}F]FLT uptake in the tumour were unchanged between all three groups (Figure 78).

In conclusion, [^{18}F]FLT showed no change in NUV_{60} or AUC in PC9 xenografts following 48 h gefitinib treatment. The gefitinib treated PC9 group did however show a decrease in the mean FRT value. These data highlighted the importance of the perfusion of tumours, and the influence perfusion has on differential uptake of the radiotracer in tumours. This was especially true as there was a low overall uptake of the tracer, along with necrosis of the central core of the tumours. The increase in uptake of [^{18}F]FLT in PC9ER group following treatment was surprising and warrants further investigation.

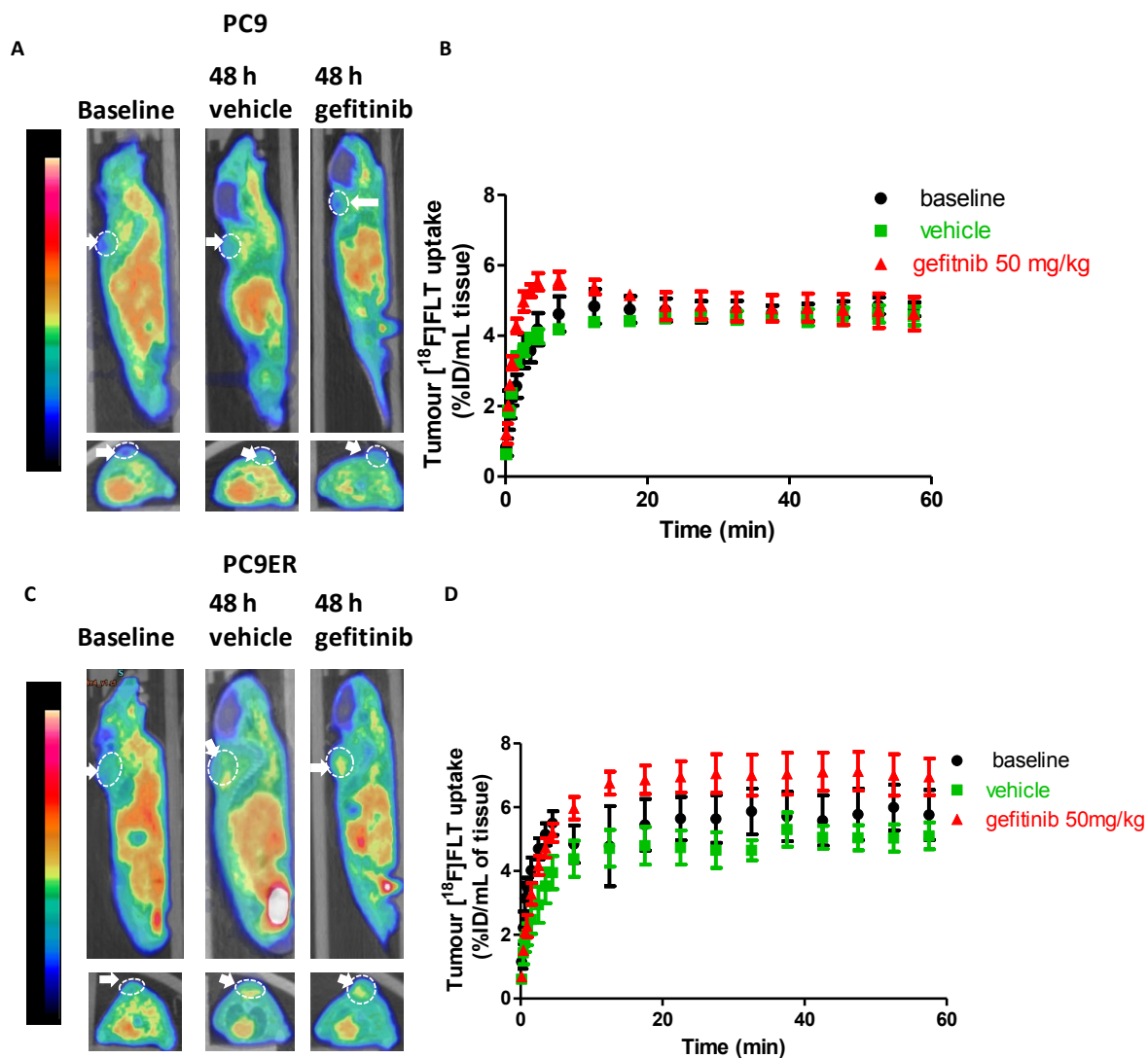


Figure 77: [¹⁸F]FLT PET imaging of PC9 and PC9ER xenografts following 48h gefitinib treatment.

A,C- Merged PET/CT image of representative sagittal (top) and frontal (bottom) cross section of PC9 (A) and PC9ER (C) xenograft mouse at baseline and following 48 h vehicle treatment or 48 h gefitinib treatment at 50 mg/Kg at 60 min post i.v. injection of 3.7 MBq of [¹⁸F]FLT. Tumours indicated by white arrow. B, D-Tumour time activity curves of PC9 (B) and PC9ER (D) xenografts. Values show mean ± SE of n = 4 mice per group.

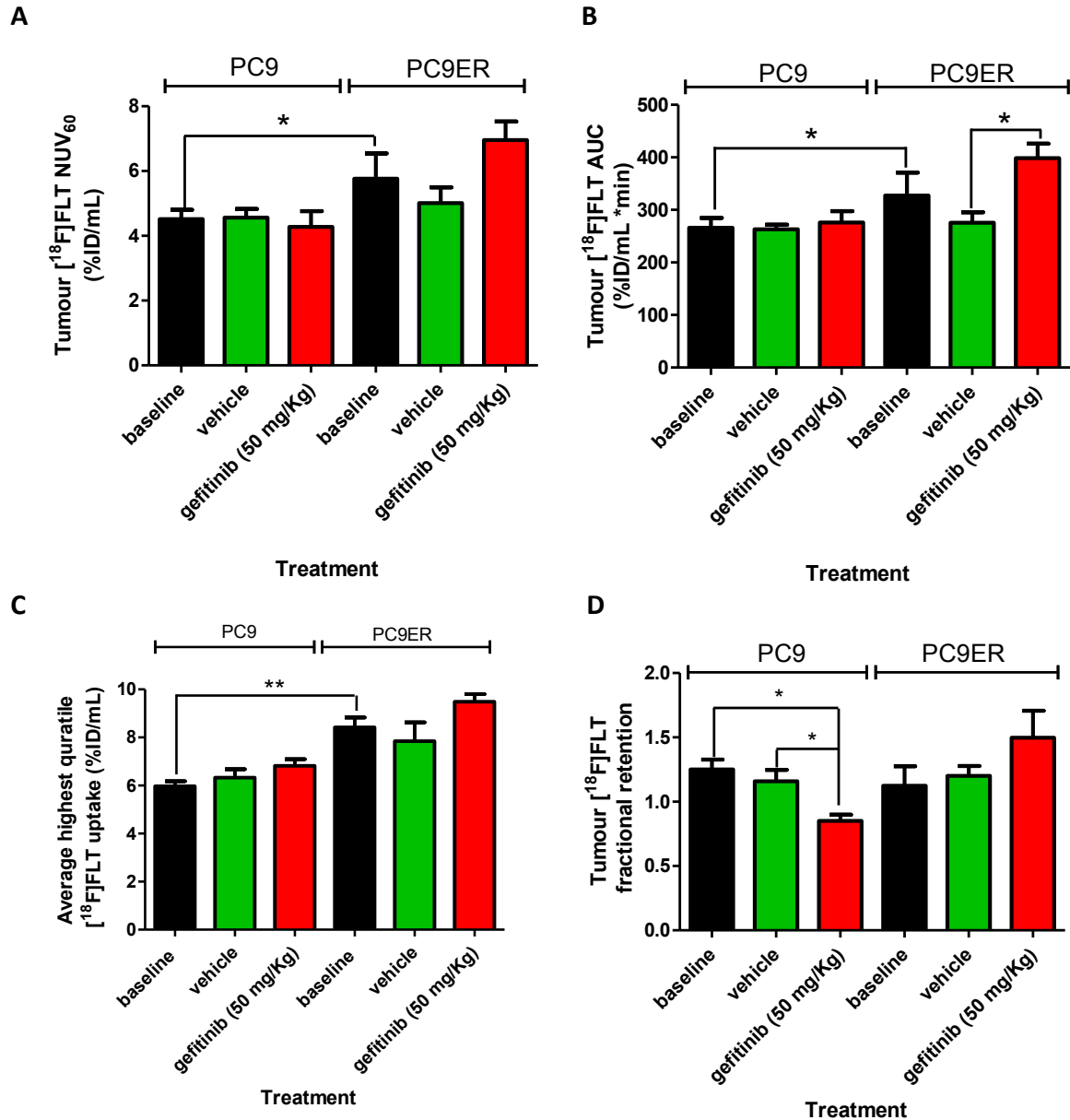


Figure 78: Tumour uptake parameters from [¹⁸F]FLT PET imaging of PC9 and PC9ER xenografts following 48 h gefitinib treatment.

A- Normalised uptake value of [¹⁸F]FLT in PC9 and PC9ER tumours at t = 60 min after tracer injection. B- Area under the curve plot. C- Average highest quartile [¹⁸F]FLT tumour uptake. D- Fractional retention of [¹⁸F]FLT in PC9 and PC9ER tumours between 3.5 and 60 min post tracer injection. Data show means ± SE of n = 4 mice per group. Statistically significant difference between data sets are indicated on the graphs (*= P ≤ 0.05 and **= P ≤ 0.01).

The tumours from the PET study were collected, processed and analysed by gel electrophoresis (Figure 79). In PC9 tumours, there was a complete inhibition of p-EGFR (Y1068) in tumours that were treated with gefitinib compared to tumour lysates from the baseline and the vehicle groups. Gefitinib treatment also led to a decrease in p-SRC Y416, Chk α , p-AKT, p-ERK and levels of total EGFR. Total levels of AKT and ERK were the same as in baseline or vehicle treated tumours.

In the PC9ER tumours, there was a decrease in the expression of p-EGFR (Y1068) in the gefitinib group. However, this decrease was significantly less than the gefitinib induced decrease in p-EGFR (Y1068) measured in the PC9 tumours. Levels of Chk α , p-AKT, AKT, p-ERK and ERK were unchanged between baseline, vehicle and gefitinib treated tumours. Levels of TK1, a key enzyme that phosphorylates [18 F]FLT resulting in its trapping in the cell was measured in the tumour samples (Wagner et al., 2003). Levels of TK1 were decreased in two out of three of the tumour lysate samples from the gefitinib treated group compared to vehicle treated tumours in PC9 but not in the PC9ER tumours (Figure 79A, B) PC9ER tumours express higher levels of TK1 than PC9 tumours (Figure 79C). The colorectal cancer cell line, HCT116, which is characterised by high levels of proliferation associated with high levels of [18 F]FLT uptake, was used as a reference. Levels of TK1, which play an important role in the tumour trapping of [18 F]FLT, were measured in PC9 and PC9ER tumours and compared to levels in HCT116 tumour lysates (Figure 79C). This low level of TK1 would therefore explain the low levels of uptake of [18 F]FLT in both tumour models and the higher baseline uptake of [18 F]FLT in PC9ER compared to PC9 xenografts.

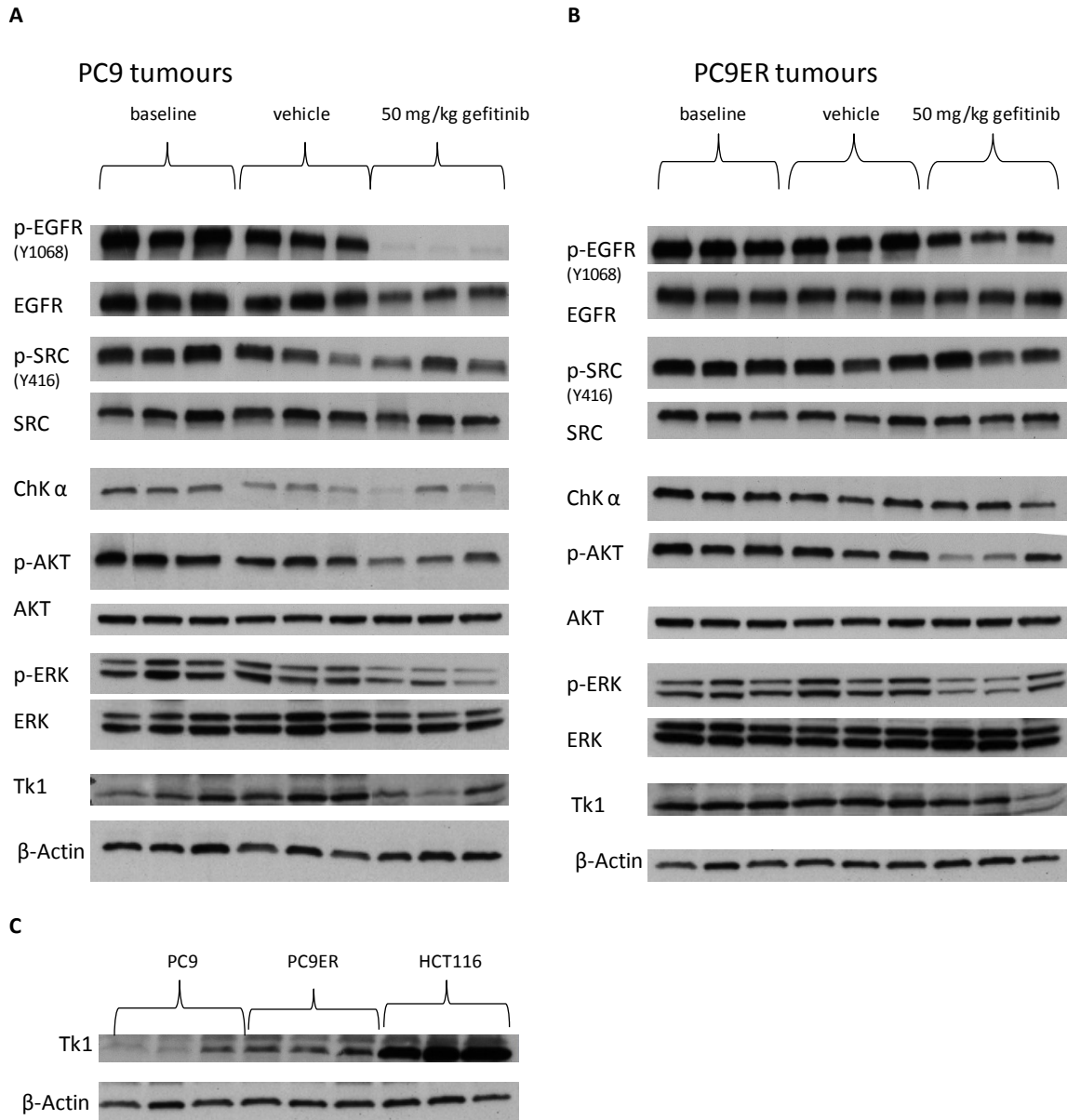


Figure 79: PC9 and PC9ER tumour lysate protein expression analysis from [¹⁸F]FLT PET imaging.

A-B- Protein expression of p-EGFR (Y1068), EGFR, ChKα, p-SRC (Y416), SRC, p-AKT, AKT, p-ERK, ERK and TK1 in tumour lysates from PC9 (A) and PC9ER (B) xenograft from baseline, 48 h vehicle or 50 mg/kg gefitinib treated groups. C- Protein expression of TK1 in HCT116, PC9 and PC9ER tumour lysates. Each column represents a lysate from one tumour.

In conclusion, the strong *in vitro* decrease in [¹⁸F]FLT uptake following gefitinib treatment in PC9 compared to PC9ER cells was not replicated in our *in vivo* studies, when assessing NUV₆₀ or AUC. However, a significantly lower measure of FRT in the gefitinib treated compared to baseline or vehicle treated PC9 group, indicated possible detection of response to gefitinib treatment via [¹⁸F]FLT. The confounds of tumour perfusion and necrosis could explain why only FRT but not NUV₆₀

or AUC were changed. The increased uptake of [¹⁸F]FLT following gefitinib treatment in PC9ER xenografts, when NUV₆₀ and AUC variables were used, was not accompanied by any changes in levels of TK1 expression and remains to be explained.

Chapter 6: Discussion

6.1 Imaging mutant EGFR

The epidermal growth factor receptor is overexpressed in several cancers including, breast, ovarian, brain and colorectal (Sebastian et al., 2006). The overexpression of EGFR and its role in cancer progression led to the development of specific TKI's directed against EGFR. However, the efficacy of gefitinib and erlotinib against wild type EGFR in patients was disappointing, with only a small fraction of unselected patients responding to TKI treatment (Thatcher et al., 2005). It was instead found that a sub group of patients, shown to express active mutant EGFR had significantly higher response rates to TKI treatment (Mok et al., 2009). Identifying patients that express mutant EGFR, non-invasively via PET imaging could assist in therapeutic selection. To date no PET tracers have been approved for the imaging of either WT or mutant EGFR in the clinic. The discovery of an L858R mutant EGFR specific [¹⁸F] PET radiotracer that showed a 7.6 fold higher uptake in H3255 (L858REGFR) compared to H1975 (L858R/T790M EGFR) xenografts was an important breakthrough in the imaging of mutant EGFR (Yeh et al., 2011). However, this radiotracer was only studied in L858R mutant EGFR and further investigation of this tracer to the other common active mutant EGFR, del 746-750 EGFR, would be important.

A series of cyanoquinoline compounds had previously been developed, in our group, for the imaging of EGFR. These molecules were structurally based on the TKI, EKB-579, and showed strong affinity, in nanomolar range, for EGFR. One compound from the series, [¹⁸F]FED6, demonstrated higher uptake in high EGFR vs low EGFR expressing xenografts as well as a favourable metabolic profile. The first part of this thesis, investigated [¹⁸F]FED6 for the imaging of mutant EGFR (Pisaneschi et al., 2010). The specificity of FED6 for EGFR was initially reaffirmed, by measuring a lower uptake of [¹⁸F]FED6 in low EGFR expressing cells, MCF7, vs high EGFR expressing cells, A431. A431 cells transfected with EGFR siRNA also had a reduced uptake of [¹⁸F]FED6 compared to untransfected cells, confirming selectivity of [¹⁸F]FED6 for EGFR.

To investigate FED6 for the imaging of mutant EGFR, del 746-750 mutant EGFR expressing H1650 NSCLC cells, were compared to WT EGFR expressing A549 and H358 cells. When probe inhibitory activity, against EGFR phosphorylation at pharmacological concentrations, was used as a surrogate for potential tracer affinity for imaging, western blot analysis showed that FED6 had a significantly higher inhibition potential against del 746-750 mutant EGFR expressing cells compared to WT EGFR expressing cells. This differential affinity of FED6 for active mutant vs wild type did not however translate into higher *in vitro* uptake of [¹⁸F]FED6 in the H1650 cells. Instead, WT EGFR expressing A549 and H358 cells showed higher levels of [¹⁸F]FED6 uptake. Furthermore the difference in [¹⁸F]FED6 uptake was not linked to differentially EGFR expression, as A549 and H1650 cells expressed

higher levels of EGFR than H358 cells. The *in vivo* PET imaging, of H1650 and A549 xenografts with [¹⁸F]FED6, showed no statistical difference in the tumour uptake of [¹⁸F]FED6 in both A549 and H1650 xenografts. The levels of tracer uptake in the tumour were low in comparison to the high uptake in the GI tract. Furthermore, the time activity curve of [¹⁸F]FED6 showed a gradual wash out of the tracer from the tumour over time. The high non-specific binding of [¹⁸F]FED6 and the lack of accumulation in the tumour could explain why no differential uptake of [¹⁸F]FED6 was measured between both tumour models.

Other mutant EGFR expressing NSCLC cell lines were investigated to further evaluate a possible correlation between the affinity of FED6 for mutant EGFR and [¹⁸F]FED6 uptake. As in del 746-750 EGFR expressing H1650 cells, FED6 showed a higher affinity against active mutant EGFR in PC9 (del 746-750 EGFR) and H3255 (L858R EGFR) cells compared to resistant mutant EGFR expressing PC9ER (del 746-750/ T790M EGFR) and H1975 (L858R/T790M EGFR) cells.

The uptake of [¹⁸F]FED6 was greater in the H3255 and the PC9 cells and lowest in H1975 cells. The higher uptake of [¹⁸F]FED6 in H3255 cells as opposed to the low uptake in H1975 cells correlated with the differential potency (affinity) of FED6 in these two cell lines, assessed by western blot. However, it is important to note that both expression levels of EGFR and mutant status will impact on the uptake of [¹⁸F]FED6. H3255 cells had the highest expression of EGFR compared to the other NSCLC cell lines investigated. It is not possible to confirm that the higher uptake of [¹⁸F]FED6, in the H3255 cells, is a consequence of the higher affinity of FED6 for L858R mutant EGFR, higher expression of EGFR or a combination of both. To address this problem and to be able to characterise the uptake of [¹⁸F]FED6 based on the mutational status of EGFR rather than levels of expression of EGFR, cell lines that have the same levels of expression of EGFR but differ in mutational status should be used for comparison. The PC9 and PC9ER cell lines are isogenic with similar expression levels of EGFR but different mutational status. When comparing these two cell lines, no statistical difference in the uptake of [¹⁸F]FED6 was measured. This could be explained by the fact that IC₅₀ values of FED6 obtained from the % inhibition of p-EGFR were in the same order of magnitude for both PC9 and PC9ER cells. Another confounding effect, which will be discussed further in the subsequent parts of this discussion, and impacted on the uptake of [¹⁸F]FED6 in the NSCLC was the expression of ABC transporter molecules. In order to image mutant EGFR preferentially over WT EGFR, irrespective of the total levels of EGFR, the tracer needs to have high specificity for mutant EGFR. In imaging L858R EGFR, Yeh *et al.* screened a series of compounds and selected the compound that showed the highest affinity for active mutant vs wild type EGFR. They showed a higher affinity

of their tracer in L858R EGFR expressing cells compared to cells that overexpressed WT EGFR (Yeh et al., 2011).

Different levels of expression of EGFR will result in different levels of uptake of the radiotracer. Unless, the radiotracer is designed in such a way that the affinity for WT EGFR is so low that even in cases where the expression levels of WT EGFR are ten folds greater than that of mutant EGF, it would not lead to higher levels of uptake of the tracer. This aspect needs to be carefully considered before stating the sensitive and selective imaging of mutant Vs WT EGFR.

Although FED6 showed higher levels of binding to high vs low EGFR cells *in vivo*, there was a lack of accumulation over time of the radiotracer in the tumour with TACs indicative of a washout of the radiotracer.

To support the design of an optimal imaging cyanoquinoline radiotracer, it was imperative to further elucidate additional properties of FED6 that contributed to its non-specific actions.

Non radiolabelled FED6 blocking studies led to an increase rather than a decrease in [¹⁸F]FED6 uptake. One hypothesis was the involvement of an interaction between FED6 and members of the ABC transporters. By hypothesizing that FED6 is both a substrate and an inhibitor of the ABC transporters, non-radiolabelled FED6 would act as an inhibitor of the ABC transporters leading to an increased uptake of [¹⁸F]FED6 which would no longer be effluxed from the cells. This is in line with work carried out by Mishani *et al.* who developed the quinoline containing EGFR radiotracer, ML04, similar in structure to FED6. Mishani *et al.* demonstrated the involvement of the ABCB1 ABC transporter in the active efflux of ML04 from cells (Abourbeh et al., 2007). Based on the similarity of structure of FED6 to ML04 and on the findings above, the possible substrate specificity of FED6 for the ABC transporters was investigated. In addition, it has been reported that compounds that exhibit substrate specificity for the ABC transporters can also act as inhibitors (Wang and Fu, 2010). We therefore hypothesized that FED6 could be both a substrate and an inhibitor of the ABC transporters.

6.2 FED6 substrate specificity for the ABC transporters.

Multi-drug resistance phenotype is a common feature in cancer patients. Indeed, prolonged treatment, with chemotherapeutic or target specific therapies, commonly leads to acquired resistance. One of the key components of MDR is the increase in expression of ABC transporters on the surface of tumours (Szakacs et al., 2006, Fletcher et al., 2010). The increased expression of ABC transporters will result in tumour efflux of cancer therapies, thus reducing their efficacy. In the

context of PET imaging, ABC transporter substrate specificity also plays its part. As only tracer amounts of the radiolabelled probe are injected into the patients, efflux via such transporters will significantly decrease the potential accumulation of the radioligand in the tumour. Several TKIs, including EKB-569 from which the FED series of compounds were synthesised, have been shown to be substrates for members of the ABC transporter family (Hegedus et al., 2012). As discussed above, we hypothesized that FED6 interacts with one or several of the ABC transporters. A series of experiments were performed in order to find out if this was the case and if so, which ABC transporters were involved.

6.2.1 FED6 is a substrate for ABCB1 and ABCG2.

We focused on the three main ABC transporters reported to be involved in MDR, ABCB1, ABCG2 and ABCC1 (Mizuno et al., 2003). The initial *in silico* characterisation of the FED series of compounds, indicated that these compounds had several characteristics which made them potential substrates for both ABCB1 and ABCG2 transporters including MW > 400, log P > 3 (ABCB1 substrate) and PSA > 85 Å² (ABCG2 substrate) (Varma et al., 2005, Dellinger et al., 1992, Didziapetris et al., 2003). We therefore predicted that FED6, FED2, and FED9 would be substrates for ABCB1 and ABCG2, whereas FED14, that had a reduced molecular weight, would not. The cell viability - SRB - assays performed in the paired cell lines that expressed or not the specific ABC transporters, allowed us to indirectly assess the substrate specificity of the series of compounds for the transporters, by exploiting their cytotoxicity. The higher GI₅₀ values of FED6 in both the ABCB1 expressing 3T3-MDR1 cells and the ABCG2 expressing MCF7MX cells compared to the paired cells that expressed no transporters were indicative of the substrate specificity of FED6 for both transporters. The substrate specificity of FED6 for both transporters was further confirmed by a decrease in the GI₅₀ values following inhibition of the transporters with specific inhibitors, zosuquidar or FTC. Other molecules in the cyanoquinoline series were also found to be substrates for these two transporters. As predicted from its structure, FED14, which corresponds to the cyanoquinoline core, showed no substrate specificity for the ABC transporters tested. For further expansion of the cyanoquinoline library of compounds, in the view of designing out any ABC transporter substrate specificity, knowing that the cyanoquinoline core was non-substrate was an important finding. The substrate specificity of FED6 and any of the other tested compounds for ABCC1 was ruled out as the ratio of the GI₅₀ values was less than 2. However, it is important to note that the A549 cells also express low levels of ABCG2 and this will have affected the GI₅₀ values measured.

The low uptake of radiolabelled [¹⁸F]FED6 in the MCF7MX and 3T3-MDR1 cells, which was increased with FTC and zosuquidar pre-treatment, respectively, compared to the higher uptake in the MCF7 and 3T3 cells further confirmed the substrate specificity of [¹⁸F]FED6 for both the ABCB1 and ABCG2 transporters.

The Caco2 model permitted investigation of the interaction between members of the cyanoquinoline family and the ABC transporters, ABCB1 and ABCG2, expressed at physiological levels. By measuring the efflux ratios corresponding to the ratio between the rate of secretion over the rate of absorption of a compound, the active extrusion of a compound from the cell could be determined. Efflux ratios above 1 were indicative of active ABC transporter efflux (Szakacs et al., 2006). EKB-569, FED2 and FED6 all had efflux ratios indicative of active efflux. The efflux of FED6 was partially reduced in the presence of FTC but not in the presence of zosuquidar. The largest decrease in the efflux of FED6 was measured following pre-treatment with Verapamil. Verapamil is a non-specific drug that has higher potency against ABCB1 but also inhibits other members of the ABC transporters including ABCG2 (Liu et al., 2012). These results would indicate that FED6 is a substrate for both ABCB1 and ABCG2. Verapamil led to the highest decrease in the efflux ratio due to inhibition of both ABCB1 and ABCG2. Zosuquidar alone did not lead to a significant decrease in the efflux ratio as FED6 was still being effluxed via the ABCG2 transporter.

6.2.2 Overcoming ABCG2 efflux of FED6

Having shown that FED6 is a substrate for ABCB1 and ABCG2, the goal was to determine which if any of these two transporters were expressed in the cell lines previously selected to study [¹⁸F]FED6. No ABCB1 was detected in any of the cell lines studied. ABCG2 was expressed in all the cell lines studied with the exception of the H3255 and H358 cells. The levels of ABCG2 were moderate to low in comparison to that in MCF7MX cells, which overexpressed ABCG2. The rest of our work focused on the role of the ABCG2 transporter in the efflux of FED6 and how this efflux could be overcome. To investigate the inhibition of efflux via ABCG2, FTC, a well-characterised inhibitor of ABCG2 and gefitinib, was investigated. The role of gefitinib as an ABCG2 inhibitor has been demonstrated in several studies (Lopez et al., 2007, Nakamura et al., 2005, Yanase et al., 2004, Chen et al., 2011).

The ABCG2 substrate specificity of the fluorescence dye Hoechst 33324 (Scharenberg et al., 2002) was used to assess the effect of knocking down ABCG2 via siRNA or inhibiting ABCG2 with FTC, gefitinib or FED6. In the MCF7MX, ABCG2 overexpressing cells, the increase in fluorescence measured with increasing concentration of FTC and gefitinib was indicative of a reduction in the efflux of Hoechst by ABCG2 following its inhibition. The lack of increase in Hoechst 33324 following

pre-treatment with FED6 indicated that unlike previously hypothesized, FED6 was not an inhibitor of ABCG2. The decrease in efflux and increase in fluorescence of Hoechst 33324 was also measured following ABCG2 siRNA transfection. The trends seen in the Hoechst assay were replicated in the uptake of [¹⁸F]FED6 in MCF7MX cells. There was a significant decrease in radiotracer efflux, and conversely, an increase in uptake of [¹⁸F]FED6 following ABCG2 siRNA transfection or pre-treatment with FTC or gefitinib. Western blot analysis showed that ABCG2 siRNA transfection did not lead to a complete knock down of the expression of ABCG2; this could explain why both the levels of fluorescence in the Hoechst experiment and the uptake of [¹⁸F]FED6 following siRNA treatment, did not reach the levels of those measured following FTC and gefitinib pre-treatment.

Having shown the inhibitory role of gefitinib and FTC on the efflux of [¹⁸F]FED6 in the ABCG2 overexpressing cellular model, both drugs were investigated as inhibitors of [¹⁸F]FED6 efflux in A431 cells that express moderate levels of ABCG2. The fluorescence of Hoechst 33324 at baseline was significantly higher in the A431 cells compared to the MCF7MX cells, indicating an accumulation of Hoechst dye and little efflux by ABCG2. The moderate levels of expression of ABCG2 in the A431 did not appear to impact on the retention of the Hoechst 33324 dye, present in excess concentrations. This could explain why ABCG2 siRNA transfection did not cause an increase in fluorescence in the A431 cells. On the other hand, the uptake of [¹⁸F]FED6 was increased in A431 cells treated with ABCG2 siRNA. In contrast to the Hoechst assay, [¹⁸F]FED6 was added in tracer amounts. We hypothesized that in tracer amounts the accumulation of [¹⁸F]FED6 would be more sensitive to events such as ABC transporter efflux. Pre-treatment with both FTC and gefitinib led to an increase in fluorescence in the Hoechst assay and [¹⁸F]FED6 uptake. The uptake of [¹⁸F]FED6 following gefitinib pre-treatment was over 2 fold higher than the uptake following ABCG2 siRNA transfected cells. We hypothesized that the increase in [¹⁸F]FED6 uptake following gefitinib pre-treatment was only partly caused by an inhibition of ABCG2, and that gefitinib may also have caused an increase in membrane interactions. This would have led to an increased affinity of [¹⁸F]FED6 for proteins of the cellular membrane. Compared to Hegedus *et al.* the concentration of gefitinib selected for the inhibition of ABCG2 in this study was 10 fold higher (Hegedus *et al.*, 2012). At a concentration of 100 μM, gefitinib could be involved in non-specific binding, that could modify the permeability of the cells to Hoechst 33324 and [¹⁸F]FED6. Alongside the inhibitory role of gefitinib for ABCG2, it is important to highlight that gefitinib will ultimately be binding to EGFR, the same target probed by [¹⁸F]FED6. Owing to the increase in uptake following gefitinib treatment, it was suggested that the inhibition of ABCG2 and subsequent decrease in efflux of [¹⁸F]FED6 played a dominant role over changes in [¹⁸F]FED6 uptake caused by blocking of EGFR receptor by gefitinib. However, further investigation into other potential actions of gefitinib in this context is needed. The increase in

[¹⁸F]FED6 uptake following pre-treatment with gefitinib measured *in vitro* was replicated *in vivo* in A431 xenograft. The uptake of [¹⁸F]FED6 in the A431 xenografts that were not pre-treated with gefitinib was low with values under 1 % ID/mL tissue. Pre-treatment with an i.p. injection of 100 mg/Kg of gefitinib led to a doubling of the tracer uptake in the tumour.

In conclusion, having demonstrated the substrate specificity of FED6 for both ABCB1 and ABCG2, ABCG2 was the transporter which was expressed in the majority of the cellular models investigated. The uptake of [¹⁸F]FED6 could be increased both *in vitro* and *in vivo* following gefitinib pre-treatment. However, the effects of gefitinib pre-treatment were not solely caused by the inhibition of ABCG2. Future work could involve the investigation of novel inhibitors of ABCG2, which don't interact with EGFR, and their role in modulating the uptake of [¹⁸F]FED6 both *in vitro* and *in vivo*. One such example could be sorafenib, which has recently been shown to act as an inhibitor of ABCG2 (Wei et al., 2012). In addition, FED6 did not appear to act as an inhibitor of ABCG2. Therefore, further work needs to be carried out, to understand why pre-treatment with non radiolabelled FED6 lead to an increase in [¹⁸F]FED6 in A431 cells.

Rather than having to block the effect of the ABC transporters to which our radiotracer is a substrate, designing a radiotracer that lacks the ABC transporter substrate specificity is preferred

The potential substrate specificity of a radiotracer for the ABC transporters, involved in MDR, should be investigated early in the development stages of the radiotracer. Indeed, structure activity relationship studies could be implemented during the design of the radiotracers. Furthermore, the substrate specificity could be probed through a series of *in vitro* assays once lead compounds have been selected. Carrying out these investigations, an selecting radiotracers that are not substrates of the ABC transporters, would insure that efflux of the radiotracer, due to MDR, would not impede on the uptake and accumulation of the radiotracer in the tumour.

6.2.3 Investigation of an alternative cyanoquinoline molecule: FED20

The main goal in the design of a "second" generation cyanoquinoline compound was to eliminate the substrate specificity of these compounds to the ABC transporters, whilst maintaining high affinity against EGFR. The addition of a glucose moiety to form FED20, led to a decrease in Log P (2.1) compared to 3.9 for FED6. The affinity of FED20 for EGFR was shown to be in the low nanomolar range, and the higher uptake of [¹⁸F]FED20 in the A431 vs MCF7 cells was indicative of the specificity of the tracer for EGFR. The lack of significant decrease in the uptake of [¹⁸F]FED20 following blocking

with cold FED20, would indicate a degree of non-specific binding, which has been reported for other EGFR tracers (Abourbeh et al., 2007). Furthermore, compared to FED6 the uptake values of FED20 were significantly lower with values of under 2 CCPMA/ μg of protein compared to values of 10 to 100 CCPMA/ μg of protein for [^{18}F]FED6. It was hypothesized that the higher lipophilicity of FED6 could cause a high level of non-specific binding in the cell membrane leading to the much higher values of uptake of [^{18}F]FED6. One of the main drawbacks of FED6, which was discussed above, was the substrate specificity for the ABC transporters, and the confounding effect this had on PET imaging of WT and mutant EGFR. It was therefore important that this characteristic be designed out of any new molecules in the series. Caco2 and [^{18}F]FED20 uptake experiments in paired cells that expressed or not ABCB1 and ABCG2 showed no substrate specificity of FED20 for either transporter. The lower Log P of FED20 could explain the lack of substrate specificity for the transporters, as this is a feature known to contribute to the substrate specificity of a compound (Dellinger et al., 1992).

The second goal with [^{18}F]FED20 was to investigate this tracer for the imaging of mutant vs WT EGFR. NSCLC cell lines expressing active mutant EGFR showed the highest affinity for FED20. However, there was not a clear correlation between this data and the uptake values of [^{18}F]FED20. There was a strong correlation between high affinity with high uptake and low affinity with low uptake, in some cell lines (H3255, PC9, and H1975) but not in others (H1650 and A549). One of the main explanations for this lack of clear correlation, which was discussed above for FED6, was the differential expression of p-EGFR (Y1068) and EGFR in the NSCLC studied. Indeed, this will impact on the uptake of [^{18}F]FED20 and make it difficult to specifically attribute [^{18}F]FED20 uptake values to the affinity (correlating to mutational status of EGFR) of FED20 in the NSCLC cell lines. However, the higher uptake of [^{18}F]FED20 in the active mutant PC9 vs resistant mutant PC9ER cells, which both express similar levels of EGFR, was promising for the further investigation of [^{18}F]FED20 in the context of selective imaging of active vs resistant mutant EGFR expressing cells.

The assessment of the uptake, metabolism and biodistribution of [^{18}F]FED20 *in vivo*, which was not completed due to lack of time, will be necessary for further investigation of this molecule for the imaging of WT and mutant EGFR.

PET imaging of EGFR and particularly mutant EGFR could be used for several application: *in vivo* EGFR mutational status determination, treatment response monitoring and identification of the development of drug resistance (Bahce et al., 2013, Yeh et al., 2011). The current recommendation are that, NSCLC patients undergo screening for mutations to EGFR before the start of therapy (Lindeman et al., 2013). This allows the selection of patients with active mutant to be given TKI gefitinib or erlotinib. In fact, gefitinib was approved by NICE in 2009 for first line treatment for

advanced metastatic NSCLC, with active mutant EGFR (NICE, 2010). PET imaging of active mutant EGFR could complement this screening. Biopsies are not always possible and different nodules may present different mutational expression that would not be picked up if one site was biopsied.

The area in which PET imaging of EGFR could be indispensable is in the early detection of resistance to therapy. Following prolonged TKI treatment, patients inevitably acquire drug resistance (Oxnard et al., 2011). Clinical signs of resistance to therapy may occur a long time after the initial molecular changes have arisen. This means that patients may remain on non-effective treatment until the clinical signs of resistance are measured. Being able to detect acquired resistance at an early stage would significantly reduce the time a patient remains on drugs that are no longer effective and would allow new therapy options to be given to the patient. In NSCLC patients, treated with TKI therapies such as gefitinib or erlotinib, 50 % of cases of acquired resistance are the result of T790M mutation to EGFR (Kobayashi et al., 2005, Balak et al., 2006). PET imaging could allow early detection of acquired resistance caused by T790M mutant EGFR, as well as the potential to detect subpopulations of tumour cells that have been shown to express T790M before the start of treatment (Inukai et al., 2006). In 2009, a drug that is selective for T790M mutant EGFR was discovered (Zhou et al., 2009, Zhou et al., 2011b). Using a similar approach, one could design a PET tracer that binds selectively to T790M mutant EGFR, allowing for early detection of resistance to TKI therapy in NSCLC patients. It is important to note that such approaches are however limited. Indeed, the T790M mutation only accounts for 50 % of cases of resistance to gefitinib or erlotinib therapy. Acquired resistance caused by other pathways including MET amplification (Engelman et al., 2007) and K-RAS mutations (Massarelli et al., 2007) would not be detected.

6.3 Chk α as a biomarker of response to gefitinib treatment.

Novel radiotracers for the imaging of EGFR, such as the cyanoquinoline compounds discussed above, could be used to measure pharmacodynamic effects of EGFR directed therapies, by giving a read out of the activity of the receptor. These radiotracers may also be used to monitor response to treatment by measuring a cell viability response. Yeh *et al* demonstrated such effect with [¹⁸F]-PEG(6)-IPQA, whereby a decrease in EGFR activity following gefitinib treatment was associated with a decrease in radiotracer uptake (Yeh et al., 2011).

Another approach is to monitor response to EGFR treatment by measuring changes in other molecules. In this regard, the roles of both Chk α and SRC as key components in the regulation of the activity of EGFR have been elucidated in breast cancer. The mechanistic involvement of Chk α as part of this complex makes it an important molecule to investigate in the assessment of response to

therapies directed against EGFR. As well as the mechanistic link between ChK α and EGFR, the biological relevance of studying ChK α in the context of lung cancer is also significant. In fact, ChK α expression and activity have been shown to be upregulated in several cancers, including lung cancer (Lenkinski et al., 2008, Iorio et al., 2010, Ramirez de Molina et al., 2002a). Furthermore, higher levels of expression of ChK α were also shown to be linked to poorer prognostic of survival in NSCLC patients (Ramirez de Molina et al., 2007). Finally, ChK α has previously been examined as a novel pharmacodynamic or response to treatment biomarker following both TKI and antibody treatment. Preclinical work from our group by Leyton *et al* showed a decrease in uptake of [^{18}F]D4Choline in mouse xenografts following MAPK inhibitor treatment (Leyton et al., 2009). A clinical study investigated [^{11}C]Choline imaging in the context of measuring response to antibody therapy in breast cancer patients. Kenny *et al* showed a decrease in tumour uptake of [^{11}C]Choline following trastuzumab treatment (Kenny et al., 2010).

The mechanistic, biological relevance and previous investigation of ChK α as a biomarker of response to treatment led us to investigate ChK α as a biomarker of response to gefitinib treatment in NSCLC. For this, the effect of gefitinib treatment on ChK α in a gefitinib sensitive NSCLC cell line, PC9, and its isogenic gefitinib resistant PC9ER cell line was determined.

6.3.1 *In vitro* assessment of ChK α as a biomarker of response to gefitinib treatment in PC9 and PC9ER cells.

PC9 and PC9ER cells showed differential response to gefitinib treatment, with cell viability assays indicating a 160 fold higher sensitivity to gefitinib in PC9 vs PC9ER cells. The aim of this *in vitro* work was to determine the potential role of ChK α as a biomarker of the differential response to gefitinib treatment. [^3H]Choline uptake was used as a surrogate of ChK α activity assessment. The extraction of [^3H]phosphocholine and the uptake values measured from the whole cell lysate, indicated that [^3H]choline uptake, measured in the whole cell lysate, was representative of the phosphocholine component. Levels of phosphocholine are linked to the activity of ChK α which catalyses the phosphorylation of choline to phosphocholine (Gibellini and Smith, 2010). At baseline a higher uptake of [^3H]choline was measured in PC9 than in PC9ER cells. This could be a result of increased basal levels of ChK α activity and, or, increased protein expression which was measured in the PC9 cells. Gefitinib treatment, led to a greater decrease in [^3H]choline uptake in the PC9 cells compared to the PC9ER cells at both 6 and 24 h treatment. The highest concentrations of gefitinib which were used also caused high levels of apoptosis in both cell lines at the 24 h time point, and this cell death could be a confounding effect on the changes measured in [^3H]choline uptake. Furthermore, at these concentrations, gefitinib could be directly inhibiting ChK α , leading to a decrease in phosphocholine

formation and hence a decrease in the radioactivity uptake measured. Indeed, at concentrations of 10 and 20 μM gefitinib is also binding to many off targets. This has been reported in a kinase screen carried out on over 113 kinase (Fabian et al., 2005). The lower concentrations of gefitinib used for 48 h treatment, reduced the likelihood of direct inhibitory role of gefitinib on the activity of ChK α . The absence of change in [^3H]choline uptake in the PC9ER cells following 48 h treatment was opposed by a marked decrease in [^3H]choline uptake in the PC9 cells. Decrease in ChK α protein expression in PC9 and increase in ChK α protein and mRNA expression in PC9ER cells may also contribute to this distinct profile of response to gefitinib treatment. This differential uptake of [^3H]choline in the sensitive PC9 and resistant PC9ER cells after 48 h gefitinib was indicative of the potential usefulness of ChK α as a biomarker of response vs resistance to gefitinib treatment in NSCLC. One aspect that warrants further investigation is the role of choline transporter molecules in the uptake of [^3H]choline. Possible changes to expression or activity of these transporters following gefitinib treatment, especially after the 48 h time point, would be necessary to rule out their involvement in the changes measured in [^3H]choline uptake, and to confirm that the changes measured were a surrogate of ChK α activity.

In this present study we focused on one model of resistance. It will be important to further characterise the role of ChK α , in other sensitive and resistant NSCLC cell lines, to affirm it's use as a biomarker of response, failure of response to TKIs such as gefitinib.

6.3.2 Role of SRC and EGFR activity on ChK α activity.

Miyake *et al* investigated the interaction between EGFR, ChK α and c-SRC. In a breast cancer model they showed that ChK α interacted with EGFR in a c-SRC dependant manner. C-SRC but not EGFR kinase activity was necessary for the EGFR-ChK α interaction to occur (Miyake and Parsons, 2012). To investigate whether EGFR and c-SRC activity were required for ChK α activity in the PC9 and PC9ER NSCLC the effect of inhibiting either EGFR or SRC activity, or protein expression were assessed.

Gefitinib dependant loss of EGFR activity occurred rapidly and in a dose dependant manner in both cell lines. However, after 1 and 6 h treatment, ChK α activity was not decreased in the PC9 cells and only the highest concentrations of gefitinib led to a decrease in ChK α in the PC9ER cells. As discussed above, the decrease in ChK α activity, measured at these concentrations of gefitinib could result from a direct inhibition of ChK α activity by gefitinib. After 24 h, significant levels of apoptosis rendered the use of this model to understand regulation of ChK α activity by EGFR complicated. These results indicated that EGFR activity would not be necessary for ChK α activity.

Dasatinib dependant loss of SRC activity occurred rapidly and at all dose levels used. In contrast, ChK α activity had a longer latency and changes were measured at 6 h. After 24 h, significant levels of apoptosis rendered the use of this model to understand regulation of ChK α activity by SRC complicated. The lack of complete knock down of SRC protein expression following siRNA treatment made it difficult to assign SRC protein expression rather than SRC activity to the regulation of ChK α activity. EGFR knock down was indicative of the importance of EGFR protein expression for the activity of ChK α but its knock down alone did not cause complete loss of ChK α activity.

In conclusion, it would appear that SRC but not EGFR activity may play a part in the regulation of ChK α in NSCLC and further experiments should be carried out to confirm this.

The investigation of the interaction of EGFR, ChK α and SRC was investigated at the cellular level. This was deemed important in order to ensure that all the possible co factors required for their interaction were present. However, investigating the interaction of these proteins in isolation would allow further elucidation of specific sites of binding and this should be carried out with mutant forms of EGFR, to measure how these mutations would impact on the interaction of EGFR with SRC and ChK α .

6.3.3 *In vivo* [^{18}F]D4 choline uptake in PC9 and PC9ER xenografts

In vivo imaging of choline kinase metabolism has been carried out in a number of cancers including lung, prostate and breast cancer; both [^{11}C] and [^{18}F] analogues of Choline have been used (DeGrado et al., 2001a, DeGrado et al., 2001b, Hara et al., 2002, Contractor et al., 2011b). Imaging of choline metabolism has been used for tumour detection but also for assessment of response to treatment (Leyton et al., 2009, Kenny et al., 2010) with this in mind and following the positive *in vitro* results the investigation of [^{18}F]D4choline as an early biomarker of response or failure of response to gefitinib treatment in NSCLC was performed.

The difference in ChK α activity, which was measured, between PC9 and PC9ER cells *in vitro* was not reproduced *in vivo*. In fact, the NUV₆₀ and AUC measures of [^{18}F]D4choline tumour uptake were similar in both tumour models. In addition, there were no changes to NUV₆₀ or AUC values following 48 h gefitinib treatment compared to vehicle in the PC9 and PC9ER xenografts. Western blot analysis of tumour lysates indicated that gefitinib treatment induced a marked decrease in ChK α protein expression in PC9 but not PC9ER tumours. ChK α activity is not directly correlated to expression of ChK α and this could explain why a decrease in protein expression did not cause a decrease in [^{18}F]D4choline uptake in the PC9 xenograft, as assessed by NUV₆₀ or AUC measurements.

The lack of decrease in [¹⁸F]D4choline uptake following 48 h gefitinib treatment in the PC9 xenografts could be caused by confounding factors. The two main confounding factors were tumour necrosis and differential tumour perfusion. The presence of possible necrotic core at the centre of the tumours was characterised on the PET images by low uptake of the radiotracer, at the very centre of the tumour. Measuring the values that corresponded to the highest quartile of tumour radiotracer uptake, should allow for only the uptake in viable tissue to be measured. The highest quartile NUV data did not indicate any statistical difference following gefitinib compared to vehicle treatment in the PC9 tumours. The values of tumour uptake of [¹⁸F]D4choline were however closer between both groups. This could indicate that necrosis played a more significant role in confounding the uptake of the radiotracer in the vehicle treated group compared to the gefitinib treated group. One explanation could be that gefitinib treatment halted the growth of the tumours decreasing the development of necrosis, which can be associated with larger tumours. The second confound was tumour perfusion. The uptake of any radiotracer within a tumour is dependent on the perfusion of this tumour (Huang et al., 2012). Tumours that display different degrees of perfusion will show different levels of uptake of the radiotracer, regardless of the expression levels of the specific target imaged by the tracer. FRT values have been previously reported as a means of comparing the tumour uptake of a radiotracer in models where perfusion may play an important role (Leyton et al., 2008). The FRT value decreased in PC9 xenografts following gefitinib treatment compared to the vehicle treated group. In the PC9ER xenografts there were no changes in FRT values between both groups. These results indicated that measuring FRT was a better read out for the response to gefitinib treatment compared to NUV₆₀ or AUC and this was due to the role of perfusion in the initial tumour uptake of [¹⁸F]D4choline.

Based on the reported impact of necrosis and perfusion on the uptake of [¹⁸F]D4choline, it will be important to screen other TKI sensitive and resistant tumour models. Although necrosis is an inherent characteristic of tumours, using models in which the impact of necrosis isn't so great will allow a more thorough investigation of the impact of the uptake of [¹⁸F]D4choline in sensitive VS resistant tumours.

6.4 [¹⁸F]FDG and [¹⁸F]FLT PET imaging of response to gefitinib treatment in comparison to [¹⁸F]D4choline.

[¹⁸F]FDG and [¹⁸F]FLT have both been studied as biomarkers of response to TKI treatment in NSCLC. Several NSCLC xenograft studies showed a decrease in the uptake of [¹⁸F]FLT following TKI treatment (Ullrich et al., 2008, Zannetti et al., 2012), others showed a decrease in [¹⁸F]FDG uptake following TKI

treatment (Su et al., 2006). Having investigated [¹⁸F]D4choline as a biomarker of early response to gefitinib treatment, [¹⁸F]FDG and [¹⁸F]FLT were used in the same models as means of comparison.

The tumour uptake of [¹⁸F]FDG as measured by NUV₆₀, AUC, highest quartile NUV and FRT all indicated a decrease in uptake of the radiotracer following gefitinib compared to vehicle treatment in the PC9 but not PC9ER xenografts. This is in line with the finding of Su *et al.*, that demonstrated a decrease in [¹⁸F]FDG uptake following TKI treatment in sensitive NSCLC tumours (Su et al., 2006). In comparison to [¹⁸F]D4choline, the decrease in uptake of [¹⁸F]FDG following gefitinib treatment compared to vehicle treatment, as measured by FRT, was greater. This could be explained by higher overall values of tumour uptake with [¹⁸F]FDG than with [¹⁸F]D4choline, allowing for a larger decrease in signal following treatment. Further *ex vivo* analysis of gefitinib and vehicle tumours from both models, to determine hexokinase activity but also immunohistochemistry staining for GLUT1, could elucidate the molecular mechanisms behind the differential uptake of [¹⁸F]FDG following gefitinib treatment in PC9 but not PC9ER tumours (Phelps, 2000, Jadvar et al., 2009).

The uptake of [¹⁸F]FLT was significantly higher in the PC9ER than the PC9 tumours. This could in part be a result of higher expression of TK1 in the PC9ER tumours. TK1 phosphorylates [¹⁸F]FLT resulting in its trapping in the cell and the expression of TK1 has been correlated to [¹⁸F]FLT uptake (Barthel et al., 2005). However, TK1 activity may correlate better with changes to [¹⁸F]FLT uptake, and differential activity of TK1 in both models may account for the difference in basal levels of [¹⁸F]FLT uptake. As for [¹⁸F]D4choline only the FRT values were decreased following gefitinib treatment in the PC9 cells, with no change measured in the NUV₆₀ or AUC. This was indicative that again tumour perfusion influenced the initial uptake of the radiotracer in the tumour.

In conclusion, a decrease in FRT following gefitinib treatment was measured using all three radiotracers in the PC9 but not the PC9ER tumours, indicating that all three probes could be used for the detection of sensitivity and or resistance to gefitinib therapy. Further work should include the comparison of all three radiotracers in other NSCLC models to potentially reduce the confound of necrosis and perfusion of the PC9 and PC9ER models. In addition, immunohistochemistry analysis of the tumour sections would allow further confirmation of the PET imaging data.

The different results published in the literature highlight the need for better standardisation of studies and parameters which are measured. This would allow robust comparison of different investigations in order to select the most appropriate tracer for monitoring response to gefitinib treatment in NSCLC.

References

- A. INOUE, K. K., M. MAEMONDO, S. SUGAWARA, S. OIZUM, H. ISOBE, A. GEMMA, M. HARADA, H. YOSHIZAWA, I. KINOSHITA, Y. FUJITA, S. OKINAGA, H. HIRANO, K. YOSHIMORI, T. HARADA, Y. SAIJO, K. HAGIWARA, S. MORITA, T. NUKIWA (2012) Updated overall survival results from a randomized phase III trial comparing gefitinib with carboplatin-paclitaxel for chemo-naïve non-small cell lung cancer with sensitive EGFR gene mutations (NEJ002). *Annals of oncology*, 24, p54-59.
- A.O. WALTER, R. T., H. HARINGSMA, K. LIN, A. DUBROVSKIY, K. LEE ET AL. (2011) CO-1686 an orally available, mutant-selective inhibitor of the epidermal growth factor receptor (EGFR), causes tumor shrinkage in non-small cell lung cancer (NSCLC) with T790M mutations *Molecular cancer therapy*, 10.
- ABOAGYE, E. O. & BHUJWALLA, Z. M. (1999) Malignant transformation alters membrane choline phospholipid metabolism of human mammary epithelial cells. *Cancer Res*, 59, 80-4.
- ABOURBEH, G., DISSOKI, S., JACOBSON, O., LITCHI, A., BEN DANIEL, R., LAKI, D., LEVITZKI, A. & MISHANI, E. (2007) Evaluation of radiolabeled ML04, a putative irreversible inhibitor of epidermal growth factor receptor, as a bioprobe for PET imaging of EGFR-overexpressing tumors. *Nucl Med Biol*, 34, 55-70.
- ACKERSTAFF, E., GLUNDE, K. & BHUJWALLA, Z. M. (2003) Choline phospholipid metabolism: a target in cancer cells? *J Cell Biochem*, 90, 525-33.
- AKCA, H., DEMIRAY, A., YAREN, A., BIR, F., KOSELER, A., IWAKAWA, R., BAGCI, G. & YOKOTA, J. (2013) Utility of serum DNA and pyrosequencing for the detection of EGFR mutations in non-small cell lung cancer. *Cancer Genet*, 206, 73-80.
- AMBUDKAR, S. V., DEY, S., HRYCYNA, C. A., RAMACHANDRA, M., PASTAN, I. & GOTTESMAN, M. M. (1999) Biochemical, cellular, and pharmacological aspects of the multidrug transporter. *Annu Rev Pharmacol Toxicol*, 39, 361-98.
- AOYAMA, C., LIAO, H. & ISHIDATE, K. (2004) Structure and function of choline kinase isoforms in mammalian cells. *Prog Lipid Res*, 43, 266-81.
- ARTURSSON, P. & KARLSSON, J. (1991) Correlation between oral drug absorption in humans and apparent drug permeability coefficients in human intestinal epithelial (Caco-2) cells. *Biochem Biophys Res Commun*, 175, 880-5.
- BAGHAEI, H. W., W-H; URIBE, J. (2003) *Principles of positron emission tomography imaging*, springer.
- BAHCE, I., SMIT, E. F., LUBBERINK, M., VAN DER VELDT, A. A., YAQUB, M., WINDHORST, A. D., SCHUIT, R. C., THUNNISSEN, E., HEIDEMAN, D. A., POSTMUS, P. E., LAMMERTSMA, A. A. & HENDRIKSE, N. H. (2013) Development of [(11)C]erlotinib positron emission tomography for in vivo evaluation of EGF receptor mutational status. *Clin Cancer Res*, 19, 183-93.
- BALAK, M. N., GONG, Y., RIELY, G. J., SOMWAR, R., LI, A. R., ZAKOWSKI, M. F., CHIANG, A., YANG, G., OUFERELLI, O., KRIS, M. G., LADANYI, M., MILLER, V. A. & PAO, W. (2006) Novel D761Y and common secondary T790M mutations in epidermal growth factor receptor-mutant lung adenocarcinomas with acquired resistance to kinase inhibitors. *Clin Cancer Res*, 12, 6494-501.
- BARKER, A. J., GIBSON, K. H., GRUNDY, W., GODFREY, A. A., BARLOW, J. J., HEALY, M. P., WOODBURN, J. R., ASHTON, S. E., CURRY, B. J., SCARLETT, L., HENTHORN, L. & RICHARDS, L. (2001) Studies leading to the identification of ZD1839 (IRESSA): an orally active, selective epidermal growth factor receptor tyrosine kinase inhibitor targeted to the treatment of cancer. *Bioorg Med Chem Lett*, 11, 1911-4.
- BARTHEL, H., PERUMAL, M., LATIGO, J., HE, Q., BRADY, F., LUTHRA, S. K., PRICE, P. M. & ABOAGYE, E. O. (2005) The uptake of 3'-deoxy-3'-[18F]fluorothymidine into L5178Y tumours in vivo is dependent on thymidine kinase 1 protein levels. *Eur J Nucl Med Mol Imaging*, 32, 257-63.
- BASU, S., KWEE, T. C., SURTI, S., AKIN, E. A., YOO, D. & ALAVI, A. (2011) Fundamentals of PET and PET/CT imaging. *Ann N Y Acad Sci*, 1228, 1-18.
- BEAN, J., RIELY, G. J., BALAK, M., MARKS, J. L., LADANYI, M., MILLER, V. A. & PAO, W. (2008) Acquired resistance to epidermal growth factor receptor kinase inhibitors associated with a novel

- T854A mutation in a patient with EGFR-mutant lung adenocarcinoma. *Clin Cancer Res*, 14, 7519-25.
- BHATTACHARYYA, S., KURDZIEL, K., WEI, L., RIFFLE, L., KAUR, G., HILL, G. C., JACOBS, P. M., TATUM, J. L., DOROSHOW, J. H. & KALEN, J. D. (2013) Zirconium-89 labeled panitumumab: a potential immuno-PET probe for HER1-expressing carcinomas. *Nucl Med Biol*, 40, 451-7.
- BRYCE, A. H., RAO, R., SARKARIA, J., REID, J. M., QI, Y., QIN, R., JAMES, C. D., JENKINS, R. B., BONI, J., ERLICHMAN, C. & HALUSKA, P. (2012) Phase I study of temsirolimus in combination with EKB-569 in patients with advanced solid tumors. *Invest New Drugs*, 30, 1934-41.
- BURGESS, A. W. (2008) EGFR family: structure physiology signalling and therapeutic targets. *Growth Factors*, 26, 263-74.
- C.-H. YANG, M. H. S., N. YAMAMOTO, K.J. O'BYRNE, V. HIRSH, T. MOK, S.L. GEATER ET AL. (2012) LUX-Lung 3: A randomized, open-label, phase III study of afatinib versus pemetrexed and cisplatin as first-line treatment for patients with advanced adenocarcinoma of the lung harboring EGFR-activating mutations *Journal of clinical oncology*, 30.
- CAI, W., CHEN, K., HE, L., CAO, Q., KOONG, A. & CHEN, X. (2007) Quantitative PET of EGFR expression in xenograft-bearing mice using ⁶⁴Cu-labeled cetuximab, a chimeric anti-EGFR monoclonal antibody. *Eur J Nucl Med Mol Imaging*, 34, 850-8.
- CAPPUZZO, F., MAGRINI, E., CERESOLI, G. L., BARTOLINI, S., ROSSI, E., LUDOVINI, V., GREGORC, V., LIGORIO, C., CANCELLIERI, A., DAMIANI, S., SPREAFICO, A., PATIES, C. T., LOMBARDO, L., CALANDRI, C., BELLEZZA, G., TONATO, M. & CRINO, L. (2004) Akt phosphorylation and gefitinib efficacy in patients with advanced non-small-cell lung cancer. *J Natl Cancer Inst*, 96, 1133-41.
- CAREY, K. D., GARTON, A. J., ROMERO, M. S., KAHLER, J., THOMSON, S., ROSS, S., PARK, F., HALEY, J. D., GIBSON, N. & SLIWKOWSKI, M. X. (2006) Kinetic analysis of epidermal growth factor receptor somatic mutant proteins shows increased sensitivity to the epidermal growth factor receptor tyrosine kinase inhibitor, erlotinib. *Cancer Res*, 66, 8163-71.
- CHEN, G., NOOR, A., KRONENBERGER, P., TEUGELS, E., UMELO, I. A. & DE GREVE, J. (2013a) Synergistic effect of afatinib with su11274 in non-small cell lung cancer cells resistant to gefitinib or erlotinib. *PLoS One*, 8, e59708.
- CHEN, X., ZHU, Q., ZHU, L., PEI, D., LIU, Y., YIN, Y., SCHULER, M. & SHU, Y. (2013b) Clinical perspective of afatinib in non-small cell lung cancer. *Lung Cancer*.
- CHEN, Y. J., HUANG, W. C., WEI, Y. L., HSU, S. C., YUAN, P., LIN, H. Y., WISTUBA, II, LEE, J. J., YEN, C. J., SU, W. C., CHANG, K. Y., CHANG, W. C., CHOU, T. C., CHOU, C. K., TSAI, C. H. & HUNG, M. C. (2011) Elevated BCRP/ABCG2 Expression Confers Acquired Resistance to Gefitinib in Wild-Type EGFR-Expressing Cells. *PLoS One*, 6, e21428.
- CHOI, B. K., FAN, X., DENG, H., ZHANG, N. & AN, Z. (2012) ERBB3 (HER3) is a key sensor in the regulation of ERBB-mediated signaling in both low and high ERBB2 (HER2) expressing cancer cells. *Cancer Med*, 1, 28-38.
- COBO, M., ISLA, D., MASSUTI, B., MONTES, A., SANCHEZ, J. M., PROVENCIO, M., VINOLAS, N., PAZ-ARES, L., LOPEZ-VIVANCO, G., MUNOZ, M. A., FELIP, E., ALBEROLA, V., CAMPS, C., DOMINE, M., SANCHEZ, J. J., SANCHEZ-RONCO, M., DANENBERG, K., TARON, M., GANDARA, D. & ROSELL, R. (2007) Customizing cisplatin based on quantitative excision repair cross-complementing 1 mRNA expression: a phase III trial in non-small-cell lung cancer. *J Clin Oncol*, 25, 2747-54.
- COLE, S. P., BHARDWAJ, G., GERLACH, J. H., MACKIE, J. E., GRANT, C. E., ALMQUIST, K. C., STEWART, A. J., KURZ, E. U., DUNCAN, A. M. & DEELEY, R. G. (1992) Overexpression of a transporter gene in a multidrug-resistant human lung cancer cell line. *Science*, 258, 1650-4.
- CONTRACTOR, K., CHALLAPALLI, A., BARWICK, T., WINKLER, M., HELLAWELL, G., HAZELL, S., TOMASI, G., AL-NAHHAS, A., MAPELLI, P., KENNY, L. M., TADROUS, P., COOMBES, R. C., ABOAGYE, E. O. & MANGAR, S. (2011a) Use of [¹¹C]choline PET-CT as a noninvasive method for detecting

- pelvic lymph node status from prostate cancer and relationship with choline kinase expression. *Clin Cancer Res*, 17, 7673-83.
- CONTRACTOR, K. B., KENNY, L. M., STEBBING, J., CHALLAPALLI, A., AL-NAHHAS, A., PALMIERI, C., SHOUSHA, S., LEWIS, J. S., HOGBEN, K., DE NGUYEN, Q., COOMBES, R. C. & ABOAGYE, E. O. (2011b) Biological basis of [(1)(1)C]choline-positron emission tomography in patients with breast cancer: comparison with [(1)(8)F]fluorothymidine positron emission tomography. *Nucl Med Commun*, 32, 997-1004.
- CONTRACTOR, K. B., KENNY, L. M., STEBBING, J., ROSSO, L., AHMAD, R., JACOB, J., CHALLAPALLI, A., TURKHEIMER, F., AL-NAHHAS, A., SHARMA, R., COOMBES, R. C. & ABOAGYE, E. O. (2011c) [18F]-3'Deoxy-3'-fluorothymidine positron emission tomography and breast cancer response to docetaxel. *Clin Cancer Res*, 17, 7664-72.
- DAHABREH, I. J., LINARDOU, H., SIANNIS, F., KOSMIDIS, P., BAFALOUKOS, D. & MURRAY, S. (2010) Somatic EGFR mutation and gene copy gain as predictive biomarkers for response to tyrosine kinase inhibitors in non-small cell lung cancer. *Clin Cancer Res*, 16, 291-303.
- DEAN, M., RZHETSKY, A. & ALLIKMETS, R. (2001) The human ATP-binding cassette (ABC) transporter superfamily. *Genome Res*, 11, 1156-66.
- DEELEY, R. G. & COLE, S. P. (2006) Substrate recognition and transport by multidrug resistance protein 1 (ABCC1). *FEBS Lett*, 580, 1103-11.
- DEGRADO, T. R., BALDWIN, S. W., WANG, S., ORR, M. D., LIAO, R. P., FRIEDMAN, H. S., REIMAN, R., PRICE, D. T. & COLEMAN, R. E. (2001a) Synthesis and evaluation of (18)F-labeled choline analogs as oncologic PET tracers. *J Nucl Med*, 42, 1805-14.
- DEGRADO, T. R., COLEMAN, R. E., WANG, S., BALDWIN, S. W., ORR, M. D., ROBERTSON, C. N., POLASCIAK, T. J. & PRICE, D. T. (2001b) Synthesis and evaluation of 18F-labeled choline as an oncologic tracer for positron emission tomography: initial findings in prostate cancer. *Cancer Res*, 61, 110-7.
- DELLINGER, M., PRESSMAN, B. C., CALDERON-HIGGINSON, C., SAVARAJ, N., TAPIERO, H., KOLONIAS, D. & LAMPIDIS, T. J. (1992) Structural requirements of simple organic cations for recognition by multidrug-resistant cells. *Cancer Res*, 52, 6385-9.
- DI FIORE, P. P., PIERCE, J. H., FLEMING, T. P., HAZAN, R., ULLRICH, A., KING, C. R., SCHLESSINGER, J. & AARONSON, S. A. (1987) Overexpression of the human EGF receptor confers an EGF-dependent transformed phenotype to NIH 3T3 cells. *Cell*, 51, 1063-70.
- DIDZIAPETRIS, R., JAPERTAS, P., AVDEEF, A. & PETRAUSKAS, A. (2003) Classification analysis of P-glycoprotein substrate specificity. *J Drug Target*, 11, 391-406.
- DOWNING, G. J. E. A. (2001) Biomarkers and surrogate endpoints: preferred definitions and conceptual framework. *Clin Pharmacol Ther*, 69, 89-95.
- DOWNWARD, J., PARKER, P. & WATERFIELD, M. D. (1984a) Autophosphorylation sites on the epidermal growth factor receptor. *Nature*, 311, 483-5.
- DOWNWARD, J., YARDEN, Y., MAYES, E., SCRACE, G., TOTTY, N., STOCKWELL, P., ULLRICH, A., SCHLESSINGER, J. & WATERFIELD, M. D. (1984b) Close similarity of epidermal growth factor receptor and v-erb-B oncogene protein sequences. *Nature*, 307, 521-7.
- DOYLE, L. & ROSS, D. D. (2003) Multidrug resistance mediated by the breast cancer resistance protein BCRP (ABCG2). *Oncogene*, 22, 7340-58.
- DOYLE, L. A., YANG, W., ABRUZZO, L. V., KROGMANN, T., GAO, Y., RISHI, A. K. & ROSS, D. D. (1998) A multidrug resistance transporter from human MCF-7 breast cancer cells. *Proc Natl Acad Sci U S A*, 95, 15665-70.
- EISENHAEUER, E. A., THERASSE, P., BOGAERTS, J., SCHWARTZ, L. H., SARGENT, D., FORD, R., DANCEY, J., ARBUCK, S., GWYTHYER, S., MOONEY, M., RUBINSTEIN, L., SHANKAR, L., DODD, L., KAPLAN, R., LACOMBE, D. & VERWEIJ, J. (2009) New response evaluation criteria in solid tumours: revised RECIST guideline (version 1.1). *Eur J Cancer*, 45, 228-47.
- ENGELMAN, J. A., ZEJNULLAHU, K., MITSUDOMI, T., SONG, Y., HYLAND, C., PARK, J. O., LINDEMAN, N., GALE, C. M., ZHAO, X., CHRISTENSEN, J., KOSAKA, T., HOLMES, A. J., ROGERS, A. M.,

- CAPPUZZO, F., MOK, T., LEE, C., JOHNSON, B. E., CANTLEY, L. C. & JANNE, P. A. (2007) MET amplification leads to gefitinib resistance in lung cancer by activating ERBB3 signaling. *Science*, 316, 1039-43.
- ERCAN, D., ZEJNULLAHU, K., YONESAKA, K., XIAO, Y., CAPELLETTI, M., ROGERS, A., LIFSHITS, E., BROWN, A., LEE, C., CHRISTENSEN, J. G., KWIATKOWSKI, D. J., ENGELMAN, J. A. & JANNE, P. A. (2010) Amplification of EGFR T790M causes resistance to an irreversible EGFR inhibitor. *Oncogene*, 29, 2346-56.
- ESKENS, F. A., MOM, C. H., PLANTING, A. S., GIETEMA, J. A., AMELSBURG, A., HUISMAN, H., VAN DOORN, L., BURGER, H., STOPFER, P., VERWEIJ, J. & DE VRIES, E. G. (2008) A phase I dose escalation study of BIBW 2992, an irreversible dual inhibitor of epidermal growth factor receptor 1 (EGFR) and 2 (HER2) tyrosine kinase in a 2-week on, 2-week off schedule in patients with advanced solid tumours. *Br J Cancer*, 98, 80-5.
- FABIAN, M. A., BIGGS, W. H., 3RD, TREIBER, D. K., ATTERIDGE, C. E., AZIMIOARA, M. D., BENEDETTI, M. G., CARTER, T. A., CICERI, P., EDEEN, P. T., FLOYD, M., FORD, J. M., GALVIN, M., GERLACH, J. L., GROTZFELD, R. M., HERRGARD, S., INSKO, D. E., INSKO, M. A., LAI, A. G., LELIAS, J. M., MEHTA, S. A., MILANOV, Z. V., VELASCO, A. M., WODICKA, L. M., PATEL, H. K., ZARRINKAR, P. P. & LOCKHART, D. J. (2005) A small molecule-kinase interaction map for clinical kinase inhibitors. *Nat Biotechnol*, 23, 329-36.
- FELIP, E. & ROSELL, R. (2006) Clinical experience with erlotinib in non-small-cell lung cancer. *Drugs Today (Barc)*, 42, 147-56.
- FLANIGAN, J., DESHPANDE, H. & GETTINGER, S. (2010) Current status of vandetanib (ZD6474) in the treatment of non-small cell lung cancer. *Biologics*, 4, 237-43.
- FLETCHER, J. I., HABER, M., HENDERSON, M. J. & NORRIS, M. D. (2010) ABC transporters in cancer: more than just drug efflux pumps. *Nat Rev Cancer*, 10, 147-56.
- FOLPRECHT, G., TABERNERO, J., KOHNE, C. H., ZACHARCHUK, C., PAZ-ARES, L., ROJO, F., QUINN, S., CASADO, E., SALAZAR, R., ABBAS, R., LEJEUNE, C., MARIMON, I., ANDREU, J., UBBELOHDE, U., CORTES-FUNES, H. & BASELGA, J. (2008) Phase I pharmacokinetic/pharmacodynamic study of EKB-569, an irreversible inhibitor of the epidermal growth factor receptor tyrosine kinase, in combination with irinotecan, 5-fluorouracil, and leucovorin (FOLFIRI) in first-line treatment of patients with metastatic colorectal cancer. *Clin Cancer Res*, 14, 215-23.
- FRIEDMAN, M., ORLOVA, A., JOHANSSON, E., ERIKSSON, T. L., HOIDEN-GUTHENBERG, I., TOLMACHEV, V., NILSSON, F. Y. & STAHL, S. (2008) Directed evolution to low nanomolar affinity of a tumor-targeting epidermal growth factor receptor-binding affibody molecule. *J Mol Biol*, 376, 1388-402.
- FRY, D. W. (1999) Inhibition of the epidermal growth factor receptor family of tyrosine kinases as an approach to cancer chemotherapy: progression from reversible to irreversible inhibitors. *Pharmacol Ther*, 82, 207-18.
- FUKUOKA, M., YANO, S., GIACCONE, G., TAMURA, T., NAKAGAWA, K., DOUILLARD, J. Y., NISHIWAKI, Y., VANSTEENKISTE, J., KUDOH, S., RISCHIN, D., EEK, R., HORAI, T., NODA, K., TAKATA, I., SMIT, E., AVERBUCH, S., MACLEOD, A., FEYEREISLOVA, A., DONG, R. P. & BASELGA, J. (2003) Multi-institutional randomized phase II trial of gefitinib for previously treated patients with advanced non-small-cell lung cancer (The IDEAL 1 Trial) [corrected]. *J Clin Oncol*, 21, 2237-46.
- GALLEGO-ORTEGA, D., RAMIREZ DE MOLINA, A., RAMOS, M. A., VALDES-MORA, F., BARDERAS, M. G., SARMENTERO-ESTRADA, J. & LACAL, J. C. (2009) Differential role of human choline kinase alpha and beta enzymes in lipid metabolism: implications in cancer onset and treatment. *PLoS One*, 4, e7819.
- GAN, H. K., KAYE, A. H. & LUWOR, R. B. (2009) The EGFRvIII variant in glioblastoma multiforme. *J Clin Neurosci*, 16, 748-54.
- GAZDAR, A. F. (2009) Activating and resistance mutations of EGFR in non-small-cell lung cancer: role in clinical response to EGFR tyrosine kinase inhibitors. *Oncogene*, 28 Suppl 1, S24-31.

- GELOVANI, J. G. (2008) Molecular imaging of epidermal growth factor receptor expression-activity at the kinase level in tumors with positron emission tomography. *Cancer Metastasis Rev*, 27, 645-53.
- GIACCONE, G., HERBST, R. S., MANEGOLD, C., SCAGLIOTTI, G., ROSELL, R., MILLER, V., NATALE, R. B., SCHILLER, J. H., VON PAWEL, J., PLUZANSKA, A., GATZEMEIER, U., GROUS, J., OCHS, J. S., AVERBUCH, S. D., WOLF, M. K., RENNIE, P., FANDI, A. & JOHNSON, D. H. (2004) Gefitinib in combination with gemcitabine and cisplatin in advanced non-small-cell lung cancer: a phase III trial--INTACT 1. *J Clin Oncol*, 22, 777-84.
- GIBELLINI, F. & SMITH, T. K. (2010) The Kennedy pathway--De novo synthesis of phosphatidylethanolamine and phosphatidylcholine. *IUBMB Life*, 62, 414-28.
- GLUNDE, K., BHUJWALLA, Z. M. & RONEN, S. M. (2011) Choline metabolism in malignant transformation. *Nat Rev Cancer*, 11, 835-48.
- GOTO, K., ICHINOSE, Y., OHE, Y., YAMAMOTO, N., NEGORO, S., NISHIO, K., ITOH, Y., JIANG, H., DUFFIELD, E., MCCORMACK, R., SAIJO, N., MOK, T. & FUKUOKA, M. (2012) Epidermal growth factor receptor mutation status in circulating free DNA in serum: from IPASS, a phase III study of gefitinib or carboplatin/paclitaxel in non-small cell lung cancer. *J Thorac Oncol*, 7, 115-21.
- GOTTESMAN, M. M. & PASTAN, I. (1993) Biochemistry of multidrug resistance mediated by the multidrug transporter. *Annu Rev Biochem*, 62, 385-427.
- GRIFFITHS, J. R., CADY, E., EDWARDS, R. H., MCCREADY, V. R., WILKIE, D. R. & WILTSHAW, E. (1983) 31P-NMR studies of a human tumour in situ. *Lancet*, 1, 1435-6.
- HABERKORN, U., MARKERT, A., MIER, W., ASKOXYLAKIS, V. & ALTMANN, A. (2011) Molecular imaging of tumor metabolism and apoptosis. *Oncogene*, 30, 4141-51.
- HAN, J. Y., PARK, K., KIM, S. W., LEE, D. H., KIM, H. Y., KIM, H. T., AHN, M. J., YUN, T., AHN, J. S., SUH, C., LEE, J. S., YOON, S. J., HAN, J. H., LEE, J. W., JO, S. J. & LEE, J. S. (2012) First-SIGNAL: first-line single-agent iressa versus gemcitabine and cisplatin trial in never-smokers with adenocarcinoma of the lung. *J Clin Oncol*, 30, 1122-8.
- HARA, T., KOSAKA, N. & KISHI, H. (1998) PET imaging of prostate cancer using carbon-11-choline. *J Nucl Med*, 39, 990-5.
- HARA, T., KOSAKA, N. & KISHI, H. (2002) Development of (18)F-fluoroethylcholine for cancer imaging with PET: synthesis, biochemistry, and prostate cancer imaging. *J Nucl Med*, 43, 187-99.
- HE, M. & WEI, M. J. (2012) Reversing multidrug resistance by tyrosine kinase inhibitors. *Chin J Cancer*, 31, 126-33.
- HEGEDUS, C., OZVEGY-LACZKA, C., APATI, A., MAGOCSI, M., NEMET, K., ORFI, L., KERI, G., KATONA, M., TAKATS, Z., VARADI, A., SZAKACS, G. & SARKADI, B. (2009) Interaction of nilotinib, dasatinib and bosutinib with ABCB1 and ABCG2: implications for altered anti-cancer effects and pharmacological properties. *Br J Pharmacol*, 158, 1153-64.
- HEGEDUS, C., TRUTA-FELES, K., ANTALFFY, G., VARADY, G., NEMET, K., OZVEGY-LACZKA, C., KERI, G., ORFI, L., SZAKACS, G., SETTLEMAN, J., VARADI, A. & SARKADI, B. (2012) Interaction of the EGFR inhibitors gefitinib, vandetanib, pelitinib and neratinib with the ABCG2 multidrug transporter: implications for the emergence and reversal of cancer drug resistance. *Biochem Pharmacol*, 84, 260-7.
- HERBST, R. S., HEYMACH, J. V. & LIPPMAN, S. M. (2008) Lung cancer. *N Engl J Med*, 359, 1367-80.
- HERNANDO, E., SARMENTERO-ESTRADA, J., KOPPIE, T., BELDA-INIESTA, C., RAMIREZ DE MOLINA, V., CEJAS, P., OZU, C., LE, C., SANCHEZ, J. J., GONZALEZ-BARON, M., KOUTCHER, J., CORDON-CARDO, C., BOCHNER, B. H., LACAL, J. C. & RAMIREZ DE MOLINA, A. (2009) A critical role for choline kinase-alpha in the aggressiveness of bladder carcinomas. *Oncogene*, 28, 2425-35.
- HICKS, R. J. (2009) Role of 18F-FDG PET in assessment of response in non-small cell lung cancer. *J Nucl Med*, 50 Suppl 1, 31S-42S.
- HIRSCH, F. R., VARELLA-GARCIA, M., MCCOY, J., WEST, H., XAVIER, A. C., GUMERLOCK, P., BUNN, P. A., JR., FRANKLIN, W. A., CROWLEY, J. & GANDARA, D. R. (2005) Increased epidermal growth

- factor receptor gene copy number detected by fluorescence in situ hybridization associates with increased sensitivity to gefitinib in patients with bronchioloalveolar carcinoma subtypes: a Southwest Oncology Group Study. *J Clin Oncol*, 23, 6838-45.
- HOLLO, Z., HOMOLYA, L., DAVIS, C. W. & SARKADI, B. (1994) Calcein accumulation as a fluorometric functional assay of the multidrug transporter. *Biochim Biophys Acta*, 1191, 384-8.
- HUANG, T., CIVELEK, A. C., LI, J., JIANG, H., NG, C. K., POSTEL, G. C., SHEN, B. & LI, X. F. (2012) Tumor microenvironment-dependent 18F-FDG, 18F-fluorothymidine, and 18F-misonidazole uptake: a pilot study in mouse models of human non-small cell lung cancer. *J Nucl Med*, 53, 1262-8.
- HUANG, W. C., CHEN, Y. J., LI, L. Y., WEI, Y. L., HSU, S. C., TSAI, S. L., CHIU, P. C., HUANG, W. P., WANG, Y. N., CHEN, C. H., CHANG, W. C., CHEN, A. J., TSAI, C. H. & HUNG, M. C. (2011) Nuclear translocation of epidermal growth factor receptor by Akt-dependent phosphorylation enhances breast cancer-resistant protein expression in gefitinib-resistant cells. *J Biol Chem*, 286, 20558-68.
- HUTCHINS GD, M. M., SOON VC, RECEVEUR T. (2008) Small animal PET imaging. *ILAR J.*, 49, 54-65.
- HYNES, N. E. & LANE, H. A. (2005) ERBB receptors and cancer: the complexity of targeted inhibitors. *Nat Rev Cancer*, 5, 341-54.
- INUKAI, M., TOYOOKA, S., ITO, S., ASANO, H., ICHIHARA, S., SOH, J., SUEHISA, H., OUCHIDA, M., AOE, K., AOE, M., KIURA, K., SHIMIZU, N. & DATE, H. (2006) Presence of epidermal growth factor receptor gene T790M mutation as a minor clone in non-small cell lung cancer. *Cancer Res*, 66, 7854-8.
- IORIO, E., RICCI, A., BAGNOLI, M., PISANU, M. E., CASTELLANO, G., DI VITO, M., VENTURINI, E., GLUNDE, K., BHUJWALLA, Z. M., MEZZANZANICA, D., CANEVARI, S. & PODO, F. (2010) Activation of phosphatidylcholine cycle enzymes in human epithelial ovarian cancer cells. *Cancer Res*, 70, 2126-35.
- JADVAR, H., ALAVI, A. & GAMBHIR, S. S. (2009) 18F-FDG uptake in lung, breast, and colon cancers: molecular biology correlates and disease characterization. *J Nucl Med*, 50, 1820-7.
- JORISSEN, R. N., WALKER, F., POULIOT, N., GARRETT, T. P., WARD, C. W. & BURGESS, A. W. (2003) Epidermal growth factor receptor: mechanisms of activation and signalling. *Exp Cell Res*, 284, 31-53.
- KALISZCZAK, M., ANTONOW, D., PATEL, K. I., HOWARD, P., JODRELL, D. I., THURSTON, D. E. & GUICHARD, S. M. (2010) Optimization of the antitumor activity of sequence-specific pyrrolobenzodiazepine derivatives based on their affinity for ABC transporters. *AAPS J*, 12, 617-27.
- KATZ-BRULL, R., LAVIN, P. T. & LENKINSKI, R. E. (2002) Clinical utility of proton magnetic resonance spectroscopy in characterizing breast lesions. *J Natl Cancer Inst*, 94, 1197-203.
- KAUPPINEN, R. A. & PEET, A. C. (2011) Using magnetic resonance imaging and spectroscopy in cancer diagnostics and monitoring: preclinical and clinical approaches. *Cancer Biol Ther*, 12, 665-79.
- KENNY, L. M., CONTRACTOR, K. B., HINZ, R., STEBBING, J., PALMIERI, C., JIANG, J., SHOUSHA, S., AL-NAHHAS, A., COOMBES, R. C. & ABOAGYE, E. O. (2010) Reproducibility of [11C]choline-positron emission tomography and effect of trastuzumab. *Clin Cancer Res*, 16, 4236-45.
- KIM, M., TURNQUIST, H., JACKSON, J., SGAGIAS, M., YAN, Y., GONG, M., DEAN, M., SHARP, J. G. & COWAN, K. (2002) The multidrug resistance transporter ABCG2 (breast cancer resistance protein 1) effluxes Hoechst 33342 and is overexpressed in hematopoietic stem cells. *Clin Cancer Res*, 8, 22-8.
- KITAJIMA, K., MURPHY, R. C. & NATHAN, M. A. (2013) Choline PET/CT for imaging prostate cancer: an update. *Ann Nucl Med*.
- KITAZAKI, T., OKA, M., NAKAMURA, Y., TSURUTANI, J., DOI, S., YASUNAGA, M., TAKEMURA, M., YABUUCHI, H., SODA, H. & KOHNO, S. (2005) Gefitinib, an EGFR tyrosine kinase inhibitor, directly inhibits the function of P-glycoprotein in multidrug resistant cancer cells. *Lung Cancer*, 49, 337-43.

- KOBAYASHI, S., BOGGON, T. J., DAYARAM, T., JANNE, P. A., KOCHER, O., MEYERSON, M., JOHNSON, B. E., ECK, M. J., TENEN, D. G. & HALMOS, B. (2005) EGFR mutation and resistance of non-small-cell lung cancer to gefitinib. *N Engl J Med*, 352, 786-92.
- KOBE, C., SCHEFFLER, M., HOLSTEIN, A., ZANDER, T., NOGOVA, L., LAMMERTSMA, A. A., BOELLAARD, R., NEUMAIER, B., ULLRICH, R. T., DIETLEIN, M., WOLF, J. & KAHRAMAN, D. (2012) Predictive value of early and late residual 18F-fluorodeoxyglucose and 18F-fluorothymidine uptake using different SUV measurements in patients with non-small-cell lung cancer treated with erlotinib. *Eur J Nucl Med Mol Imaging*, 39, 1117-27.
- KOLB, H. C., FINN, M. G. & SHARPLESS, K. B. (2001) Click Chemistry: Diverse Chemical Function from a Few Good Reactions. *Angew Chem Int Ed Engl*, 40, 2004-2021.
- KOSAKA, T., YATABE, Y., ENDOH, H., KUWANO, H., TAKAHASHI, T. & MITSUDOMI, T. (2004) Mutations of the epidermal growth factor receptor gene in lung cancer: biological and clinical implications. *Cancer Res*, 64, 8919-23.
- KRIS, M. G., NATALE, R. B., HERBST, R. S., LYNCH, T. J., JR., PRAGER, D., BELANI, C. P., SCHILLER, J. H., KELLY, K., SPIRIDONIDIS, H., SANDLER, A., ALBAIN, K. S., CELLA, D., WOLF, M. K., AVERBUCH, S. D., OCHS, J. J. & KAY, A. C. (2003) Efficacy of gefitinib, an inhibitor of the epidermal growth factor receptor tyrosine kinase, in symptomatic patients with non-small cell lung cancer: a randomized trial. *JAMA*, 290, 2149-58.
- KUBO, T., YAMAMOTO, H., LOCKWOOD, W. W., VALENCIA, I., SOH, J., PEYTON, M., JIDA, M., OTANI, H., FUJII, T., OUCHIDA, M., TAKIGAWA, N., KIURA, K., SHIMIZU, K., DATE, H., MINNA, J. D., VARELLA-GARCIA, M., LAM, W. L., GAZDAR, A. F. & TOYOOKA, S. (2009) MET gene amplification or EGFR mutation activate MET in lung cancers untreated with EGFR tyrosine kinase inhibitors. *Int J Cancer*, 124, 1778-84.
- KUMAR, A., PETRI, E. T., HALMOS, B. & BOGGON, T. J. (2008) Structure and clinical relevance of the epidermal growth factor receptor in human cancer. *J Clin Oncol*, 26, 1742-51.
- KURHANEWICZ, J., VIGNERON, D. B. & NELSON, S. J. (2000) Three-dimensional magnetic resonance spectroscopic imaging of brain and prostate cancer. *Neoplasia*, 2, 166-89.
- KWEE, S. A., COEL, M. N., LIM, J. & KO, J. P. (2004) Combined use of F-18 fluorocholine positron emission tomography and magnetic resonance spectroscopy for brain tumor evaluation. *J Neuroimaging*, 14, 285-9.
- LAHERU, D., CROGHAN, G., BUKOWSKI, R., RUDEK, M., MESSERSMITH, W., ERLICHMAN, C., PELLEY, R., JIMENO, A., DONEHOWER, R., BONI, J., ABBAS, R., MARTINS, P., ZACHARCHUK, C. & HIDALGO, M. (2008) A phase I study of EKB-569 in combination with capecitabine in patients with advanced colorectal cancer. *Clin Cancer Res*, 14, 5602-9.
- LAMMERTS VAN BUEREN, J. J., BLEEKER, W. K., BRANNSTROM, A., VON EULER, A., JANSSON, M., PEIPP, M., SCHNEIDER-MERCK, T., VALERIUS, T., VAN DE WINKEL, J. G. & PARREN, P. W. (2008) The antibody zalutumumab inhibits epidermal growth factor receptor signaling by limiting intra- and intermolecular flexibility. *Proc Natl Acad Sci U S A*, 105, 6109-14.
- LEACH, M. O., VERRILL, M., GLAHOLM, J., SMITH, T. A., COLLINS, D. J., PAYNE, G. S., SHARP, J. C., RONEN, S. M., MCCREADY, V. R., POWLES, T. J. & SMITH, I. E. (1998) Measurements of human breast cancer using magnetic resonance spectroscopy: a review of clinical measurements and a report of localized 31P measurements of response to treatment. *NMR Biomed*, 11, 314-40.
- LENKINSKI, R. E., BLOCH, B. N., LIU, F., FRANGIONI, J. V., PERNER, S., RUBIN, M. A., GENEGA, E. M., ROFSKY, N. M. & GASTON, S. M. (2008) An illustration of the potential for mapping MRI/MRS parameters with genetic over-expression profiles in human prostate cancer. *MAGMA*, 21, 411-21.
- LEYTON, J., SMITH, G., LEES, M., PERUMAL, M., NGUYEN, Q. D., AIGBIRHIO, F. I., GOLOVKO, O., HE, Q., WORKMAN, P. & ABOAGYE, E. O. (2008) Noninvasive imaging of cell proliferation following mitogenic extracellular kinase inhibition by PD0325901. *Mol Cancer Ther*, 7, 3112-21.

- LEYTON, J., SMITH, G., ZHAO, Y., PERUMAL, M., NGUYEN, Q. D., ROBINS, E., ARSTAD, E. & ABOAGYE, E. O. (2009) [18F]fluoromethyl-[1,2-2H4]-choline: a novel radiotracer for imaging choline metabolism in tumors by positron emission tomography. *Cancer Res*, 69, 7721-8.
- LI, D., AMBROGIO, L., SHIMAMURA, T., KUBO, S., TAKAHASHI, M., CHIRIEAC, L. R., PADERA, R. F., SHAPIRO, G. I., BAUM, A., HIMMELSBACH, F., RETTIG, W. J., MEYERSON, M., SOLCA, F., GREULICH, H. & WONG, K. K. (2008) BIBW2992, an irreversible EGFR/HER2 inhibitor highly effective in preclinical lung cancer models. *Oncogene*, 27, 4702-11.
- LIMTRAKUL, P., CHEARWAE, W., SHUKLA, S., PHISALPHONG, C. & AMBUDKAR, S. V. (2007) Modulation of function of three ABC drug transporters, P-glycoprotein (ABCB1), mitoxantrone resistance protein (ABCG2) and multidrug resistance protein 1 (ABCC1) by tetrahydrocurcumin, a major metabolite of curcumin. *Mol Cell Biochem*, 296, 85-95.
- LINARDOU, H., DAHABREH, I. J., KANALOUPI, D., SIANNIS, F., BAFALOUKOS, D., KOSMIDIS, P., PAPANIMITRIOU, C. A. & MURRAY, S. (2008) Assessment of somatic k-RAS mutations as a mechanism associated with resistance to EGFR-targeted agents: a systematic review and meta-analysis of studies in advanced non-small-cell lung cancer and metastatic colorectal cancer. *Lancet Oncol*, 9, 962-72.
- LINDEMAN, N. I., CAGLE, P. T., BEASLEY, M. B., CHITALE, D. A., DACIC, S., GIACCONE, G., JENKINS, R. B., KWIATKOWSKI, D. J., SALDIVAR, J. S., SQUIRE, J., THUNNISSEN, E. & LADANYI, M. (2013) Molecular Testing Guideline for Selection of Lung Cancer Patients for EGFR and ALK Tyrosine Kinase Inhibitors: Guideline from the College of American Pathologists, International Association for the Study of Lung Cancer, and Association for Molecular Pathology. *J Mol Diagn*.
- LITMAN, T., DRULEY, T. E., STEIN, W. D. & BATES, S. E. (2001) From MDR to MXR: new understanding of multidrug resistance systems, their properties and clinical significance. *Cell Mol Life Sci*, 58, 931-59.
- LIU, W., LIU, H., GAO, D., GE, G., ZHANG, P., SUN, S., WANG, H. & LIU, S. (2012) ABCG2 protects kidney side population cells from hypoxia/reoxygenation injury through activation of the MEK/ERK pathway. *Cell Transplant*.
- LOPEZ, J. P., WANG-RODRIGUEZ, J., CHANG, C., CHEN, J. S., PARDO, F. S., AGUILERA, J. & ONGKEKO, W. M. (2007) Gefitinib inhibition of drug resistance to doxorubicin by inactivating ABCG2 in thyroid cancer cell lines. *Arch Otolaryngol Head Neck Surg*, 133, 1022-7.
- LYNCH, T. J., BELL, D. W., SORDELLA, R., GURUBHAGAVATULA, S., OKIMOTO, R. A., BRANNIGAN, B. W., HARRIS, P. L., HASERLAT, S. M., SUPKO, J. G., HALUSKA, F. G., LOUIS, D. N., CHRISTIANI, D. C., SETTLEMAN, J. & HABER, D. A. (2004) Activating mutations in the epidermal growth factor receptor underlying responsiveness of non-small-cell lung cancer to gefitinib. *N Engl J Med*, 350, 2129-39.
- MAEMONDO, M., INOUE, A., KOBAYASHI, K., SUGAWARA, S., OIZUMI, S., ISOBE, H., GEMMA, A., HARADA, M., YOSHIZAWA, H., KINOSHITA, I., FUJITA, Y., OKINAGA, S., HIRANO, H., YOSHIMORI, K., HARADA, T., OGURA, T., ANDO, M., MIYAZAWA, H., TANAKA, T., SAIJO, Y., HAGIWARA, K., MORITA, S. & NUKIWA, T. (2010) Gefitinib or chemotherapy for non-small-cell lung cancer with mutated EGFR. *N Engl J Med*, 362, 2380-8.
- MAHESWARAN, S., SEQUIST, L. V., NAGRATH, S., ULKUS, L., BRANNIGAN, B., COLLURA, C. V., INSERRA, E., DIEDERICHS, S., IAFRATE, A. J., BELL, D. W., DIGUMARTHY, S., MUZIKANSKY, A., IRIMIA, D., SETTLEMAN, J., TOMPKINS, R. G., LYNCH, T. J., TONER, M. & HABER, D. A. (2008) Detection of mutations in EGFR in circulating lung-cancer cells. *N Engl J Med*, 359, 366-77.
- MAO, C., LIAO, R. Y. & CHEN, Q. (2010) BRAF mutation predicts resistance to anti-EGFR monoclonal antibodies in wild-type KRAS metastatic colorectal cancer. *J Cancer Res Clin Oncol*, 136, 1293-4.
- MASCHAUER, S. & PRANTE, O. (2009) A series of 2-O-trifluoromethylsulfonyl-D-mannopyranosides as precursors for concomitant 18F-labeling and glycosylation by click chemistry. *Carbohydr Res*, 344, 753-61.

- MASSARELLI, E., VARELLA-GARCIA, M., TANG, X., XAVIER, A. C., OZBURN, N. C., LIU, D. D., BEKELE, B. N., HERBST, R. S. & WISTUBA, II (2007) KRAS mutation is an important predictor of resistance to therapy with epidermal growth factor receptor tyrosine kinase inhibitors in non-small-cell lung cancer. *Clin Cancer Res*, 13, 2890-6.
- MAZZOLENI, S., POLITI, L. S., PALA, M., COMINELLI, M., FRANZIN, A., SERGI SERGI, L., FALINI, A., DE PALMA, M., BULFONE, A., POLIANI, P. L. & GALLI, R. (2010) Epidermal growth factor receptor expression identifies functionally and molecularly distinct tumor-initiating cells in human glioblastoma multiforme and is required for gliomagenesis. *Cancer Res*, 70, 7500-13.
- MCKINLEY, E. T., AYERS, G. D., SMITH, R. A., SALEH, S. A., ZHAO, P., WASHINGTON, M. K., COFFEY, R. J. & MANNING, H. C. (2013) Limits of [¹⁸F]-FLT PET as a biomarker of proliferation in oncology. *PLoS One*, 8, e58938.
- MCKNIGHT, T. R., LAMBORN, K. R., LOVE, T. D., BERGER, M. S., CHANG, S., DILLON, W. P., BOLLEN, A. & NELSON, S. J. (2007) Correlation of magnetic resonance spectroscopic and growth characteristics within Grades II and III gliomas. *J Neurosurg*, 106, 660-6.
- MEMON, A. A., JAKOBSEN, S., DAGNAES-HANSEN, F., SORENSEN, B. S., KEIDING, S. & NEXO, E. (2009) Positron emission tomography (PET) imaging with [¹¹C]-labeled erlotinib: a micro-PET study on mice with lung tumor xenografts. *Cancer Res*, 69, 873-8.
- MENDELSON, J. & BASELGA, J. (2006) Epidermal growth factor receptor targeting in cancer. *Semin Oncol*, 33, 369-85.
- MIAO, Z., REN, G., LIU, H., JIANG, L. & CHENG, Z. (2010) Small-animal PET imaging of human epidermal growth factor receptor positive tumor with a ⁶⁴Cu labeled affibody protein. *Bioconjug Chem*, 21, 947-54.
- MILANO, G., SPANO, J. P. & LEYLAND-JONES, B. (2008) EGFR-targeting drugs in combination with cytotoxic agents: from bench to bedside, a contrasted reality. *Br J Cancer*, 99, 1-5.
- MISHANI, E., ABOURBEH, G., EIBLMAIER, M. & ANDERSON, C. J. (2008) Imaging of EGFR and EGFR tyrosine kinase overexpression in tumors by nuclear medicine modalities. *Curr Pharm Des*, 14, 2983-98.
- MITSU DOMI, T., MORITA, S., YATABE, Y., NEGORO, S., OKAMOTO, I., TSURUTANI, J., SETO, T., SATOUCHI, M., TADA, H., HIRASHIMA, T., ASAMI, K., KATAKAMI, N., TAKADA, M., YOSHIOKA, H., SHIBATA, K., KUDOH, S., SHIMIZU, E., SAITO, H., TOYOOKA, S., NAKAGAWA, K., FUKUOKA, M. & WEST JAPAN ONCOLOGY, G. (2010) Gefitinib versus cisplatin plus docetaxel in patients with non-small-cell lung cancer harbouring mutations of the epidermal growth factor receptor (WJTOG3405): an open label, randomised phase 3 trial. *Lancet Oncol*, 11, 121-8.
- MIYAKE, T. & PARSONS, S. J. (2012) Functional interactions between Choline kinase alpha, epidermal growth factor receptor and c-Src in breast cancer cell proliferation. *Oncogene*.
- MIZUNO, N., NIWA, T., YOTSUMOTO, Y. & SUGIYAMA, Y. (2003) Impact of drug transporter studies on drug discovery and development. *Pharmacol Rev*, 55, 425-61.
- MO, W. & ZHANG, J. T. (2012) Human ABCG2: structure, function, and its role in multidrug resistance. *Int J Biochem Mol Biol*, 3, 1-27.
- MOK, T. S., WU, Y. L., THONGPRASERT, S., YANG, C. H., CHU, D. T., SAIJO, N., SUNPAWERAVONG, P., HAN, B., MARGONO, B., ICHINOSE, Y., NISHIWAKI, Y., OHE, Y., YANG, J. J., CHEWASKULYONG, B., JIANG, H., DUFFIELD, E. L., WATKINS, C. L., ARMOUR, A. A. & FUKUOKA, M. (2009) Gefitinib or carboplatin-paclitaxel in pulmonary adenocarcinoma. *N Engl J Med*, 361, 947-57.
- MOYER, J. D., BARBACCI, E. G., IWATA, K. K., ARNOLD, L., BOMAN, B., CUNNINGHAM, A., DIORIO, C., DOTY, J., MORIN, M. J., MOYER, M. P., NEVEU, M., POLLACK, V. A., PUSTILNIK, L. R., REYNOLDS, M. M., SLOAN, D., THELEMAN, A. & MILLER, P. (1997) Induction of apoptosis and cell cycle arrest by CP-358,774, an inhibitor of epidermal growth factor receptor tyrosine kinase. *Cancer Res*, 57, 4838-48.
- MUNOZ, M., HENDERSON, M., HABER, M. & NORRIS, M. (2007) Role of the MRP1/ABCC1 multidrug transporter protein in cancer. *IUBMB Life*, 59, 752-7.

- MURRAY, S., KARAVASILIS, V., BOBOS, M., RAZIS, E., PAPADOPOULOS, S., CHRISTODOULOU, C., KOSMIDIS, P. & FOUNTZILAS, G. (2012) Molecular predictors of response to tyrosine kinase inhibitors in patients with Non-Small-Cell Lung Cancer. *J Exp Clin Cancer Res*, 31, 77.
- NAKAGAWA, H., SAITO, H., IKEGAMI, Y., AIDA-HYUGAJI, S., SAWADA, S. & ISHIKAWA, T. (2006) Molecular modeling of new camptothecin analogues to circumvent ABCG2-mediated drug resistance in cancer. *Cancer Lett*, 234, 81-9.
- NAKAMURA, Y., OKA, M., SODA, H., SHIOZAWA, K., YOSHIKAWA, M., ITOH, A., IKEGAMI, Y., TSURUTANI, J., NAKATOMI, K., KITAZAKI, T., DOI, S., YOSHIDA, H. & KOHNO, S. (2005) Gefitinib ("Iressa", ZD1839), an epidermal growth factor receptor tyrosine kinase inhibitor, reverses breast cancer resistance protein/ABCG2-mediated drug resistance. *Cancer Res*, 65, 1541-6.
- NAYAK, T. K., GARMESTANI, K., BAIDOO, K. E., MILENIC, D. E. & BRECHBIEL, M. W. (2010) Preparation, biological evaluation, and pharmacokinetics of the human anti-HER1 monoclonal antibody panitumumab labeled with ⁸⁶Y for quantitative PET of carcinoma. *J Nucl Med*, 51, 942-50.
- NAYAK, T. K., GARMESTANI, K., MILENIC, D. E., BAIDOO, K. E. & BRECHBIEL, M. W. (2011) HER1-targeted ⁸⁶Y-panitumumab possesses superior targeting characteristics than ⁸⁶Y-cetuximab for PET imaging of human malignant mesothelioma tumors xenografts. *PLoS One*, 6, e18198.
- NICE (2010) Gefitinib for the first-line treatment of locally advanced or metastatic non-small-cell lung cancer IN NICE (Ed.).
- NICHOLSON, R. I., GEE, J. M. & HARPER, M. E. (2001) EGFR and cancer prognosis. *Eur J Cancer*, 37 Suppl 4, S9-15.
- NIMMAGADDA, S., GLUNDE, K., POMPER, M. G. & BHUJWALLA, Z. M. (2009) Pharmacodynamic markers for choline kinase down-regulation in breast cancer cells. *Neoplasia*, 11, 477-84.
- NYATI, M. K., MORGAN, M. A., FENG, F. Y. & LAWRENCE, T. S. (2006) Integration of EGFR inhibitors with radiochemotherapy. *Nat Rev Cancer*, 6, 876-85.
- OGISO, H., ISHITANI, R., NUREKI, O., FUKAI, S., YAMANAKA, M., KIM, J. H., SAITO, K., SAKAMOTO, A., INOUE, M., SHIROUZU, M. & YOKOYAMA, S. (2002) Crystal structure of the complex of human epidermal growth factor and receptor extracellular domains. *Cell*, 110, 775-87.
- ORTU, G., BEN-DAVID, I., ROZEN, Y., FREEDMAN, N. M., CHISIN, R., LEVITZKI, A. & MISHANI, E. (2002) Labeled EGFR-TK irreversible inhibitor (ML03): in vitro and in vivo properties, potential as PET biomarker for cancer and feasibility as anticancer drug. *Int J Cancer*, 101, 360-70.
- OXNARD, G. R., ARCILA, M. E., CHMIELECKI, J., LADANYI, M., MILLER, V. A. & PAO, W. (2011) New strategies in overcoming acquired resistance to epidermal growth factor receptor tyrosine kinase inhibitors in lung cancer. *Clin Cancer Res*, 17, 5530-7.
- OZVEGY-LACZKA, C., HEGEDUS, T., VARADY, G., UJHELLY, O., SCHUETZ, J. D., VARADI, A., KERI, G., ORFI, L., NEMET, K. & SARKADI, B. (2004) High-affinity interaction of tyrosine kinase inhibitors with the ABCG2 multidrug transporter. *Mol Pharmacol*, 65, 1485-95.
- OZVEGY, C., LITMAN, T., SZAKACS, G., NAGY, Z., BATES, S., VARADI, A. & SARKADI, B. (2001) Functional characterization of the human multidrug transporter, ABCG2, expressed in insect cells. *Biochem Biophys Res Commun*, 285, 111-7.
- PAEZ, J. G., JANNE, P. A., LEE, J. C., TRACY, S., GREULICH, H., GABRIEL, S., HERMAN, P., KAYE, F. J., LINDEMAN, N., BOGGON, T. J., NAOKI, K., SASAKI, H., FUJII, Y., ECK, M. J., SELLERS, W. R., JOHNSON, B. E. & MEYERSON, M. (2004) EGFR mutations in lung cancer: correlation with clinical response to gefitinib therapy. *Science*, 304, 1497-500.
- PAL, A., GLEKAS, A., DOUBROVIN, M., BALATONI, J., NAMAVARI, M., BERESTEN, T., MAXWELL, D., SOGHOMONYAN, S., SHAVRIN, A., AGEYEVA, L., FINN, R., LARSON, S. M., BORNMANN, W. & GELOVANI, J. G. (2006) Molecular imaging of EGFR kinase activity in tumors with ¹²⁴I-labeled small molecular tracer and positron emission tomography. *Mol Imaging Biol*, 8, 262-77.

- PANTALEO, M. A., MISHANI, E., NANNI, C., LANDUZZI, L., BOSCHI, S., NICOLETTI, G., DISSOKI, S., PATERINI, P., PICCALUGA, P. P., LODI, F., LOLLINI, P. L., FANTI, S. & BIASCO, G. (2010) Evaluation of Modified PEG-Anilinoquinazoline Derivatives as Potential Agents for EGFR Imaging in Cancer by Small Animal PET. *Mol Imaging Biol.*
- PANTALEO, M. A., NANNINI, M., MALEDDU, A., FANTI, S., NANNI, C., BOSCHI, S., LODI, F., NICOLETTI, G., LANDUZZI, L., LOLLINI, P. L. & BIASCO, G. (2009) Experimental results and related clinical implications of PET detection of epidermal growth factor receptor (EGFr) in cancer. *Ann Oncol*, 20, 213-26.
- PAO, W. & HUTCHINSON, K. E. (2012) Chipping away at the lung cancer genome. *Nat Med*, 18, 349-51.
- PAO, W. & MILLER, V. A. (2005) Epidermal growth factor receptor mutations, small-molecule kinase inhibitors, and non-small-cell lung cancer: current knowledge and future directions. *J Clin Oncol*, 23, 2556-68.
- PAO, W., WANG, T. Y., RIELY, G. J., MILLER, V. A., PAN, Q., LADANYI, M., ZAKOWSKI, M. F., HEELAN, R. T., KRIS, M. G. & VARMUS, H. E. (2005) KRAS mutations and primary resistance of lung adenocarcinomas to gefitinib or erlotinib. *PLoS Med*, 2, e17.
- PETAK, I., SCHWAB, R., ORFI, L., KOPPER, L. & KERI, G. (2010) Integrating molecular diagnostics into anticancer drug discovery. *Nat Rev Drug Discov*, 9, 523-35.
- PHAM, A. N., WANG, J., FANG, J., GAO, X., ZHANG, Y., BLOWER, P. E., SADEE, W. & HUANG, Y. (2009) Pharmacogenomics approach reveals MRP1 (ABCC1)-mediated resistance to geldanamycins. *Pharm Res*, 26, 936-45.
- PHELPS, M. E. (2000) Positron emission tomography provides molecular imaging of biological processes. *Proc Natl Acad Sci U S A*, 97, 9226-33.
- PICK, A. & WIESE, M. (2012) Tyrosine kinase inhibitors influence ABCG2 expression in EGFR-positive MDCK BCRP cells via the PI3K/Akt signaling pathway. *ChemMedChem*, 7, 650-62.
- PINES, G., HUANG, P. H., ZWANG, Y., WHITE, F. M. & YARDEN, Y. (2010) EGFRvIV: a previously uncharacterized oncogenic mutant reveals a kinase autoinhibitory mechanism. *Oncogene*.
- PING LI, W., MEYER, L. A., CAPRETTO, D. A., SHERMAN, C. D. & ANDERSON, C. J. (2008) Receptor-binding, biodistribution, and metabolism studies of ⁶⁴Cu-DOTA-cetuximab, a PET-imaging agent for epidermal growth-factor receptor-positive tumors. *Cancer Biother Radiopharm*, 23, 158-71.
- PISANESCHI, F., NGUYEN, Q. D., SHAMSAEI, E., GLASER, M., ROBINS, E., KALISZCZAK, M., SMITH, G., SPIVEY, A. C. & ABOAGYE, E. O. (2010) Development of a new epidermal growth factor receptor positron emission tomography imaging agent based on the 3-cyanoquinoline core: synthesis and biological evaluation. *Bioorg Med Chem*, 18, 6634-45.
- PRENZEL, N., FISCHER, O. M., STREIT, S., HART, S. & ULLRICH, A. (2001) The epidermal growth factor receptor family as a central element for cellular signal transduction and diversification. *Endocr Relat Cancer*, 8, 11-31.
- RABINDRAN, S. K., ROSS, D. D., DOYLE, L. A., YANG, W. & GREENBERGER, L. M. (2000) Fumitremorgin C reverses multidrug resistance in cells transfected with the breast cancer resistance protein. *Cancer Res*, 60, 47-50.
- RAMIREZ DE MOLINA, A., GALLEGU-ORTEGA, D., SARMENTERO-ESTRADA, J., LAGARES, D., GOMEZ DEL PULGAR, T., BANDRES, E., GARCIA-FONCILLAS, J. & LACAL, J. C. (2008) Choline kinase as a link connecting phospholipid metabolism and cell cycle regulation: implications in cancer therapy. *Int J Biochem Cell Biol*, 40, 1753-63.
- RAMIREZ DE MOLINA, A., GALLEGU-ORTEGA, D., SARMENTERO, J., BANEZ-CORONEL, M., MARTIN-CANTALEJO, Y. & LACAL, J. C. (2005) Choline kinase is a novel oncogene that potentiates RhoA-induced carcinogenesis. *Cancer Res*, 65, 5647-53.
- RAMIREZ DE MOLINA, A., GUTIERREZ, R., RAMOS, M. A., SILVA, J. M., SILVA, J., BONILLA, F., SANCHEZ, J. J. & LACAL, J. C. (2002a) Increased choline kinase activity in human breast

- carcinomas: clinical evidence for a potential novel antitumor strategy. *Oncogene*, 21, 4317-22.
- RAMIREZ DE MOLINA, A., PENALVA, V., LUCAS, L. & LACAL, J. C. (2002b) Regulation of choline kinase activity by Ras proteins involves Ral-GDS and PI3K. *Oncogene*, 21, 937-46.
- RAMIREZ DE MOLINA, A., SARMENTERO-ESTRADA, J., BELDA-INIESTA, C., TARON, M., RAMIREZ DE MOLINA, V., CEJAS, P., SKRZYPSKI, M., GALLEGU-ORTEGA, D., DE CASTRO, J., CASADO, E., GARCIA-CABEZAS, M. A., SANCHEZ, J. J., NISTAL, M., ROSELL, R., GONZALEZ-BARON, M. & LACAL, J. C. (2007) Expression of choline kinase alpha to predict outcome in patients with early-stage non-small-cell lung cancer: a retrospective study. *Lancet Oncol*, 8, 889-97.
- REGINA, A., KOMAN, A., PICIOTTI, M., EL HAFNY, B., CENTER, M. S., BERGMANN, R., COURAUD, P. O. & ROUX, F. (1998) Mrp1 multidrug resistance-associated protein and P-glycoprotein expression in rat brain microvessel endothelial cells. *J Neurochem*, 71, 705-15.
- RIELY, G. J., PAO, W., PHAM, D., LI, A. R., RIZVI, N., VENKATRAMAN, E. S., ZAKOWSKI, M. F., KRIS, M. G., LADANYI, M. & MILLER, V. A. (2006) Clinical course of patients with non-small cell lung cancer and epidermal growth factor receptor exon 19 and exon 21 mutations treated with gefitinib or erlotinib. *Clin Cancer Res*, 12, 839-44.
- ROBEY, R. W., HONJO, Y., VAN DE LAAR, A., MIYAKE, K., REGIS, J. T., LITMAN, T. & BATES, S. E. (2001) A functional assay for detection of the mitoxantrone resistance protein, MXR (ABCG2). *Biochim Biophys Acta*, 1512, 171-82.
- ROGAN, A. M., HAMILTON, T. C., YOUNG, R. C., KLECKER, R. W., JR. & OZOLS, R. F. (1984) Reversal of adriamycin resistance by verapamil in human ovarian cancer. *Science*, 224, 994-6.
- ROSELL, R., CARCERENY, E., GERVAIS, R., VERGNENEGRE, A., MASSUTI, B., FELIP, E., PALMERO, R., GARCIA-GOMEZ, R., PALLARES, C., SANCHEZ, J. M., PORTA, R., COBO, M., GARRIDO, P., LONGO, F., MORAN, T., INSA, A., DE MARINIS, F., CORRE, R., BOVER, I., ILLIANO, A., DANSIN, E., DE CASTRO, J., MILELLA, M., REGUART, N., ALTAVILLA, G., JIMENEZ, U., PROVENCIO, M., MORENO, M. A., TERRASA, J., MUNOZ-LANGA, J., VALDIVIA, J., ISLA, D., DOMINE, M., MOLINIER, O., MAZIERES, J., BAIZE, N., GARCIA-CAMPELO, R., ROBINET, G., RODRIGUEZ-ABREU, D., LOPEZ-VIVANCO, G., GEBBIA, V., FERRERA-DELGADO, L., BOMBARON, P., BERNABE, R., BEARZ, A., ARTAL, A., CORTESI, E., ROLFO, C., SANCHEZ-RONCO, M., DROZDOWSKYJ, A., QUERALT, C., DE AGUIRRE, I., RAMIREZ, J. L., SANCHEZ, J. J., MOLINA, M. A., TARON, M., PAZ-ARES, L., PNEUMOCANCEROLOGIE, G. F. & TORACICA, A. I. O. (2012) Erlotinib versus standard chemotherapy as first-line treatment for European patients with advanced EGFR mutation-positive non-small-cell lung cancer (EURTAC): a multicentre, open-label, randomised phase 3 trial. *Lancet Oncology*, 13, 239-246.
- ROSEN, E. L., EUBANK, W. B. & MANKOFF, D. A. (2007) FDG PET, PET/CT, and breast cancer imaging. *Radiographics*, 27 Suppl 1, S215-29.
- ROSSI, A., PASQUALE, R., ESPOSITO, C. & NORMANNO, N. (2013) Should epidermal growth factor receptor tyrosine kinase inhibitors be considered ideal drugs for the treatment of selected advanced non-small cell lung cancer patients? *Cancer Treat Rev*, 39, 489-97.
- ROWINSKY, E. K. (2004) The erbB family: targets for therapeutic development against cancer and therapeutic strategies using monoclonal antibodies and tyrosine kinase inhibitors. *Annu Rev Med*, 55, 433-57.
- SAITO, H., HIRANO, H., NAKAGAWA, H., FUKAMI, T., OOSUMI, K., MURAKAMI, K., KIMURA, H., KOUCHI, T., KONOMI, M., TAO, E., TSUJIKAWA, N., TARUI, S., NAGAKURA, M., OSUMI, M. & ISHIKAWA, T. (2006) A new strategy of high-speed screening and quantitative structure-activity relationship analysis to evaluate human ATP-binding cassette transporter ABCG2-drug interactions. *J Pharmacol Exp Ther*, 317, 1114-24.
- SALOMON, D. S., BRANDT, R., CIARDIELLO, F. & NORMANNO, N. (1995) Epidermal growth factor-related peptides and their receptors in human malignancies. *Crit Rev Oncol Hematol*, 19, 183-232.

- SARKADI, B., HOMOLYA, L., SZAKACS, G. & VARADI, A. (2006) Human multidrug resistance ABCB and ABCG transporters: participation in a chemoinnity defense system. *Physiol Rev*, 86, 1179-236.
- SCHARENBERG, C. W., HARKEY, M. A. & TOROK-STORB, B. (2002) The ABCG2 transporter is an efficient Hoechst 33342 efflux pump and is preferentially expressed by immature human hematopoietic progenitors. *Blood*, 99, 507-12.
- SCHEFFLER, M., ZANDER, T., NOGOVA, L., KOBE, C., KAHRAMAN, D., DIETLEIN, M., PAPACHRISTOU, I., HEUKAMP, L., BUTTNER, R., BOELLAARD, R., LAMMERTSMA, A. A., QUERINGS, S., STOELBEN, E., ENGEL-RIEDEL, W., NEUMAIER, B. & WOLF, J. (2013) Prognostic impact of [18F]fluorothymidine and [18F]fluoro-D-glucose baseline uptakes in patients with lung cancer treated first-line with erlotinib. *PLoS One*, 8, e53081.
- SCHMITTGEN, T. D. & LIVAK, K. J. (2008) Analyzing real-time PCR data by the comparative C(T) method. *Nat Protoc*, 3, 1101-8.
- SEBASTIAN, S., SETTLEMAN, J., RESHKIN, S. J., AZZARITI, A., BELLIZZI, A. & PARADISO, A. (2006) The complexity of targeting EGFR signalling in cancer: from expression to turnover. *Biochim Biophys Acta*, 1766, 120-39.
- SEBASTIAN TROUSIL, A. L. C., A ANDREW KALUSA, A OLA ABERG, A MACIEJ KALISZCZAKA AND ERIC O. ABOAGYE (2013) Design of symmetrical and nonsymmetrical N,N-dimethylaminopyridine derivatives as highly potent choline kinase alpha inhibitors *MedChemComm*.
- SEQUIST, L. V., WALTMAN, B. A., DIAS-SANTAGATA, D., DIGUMARTHY, S., TURKE, A. B., FIDIAS, P., BERGETHON, K., SHAW, A. T., GETTINGER, S., COSPER, A. K., AKHAVANFARD, S., HEIST, R. S., TEMEL, J., CHRISTENSEN, J. G., WAIN, J. C., LYNCH, T. J., VERNOVSKY, K., MARK, E. J., LANUTI, M., IAFRATE, A. J., MINO-KENUDSON, M. & ENGELMAN, J. A. (2011) Genotypic and histological evolution of lung cancers acquiring resistance to EGFR inhibitors. *Sci Transl Med*, 3, 75ra26.
- SHAH, T., WILDES, F., PENET, M. F., WINNARD, P. T., JR., GLUNDE, K., ARTEMOV, D., ACKERSTAFF, E., GIMI, B., KAKKAD, S., RAMAN, V. & BHUJWALLA, Z. M. (2010) Choline kinase overexpression increases invasiveness and drug resistance of human breast cancer cells. *NMR Biomed*, 23, 633-42.
- SHARMA, S. V., BELL, D. W., SETTLEMAN, J. & HABER, D. A. (2007) Epidermal growth factor receptor mutations in lung cancer. *Nat Rev Cancer*, 7, 169-81.
- SHEPARD, R. L., CAO, J., STARLING, J. J. & DANTZIG, A. H. (2003) Modulation of P-glycoprotein but not MRP1- or BCRP-mediated drug resistance by LY335979. *Int J Cancer*, 103, 121-5.
- SHI, Z., PENG, X. X., KIM, I. W., SHUKLA, S., SI, Q. S., ROBEY, R. W., BATES, S. E., SHEN, T., ASHBY, C. R., JR., FU, L. W., AMBUDKAR, S. V. & CHEN, Z. S. (2007) Erlotinib (Tarceva, OSI-774) antagonizes ATP-binding cassette subfamily B member 1 and ATP-binding cassette subfamily G member 2-mediated drug resistance. *Cancer Res*, 67, 11012-20.
- SHIELDS, A. F. (2003) PET imaging with 18F-FLT and thymidine analogs: promise and pitfalls. *J Nucl Med*, 44, 1432-4.
- SHIELDS, A. F., GRIERSON, J. R., DOHMEN, B. M., MACHULLA, H. J., STAYANOFF, J. C., LAWHORN-CREWS, J. M., OBRADOVICH, J. E., MUZIK, O. & MANGNER, T. J. (1998) Imaging proliferation in vivo with [F-18]FLT and positron emission tomography. *Nat Med*, 4, 1334-6.
- SHOLL, L. M., XIAO, Y., JOSHI, V., YEAP, B. Y., CIOFFREDI, L. A., JACKMAN, D. M., LEE, C., JANNE, P. A. & LINDEMAN, N. I. (2010) EGFR mutation is a better predictor of response to tyrosine kinase inhibitors in non-small cell lung carcinoma than FISH, CISH, and immunohistochemistry. *Am J Clin Pathol*, 133, 922-34.
- SKEHAN, P., STORENG, R., SCUDIERO, D., MONKS, A., MCMAHON, J., VISTICA, D., WARREN, J. T., BOKESCH, H., KENNEY, S. & BOYD, M. R. (1990) New colorimetric cytotoxicity assay for anticancer-drug screening. *J Natl Cancer Inst*, 82, 1107-12.

- SOHN, H. J., YANG, Y. J., RYU, J. S., OH, S. J., IM, K. C., MOON, D. H., LEE, D. H., SUH, C., LEE, J. S. & KIM, S. W. (2008) [18F]Fluorothymidine positron emission tomography before and 7 days after gefitinib treatment predicts response in patients with advanced adenocarcinoma of the lung. *Clin Cancer Res*, 14, 7423-9.
- SOS, M. L., KOKER, M., WEIR, B. A., HEYNCK, S., RABINOVSKY, R., ZANDER, T., SEEGER, J. M., WEISS, J., FISCHER, F., FROMMOLT, P., MICHEL, K., PEIFER, M., MERMEL, C., GIRARD, L., PEYTON, M., GAZDAR, A. F., MINNA, J. D., GARRAWAY, L. A., KASHKAR, H., PAO, W., MEYERSON, M. & THOMAS, R. K. (2009) PTEN Loss Contributes to Erlotinib Resistance in EGFR-Mutant Lung Cancer by Activation of Akt and EGFR. *Cancer Research*, 69, 3256-3261.
- SPICER, J. F. & RUDMAN, S. M. (2010) EGFR inhibitors in non-small cell lung cancer (NSCLC): the emerging role of the dual irreversible EGFR/HER2 inhibitor BIBW 2992. *Target Oncol*.
- SQUILLACI, E., MANENTI, G., MANCINO, S., CARLANI, M., DI ROMA, M., COLANGELO, V. & SIMONETTI, G. (2005) MR spectroscopy of prostate cancer. Initial clinical experience. *J Exp Clin Cancer Res*, 24, 523-30.
- SU, H., BODENSTEIN, C., DUMONT, R. A., SEIMBILLE, Y., DUBINETT, S., PHELPS, M. E., HERSCHMAN, H., CZERNIN, J. & WEBER, W. (2006) Monitoring tumor glucose utilization by positron emission tomography for the prediction of treatment response to epidermal growth factor receptor kinase inhibitors. *Clin Cancer Res*, 12, 5659-67.
- SU, H., SEIMBILLE, Y., FERL, G. Z., BODENSTEIN, C., FUEGER, B., KIM, K. J., HSU, Y. T., DUBINETT, S. M., PHELPS, M. E., CZERNIN, J. & WEBER, W. A. (2008) Evaluation of [(18)F]gefitinib as a molecular imaging probe for the assessment of the epidermal growth factor receptor status in malignant tumors. *Eur J Nucl Med Mol Imaging*, 35, 1089-99.
- SUNAGA, N., ORIUCHI, N., KAIRA, K., YANAGITANI, N., TOMIZAWA, Y., HISADA, T., ISHIZUKA, T., ENDO, K. & MORI, M. (2008) Usefulness of FDG-PET for early prediction of the response to gefitinib in non-small cell lung cancer. *Lung Cancer*, 59, 203-10.
- SWAISLAND, H., LAIGHT, A., STAFFORD, L., JONES, H., MORRIS, C., DANE, A. & YATES, R. (2001) Pharmacokinetics and tolerability of the orally active selective epidermal growth factor receptor tyrosine kinase inhibitor ZD1839 in healthy volunteers. *Clin Pharmacokinet*, 40, 297-306.
- SZAKACS, G., PATERSON, J. K., LUDWIG, J. A., BOOTH-GENTHE, C. & GOTTESMAN, M. M. (2006) Targeting multidrug resistance in cancer. *Nat Rev Drug Discov*, 5, 219-34.
- SZAKACS, G., VARADI, A., OZVEGY-LACZKA, C. & SARKADI, B. (2008) The role of ABC transporters in drug absorption, distribution, metabolism, excretion and toxicity (ADME-Tox). *Drug Discov Today*, 13, 379-93.
- TAKAHASHI, R., HIRATA, H., TACHIBANA, I., SHIMOSEGAWA, E., INOUE, A., NAGATOMO, I., TAKEDA, Y., KIDA, H., GOYA, S., KIJIMA, T., YOSHIDA, M., KUMAGAI, T., KUMANOGOH, A., OKUMURA, M., HATAZAWA, J. & KAWASE, I. (2012) Early [18F]fluorodeoxyglucose positron emission tomography at two days of gefitinib treatment predicts clinical outcome in patients with adenocarcinoma of the lung. *Clin Cancer Res*, 18, 220-8.
- TANAKA, T., MATSUOKA, M., SUTANI, A., GEMMA, A., MAEMONDO, M., INOUE, A., OKINAGA, S., NAGASHIMA, M., OIZUMI, S., UEMATSU, K., NAGAI, Y., MORIYAMA, G., MIYAZAWA, H., IKEBUCHI, K., MORITA, S., KOBAYASHI, K. & HAGIWARA, K. (2010) Frequency of and variables associated with the EGFR mutation and its subtypes. *Int J Cancer*, 126, 651-5.
- TAYLOR, R. C., CULLEN, S. P. & MARTIN, S. J. (2008) Apoptosis: controlled demolition at the cellular level. *Nat Rev Mol Cell Biol*, 9, 231-41.
- TETSUYA MITSUDOMI, S. M., YASUSHI YATABE, SHUNICHI NEGORO, ISAMU OKAMOTO, TAKASHI SETO, MIYAKO SATOUCHI, HIROHITO TADA, TOMONORI HIRASHIMA, KAZUHIRO ASAMI, NOBUYUKI KATAKAMI, MINORU TAKADA, HIROSHIGE YOSHIOKA, KAZUHIKO SHIBATA, SHINZOH KUDOH, EIJI SHIMIZU, HIROSHI SAITO, SHINICHI TOYOOKA, KAZUHIKO NAKAGAWA, MASAHIRO FUKUOKA, (2012) Updated overall survival results of WJTOG 3405, a randomized phase III trial comparing gefitinib (G) with cisplatin plus docetaxel (CD) as the first-line

- treatment for patients with non-small cell lung cancer harboring mutations of the epidermal growth factor receptor (EGFR). *Journal of clinical oncology*, 30.
- THATCHER, N., CHANG, A., PARIKH, P., RODRIGUES PEREIRA, J., CIULEANU, T., VON PAWEL, J., THONGPRASERT, S., TAN, E. H., PEMBERTON, K., ARCHER, V. & CARROLL, K. (2005) Gefitinib plus best supportive care in previously treated patients with refractory advanced non-small-cell lung cancer: results from a randomised, placebo-controlled, multicentre study (Iressa Survival Evaluation in Lung Cancer). *Lancet*, 366, 1527-37.
- THERASSE, P., ARBUCK, S. G., EISENHAUER, E. A., WANDERS, J., KAPLAN, R. S., RUBINSTEIN, L., VERWEIJ, J., VAN GLABBEKE, M., VAN OOSTEROM, A. T., CHRISTIAN, M. C. & GWYTHYER, S. G. (2000) New guidelines to evaluate the response to treatment in solid tumors. European Organization for Research and Treatment of Cancer, National Cancer Institute of the United States, National Cancer Institute of Canada. *J Natl Cancer Inst*, 92, 205-16.
- TIAN, M., OGAWA, K., WENDT, R., MUKHOPADHYAY, U., BALATONI, J., FUKUMITSU, N., UTHAMANTHIL, R., BORNE, A., BRAMMER, D., JACKSON, J., MAWLAWI, O., YANG, B., ALAUDDIN, M. M. & GELOVANI, J. G. (2011) Whole-body biodistribution kinetics, metabolism, and radiation dosimetry estimates of 18F-PEG6-IPQA in nonhuman primates. *J Nucl Med*, 52, 934-41.
- TOLMACHEV, V., ROSIK, D., WALLBERG, H., SJOBERG, A., SANDSTROM, M., HANSSON, M., WENNBORG, A. & ORLOVA, A. (2010) Imaging of EGFR expression in murine xenografts using site-specifically labelled anti-EGFR 111In-DOTA-Z EGFR:2377 Affibody molecule: aspect of the injected tracer amount. *Eur J Nucl Med Mol Imaging*, 37, 613-22.
- ULLRICH, R. T., ZANDER, T., NEUMAIER, B., KOKER, M., SHIMAMURA, T., WAERZEGGERS, Y., BORGMAN, C. L., TAWADROS, S., LI, H., SOS, M. L., BACKES, H., SHAPIRO, G. I., WOLF, J., JACOBS, A. H., THOMAS, R. K. & WINKELER, A. (2008) Early detection of erlotinib treatment response in NSCLC by 3'-deoxy-3'-[F]-fluoro-L-thymidine ([F]FLT) positron emission tomography (PET). *PLoS One*, 3, e3908.
- VAN CUTSEM, E., PEETERS, M., SIENA, S., HUMBLET, Y., HENDLISZ, A., NEYNS, B., CANON, J. L., VAN LAETHEM, J. L., MAUREL, J., RICHARDSON, G., WOLF, M. & AMADO, R. G. (2007) Open-label phase III trial of panitumumab plus best supportive care compared with best supportive care alone in patients with chemotherapy-refractory metastatic colorectal cancer. *J Clin Oncol*, 25, 1658-64.
- VARMA, M. V., SATEESH, K. & PANCHAGNULA, R. (2005) Functional role of P-glycoprotein in limiting intestinal absorption of drugs: contribution of passive permeability to P-glycoprotein mediated efflux transport. *Mol Pharm*, 2, 12-21.
- WAGNER, M., SEITZ, U., BUCK, A., NEUMAIER, B., SCHULTHEISS, S., BANGERTER, M., BOMMER, M., LEITHAUSER, F., WAWRA, E., MUNZERT, G. & RESKE, S. N. (2003) 3'-[18F]fluoro-3'-deoxythymidine ([18F]-FLT) as positron emission tomography tracer for imaging proliferation in a murine B-Cell lymphoma model and in the human disease. *Cancer Res*, 63, 2681-7.
- WANG, X. K. & FU, L. W. (2010) Interaction of tyrosine kinase inhibitors with the MDR- related ABC transporter proteins. *Curr Drug Metab*, 11, 618-28.
- WEBER, W. A., DIETLEIN, M., HELLWIG, D., KIRSCH, C. M., SCHICHA, H. & SCHWAIGER, M. (2003) PET with F-18-fluorodeoxyglucose for staging of non-small cell lung cancer - Evidence-based recommendations and cost-effectiveness. *Nuklearmedizin-Nuclear Medicine*, 42, 135-144.
- WEI, Y., MA, Y., ZHAO, Q., REN, Z., LI, Y., HOU, T. & PENG, H. (2012) New use for an old drug: inhibiting ABCG2 with sorafenib. *Mol Cancer Ther*, 11, 1693-702.
- WEISSLEDER, R. & PITTET, M. J. (2008) Imaging in the era of molecular oncology. *Nature*, 452, 580-9.
- WHEELER, D. L., DUNN, E. F. & HARARI, P. M. (2010) Understanding resistance to EGFR inhibitors- impact on future treatment strategies. *Nat Rev Clin Oncol*.
- WISSNER, A., OVERBEEK, E., REICH, M. F., FLOYD, M. B., JOHNSON, B. D., MAMUYA, N., ROSFJORD, E. C., DISCAFANI, C., DAVIS, R., SHI, X., RABINDRAN, S. K., GRUBER, B. C., YE, F., HALLETT, W. A., NILAKANTAN, R., SHEN, R., WANG, Y. F., GREENBERGER, L. M. & TSOU, H. R. (2003) Synthesis

- and structure-activity relationships of 6,7-disubstituted 4-anilinoquinoline-3-carbonitriles. The design of an orally active, irreversible inhibitor of the tyrosine kinase activity of the epidermal growth factor receptor (EGFR) and the human epidermal growth factor receptor-2 (HER-2). *J Med Chem*, 46, 49-63.
- WITNEY, T. H., ALAM, I. S., TURTON, D. R., SMITH, G., CARROLL, L., BRICKUTE, D., TWYMAN, F. J., NGUYEN, Q. D., TOMASI, G., AWAIS, R. O. & ABOAGYE, E. O. (2012) Evaluation of deuterated 18F- and 11C-labeled choline analogs for cancer detection by positron emission tomography. *Clin Cancer Res*, 18, 1063-72.
- WONG, K. L. I. (2004) *Clinical PET Principles and applications*, Springer.
- WORKMAN, P., ABOAGYE, E. O., BALKWILL, F., BALMAIN, A., BRUDER, G., CHAPLIN, D. J., DOUBLE, J. A., EVERITT, J., FARNINGHAM, D. A., GLENNIE, M. J., KELLAND, L. R., ROBINSON, V., STRATFORD, I. J., TOZER, G. M., WATSON, S., WEDGE, S. R. & ECCLES, S. A. (2010) Guidelines for the welfare and use of animals in cancer research. *Br J Cancer*, 102, 1555-77.
- YAMADA, T., MATSUMOTO, K., WANG, W., LI, Q., NISHIOKA, Y., SEKIDO, Y., SONE, S. & YANO, S. (2010) Hepatocyte growth factor reduces susceptibility to an irreversible epidermal growth factor receptor inhibitor in EGFR-T790M mutant lung cancer. *Clin Cancer Res*, 16, 174-83.
- YANASE, K., TSUKAHARA, S., ASADA, S., ISHIKAWA, E., IMAI, Y. & SUGIMOTO, Y. (2004) Gefitinib reverses breast cancer resistance protein-mediated drug resistance. *Mol Cancer Ther*, 3, 1119-25.
- YARDEN, Y. & SLIWKOWSKI, M. X. (2001) Untangling the ErbB signalling network. *Nat Rev Mol Cell Biol*, 2, 127-37.
- YEH, H. H., OGAWA, K., BALATONI, J., MUKHAPADHYAY, U., PAL, A., GONZALEZ-LEPERA, C., SHAVRIN, A., SOGHOMONYAN, S., FLORES, L., 2ND, YOUNG, D., VOLGIN, A. Y., NAJJAR, A. M., KRASNYKH, V., TONG, W., ALAUDDIN, M. M. & GELOVANI, J. G. (2011) Molecular imaging of active mutant L858R EGF receptor (EGFR) kinase-expressing non-small cell lung carcinomas using PET/CT. *Proc Natl Acad Sci U S A*, 108, 1603-8.
- YOSHIDA, T., ZHANG, G. & HAURA, E. B. (2010) Targeting epidermal growth factor receptor: central signaling kinase in lung cancer. *Biochem Pharmacol*, 80, 613-23.
- YOSHIMURA, N., KUDOH, S., KIMURA, T., MITSUOKA, S., MATSUURA, K., HIRATA, K., MATSUI, K., NEGORO, S., NAKAGAWA, K. & FUKUOKA, M. (2006) EKB-569, a new irreversible epidermal growth factor receptor tyrosine kinase inhibitor, with clinical activity in patients with non-small cell lung cancer with acquired resistance to gefitinib. *Lung Cancer*, 51, 363-8.
- YUN, C. H., BOGGON, T. J., LI, Y., WOO, M. S., GREULICH, H., MEYERSON, M. & ECK, M. J. (2007) Structures of lung cancer-derived EGFR mutants and inhibitor complexes: mechanism of activation and insights into differential inhibitor sensitivity. *Cancer Cell*, 11, 217-27.
- YUN, C. H., MENGWASSER, K. E., TOMS, A. V., WOO, M. S., GREULICH, H., WONG, K. K., MEYERSON, M. & ECK, M. J. (2008) The T790M mutation in EGFR kinase causes drug resistance by increasing the affinity for ATP. *Proc Natl Acad Sci U S A*, 105, 2070-5.
- ZANDER, T., SCHEFFLER, M., NOGOVA, L., KOBE, C., ENGEL-RIEDEL, W., HELLMICH, M., PAPACHRISTOU, I., TOEPELT, K., DRAUBE, A., HEUKAMP, L., BUETTNER, R., KO, Y. D., ULLRICH, R. T., SMIT, E., BOELLAARD, R., LAMMERTSMA, A. A., HALLEK, M., JACOBS, A. H., SCHLESINGER, A., SCHULTE, K., QUERINGS, S., STOELBEN, E., NEUMAIER, B., THOMAS, R. K., DIETLEIN, M. & WOLF, J. (2011) Early prediction of nonprogression in advanced non-small-cell lung cancer treated with erlotinib by using [(18)F]fluorodeoxyglucose and [(18)F]fluorothymidine positron emission tomography. *J Clin Oncol*, 29, 1701-8.
- ZANNETTI, A., IOMMELLI, F., SPERANZA, A., SALVATORE, M. & DEL VECCHIO, S. (2012) 3'-Deoxy-3'-F-18-Fluorothymidine PET/CT to Guide Therapy with Epidermal Growth Factor Receptor Antagonists and Bcl-x(L) Inhibitors in Non-Small Cell Lung Cancer. *Journal of Nuclear Medicine*, 53, 443-450.
- ZHANG, M. R., KUMATA, K., HATORI, A., TAKAI, N., TOYOHARA, J., YAMASAKI, T., YANAMOTO, K., YUI, J., KAWAMURA, K., KOIKE, S., ANDO, K. & SUZUKI, K. (2010) [11C]Gefitinib ([11C]Iressa):

- radiosynthesis, in vitro uptake, and in vivo imaging of intact murine fibrosarcoma. *Mol Imaging Biol*, 12, 181-91.
- ZHAO, W., YANG, Z., LIU, X., TIAN, Q., LV, Y., LIANG, Y., LI, C., GAO, X. & CHEN, L. (2013) Identification of alpha1-antitrypsin as a potential prognostic biomarker for advanced nonsmall cell lung cancer treated with epidermal growth factor receptor tyrosine kinase inhibitors by proteomic analysis. *J Int Med Res*.
- ZHOU, C. C., WU, Y. L., CHEN, G. Y., FENG, J. F., LIU, X. Q., WANG, C. L., ZHANG, S. C., WANG, J., ZHOU, S. W., REN, S. X., LU, S., ZHANG, L., HU, C. P., HU, C. H., LUO, Y., CHEN, L., YE, M., HUANG, J. N., ZHI, X. Y., ZHANG, Y. P., XIU, Q. Y., MA, J., ZHANG, L. & YOU, C. X. (2011a) Erlotinib versus chemotherapy as first-line treatment for patients with advanced EGFR mutation-positive non-small-cell lung cancer (OPTIMAL, CTONG-0802): a multicentre, open-label, randomised, phase 3 study. *Lancet Oncology*, 12, 735-742.
- ZHOU, W., ERCAN, D., CHEN, L., YUN, C. H., LI, D., CAPELLETTI, M., CORTOT, A. B., CHIRIEAC, L., IACOB, R. E., PADERA, R., ENGEN, J. R., WONG, K. K., ECK, M. J., GRAY, N. S. & JANNE, P. A. (2009) Novel mutant-selective EGFR kinase inhibitors against EGFR T790M. *Nature*, 462, 1070-4.
- ZHOU, W., ERCAN, D., JANNE, P. A. & GRAY, N. S. (2011b) Discovery of selective irreversible inhibitors for EGFR-T790M. *Bioorg Med Chem Lett*, 21, 638-43.

Appendix

Conference abstracts

Poster presentation at ACCR/SNMMI San Diego, CA, February 2013.

Cyanoquinoline based tracers and their interaction with the ABC transporters for the imaging of EGFR in cancer

Slade R.; Pisaneschi F ;Kaliszczak M.; Smith G.; Nguyen Q.D.; Aboagye EO.

The epidermal growth factor receptor (EGFR) plays a key role in biological processes including proliferation and cell cycle regulation through the activation of downstream signal transduction pathways. Furthermore, this tyrosine kinase receptor is overexpressed in many cancers including ovarian, breast, head and neck and Brain. Imaging EGFR using positron emission tomography (PET) linked to EGFR mutational status could help select patients who are more likely to respond to small molecule tyrosine kinase inhibitors such as Gefitinib. We previously showed by PET that ^{18}F -FED6, a radiolabeled cyanoquinoline EGFR antagonist, had higher uptake in A431 xenograft tumors (high EGFR; high ABCG2, no ABCB1) compared to HCT116 xenograft tumors (low EGFR; low ABCG2, no ABCB1). However the overall tumor radiotracer uptake is low possibly due to the ATP binding cassette transporters, frequently overexpressed in tumor cells and actively extruding drugs from the cytosol.

The aim of this study is to further characterise cyanoquinoline tracers for ^{18}F PET imaging of EGFR, investigating the role of the ABC transporters. Following exposure of isogenic wild-type and ABC transporter over-expressing cells to the cyanoquinoline series (FED1-9) several of the compounds were found to be potential substrates of ABCB1 (P-glycoprotein) and ABCG2 transporters. Transwell caco2 cell permeability assays confirmed compound efflux and hence ABC transporter substrate specificity. Efflux of the cyanoquinolines was significantly decreased in the presence of inhibitors of both ABCB1 and ABCG2 transporters, further confirming specificity. Radiolabeled ^{18}F -FED6, was shown to have a four-fold lower *in vitro* uptake in ABCB1 or ABCG2 overexpressing cell lines compared to the isogenic counterpart. Finally, *in vivo* PET imaging in A431 xenografts with ^{18}F -FED6, showed over a two-fold increase in the tumor uptake of the radiolabeled cyanoquinoline, when mice were pre-treated with gefitinib. *In vitro* studies confirmed gefitinib's role as an ABCG2 inhibitor. We confirm that ABC transporter expression can confound PET imaging of EGFR using ^{18}F -FED6. Further development and investigation into a second generation of compounds, devoid of ABC transporters interaction and improved tumor uptake are required. Initial studies have commenced on one such second generation cyanoquinoline.

Poster presentation at CRUK imaging conference, London, April 2012.

Cyanoquinoline based tracers for the imaging of mutant EGFR in cancer.

Rozanna Slade; Pisaneschi F.; Aboagye E.

The epidermal growth factor receptor (EGFR) plays a key role in biological processes including proliferation and cell cycle regulation through the activation of downstream signal transduction pathways^[1]. Furthermore, this tyrosine kinase receptor is overexpressed in many cancers including ovarian, breast, head and neck and Brain.^[2] In NSCLC the presence of so called activation mutations to EGFR such as del747-750 have been shown to lead to improved response to small molecular TKI (TKI) such as gefitinib. Imaging EGFR using positron emission tomography, PET, could be used to select, monitor and assess therapeutic response to inhibitors such as gefitinib. A series of ¹⁸F radiolabeled EGFR specific cyanoquinoline based compounds, have been previously characterised showing higher radiotracer uptake in A431 xenograft tumours (High EGFR) compared to HCT116 xenograft tumours (low EGFR).^[3]

The aim of this study is to further characterise the cyanoquinoline tracers for ¹⁸F PET imaging of EGFR, investigating their specificity and selectivity for different mutant forms of EGFR. First, a series of western blots were carried out to assess the inhibition of p-EGFR in a series of cell lines expressing different mutant forms of EGFR. P-EGFR was more strongly inhibited by the cyanoquinoline compounds in cell lines containing active mutant forms of EGFR compared to wild type EGFR expressing cell lines.

Second, both cell uptake and *in vivo* imaging were performed with a selected ¹⁸F labelled cyanoquinoline. These studies showed no difference in tracer uptake between mutant and wild type EGFR expressing NSCLC cell lines.

However the overall tumour radiotracer uptake is low possibly due to the ATP binding cassette transporters, actively extruding substrates from the cytosol.^[4]

A second generation of compounds are needed that have little or no interaction with the ABC transporters and thus improve the tumour uptake of the tracer.

(1) Sebastian, S., J. Settleman, et al. (2006). Biochim Biophys Acta **1766**(1): 120-39.

(2) Wells, A. (1999). "EGF receptor." Int J Biochem Cell Biol **31**(6): 637-43.

(3) Pisaneschi, F., Q.D. Nguyen, et al. (2010) Bioorg MED Chem **18**(18)66343-45

(4) Abourbeh, G., S. Dissoki, et al. (2007) Nucl Med Biol **34** (1): 55-70

Publications planned

ABC transporter interaction of cyanoquinoline PET imaging molecule.

Rozanna Slade, Federica Pisaneschi, and Eric O. Aboagye.

Comprehensive Cancer Imaging Centre, Imperial College London, Faculty of Medicine, Hammersmith Hospital Campus, Du Cane Road, London W12 0NN, United Kingdom